ADVANCE TREATMENT FOR REMOVAL OF CHROMIUM AND FLUORIDE FROM INDUSTRIAL WASTEWATER

Ph.D. THESIS

by

GAIKWAD MAHENDRA SHIVAJI

DEPARTMENT OF CHEMICAL ENGINEERING
INDIAN INSTITUTE OF TECHNOLOGY ROORKEE
ROORKEE-247667 (INDIA)
MARCH, 2018

ADVANCE TREATMENT FOR REMOVAL OF CHROMIUM AND FLUORIDE FROM INDUSTRIAL WASTEWATER

A THESIS

Submitted in partial fulfilment of the requirements for the award of the degree

of
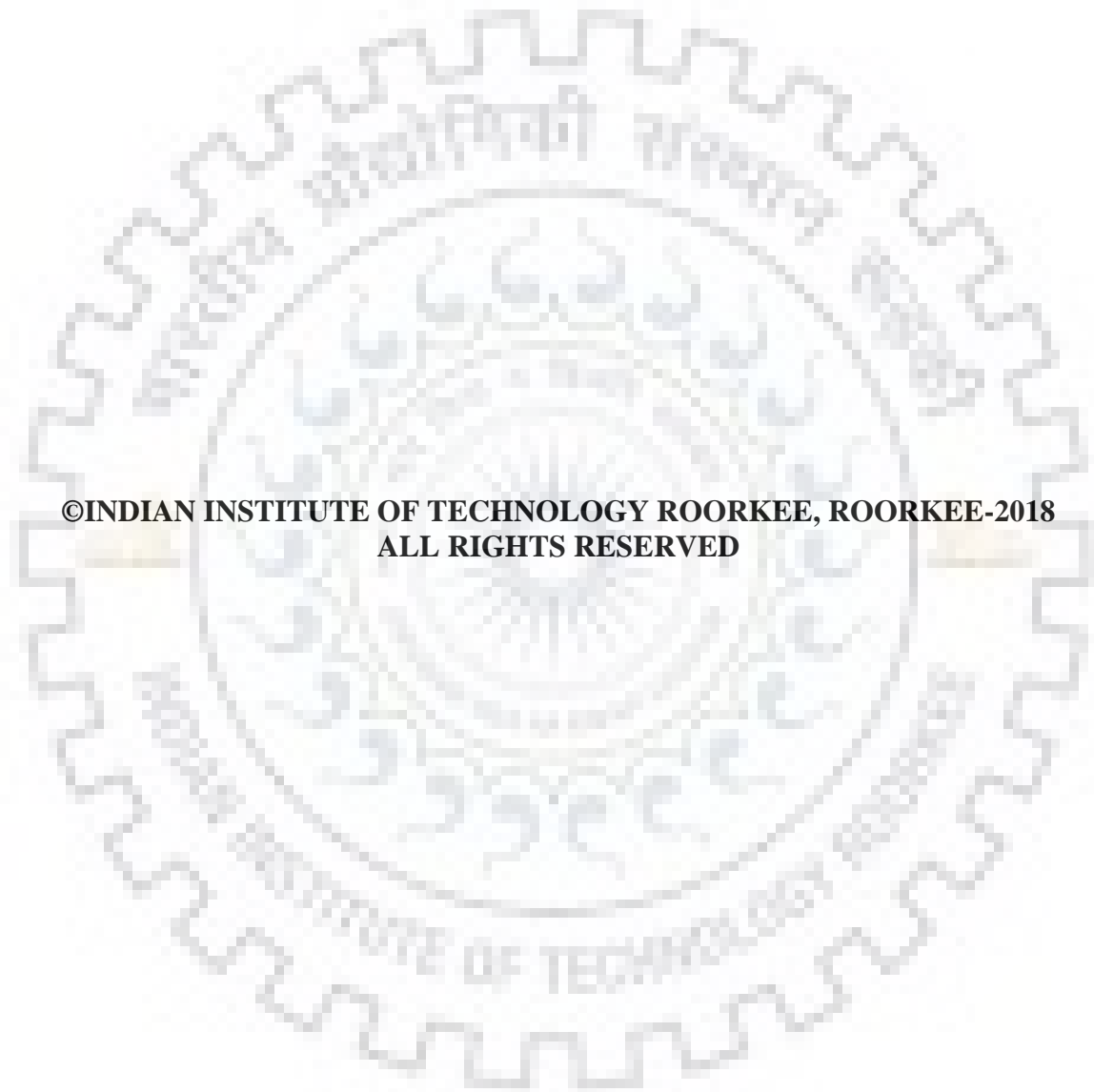
DOCTOR OF PHILOSOPHY

in

CHEMICAL ENGINEERING

by

GAIKWAD MAHENDRA SHIVAJI

**DEPARTMENT OF CHEMICAL ENGINEERING
INDIAN INSTITUTE OF TECHNOLOGY ROORKEE
ROORKEE – 247 667 (INDIA)
MARCH, 2018**

INDIAN INSTITUTE OF TECHNOLOGY ROORKEE
ROORKEE

<u>CANDIDATE'S DECLARATION</u>

I hereby certify that the work which is being presented in the thesis entitled **"ADVANCE TREATMENT FOR REMOVAL OF CHROMIUM AND FLUORIDE FROM INDUSTRIAL WASTEWATER"** in partial fulfilment of the requirements for the award of the Degree of Doctor of Philosophy and submitted in the Department of Chemical Engineering of the Indian Institute of Technology Roorkee, Roorkee, is an authentic record of my own work carried out during a period from July, 2014 to March, 2018 under the supervision of Dr. Chandrajit Balomajumder, Professor, Department of Chemical Engineering, Indian Institute of Technology Roorkee, Roorkee.

The matter presented in this thesis has not been submitted by me for the award of any other degree of this or any other institution.

(GAIKWAD MAHENDRA SHIVAJI)

This is to certify that the above statement made by the candidate is correct to the best of my knowledge.

Dated:

(Chandrajit Balomajumder)
Supervisor

ABSTRACT

The water pollution is enhanced due to high industrialization and random discharge of toxic metal ions, chemical, organic compounds, toxic chemicals, from various industries. The chromium and fluoride like toxic ions are coming in to wastewater from electronic process industries. Especially in the semiconductor industry for wafer surface etching process produces some waste like chromic acids, sulfuric, phosphoric, hydrofluoric etc. Thus, Cr(VI) and fluoride like toxic ions are found in semiconductor effluents. Cr(VI) also coming in waste stream from other industrial activities like steel-works, metal finishing, electroplating, petroleum refining, leather tanning, etc. The high release of fluoride into water bodies of environment from industries such as semiconductor manufacturing, electroplating, glass and ceramic production and many more. Cr(VI) is highly toxic, carcinogenic and tera-togenic. It is harmful for human, animals and plants causing harmful effects on human like lung cancer, damage to liver, kidney and gastric system. General sign of high fluoride consumption is fluorosis, which is identified by mottling of teeth in mild cases and embrittlement of bones and neurological damage in severe cases. The permissible limit as per CPCB standards for Cr (VI) discharge of industrial effluents in different water bodies, viz., inland surface water, public sewers and marine coastal areas are 0.1, 2.0 and 1.0 mg/L, respectively (CPCB 2012). The permissible limit as per CPCB standards for fluoride discharge of industrial effluents is 15 mg/L (CPCB 2012). The fluoride effluent limit as per USEPA from the wastewater treatment facilities has been set to 4 mg/L (USEPA 1985, 2008).

In the present study membrane separation (nanofiltration and reverse osmosis) and capacitive deionization process have been selected for simultaneous removal of Cr (VI) and fluoride. In membrane separation various commercial polyamide flat sheet membranes namely NF300, NF500, PN40 and RO membrane were selected for the simultaneous removal of Cr(VI) and fluoride from synthetic and industrial wastewater. The present work aims to study the influence of various operating variables to remove Cr(VI) and fluoride simultaneously from feed synthetic and real industrial wastewater with various nanofiltration (NF300, NF500, PN40) and RO flat sheet membranes.

The characterization studies for identification of morphology, surface roughness and chemical composition of NF300, NF500, PN40, RO membranes were carried out with SEM, AFM, and FTIR, respectively. In this experiment influence of pressure on removal of Cr(VI) and fluoride

was studied by changing the pressure from 2 to 10 bar with a concentration range of 5-100 mg/L of Cr(VI) and fluoride each and at different pH (2 to 10).

It was observed that the simultaneous rejection of Cr(VI) and fluoride ions increases with the increase in feed pressure and decreases with an increase in feed concentration. This rejection of Cr(VI) and fluoride ions were significantly influenced by the pH of feed solution. The optimized values of experimental parameters were evaluated found and the optimized value of operating pressure was 10 bar for nanofiltration and 16 bar for reverse osmosis, pH 8 was found best for simultaneous rejection of Cr(VI) and fluoride ions. The highest percent rejection of Cr(VI) and fluoride were found to be 97% and 92% with NF300; 91% and 84% with NF500 and 88% and 82% with PN40 membranes for lower concentration of 5 mg/L feed, respectively. The highest removal of Cr(VI) and fluoride by RO flat sheet membrane were found 99.98% and 95.1% for 5 mg/L feed respectively at 16 bar pressure. The highest percent rejection of Cr(VI) and fluoride were found to be 77% and 70% with NF300; 71% and 64% with NF500 and 68% and 61% with PN40 membranes for higher concentration 100 mg/L feed, respectively. The highest removal of Cr(VI) and fluoride by RO flat sheet membrane were found 99.10% and 94% for 100 mg/L feed, respectively at 16 bar pressure. The rejection performances of membranes are found in the sequence as RO > NF300 > NF500> PN40. The maximum percent rejection of Cr(VI) and fluoride were found 92.2% and 83% with NF300; 99.96% and 94.97% with RO flat sheet membrane from industrial wastewater concentration [11 mg/L Cr(VI) and 35.24 mg/L fluoride] respectively.

The estimation of membrane transport parameters and membrane performance evaluation were carried out with CFSK model and CFSD model. The values of flux and rejection estimated using membrane transport parameters are in good agreement with the experimental results. Reasonably good agreement for experimental rejection and true rejection for Cr(VI) and fluoride estimated by CFSK and CFSD models respectively, but CFSK model predicted values are more accurate compared to CFSD model.

The capacitive deionization is recently developing and worldwide attracted techniques due to eco-friendly, having less energy consumption and less working costs than other desalination technologies, simplicity in regeneration and maintenance compared with other conventional techniques of desalination. The CDI technology is used in the application of the desalination and water treatment application.

In this work, different activated carbon were prepared from tea waste biomass, rice husk, and limonia acidissma (wood apple) shell with acid treatment and thermal modification. The TGA,

DTA, DTG analyses of waste biomass were carried out using a thermal analysis instrument. The characterization of prepared activated carbon was done for morphological, chemical composition analysis using SEM and FTIR, respectively. Different activated carbon electrodes were prepared from commercial activated carbon, tea waste activated carbon, rice husk activated carbon, and limmonia acidissma activated carbon.

The CAC electrode was fabricated from commercial activated carbon and successfully applied in CDI for simultaneous electrosorptive treatment of Cr(VI) and fluoride binary feed. The different parameters optimization was carried out with CAC electrode. The optimized values of operating parameters were found as operating voltage 1.2 V, optimum feed flow rate 16 mL/min and pH above 7 were found best for simultaneous rejection of Cr(VI) and fluoride. All the optimized parameters were set for all further experiments. The result shows that maximum electrosorption capacity for Cr(VI) and fluoride were 0.85 mg/g and 0.82 mg/g for 10 mg/L; 3.67 mg/g and 3.22 mg/g for 100 mg/L Cr(VI) and fluoride binary feed, respectively at 1.2 V. Effective purification and regeneration of electrode were found for binary feed solution of Cr(VI) and fluoride.

Similarly, other electrodes namely TWBAC electrode, RHAC electrode, LASAC electrode were successfully prepared from tea waste biomass activated carbon, rice husk activated carbon, limonia acidissima shells activated carbon respectively. The prepared electrodes were tested out in CDI application for simultaneous removal of Cr(VI) and fluoride. The TWBAC, RHAC, LASAC electrodes were found an effective removal performance at low concentration of feed. The percent removal of Cr(VI) and fluoride were found 88.5% and 85.20% for 10 mg L^{-1} mix feed solution respectively with TWBAC electrode. The percent removal of Cr(VI) and fluoride was found 83.1 % and 80.4 % for 10 mg L^{-1} mix feed solution respectively with RHAC electrode. The LASAC electrode was assembled in the MCDI system for simultaneous removal of Cr(VI) and fluoride from feed solution. The percent removal of Cr(VI) and fluoride came out to 92.2 % and 89.23% for 10 mg/L.

In the present work, mono and multicomponent isotherm models were done. The Langmuir, Freundlich and Redlich Peterson isotherm models were used for the mono component system. The multicomponent isotherm models, namely modified Langmuir, non modified Langmuir, extended Langmuir, extended Freundlich, modified Redlich Peterson and non modified Redlich Peterson were used for multicomponent system. In isotherm study it was found that the removal of Cr(VI) and fluoride by CAC electrode follows Freundlich isotherm model and Redlich Peterson model was found to be best agreement for both Cr(VI) and fluoride in mono

component models. Extended Freundlich model and Non modified R–P model among six applied multicomponent isotherm models were found to fit well with the experimental data for both Cr(VI) and fluoride electropsorption performance. The ion sorption process with TWBAC, RHAC and LASAC electrode follows Langmuir isotherm model and Redlich Peterson model for mono component; Extended Langmuir and Non modified Redlich Peterson for multicomponent isotherm modelling.

A Kinetic model study was carried out for investigating the nature of sorption process. It is useful to find out equilibrium time and the mechanism of adsorption, such as physisorption and chemisorption. In kinetic study, it was found that Pseudo first order kinetic model is good agreement with experimental data for both Cr(VI) and fluoride by CAC, TWBAC, RHAC, and LASAC electrode. The sorption performance electrodes were found in the sequence as CAC electrode > LASAC electrode > TWBAC electrode > RHAC electrode.

The maximum percent rejection of Cr(VI) and fluoride was found 94.35% and 80.1% with CAC electrode; 90.2 % and 76 % with LASAC electrode from industrial wastewater concentration [11 mg/L Cr(VI) and 35.24 mg/L fluoride] respectively.

Thus, membrane separation with NF300 and RO flat sheet membrane and CDI with CAC electrode and LASAC electrode could be a promising treatment for simultaneous electrosorptive removal of low concentrated Cr(VI) and fluoride from industrial wastewater.

ACKNOWLEDGEMENT

Kumar Sandhawar, Mr. Kartikeya Shukla, Mr. Bahiru Tsegaye, Ms. Parminder Kaur, Ms. Bharti Verma.

I would like to acknowledge all of them for their prayers, for the encouragement they have given me whenever I was depressed and for the support, they have rendered me throughout my life and especially throughout this work.

Finally, I would like to thank all those who have helped me during the research work. Above all, I thank 'Almighty' with whose beatitude, I could reach this far.

GAIKWAD MAHENDRA SHIVAJI

TABLE OF CONTENTS

LIST OF FIGURES

LIST OF TABLES

ABBREVIATIONS AND NOTATIONS

ABBREVIATIONS

ACF	Active carbon fiber
AFM	Atomic force microscopy
ARE	Average relative error
CAC	Commercial activated carbon
CDI	Capacitive deionization
CFSD	Combined film theory-solution diffusion
CFSK	Combined film theory-Spiegler-Kedem model
CPCB	Central Pollution Control Board
DI	Deionized water
DTA	Differential thermal analysis
DTG	Derivative thermal gravimetric analysis
DTPA	Diethylene triamine penta acetic acid
ED	Electrodialysis
EDL	Electric double layer
EDTA	Ethylene diamine tetra acetic acid
FTIR	Fourier transform infrared (spectroscopy)
ICP-AES	Inductively coupled plasma atomic emission spectroscopy
ICP-MS	Inductively coupled plasma mass spectrometry
LAS	Limonia acidissima shell
LASAC	Limonia acidissima activated carbon
MCDI	Membrane capacitive deionization
MF	Microfiltration

MO	Manganese oxide
MPSD	Marquardt's percent standard deviation
MTC	Mass transfer coefficient
MWCO	Molecular weight cut off
NF	Nanofiltration
PWP	Pure water permeability
RH	Rice husk
RHAC	Rice husk activated carbon
RMS	Root mean square
RO	Reverse osmosis
SEM	Scanning electron microscopy
TGA	Thermal gravimetric analysis
TPs	Transport parameters
TW	Tea waste
TWBAC	Tea waste biomass activated carbon
UF	Ultrafiltration
USEPA	United States Environmental Protection Agency
WHO	World Health Organization

NOTATIONS

Q_0	Langmuir model constant (mg/g)
b	Langmuir model constant (L /mg)
K_F	Freundlich model constant (mg /g) / (mg /L)$^{1/n}$
n	Freundlich model constant
K_{RP}	R–P model constant (L/g)
a_{RP}	R–P model constant (L/mg)

β	R–P model constant
$Q_{0,i}$	Modified Langmuir model constant for ith component (mg/g)
x_i, y_i, z_i	Constant in modified R–P model
K_1	Constant in Pseudo-first order model (1/min)
K_2	Constant in Pseudo-second order model (g /mg min)
N	Number of observations in the experimental Isotherm
P	Number of parameter in regression model
$Q_{e,i}^{exp}$	Experimental value of Qe (mg/g)
$Q_{e,i}^{cal}$	Predicted value of Qe (mg/g)
η_i	Correction parameter of ith component in modified Langmuir model
$\eta_{i,j}$	Correction parameter of ith component in jth experiment in modified Langmuir model
C_e	Concentration of adsorbate in solution at equilibrium (mg/l)
$C_{e,i}$	Concentration of ith component in the binary mixture at equilibrium (mg/l).
A	Permeability parameter
C_{A1}	Concentrations of solute in the feed,
C_{A2}	Concentrations of solute in the boundary layer near the membrane surface
C_{A3}	Concentrations of solute in the permeate
R_o	Observed rejection of solute,
R	True rejection of solute
Jv	Permeate flux
k	Mass transfer coefficient (m/s)
L_p	Pure water permeability coefficient,
ΔP	Trans-membrane pressure difference
$\Delta \pi$	Osmotic pressure difference.

P_m	Overall solute permeability (m/s)
$D_{AM}K/\delta$	Solute transport parameter (m/s)
V_f	Volume (L) of feed in tank
m	Mass (g) of activated carbon electrode
C_o	Initial concentration

GREEK LETTERS

σ	Reflection coefficient

INTRODUCTION

1. General

Fresh water is need of society. Due to industrialization, water is getting contaminated with various heavy metals, organic, inorganic compounds, metal ions and many more. Worldwide researchers focusing in the field of water treatment (De et al., 2013; Panigrahi et al., 2013; Verma et al., 2012; Kumar et al., 2014; Reddy et al., 2014), technology (Jo et al., 2014; Lee and Sherif, 2001), energy (Sherif et al., 2005; Das and Mitra, 1995; Gunda et al., 2011; Kumar et al., 2015; Mishra et al., 2005; Nanduri and Das, 2009; Nanduri et al., 2009), nanotechnology (Ray et al., 2010, 2011; Soin et al., 2012; Ray and Aswal, 2011; Mohammadpour et al., 2010). Water pollution is enhanced due to random discharge of toxic metal ions from the semiconductor industry, metallurgical, mining, chemical manufacturing, tannery, electroplating industries, etc. In semiconductor industry various kinds of chemicals are used (Hu et al. 2005; de Luna et al., 2009). Fluoride, toxic solvent, heavy metals, dyes and salts, suspended solids and chelating agents may found in wastewater discharge of semiconductor manufacturing industry (de Luna et al., 2009). In the wafer surface etching process produce some waste like chromic acids, sulfuric, phosphoric, hydrofluoric etc. which are highly toxic. Mainly HF/chromic acid are used in Secco and Yang etching methods (Secco d'Aragona 1972; Yang 1984). Thus the Cr(VI) and fluoride like toxic ions are found in semiconductor effluents (Aoudj et al., 2013; Aoudj et al., 2015). Cr(VI) has been also coming in waste stream from industrial activities like steel-works, metal finishing, electroplating, petroleum refining, leather tanning, etc. (Chen and Gu, 2005). Mainly anthropogenic activity is responsible for high amounts of Cr(VI) release in the environment. However, according to the literature (Gonzalez et al., 2005; Manning et al., 2015) natural geogenic activity also may release of high levels of Cr(VI). Mediterranean (Greece, Italy and Pacific (California (USA), Mexico), and different part of the world are the few populated areas are the example of having such conditions. Fluoride occurs in various parts of the world groundwater (Gaciri and Davies, 1993; Czarnowski et al., 1996; Ayoob and Gupta, 2006; Wang and Huang, 1995; Mjengera and Mkongo, 2003; Diaz-Barriga et al., 1997; Kruse and Ainchil, 2003). Geologically fluoride is widely distributed in the environment (Abe et al., 2004). The fluoride coming in to water due to fluorine containing rocks (Banks et al., 1995). Fluoride contains rocks such as granite, basalt, syenite, and shale, can be responsible for fluoride contamination of groundwater (Edmunds and

Smedley, 2005; Apambire et al., 1997; Reddy and Prasad, 2003). Other than the natural geological sources anthropogenic process are also responsible the high release of fluoride from industries (Reardon and Wang., 2000) in to water bodies of environment. These industries include semiconductor manufacturing, electroplating, glass and ceramic production and many more (Shen et al., 2003).

Chromium is exist in two form Cr (III) and Cr(VI). Cr(VI) is highly toxic compared to Cr(III) (Kowalski, 1994). Cr(VI) is highly toxic, carcinogenic and tera-togenic (Chen and Gu, 2005). It is harmful for human, animals and plants causing harmful effects on human like lung cancer, damage to liver, kidney and gastric system (US Department of Health and Human Services, 1991; Cieslak-Golonka, 1995). Worldwide groundwater contamination with fluoride is also a serious problem (Amini et al., 2008). According to World Health Organization (WHO) guidelines fluoride has come in category of contaminants in water, which cause the health problems (WHO, 2006). The smallest amount of fluoride ingested in water is beneficial for conservation formation of teeth mostly in children (Mahramanlioglu et al., 2002). Excess intakes create various kinds of diseases like cancer, arthritis, brain damage, Alzheimer syndrome and others (Chinoy, 1991; Harrison, 2005). General sign of high fluoride consumption is fluorosis, which is identified by mottling of teeth in mild cases and embrittlement of bones and neurological damage in severe cases (Fan et al., 2003).

Discharge limit of hexavalent chromium and trivalent chromium are 0.05 mg/L and 5 mg/L, respectively (Acar and Malkoc, 2004). The permissible limit as per CPCB standards for Cr(VI) discharge of industrial effluents in different water bodies, namely, inland surface water, public sewers and marine coastal areas are 0.1, 2.0 and 1.0 mg/L, respectively (CPCB, 2012).. As per guideline of WHO, maximum allowable limit for total Cr in drinking water of 50 µg/L (WHO, 2004). The fluoride discharge limit is 15 mg/L (Drouiche et al. 2009). The permissible limit as per CPCB standards for fluoride discharge of industrial effluents is 15 mg/L (CPCB, 2012). The fluoride effluent limit as per USEPA from the wastewater treatment facilities has been set to 4 mg/L (USEPA 1985, 2008).

Thus, it is essential to remove these toxic ions from the wastewaters prior to their release into the environment. Various methods were reported for water treatment, namely, biological (Kalsi and Srivastava, 1998; Srivastava and Srivastava 2006, 2008; Joshi et al., 2008), coagulation (Verma et al., 2012), membrane separation (Jana et al., 2011; Panigrahi et al., 2013; Samal et al., 2016), adsorption (De et al., 2013; Dhabhai et al., 2016; Moghal et al., 2016; Rout et al., 2014, 2015), electrochemical (Cameselle and Reddy, 2013) etc.

Different techniques have been used over recent years for individual removal of chromium and fluoride, such as adsorption (Selvi et al., 2001; Li et al. 2003), electrochemical precipitation (Kongsricharoern and Polprasert, 1995; Shen et al., 2003), liquid-liquid extraction (El-Hefny, 2009; Visser et al. 2001) and ion exchange (Atia, 2006; Onyango et al., 2004), membrane (Hu and Dickson, 2006; Kozlowski and Walkowiak, 2002) etc. Many studies have been reported on heavy metals and metals ion removal by nanofiltration (Wahab Mohammad et al., 2004; Al-Rashdi et al., 2011; Murthy and Gaikwad, 2013a, 2013b). NF is a capable method for the rejection of heavy metal ions like arsenic (Saitua et al., 2005), nickel (Ahn et al., 1999), chromium (Ahmed et al., 2002), cadmium (Ballet et al., 2004), and copper (Ku et al., 2005) from wastewater. Benefits behind NF process are the easy operation, high removal efficiency and reliable (Banerjee et al., 2007; Lhassani et al., 2001; Pontie et al., 2003). Various studies are reported on polyamide NF as a promising membrane for removal of metal ions like copper and cadmium (Mehiguene et al., 1999), praseodymium (III) (Murthy and Gaikwad, 2013a), nickel ions (Murthy and Chaudhari, 2008). Thus polyamide membranes here selected for the present study on simultaneous rejection of Cr(VI) and fluoride from binary feed solution.

The CDI process is recently developing and worldwide attracted techniques, eco-friendly, having less energy consumption and working costs than other desalination technologies, simplicity in regeneration and maintenance compared with other conventional techniques of desalination (Mezher et al., 2011; Wimalasiri and Zou, 2013). CDI working on the principle of electrostatic adsorption using porous electrodes and ion transport is due to electrostatic adsorption, not due to oxidation and reduction reactions (Farmer et al., 1996).

No study was reported on the simultaneous removal by Cr(VI) and fluoride by membrane separation and capacitive deionization. After identification this research gap following objectives have been set for the present research work.

1.1 Objective

1. Estimation and identification of best flat sheet membrane for simultaneous removal of Cr(VI) and fluoride from binary synthetic solution by nanofiltration and reverse osmosis.

2. Estimation of membrane transport parameters of membrane transport model, namely CFSK model and CFSD model. Identification of best suitable membrane transport model.

3. Best flat sheet NF and RO membrane used for simultaneous removal of Cr(VI) and fluoride from real industrial wastewater.

4. Preparation of activated carbon from different waste biomass by thermal and chemical treatment.

5. Preparation of porous activated carbon electrode from different waste biomass activated carbon for capacitive deionization.

6. Performance identification of best activated carbon electrode for simultaneous removal of Cr(VI) and fluoride from the binary synthetic solution of Cr(VI) and fluoride.

7. Estimation of single and multicomponent isotherm models parameters for simultaneous removal of Cr(VI) and fluoride from binary synthetic solution. Identification of best suitable isotherm.

8. Estimation of kinetic models parameters for simultaneous removal of Cr(VI) and fluoride from binary synthetic solution. Identification of best suitable kinetic model.

9. Application of best activated carbon electrode for simultaneous removal of Cr(VI) and fluoride from real industrial wastewater by capacitive deionization.

1.2 Organization of thesis

The thesis has been organized in total six chapters as mention below for better understanding of the subject matter.

Chapter-I: Introduction

This chapter deals with importance of topic, health effect, treatment technologies available, problem identification and objective of the work.

Chapter-II: Literature review and theory

This chapter deals with the review of all possible literature from published work for the removal of Cr(VI) and fluoride, membrane separation technology such as nanofiltration and reverse osmosis, capacitive deionization technology, types of membrane, types of electrode, current status of capacitive deionization.

Chapter-III: Experimental set up and Instrumentation

This chapter deals with experimental set up, equipment's, instruments used for the present work.

Chapter -IV: Experimental program

This chapter provides the all details of experimental program and procedure for the present work.

Chapter -V: Result and discussion

This chapter deals with the results and discussion of the present work mentioned in brief bellow.

(A) Simultaneous removal of Cr(VI) and fluoride wastewater by membrane separation (NF/RO):

The objective of the current work is to examine the simultaneous rejection of Cr(VI) and fluoride from binary aqueous feed solutions by nanofiltration (with NF300, NF500, PN40 membranes) and RO membrane with different parameter such as pressure (2-10 bar for NF and 4-20 bar for RO), feed concentration (5-100 mg/L) and pH (2-10) of the feed. Study the characterization of NF300, NF500, PN40 and RO membranes by FTIR, SEM and AFM. Experimental results indicate that, Cr(VI) and fluoride percentage of removal was improved with increasing operating pressure and declined with increasing feed concentration. Estimation of membrane transport parameters by membrane transport model such as CFSK model and CFSD model. Identification of best suitable membrane transport model for simultaneous removal of Cr(VI) and fluoride from binary synthetic solution by NF and RO. Application and performance investigation of best NF and RO membrane for actual industrial wastewater.

(B) Simultaneous removal of Cr(VI) and fluoride wastewater by capacitive deionization:

The CDI process is recently developing and worldwide attracted techniques, eco-friendly, having less energy consumption and simplicity in regeneration. In the present study different activated carbon electrodes were prepared from commercial activated carbon (CAC), tea waste biomass activated carbon (TWBAC), rice husk activated carbon (RHAC), and Limonia acidissima (wood apple) shells activated carbon (LASAC). The activated carbon electrodes have been fabricated from activated carbons and successfully applied for investigation of performance in CDI for simultaneous electrosorptive treatment of Cr(VI) and fluoride binary water system. Estimation of single and multicomponent isotherm models and kinetic models parameters for simultaneous removal of Cr(VI) and fluoride from the binary synthetic solution were carried out. Identification of best suitable isotherm and kinetic model. Application and investigation of best suitable electrodes for removal of Cr(VI) and fluoride actual industrial wastewater treatment.

Chapter-VI: Summary of present work, conclusion and scope of future work

This chapter deal with the details of summary of present work, conclusion and scope of future work of the present study as described above.

LITERATURE REVIEW AND THEORY

2 Motivation

Industrial wastewater contaminates both the surface and ground water with heavy metals, toxic ions and organic compound. The various technologies are used for the removal or treatment of such industrial effluents. From the literature, information about characterization wastewater, chemistry of solution, treatment applied to water treatment have been reviewed. The main motivation of present work is to study the current research progress and formulate the objectives of work.

2.1 Overview about chromium and fluoride

2.1.1 Introduction and sources of chromium

The chromium occurs in various oxidation states (–2 to +6). Generally the most stable oxidation states of chromium are +3 and +6 existing in an environment (Cervantes et al., 2001; Nath et al., 2009). Chromium exists naturally as in trivalent form, whereas Cr(VI) is mostly coming in to the environment from industrial discharge (Mishra and Bharagava, 2016). Schematic presentation of different oxidation states of chromium is shown in Fig. 2.1.
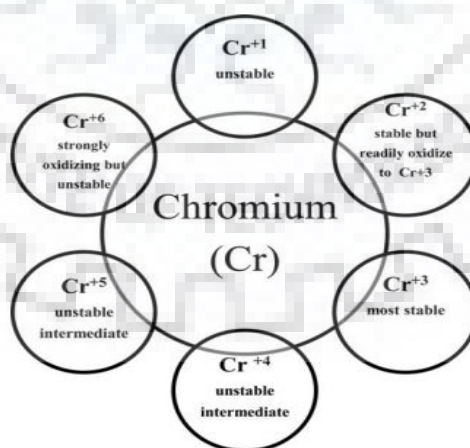
Fig. 2.1 The different oxidation states of chromium (Mishra and Bharagava, 2016).

Generally, hexavalent chromium is present in different ionic species forms such as hydro-chromate ($HCrO_4^-$), chromate (CrO_4^{2-}), and dichromate ($Cr_2O_7^{2-}$). The each ion proportion is

subject to solution pH. The chromate form is predominates at basic and neutral pH, whereas at lower pHs the concentration of hydro-chromate rises. The Cr(VI) is a strongly oxidizing agent and occur only in the oxygenated form, which is highly soluble in aqueous media. These different forms of chromium are pH-dependent as per the following equilibria (Nriagu and Nieboer, 1988; Losi and Frankenberger, 1994).

$$HCrO_4^- \longrightarrow CrO_4^{2-} + H^+ \qquad k= 10^{-5.9}$$

$$H_2CrO_4 \longrightarrow HCrO_4^- + H^+ \qquad k= 10^{+0.26}$$

$$Cr_2O_7^{2-} + H_2O \longrightarrow 2HCrO_4^- \quad k= 10^{-2.2}$$

$$HCr_2O_7^{2-} \longrightarrow Cr_2O_7^{2-} + H^+ \quad k= 10^{+0.85}$$
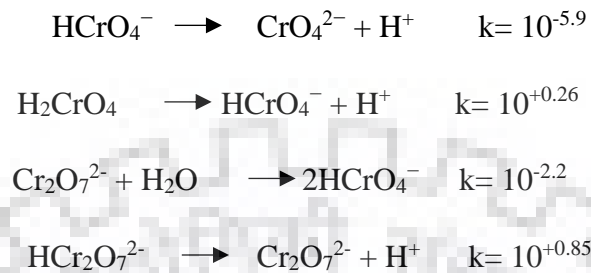
The hexavalent chromium is bound to oxygen with high oxidative capacity as dichromate and chromate. The dichromate species predominates at a very low pH, (United States of Environmental Protection Agency, 1985). Cr(VI) is highly carcinogenic, toxic, and tera-togenic (Chen and Gu, 2005). Chromium has been extensively used in various applications in industry, results in high chromium discharged issue into the environment (Jin et al., 2010). The most of the industries, which creating chromium contained polluted wastewater are electronic process, steel-works, leather tanning, electroplating, petroleum refining, mining, metal finishing, textile dyeing, and many more. The chromium level should be reduced before the discharged of wastewater is the current need (Dakiky et al., 2002; Chen and Gu, 2005; Rengaraj et al., 2003).

The product of stainless steel industries contains up to twenty weight percentage of chromium, slow oxidation of chromium containing alloys might be responsible for release of soluble Cr(III) (Zhitkovich, 2011). Moreover, there are other sources of chromium discharge like chrome plating industries (Edigaryan et al., 2002), cooling towers disposed blowdown water (where Cr(VI) is used as corrosion inhibitor) (Pellerin, and Booker, 2000), inappropriate chromite mineral processing (Stern et al., 1998). In the year 2010 china produced nearly 90 tons of discharge wastewater contaminated with Cr(VI) and most of the industrial Cr(VI) processing sources involve heavy metals and organic contamination aqueous solutions (Cao and Jin, 2015; Owlad et al., 2009).

Mainly anthropogenic activity is responsible for high amounts of Cr(VI) release in the environment. However, according to the literature (Gonzalez et al., 2005; Manning et al., 2015) natural geogenic activity also may release high levels of Cr(VI). Mediterranean (Greece, Italy

and Pacific (California (USA), Mexico), and different part of the world are the few populated areas are the example such conditions.

Hence, water pollution due to industrial activity is unescapable without an effective regulator or remediation. There is need of crucial regulatory measures, innovative research which could reduce the contaminated water and control the chromium discharge into water environments to maintain clean water sources.

2.1.2 Health effect of chromium

Cr(VI) is comparably highly toxic than other forms of chromium forms. Cr(VI) is rapid permeability through biological membranes it create teratogenic, carcinogenic, mutagenic effects in biological systems when it reacts with nucleic acids (McLean et al., 1990; Ishibashi et al.,1990; Horitsu et al., 1978). The Cr(VI) compounds have highly harmful effects on biochemical systems which leading to the skin and stomach allergies due to short-term exposure, or damage to liver, kidney and nerve tissues due to long-term exposure (Cavaco et al., 2007; Jin et al., 2011). Cr(VI) is also cause of many other health effects such as a runny nose, sneezing, nosebleeds, ulcers, itching, and holes in the nasal septum. Ingestion of very high doses of Cr(VI) can cause kidney and liver damage, nausea, stomach ulcers, convulsions, irritation of the gastrointestinal tract and death. The skin ulcers or allergic reactions through dermal exposures of chromium are also reported (Pellerin and Booker, 2000). The chromium toxicity related major health effects are shown in Table 2.1

Table 2.1 Chromium toxicity related major health effects (Mishra and Bharagava, 2016).

Sr. No.	Health effect Effects	Toxicity
1	Lung, nasal and sinus cancer are associated with the exposure through inhalation and ingestion	Carcinogenicity
2	Direct effect on blood and changes in bioelectric and mechanical activity of myocardium	Cardiovascular
3	Ulceration and perforation of nasal septum and irritation of upper airways	Respiratory
4	Skin lesions and rashes and allergic reactions	Dermatotoxicity
5	DNA damage, gene mutation, sister chromatid exchange, chromosomal aberration	Genotoxicity and mutagenicity
6	Gastric tract irritation	Gastrointestinal
7	Birth defects and decreased spermatogenesis and histopathological alterations	Reproductive and developmental

2.1.3 Regulations for Chromium

The WHO has mentioned the Cr(VI) toxic limits in waste water at the level of 0.005 ppm. Many countries have set the Cr(VI) maximum permissible limit regulations in natural or drinking water. In Poland, total chromium and Cr(VI) permissible concentration in drinking water is 0.05 ppm, 0.003 ppm (State Communicate of Standard of Poland Council of Ministers, 2000; Kozlowski and Walkowiak, 2002). The permissible limit for Cr(VI) discharge of industrial effluents in different water bodies, namely, Inland surface water, Public sewers and Marine coastal areas is 0.1, 2.0 and 1.0 mg/L, respectively as per CPCB (Central Pollution Control Board, India). (Jain and Kadivelu, 2009).

The chromium was also found in ground water due to dumping of wastewater into the unlined evaporating ponds (Lahontan Regional Water Quality Control Board, 2014). The Cr(VI) concentration was detected 580 ppb in the groundwater in Hinckley exceeded the maximum contaminant Level (MCL) of 100 ppb for total chromium currently set by the United States Environmental Protection Agency (EPA) (U.S. Environmental Protection Agency, 2008). It also exceeded the California maximum contaminant level of 50 ppb for all forms of chromium (California Department of Public Health, 2013). California first established a maximum contaminant level exactly for Cr(VI) in 2014, set at 10 ppb (California Department of Public Health, 2014) prior to that only total chromium standards applied.

2.1.4 Introduction and Sources of fluoride

Fluorine is the most electronegative and the most reactive among all chemical elements of the Periodic Table (Greenwood and Earnshaw, 1984; Gillespie et al., 1989). The fluorine cannot be found in elemental state due to its great reactivity, either it is found in the form of inorganic fluorides (including anion F^-) or organic fluoride compounds (e.g., freons). It has always exhibited -1 an oxidation number. In the worldwide environment, inorganic fluorides are abundant compared to organic fluoride compounds (Greenwood and Earnshaw, 1984; Gillespie et al., 1989). The fluoride mineral weathering is the main natural source of inorganic fluoride (Canadian Environmental Protection Act, 1994). The inorganic fluoride minerals in the earth's crust are cryolite (Na_3ALF_6), fluorite (CaF_2) and fluorapatite ($Ca_5(PO_4)_3F$). The fluoride second most natural source is Volcanoes, where gases are release along with the hydrogen fluoride (HF) into the atmosphere (Canadian Environmental Protection Act, 1994). Global release estimates propose annual emissions of inorganic fluorides between 60 and 6000 kilotonnes (CEPA, 1994, Camargo, J.A., 2003). Third major natural inorganic fluorides source is marine aerosols (Canadian Environmental Protection Act, 1994). It has been projected that marine

aerosols can globally contribute with about 20 kilo tonnes of inorganic fluorides each year (Canadian Environmental Protection Act, 1994, Camargo, J.A., 2003). Fluoride is widely distributed in the geological environment (Abe et al.2004) and generally released into the groundwater by the slow dissolution of fluorine-containing rocks (Banks et al.1995; Edmunds and Smedley 2005; Apambire et al. 1997; Reddy and Prasad 2003).

In addition, various industries are also responsible for fluoride pollution up to a great extent (Reardon and Wang 2000). The anthropogenic sources were being the most significant source of fluoride. The industries which discharge wastewater containing high fluoride concentrations include semiconductor manufacturing, fertilizers, glass-ceramic production, electroplating, coal fired power stations, beryllium extraction plants, brick and iron works, and aluminium smelters (Shen et al.2003; Farooqi 2008). The global occurrence of fluoride in the groundwater is presented in Table 2.2 (Shen and Schäfer, 2014).

Table 2.2 Global occurrences of fluoride (Shen and Schäfer, 2014).

Country	Water type and location	Fluoride concentration(mg/L)
India	Groundwater, North-West India	<19
	Groundwater, South India	<20
Germany	Wells in the Muenster region	<8.8
USA	Water supplies in Texas	<4.3
China	Groundwater , Jilin Province	<10
	Groundwater, Shanxi province	50% > 2
		<8.3
Turkey	The middle and eastern parts	<13.7
South Africa	Groundwater	<40
Argentina	Well water in the southeast regions	Median 3.8 max 182
Ethiopia	Well water of the Main Ethiopian Rift	Median 10 max 68
Tanzania	Groundwater, Shinyanga Region	<250
	Groundwater, Arusha Region	<330
Kenya	Groundwater in the Rift Valley	<180
	watercourse	<90

2.1.5 Health effects of fluoride

Fluoride is beneficial for the development of teeth and bones under consumption of concentration less than 1 mg/L. The higher intake of fluoride concentration can cause various health issues such as deformities in knee and hip bones and finally paralysis, making the person unable to walk or stand in a straight posture, crippling fluorosis (4.0–6.0 mg/L and above), Stiffened and brittle bones and joints (3.0–4.0 mg/L), Dental fluorosis (1.0–3.0 mg/L), Safe limit is (<1. 0 mg/L) (Meenakshi and Maheshwari 2006).

2.1.6 Regulations of fluoride

It is projected that globally 200 million plus people depend on drinking water contaminated with fluoride concentrations that exceed the WHO guideline of 1.5 mg/L (WHO 2004). The summary of fluoride concentrations in the groundwater occurs in worldwide places (Shen and Schäfer, 2014). The WHO recommended concentration of fluoride in drinking water is 0.5-1 mg/L (WHO, 2011). The fluoride effluent limit from the wastewater treatment facilities has been set to 4 mg/L by USEPA (Shen et al., 2003).

2.1.7 Technologies applied for chromium and fluoride removal

It is essential to remove these toxic ions from the streams of wastewater before releasing into the environment. Different techniques have been used over the recent years for individual removal of chromium and fluoride, such as adsorption (Selvi et al., 2001; Li et al. 2003), electrochemical precipitation (Kongsricharoern and Polprasert, 1995; Shen et al., 2003), liquid-liquid extraction (El-Hefny, 2009; Visser et al. 2001) and ion exchange (Atia, 2006; Onyango et al., 2004), membrane (Hu and Dickson, 2006; Kozlowski and Walkowiak, 2002). These techniques have some drawbacks such as inhibitive cost, incomplete removal and generation of toxic sludge in developing nations or elsewhere too. There is urgent need of developing better solutions for the treatment of chromium and fluoride from wastewater.

2.2 Introduction of membrane separation process

The membrane separation process is very well-known because of processes, simplicity, separation nature (do not require phase changes and high temperature), low energy consumption and less operating and capital costs (Chilekar 1993). Separation with membrane processes occur due to chemical species transport rates differences through the membrane interphase. Currently most of industries are concentrating their attention on wastes from different angles and looking for various possibilities to achieve the goal regarding environmental regulations.

The membrane process is attracted technology in the area of separation and purification process for both solid-liquid and gas-gas system. The membrane processes, demonstrate the significant role in the field of water purification and wastewater treatment. The growing need of waste minimization by recycling, recovery, and reuse to achieve very pure effluent, various membrane processes has been developed. The major difference between membrane separation and conventional processes (biological oxidation and chemical precipitation) is removal of impurities from water without the destruction of either of the components in membrane separation. The other major benefits are consumption of small space is required, continuous separation, easy up-grading of existing facilities, low energy, better effluent quality, avoidance of any chemical addition. Thus the membrane technique is the selected to achieve the pure water. The different type of membrane separation processes, namely, microfiltration, ultrafiltration, nanofiltration, and reverse osmosis are systematically discussed as follows.

Microfiltration (MF) works on sieving mechanism. The average pore size of MF is ranges from 0.1 to 10 μm and low pressures (0.1– 2 bar) requirement are adequate to attain high permeability's (> 50 L m^{-2} h^{-1} bar^{-1}). MF is commonly used as a pre-treatment stage for reverse osmosis or nanofiltration (Bungay et al., 1986).

Ultrafiltration (UF) also works on the similar sieving mechanism as MF to retain both particles and macromolecules. Characterizations of UF membranes are based on their molecular weight cutoff. Those components having molecular masses above the membrane molecular weight cut-off, they have easy removed, while those components with a less molecular mass below the cut-off are retained only partially. The UF membrane molecular weight cut-off typically comes between range of 1,000 and 100,000 Da, which relates with pore sizes in the range of a few nanometers to 0.1 μm. Permeability's between 10 and 50 L m^{-2} h^{-1} bar^{-1} are achieved with pressures between 1 and 5 bar (Bungay et al., 1986).

The reverse osmosis (RO) membrane is used to retain small ions and organic molecules from a solution. In general, dense membrane are used in this process which have a high hydrodynamic resistance, low permeability's ($0.05 - 1.4$ L m^{-2} h^{-1}bar^{-1}) operated with high pressure gradients ($10 - 100$ bar). Removal or separation occurs due to sorption and diffusion through the membrane (Bungay et al., 1986).

Nanofiltration (NF) is comes in the category between UF and RO. These membranes originated in the 1970s and the 1980s as modified RO membranes having high water fluxes. NF membranes operate at lower pressures (5–20 bars) compared to RO, which leads to significant energy savings. Additionally, NF has a high permeability ($1.5 - 15$ L m^{-2} h^{-1} bar^{-1}) with a high

retention of dissolved chemical compound with a molecular mass above 200 Da. The NF molecular weight cut-off is ranging between 150 and 1,000 Da. The membrane having charge and because charge interactions between ions and membrane, multivalent ions are also well rejected. A summary of membrane separation processes is systematically shown in table 2.3.

2.2.1 Information about membranes

The membrane is nothing but the barrier between two phases, which restrict various solute transport in a selective way. A membrane have different types it can be symmetric or asymmetric in structure, homogeneous or heterogeneous, solid or liquid can carry positive or negative charges or both. The convection or diffusion of individual molecules induced by an electric field, concentration, pressure or temperature gradient, effect on the transport performance membrane. The thickness of the membrane may generally differ between less than 100 nm to more than a centimeter (Ravanchia et al., 2009). A Summary of different type of membranes is provided in the Table 2.4.

2.2.2 Types of membranes

The appropriate selection of a membrane can be identified by the exact objective of application such as removal of dissolved solids or particulate, rejection of hardness or generation of ultra-pure water, specific chemicals/gases rejection etc. The membrane commonly used in the various membrane separation process are summaries in Table 2.4.

Table 2.3 Different membrane processes general information (Ravanchia et al. 2009).

Sr. No	Process type	Separation potential for	Permeating component	Driving force
1.	Microfiltration	Emulsions, Suspensions	Solvent	Hydrostatic pressure (0.1-500 kPa)
2.	Ultrafiltration	Emulsions, Macromolecular solutions,	Solvent	Hydrostatic pressure (100-1000kPa)
3.	Nanofiltration	Macromolecules, organics, Di- and multi-valent ions	Solvent	Hydrostatic pressure (300-1400kPa)
4.	Reverse osmosis	Organic solutions, Aqueous low molecular mass solutions	Solvent	Hydrostatic pressure (1000-10000kPa)
5.	Osmosis	Aqueous solution	Solvent	Concentration gradient
6.	Dialysis	Aqueous solution	Solute(ions)	Concentration gradient
7.	Gas separation	Gas mixture	Preferably permeating component	Hydrostatic pressure (100-10000kPa)
8.	Liquid membrane	Aq. low molecular mass solution	Solute(ions)	Concentration gradient
9.	Electrodialysis	Aqueous solution	Solute(ions)	Electrical potential gradient
10.	Membrane distillation	Ions	Solute(ions)	Temperature
11.	Pervaporation	Organic mixtures	Preferably permeating component	activity

Table 2.4 Summery for different membranes (Ravanchia et al. 2009).

Process type	Membrane type	Membrane material	Pore Size	Thickness
Microfiltration	Asymmetric porous	Polymeric, ceramic	≈0.05-10 μm	≈10-150μm
Ultrafiltration	Asymmetric porous	Polymeric, ceramic	≈1-100 nm	≈150μm
Nanofiltration	composite	Polyamide	≈2 nm	Sub layer ≈ 150μm Top layer <1μm
Reverse osmosis	Asymmetric or composite	Cellulose triacetate, aromatic polyamide	<2 nm	Sub layer ≈ 150μm Top layer <1μm
Gas separation	Asymmetric or composite membrane with an elastomeric or glassy polymeric top layer	Elastomeric and glassy polymer	Non-porous (or porous<1μm)	≈0.1 to few μm (top layer)
Pervaporation	Asymmetric or composite membrane with an elastomeric or glassy polymeric top layer	Elastomeric and glassy polymer	Non-porous	≈0.1 to few μm (top layer)
Dialysis	Ion exchange membrane	Anion and cation exchange membrane	-	(100-500μm)

2.2.2.1 Microporous membranes

Microporous membrane made of solid matrix with pores of diameter varying from below 5 nm to above 50µm. The membrane acts nearly similar a fiber filter and work on sieving mechanism which depend on the membrane pore diameter and particle size. Generally membrane can be prepared from various types of materials such as different polymer, ceramics, metal or metal oxides or graphite. The phase inversion process is used for membrane preparation, in that a particular polymer is dissolved in a suitable solvent and cast as a film with thickness 20 to 200 µm (Bungay et al. 1986).

2.2.2.2 Homogeneous membranes

A homogeneous membrane made with dense film through which a mixture of chemical species is transported under application of the driving force such as pressure, electrical potential gradient or concentration gradient. The homogeneous membrane must be thin as possible for the reason that the mass transport in these membranes is due to diffusion, thus getting low permeability (Bungay et al. 1986).

2.2.2.3 Asymmetric membranes

An asymmetric membrane consists of very thin (0.1 to 1µm) polymer film on a sub layer which is very porous. The thin layer act as active layer and it is mainly responsible for separation. Film thickness can effect on the separation characteristic pore size of membrane and membrane mass transport rate. That type of membranes is commonly applied in the membrane technique which driven pressure, namely as nanofiltration, ultrafiltration, reverse osmosis where their properties of mechanical stability and high mass transport rates can be utilized best. The casting of asymmetric membrane is carried out in two ways phase inversion method, and extremely thin polymer film depositing on a Microporous structure (Bungay et al. 1986).

2.2.2.4 Electrically charged membranes

The ion exchange membranes consisting of highly swollen gels with fixed negative or positive charges. A positively fix charge membrane is stated as anion-exchange membrane, whereas a negatively charges of membrane is known as cation exchange membrane. The performance of this membrane is mostly determined by its selectivity to ions of opposite charge, its electrical resistance and its mechanical and chemical stability. Cation exchange membranes are negatively charged they reject anions and allow cations only. Similarly anion exchange membranes are positively charged, repelled cations and allows anions only. Such type of

membranes are mostly used in the Electrodialysis. These membranes are generally prepared by polymerization of film-forming ionic monomers (Bungay et al. 1986; Xu 2005).

2.2.2.5 Liquid membranes

A liquid membrane makes use of a carrier for selectivity transport components such as metal ions at comparatively high rates across the membrane interface. It has been used in two different configurations, the first is liquid membrane composed of thin film stabilized by surfactants in an emulsion-type mixture. The second is referred as support liquid membrane (Bungay et al. 1986).

2.2.2.6 Composite membranes

In this type of membrane the actual selective membrane barrier is deposited onto the surface of a suitable fine porous substrate. The performance of this membrane is not only determined by its selective surface film. Microporous support structure, or rather the pore size, the pore distribution and the overall porosity is also taken into consideration. The most important and attractive aspect of this structure responsible for reducing costs due to the use of high performance polymer in less amount for its development. These membranes are generally prepared by interfacial polymerization techniques (Bungay et al. 1986; Hamad et al. 2005).

2.2.3.0 Membrane modules

The membrane module are classified in four different type, which is applied in the different membrane separation process.

2.2.3.1 Plate and frame module

The plate and frame module is slightly like to be plate and frame filter press with flat sheet membrane in series. This module sheets are moderately close together to decrease concentration polarization. This can be easily dismantled for cleaning purpose and this is the main benefits of such module. Mostly this module is used where the major fouling problem raise, such as applied in the food industry. These modules are applied for solvent dehydration and it can survive in corrosive environments and high temperatures, but one disadvantage associated with this module is high cost than other modules (Wankat 1990).

2.2.3.2 Spiral wound module

These type of design is best for attaining huge area per unit volume. Mostly such module is applied in ultrafiltration, reverse osmosis and gas separation. Generally the solvent dehydration purpose, such commercial modules has been used. This modules main components are

membrane, feed and permeate spacers, shell and permeate collection tube. These modules performance for a certain use is examined by the module dimensions, the membrane and the spacers. Generally net-like materials, plastic, are used as spacers and it can generate channels for flow between the layers of membrane and to decrease liquid film resistances in uses which are mass transfer limited. Thin channels can reduce or control the concentration polarization and covering the membrane around plastic netting which made turbulence. Such types of modules are cannot applicable for very dirty or fouling systems because it's difficult to clean. (Hickey & Goading 1994).

2.2.3.3 Tubular module

The cylindrical geometries are generally used and both inside and outside of the porous support tube covered (coated) with membrane. This module has less area per unit volume. These type of module has benefits in cleaning they are cleaned mechanically with the application of the sponge ball through the tubes (Wankat 1990).

2.2.3.4 Hollow fiber module

This module consists of a very huge number of fibers. The module area per unit volume is very high and such module is applicable with great practical importance in the various processes. Applications of such module are in the field of water treatment with liquid filtration membranes, adsorption with use of gas–liquid diffusion membranes, extraction with liquid–liquid contact modules. The large number of fibers can be assembled inside the module is advantages of this module. While the drawback is that particulate solids can permanently block the tiny fibers (Yantasee et al. 2009).

2.3 Theory

2.3.1 Principle of NF

The principle of NF technology is based as the separation of soluble ions from water through a semi-permeable material under the application of the pressure. The cross flow filtration is defined as which is membrane different from a dead end filter and operates under a different hydraulic profile. In crossflow filtration direction of fluid flow parallel to the surface of the membrane and perpendicular to the filtration direction. The transportation of water permeated through the membrane is due to application of transmembrane pressure and particles of permeable are transported through the membrane due to a concentration gradient. The both processes, namely, diffusion processes and convective flows are required in this process. The basic principle is schematically presented in Fig. 2.2.
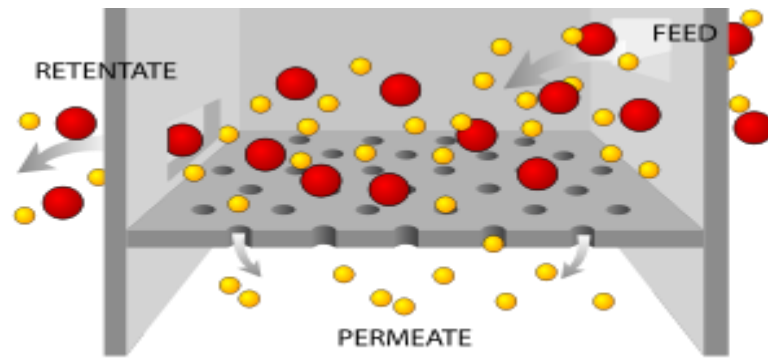
Fig. 2.2 Cross flow filtration technique.

The filtration process basic equations are given bellow:

Water transport flux: $J_v = A(\Delta P - \Delta \pi)$ (2.1)

Solute transport: $J_s = B(C_f - C_p)$ (2.2)

True rejection: $R_o = 1 - \dfrac{C_p}{C_f}$ (2.3)

where, P, π, A, B, C_p and C_f are the transmembrane pressure [bar], osmotic pressure [bar], the permeability of water [L/(m^2 h bar)], permeability of solute [L/(m^2 h)], permeate concentration [mg/L], and feed concentration [mg/L] respectively.

The NF membrane pore size is in the range of 1nm and molecular cut-offs is range between 300 and 1000 g/mol, NF can be operated in the range between reverse osmosis and ultrafiltration. (Chitry et al., 1999).

In NF process, generally separation mechanism is based on charge and sieve effects. Sieving mechanism is accountable for uncharged solutes rejection with NF.

The amount of solute permeation by the membrane is examine with mainly by the size of solute species. However, electrostatic attraction among the solute and charge on the surface of membrane surface influenced charged solute rejection by NF, which can be studied with the Donnan exclusion phenomena (Ku et al., 2005).

Additionally NF membrane separation performance can be enhanced with the application of selective complexation step, in that complexing agent formed the complex with solute species and its size and mass has increased, so it is difficult to pass through membrane hence performance will be increased (Fig. 2.3) (Chitry et al., 1999).
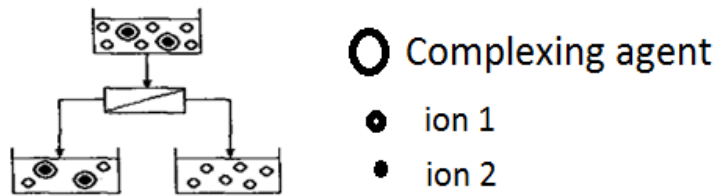
Fig. 2.3 Principle of NF with a complexation step.

2.3.2 Mass Transfer in NF
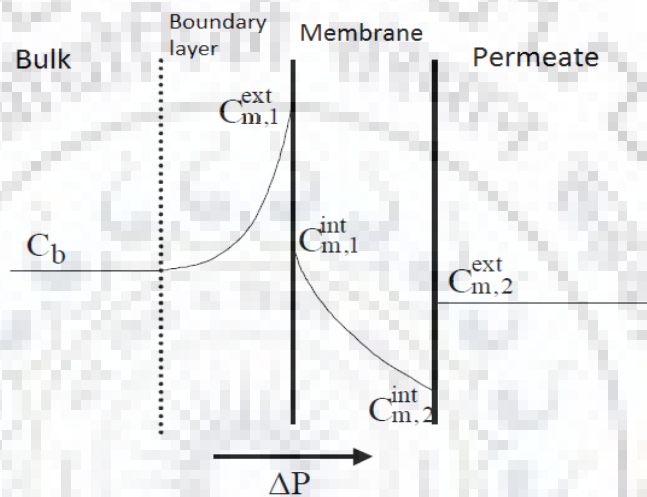
Fig. 2.4 Mass transfer in NF process.

The solvent is passed through semi-permeable membrane due to enforcement of external pressure ΔP on the liquid adjacent to the membrane surface. Mass transfer profile in NF process is shown in Fig. 2.4. When ΔP is applied on a liquid which is closer to a semi-permeable membrane, solvent will passing through the membrane. The common terms solvent flux (J_v) and the rejection (R) are used in the explanation of membrane separation processes.

The solvent flux is given by:

$$J_v = \frac{\Delta P}{\mu . R_m} \tag{2.4}$$

ΔP is effective transmembrane pressure, J_v is solvent flux, R_m is the intrinsic resistance of the membrane towards solvent flow and μ is permeate viscosity.

When membrane rejects the solute then partial permeation will take place and non-permeated solute gathers at boundary layer which leads to develop concentration profile and it is called concentration polarization (Mulder 1991; Cheryan 1998). At the membrane-solution interface

21

solute distributes and transported through the membrane due to convection and diffusion. At the permeate side, will be reached with final concentration of solute in the permeate, $C_{m,2}{}^{ext}$. A neutral solute dissolved in the solvent at a concentration level C_b will also flow towards the membrane.

$$R = 1 - \frac{C_{m2}^{ext}}{C_b} \tag{2.5}$$

In NF membrane interface (at the boundary layer) a non-charged solute distribution is considered to be estimated by a steric exclusion mechanism. The Steric exclusion is not only characteristic for NF but applies to microfiltration and ultrafiltration too. Due to its size a solute only has access to a fraction of the total surface area of a pore. This causes a geometrical exclusion of the solute from the membrane. A separation between solutes will only be accomplished when the solutes have a difference in size.

Two additional separation mechanisms for charged solutes are discussed as follow

1) Donnan exclusion: opposite charge solute i.e. counter-ions are attracted towards the membrane, whereas similar charge solute i.e. co-ions are repelled from the membrane surface because of the slightly charged behaviors of the membrane. Counter and co-ions separation occurs at surface of membrane initiating an additional separation.

2) Dielectric exclusion: This type of phenomena usually does not play a role in the case of microfiltration and ultrafiltration however major importance in the case electrodialysis. (Bontha 1994). The water molecules will show the polarization in the pore because of the membrane charge and the water dipole momentum. This polarization leads to a reduction of the dielectric constant inside the pore, thus creation it less promising for an entering of charged solute. But, even in a condition that the dielectric constant inside the pore is equivalent to the one of water, a variation in the electrostatic free energy of the ion happens when the ion is transferred from the bulk into the pore (Glueckauf 1976).This also effects in exclusion. The comparative significance of the two separation mechanisms in NF is still theme of discussion in the scientific community (Yaroshchuk 2000, 2001).

2.3.3 Performance parameter

2.3.3.1 PWP (pure water permeability) of a membrane

It is stated as the amount of water (volume) that permits through a membrane per unit time, per unit area and per unit applied pressure. It has a unit (L/m^2 h bar) in SI. Generally the PWP of the membrane is finding out to investigate the membrane characteristic. The plot of solvent

flux (J_v) is found as a function of pressure (bar), the slope of that is PWP coefficient of membrane (L_p). The plot provides a straight line as per Darcy law:

$$J_v = L_p . \Delta P \tag{2.6}$$

Another important feature while representing a membrane is PWP coefficient of membrane (L_p) which is the slope of the plot of the flux obtained versus applied pressure which is determined experimentally.

2.3.3.2 Molecular weight cut off (MWCO) of Membrane

It is a vital aspect used to characterize a membrane. It denotes to the lowest molecular weight of solute (in Daltons) in which 90% of the solute is rejected by the membrane. Generally NF membrane has MWCO in the range between 300 to 1000 Da.

2.3.3.3 Percent rejection

The rejection of solute i can be calculated according to Eq. (2.7) where C_{ip} is the concentration of solute in permeates and C_{if} is the concentration in feed.

$$R_o (\%) = 1 - \frac{C_{ip}}{C_{if}} \times 100 \tag{2.7}$$

2.3.4 Various factors affecting on NF process

The several operating parameters would consider when designing a NF process. The most important operating parameters are similar to those for most cross flow filtration processes which are affecting the performance of membranes.

2.3.4.1 Pressure

The pressure difference is the driving force accountable for a NF process. The effective driving pressure is stated the supplied hydraulic pressure less than the osmotic pressure applied on the membrane by the solutes. The effective separation performance in NF process generally at net pressures of 10 bar (150 psi) or high.

2.3.4.2 Temperature

Generally, as the NF membrane increases flux due to viscosity reduction on increasing the process temperature. The NF membrane rejection performance is not significantly dependent on the process temperature.

2.3.4.3 Cross-flow velocity

In NF membrane process when cross flow velocity increases, then the average flux also increases reason of fouling layer removed from the membrane surface. However, the maximum cross flow velocity depends on membrane strength and element construction and system hardware. There are chances of membranes and module failure if NF membrane set up is operated at too high a cross flow velocity.

2.3.4.4 pH

The pH have a significant role in NF membrane performance. At neutral pH or higher, the NF membrane having charged sites on its surface (i.e. sulfonic group and carboxylic group) are negatively charged, but lose their charge at acidic pH. It is well known that most NF and RO membranes, lower rejection performance observed at low pH. It should be noted, the pH dependency of a membrane should be determined when manufacturing different membrane. In addition to the effect of pH on the membrane itself, pH can be accountable for variations nature of feed solution, which might be leads for change the membrane performance. Two examples are a solubility change of ions at different pH regimes, which leads different rejection rate; and change in the dissociation state of ions at different pH ranges.

2.3.4.5 Salinity

The effective charged pore radius will increas as the ionic strength of the surrounding liquid increases. Thus, the monovalent ions rejection will decline as their concentration in the feed solution is enhanced. The divalent ions rejection will be affected to a lower extent.

2.3.5 Transport models for NF membranes

Models that sufficiently terms the separation membranes behavior. NF is a complex process lying between UF and RO, thus models from both these areas and their combinations can be used to define NF performance.

2.3.5.1 Film theory

Concentration of solute increases near the membrane surface due to rejection of solute by the membrane. Thus the concentration build-up at the membrane–liquid interface is called as concentration polarization. Material balance for the solute in a differential element as per film theory and relevant boundary conditions, will gives (Murthy and Gupta, 1997).

$$\left(\frac{C_{A2}-C_{A3}}{C_{A1}-C_{A3}}\right) = exp\left(\frac{J_v}{k}\right) \qquad (2.8)$$

$$R_0 = \frac{(C_{A1} - C_{A3})}{C_{A1}} \qquad (2.9)$$

$$R = \frac{(C_{A2} - C_{A3})}{C_{A2}} \qquad (2.10)$$

2.3.5.2 CFSK model

The CFSK model was the combined equation of film theory and Spiegler-Kedem model (Spiegler and Kedem, 1966). The CFSK model used for evaluation of mass transfer coefficient and membrane transport parameters simultaneously for reverse osmosis system, which can also be used for nanofiltration (Murthy and Chaudhari, 2008; Murthy and Gupta, 1998, Vaidya et al., 2001).

The film theory equation can be arranged and write as

$$\left[\frac{R_0}{1-R_0}\right] = \left[\frac{R}{1-R}\right]\left[exp\left(\frac{-J_v}{k}\right)\right] \qquad (2.11)$$

The equations of Spiegler-Kedem model are as follows (Spiegler and Kedem, 1966; Murthy and Chaudhari, 2008; Murthy and Gupta, 1998, Vaidya et al., 2001).

$$J_v = L_p(\Delta p - \sigma \Delta \pi) \qquad (2.12)$$

$$R = \sigma[1 - exp(-J_v\, a_2)]\, /[1 - \sigma(exp(-J_v a_2))] \qquad (2.13)$$

$$a_2 = \frac{(1-\sigma)}{P_m} \qquad (2.14)$$

Eq. (2.9) can be rearrange in following form

$$\left[\frac{R}{1-R}\right] = a_1[1 - exp(-J_v\, a_2)] \qquad (2.15)$$

$$a_1 = \frac{\sigma}{1-\sigma} \qquad (2.16)$$

Now substituting Eq.(2.15) in to Eq.(2.11),

$$\left[\frac{R_0}{1-R_0}\right] = a_1[1 - exp(-J_v\, a_2)]\left[exp\left(\frac{-J_v}{k}\right)\right] \qquad (2.17)$$

Eq. (2.17) is the equation for CFSK model. This equation is used for simultaneous estimation of the k , σ and P_m by providing the data of Ro and Jv with the help of a nonlinear parameter estimation method at different pressures by maintaining constant flowrate and constant concentration of feed.

2.3.5.3 CFSD model

Solution-diffusion model equations (Wijmans, and Baker, 1995) are as mention bellow

$$J_v = A(\Delta P - \Delta \pi) \tag{2.18}$$

$$J_A = \left(\frac{D_{AM}K}{\delta}\right)(C_{A2} - C_{A3}) \tag{2.19}$$

Eqs. (2.18) and (2.19) may be combined with Eq. (2.10), as illustrated by Pusch (Pusch, 1997), to provide

$$\frac{1}{R} = 1 + \left(\frac{D_{AM}K}{\delta}\right)\left(\frac{1}{J_v}\right) \tag{2.20}$$

Eq. (2.20) predicts that R approaches 1.0 for immeasurable permeate flux. This is not accurate for many solutes, which do not approach perfect rejections at high permeate flux rates (Mason and Lonsdale, 1990). Eq. (2.20) can be reshuffled to

$$\frac{R}{1-R} = \frac{J_v}{D_{AM}K/\delta} \tag{2.21}$$

Eq. (2.21) can be put into Eq. (2.11) to give

$$\frac{R_0}{1-R_0} = \left[\frac{J_v}{D_{AM}K/\delta}\right]\left[exp\left(-\frac{J_v}{k}\right)\right] \tag{2.22}$$

The Eq. (2.22) is working equation of the CFSD model. $D_{AM}K/\delta$ and k can be evaluated numerically by providing Ro vs. Jv data, taken at constant feed concentration and different pressures.

2.4 Review of Literature

2.4.1 General

The presence of toxic metals ions and harmful organic pollutants in the water environment has been known as a vital problem of environmental concern and public health. Thus, trace contaminant removal is an issue facing various industries, the study focuses mainly on CrVI) and fluoride removal from wastewater. The role of NF and RO membrane filtration process in water and wastewater treatment, and a review of current studies are presented in this section.

2.4.2 NF materials

Most NF membranes are thin-film composites of organic (polymeric) or inorganic (ceramic) nature. A membrane top layer is responsible for the separation while the support layer provides

mechanical strength. There is a large diversity of polymeric NF membranes, but mainly cellulose esters, aromatic polyamides and polyethersulfones are used (Rautenbach and Gröschl 1990; Raman et al. 1994 and Peeters et al., 1998). Cellulose esters like cellulose acetate are very suitable for desalination because of their high permeability for water in combination with a very low solubility in salts (Laine et al., 1993). However, the chemical and thermal stability of these membranes is quite poor and therefore cleaning of the membrane modules is difficult. Typical operating conditions are in the pH range of 4 to 6 and around 30 °C. The chemical stability of polyamides and polyethersulfones membranes is much better than for cellulose acetate (e.g., pH stability ≈3-10), but they are degraded by oxidizers and the feed water must therefore be dechlorinated. The polyamides and polyethersulfones materials have a high selectivity, but their water flux is generally lower than for the cellulose acetate membranes.

Inorganic NF membranes are (mixed) oxides, generally of aluminum, zirconium or titanium. Due to their material properties they all have good mechanical strength and feature very good thermal and chemical stability. Because of the latter, they can withstand high temperature cleaning treatments like sterilization. The pH stability of alumina membranes is similar to that of polyamides and polyethersulfones.

Typically the fluxes for inorganic membranes are higher than for polymeric membranes because they have larger pores and the retention of ceramic membranes is lower, especially for more concentrated (> 1 mol/m^3) electrolyte solutions.

2.4.3 NF and RO in water and wastewater treatment

NF is a pressure driven process which in ranges between ultrafiltration (UF) and reverse osmosis (RO) (Eriksson 1998). The pore size of the NF membrane is normally near to 1 nanometer. NF membranes are characteristically evaluated by MWCO rather than pore size. RO membrane has a lower flux at under application of pressure and it has applied for desalination or removal of total dissolved solid, whereas UF can deliver higher flux and it could remove macromolecules (humic acid, fulvic acid, etc) at lower operating pressure. The combination of NF process with features of RO and UF were used for effective rejection of macromolecules and multivalent ions under application of moderate operating pressures (Mallevialle et al. 1996). The NF process is typically operated with medium pressures (range 10-50 bar), have considerable higher water fluxes than RO membranes, decreasing the operating cost significantly. NF can be useful for separation between ions with different valences and for separation of low- and high-molecular weight components. NF rejects charged, uncharged, dissolved material according to the size and shape of the molecule in

question (Baker 2004). The NF membranes are generally characterized by MWCO rather than by membrane pore size (Wagner 2001). The MWCO of NF membranes is commonly provided by the manufacturers and typically in the range 200-1000 Dalton. The molecular weight is not a direct measure of the size and shape of the permeating molecule, and hence, it provides only a rough approximation of the membrane's ability to remove dissolved uncharged components.

NF has recently found its position in water and wastewater industries (Mallevialle et al. 1996). It is a well-established method and has found in industrial applications (Lipnizki et al. 1996) in various fields such as food (Butchermaker 2004), paper (Geraldes and Pinho 1995), textile (Rosa and Pinho 1995), (bio-) pharmaceutical (Burnouf and Radosevich 2003; Capelle et al. 2002), and chemical industry (Bhore et al. 1999). Thus, NF plays a major role as an advanced treatment of water and wastewater.

2.4.4 Literature review for commercial membrane (NF/RO) application various wastewater treatment

Van der Bruggen et al., (2001) reported work on the pesticides removal (namely diuron, atrazine, isoproturon and simazine) by UTC-20, UTC-60, NF70, NF45 membranes. The suitable results were found for pesticide rejections; also effective hardness removal was found, whereas a small amount of nitrate is removed achieved with membranes, except with NF70, where a 76% nitrate was removal. The economic analysis study also reported for NF. Which includes analysis of investment and operating costs. The final price was found realistic for treatment of ground water, which presentation that NF is a better option for treatment of ground water.

Vergili, (2013) investigate the NF membrane performance for the removal of three Pharmaceutical active compounds (PhACs) namely diclofenac (DIC), carbamazepine (CBZ), and ibuprofen (IBU) with cross-flow filtration equipment. The result indicates that low to moderate rejection of PhACs because of the low molecular size also presence of divalent ions in the raw water. The experimental results indicate that the overall rejection was nearly 31-39% and 55-61% for neutral (CBZ) and ionic (DIC and IBU) PhACs, respectively. This study indicates that FM NP010 membrane mostly promising for surface water treatment.

Szöke et al., (2005) reported that removal of complex of cobalt(III) EDTA by NF membrane from a drain waste water model solution, which contains mainly sodium borate at an alkaline pH. The separation the cobalt complex from the borate solution was carried with suitable NF membrane. The experiments of the NF were carried out at a 25°C constant temperature and 1-10 bar pressure. The effect of pH on rejection of cobalt complex and the borate ion as well as

the permeate flux of the membrane. The result indicates the rejection of the borate and the complex ion was enhanced at alkaline pH (at pH 8, R = 7%; at pH 11.5, R = 59% for borate; at pH 8, R = 73%; at pH 11.5, R = 96% for the cobalt complex). Thus, it was found that NF could be an appropriate separation method for the separation of the Co(III) EDTA complex from waste streams of nuclear power plant.

Radjenović et al., (2008) studied on the pharmaceuticals removal by NF and RO full-scale drinking water treatment plant with groundwater. Pharmaceutical residues identified in feed (groundwater). The maximum concentrations were detected for hydrochlorothiazide (58.6–2548 ng L^{-1}), propyphenazone (51.5–295.8 ng L^{-1}), diclofenac (60.2–219.4 ng L^{-1}), carbamazepine (8.7–166.5 ng L^{-1}) and ketoprofen (<MQL–314 ng L^{-1}) in groundwater. The result shows that NF and RO performance was found excellent with high percentages of rejection for nearly all of the pharmaceuticals (>85%).

Bellona and Drewes, (2005) studied the performance NF membranes for rejection of selected organic acids with the contribution of electrostatic interactions. Commercial NF membrane surface charge was studied with zeta potential measurements at different value of pH and feed chemistries of water. The results show that the negatively charged organic acids rejection performance was greater compared to expect based on steric exclusion and was mainly driven by the membrane surface charge. As on increase pH of the feed, which caused an increased negative surface charge which enhanced the rejection due to electrostatic repulsion. The removal of an organic acid was also depended on pH. The Result also indicates that organic solutes (with negatively charged) rejection was declined only when solute molecular weight is lower than MWCO of membranes.

Sato et al., (2002) reported that a comparative performance study of rapid sand filtration inter-chlorination system and NF to decrease the arsenic health risk of drinking water. The result outcomes show that rapid sand filtration with inter-chlorination was not found effective for arsenic removal. On the other hand, NF membrane (NaCl rejection 99.6%) was effective at relatively low-applied pressure and it could remove over 95% of As(V) and also it removes 75% of As(III) without any chemical additives.

Murthy and Chaudhari (2009) reported that, application of NF removal nickel from synthetic wastewater of nickel electroless plating industry. That industrial wastewater contains nickel, zinc, sodium and magnesium. The NF300 membrane was tested for the study of rejection performance of nickel ion in the mix ($NiSO_4$, Na_2SO_4, $MgCl_2$ and $CaCl_2$) synthetic wastewater. The results show that nickel ion removal by NF300 is 97.96% and 96.87% for 5 and 10 ppm

feed concentration, respectively. The CFSK model was used for characterization of membrane. The estimated parameters were used for the prediction of membrane performance. Predicted values were found good agreement with the experimental data.

Yoon et al., (2009) reported a study the performance of commercial membranes, including one RO membrane (RO, LFC-1), two NF membrane (NF, ESNA, and MX07), and one UF membrane (UF and GM) membranes with cross-flow flat-sheet filtration system for removal of chromate, arsenate, and perchlorate. The feed solution of arsenate, perchlorate and chromate, (approximately 100 µg L^{-1} for each anion) was prepared in the presence of other salts with model and natural both waters at different varying parameters pH and solution conductivities. The result shows that removal of target ions enhanced with increasing pH of the solution because of negative membrane charge increasing. The order of rejection performance for Cr(VI), As(V), and ClO_4^- at all pH conditions are LFC-1 (>90%) > MX07 (25–95%) ESNA $\approx$ (30–90%) > GM (3–47%). In contrast, as increasing solution conductivity, then target ions rejection by membrane was decreased due to negative membrane charge decreased.

Murthy and Gaikwad, (2013) reported that study on commercial NF membrane (NF300) application for praseodymium rejection from aqueous solutions with different operating conditions. All the feed and permeate sample were analyzed) to find concentration of praseodymium [Pr(III)] with inductively coupled plasma atomic emission spectrometry (ICP-AES). The outcome of the study indicate that rejection of Pr(III) ions enhanced with increasing applied pressure (2–10 bar) and cross flowrate (4–16 L min^{-1}). In contrast, as increase in feed concentration, then Pr(III) rejection by NF300 membrane. The highest Pr(III) rejection was found to be 89.07 and 84.20% for an initial feed concentration of 10 and 100 mg L^{-1} $PrCl_3$ respectively. It was also found that in complexation step Pr(III) rejection was increases to 99.28 and 99.30% by using ethylene EDTA and DTPA respectively, as the chelating agent has generally influenced by pH (2 –10).

Murthy and Choudhary (2011) reported a study on cerium ions separation from a synthetic feed by nanofiltration with NF300 commercial membrane to achieve cerium effective removal at different operating parameters. The ICP-AES was used to analyze the feed and permeates samples. At constant cross flowrate the results indicated that the cerium ions rejection enhanced with an increase in applied pressure and decline with increase in feed concentrations. The study also indicates that application of complexation with EDTA as a chelating agent, which improved the cerium rejection performance. Where higher cerium removal was achieved in the basic medium compared to acidic medium. The highest Ce(III) separation was found to be

94.37% (for 10 mg L^{-1} feed) and 90.03% (for 80 mg L^{-1} feed). It was also found that Ce rejection by NF was 99% with EDTA complexation.

Van der Bruggen et al., (2004) reported studies on separation of monovalent and multivalent ions by ED and NF. In this study five synthetic single salt solutions (NaCl, Na$_2$SO$_4$, MgCl$_2$, MgSO$_4$ and NaNO$_3$) were used. In the ED, Two combinations of anionic and cationic exchange membranes (ACS/CMS Tokuyama membranes and AMV/CMV Selemion membranes) were investigated and two NF membrane namely, NTR 7450 and UTC- 60 were used. The experimental result shows that good performance in separation of monovalent and divalent anions, the ED membranes performance was worse. The UTC-60 membrane was found the best for monovalent and divalent cations separation due to size exclusion effects for the larger divalent ion. The ACS/CMS membranes had a similar separation efficiency (ca. 60%); the NTR 7540 membrane and AMV/CMV ED membranes presented only a small separation.

Nguyen et al., (2013) reported that the application of two commercial NF membranes (Nitto Denko ESNA and GE Osmonics DK) for rejection study for the three model divalent cations with very similar atomic weights (Co, 58.9 Da, Ni, 58.7 Da; and Cu, 63.5 Da;) was studied in a cross flow module at range pH 3 to 5. The rejection performance was found in the order of Ni^{2+} > Cu^{2+} > Co^{2+} with the two selected membranes. The removal efficiency was improved with decreasing pH for all three metals. Moreover, DK membrane removal performance was better compared to the ESNA membrane to due to the positive charge of the DK membrane at low pH.

Murthy and Gupta, (1998) investigated the feasibility of polyamide commercial thin film composite RO membrane and its application for treatment of phenol-water binary system. The CFSD model and CFSK model were used for analyzing of experiment separation data. The study outcome indicates that the CFSK model is more accurate for the phenol-water system.

Murthy and Choudhary, (2012) reported the removal of cerium and neodymium by NF membrane process from their individual feed. The feed and permeates were tested with ICP-AES. Irreversible thermodynamics Spiegler-Kedem model, in combination with the film theory, was used to evaluation of the membrane transport parameters, viz., solute permeability, reflection coefficient of membrane and mass transfer coefficient to study their dependence on feed solute concentration. The theoretical results obtained on the application of this model are in good agreement with the experimental results. The estimated transport parameters (σ and ω) of membrane depend on salt type and the feed solution concentration.

Chaudhari and Murthy, (2010) reported in his work, nickel and cadmium ions removal from aqueous multicomponent solutions by NF membrane. The highest removal of cadmium and nickel ions were 97.26% and 98.90% for $CdSO_4$–$NiSO_4$–water system and 80.57% and 85.27% for $CdCl_2$–$NiCl_2$–water system respectively for 0.005 g/L feed concentration. The NF membrane was characterized with Spiegler–Kedem model, coupled with film theory and model predicted results show that good agreement with experimental results.

Murthy and Gupta, (1999) reported that commercial thin film composite polyamide RO membrane feasibility investigated for removal of sodium cyanide from synthetic binary aqueous solutions. The removal results are analyzed with membrane transport models, i.e. CFSK model and CFSD model. Both models were used for simultaneous estimation of membrane transport parameters and mass transfer coefficients, with a graphical method in case of CFSD model, and with a nonlinear parameter estimation method for CFSK model. The reasonable membrane performance was found with both the models, but value predicted from the model CFSK model are more accurate and the mass transfer coefficients estimated from the CFSK model are comparable with the literature values.

Application of different membrane for various wastewater treatment are well summarized in following Table 2.5.

Table 2.5 Comparison of different membranes for various wastewater treatment.

Membrane Name	Type of process	Membrane company name	Compound removal	Removal %	Operating parameters	References
NF-40HF FT-30	Nano filtration Reverse osmosis	--	Fructose	90 (NF-40HF); 98 (FT-30)	150 psi for NF-40HF 200 psi for FT-30	Freeman and Stocker, 1987
NF-70	Nanofiltration	Filmtec (Midland, MI)	Methoxychlor	100	--	Duranceau et al., 1992
Reverse osmosis thin film composite polyamide membrane	Reverse osmosis	Permionics, Vadodara, India	Sodium cyanide	around 95%	concentration in the feed (15–625 ppm), feed flow rate (300–900 ml/ m), and operating pressure (5–25 atm)	Murthy, and Gupta,1999
NF70	Nanofiltration	(Dow/FilmTec)	atrazine, simazine, diuron and isoproturon	90–95% range	--	Van der Bruggen et al., 2001
ES-10	Nanofiltration	Nitto Electric Industrial Co., Japan)	Pentavalent and Trivalent arsenic	95% As(VI) >75% As(III)	(0.3–1.1 MPa)	Sato et al., 2002

RO (BW30LE-440)	Reverse osmosis	Filmtec	Diclofenac	(99.7)	--	Heberer et al. 2002
RO (XLE)	Reverse osmosis	(Film-Tec, Vista, CA)	Diclofenac	95	--	Kimura et al. 2003
NF70	Nanofiltration	Filmtec	Metribuzin	87–97 (NF70)	--	Chen et al., 2004
NF70	Nanofiltration (MWCO) of 300 Da	Filmtec	Bentazone	100	--	Chen et al., 2004
NF90 NF-200	Nanofiltration	Dow/Filmtec (Midland, MI)	Ibuprofen	85–88 (NF90); 70–78 (NF-200)	--	Bellona and Drewes, 2005
NF200 NF90	Nanofiltration	Dow/Filmtec (Midland, MI)	1,5-dinaphthalenesulfonic acid	50–90 (NF200); 75–90 (NF90)	--	Bellona and Drewes, 2005
MPF-34	Nanofiltration	Koch Membrane Systems	Cobalt(III) EDTA complex	R >90%	if pH >9.5	Szöke et al., 2005
RO (BW30LE-440)	Reverse osmosis	Dow FilmTec	Diclofenac	99.9	--	Radjenovic et al., 2008
NF90	Nanofiltration	FilmTec	bivalent nickel	99.85%	pH = 3.2, at 5 bar	Chilyumova and

						Thöming, 2008
RO (LFC-1) ESNA MX07	Reverse osmosis Nanofiltration Nanofiltration	Hydranautics Hydranautics Desal-Osmonics	chromate, arsenate, and perchlorate	LFC-1 (>90%) > MX07 (25–95%) ≈ESNA (30–90%)	pH conditions (4, 6, 8, and 10)	Yoon et al., 2009
NF300	Nanofiltration	Permionics, Vadodara, India	cadmium and nickel ions	97.26% and 98.90%	At constant applied pressure of 20×10^5 N/m^2	Chaudhari and Murthy, 2010
NF300	Nanofiltration	Permionics, Vadodara, India	Cerium Cerium EDTA complex	90.03% 99% (8–12 pH).	at 10 bar pressure and 16 L/min for 80 mg/L cerium feed solution	Murthy and Choudhary 2011
RO (HTI)	Reverse osmosis	Hydration Technology Innovations (HTI, Albany, OR)	Diclofenac	90	--	Xie et al., 2012
NF300	Nanofiltration	Permionics, Vadodara, India	Praseodymium(III) Praseodymium(III) DTPA complex	84.20% 99.30%	at 10 bar pressure, pH 6.2±0.2 and	Murthy and Gaikwad, 2013

					a feed flowrate of 16 L min^{-1}	
NF300	Nanofiltration	Permionics, Vadodara, India	p-anisic acid	56.8%	at 4 bar	Gandhi, and Murthy, 2013
FM NP010	Nanofiltration (MWCO) of 1000 Da	Microdyn-Nadir, GmbH, Germany	Pharmaceutical active compounds	31-39% and 55-61% for neutral (CBZ) and ionic (DIC and IBU) PhACs, respectively.	transmembrane pressure =12 bar	Vergili et al., 2013

2.5 Introduction about capacitive deionization

The world's population is expected to increase from 7 billion in 2015 to 10 billion by 2050. One important issue is the increasing shortage of freshwater, as only 0.5% of earth's overall water supply is freshwater, while 97% is seawater (Lalia et al., 2013). In addition, worldwide requirements for fresh water have rapidly increased. The main consumers of water are food production and agriculture in most countries; they require 100 times more water than domestic consumers (Qadir et al., 2007). The RO membrane is currently considered to be the best desalination technique because of its superior performance in salt removal and reasonable energy requirements. The energy utilization has decreased from nearly 5 kWh/m^3 (in the 1990s) to 1.8 kWh/m^3 (today), which is comparable to other methods (Elimelech and Phillip 2011). Current desalination techniques providing fresh water are RO membranes, distillation, and electrodialysis. A promising alternative method is CDI and MCDI (AlMarzooqi et al., 2014). CDI is based on electrosorption and is ecofriendly because of its lower energy utilization and working costs, reduced secondary pollution generation, and simple regeneration and maintenance (Mezher et al., 2011; Wimalasiri and Zou 2013). The main aspects of CDI are salinity, scalability, the efficiency of electrodes, and cost-effectiveness in comparison to other desalination techniques (Zhou et al., 2006; Nadakatti et al., 2011). Welgemoed and Schutte (2005), performing one of the largest and most comprehensive studies, reported a CDI desalination unit with a capacity of $3785 \text{ m}^3/\text{day}$. For comparison, the desalination capacity of a typical reverse osmosis plant is $100,000 \text{ m}^{3/}\text{day}$. CDI is an effective method with respect to cost and efficiency. CDI may only treat high salinity if there is an important, sufficient decrease in capital investment. The desalination cost has been shown to be lower for CDI ($0.11 \text{ \$/m}^3$) compared to RO ($0.35 \text{ \$/m}^3$) for 2000 ppm feed. CDI performs better performance in the removal of divalent ions (Seo et al. 2010) and purification of insulin (Jung et al., 2012). Microbial fuel cells may serve as the power source in CDI for low-salinity feed (Yuan et al. 2012; Feng et al. 2013).

2.5.1 Capacitive deionization

CDI mainly stands for electrosorption, is an eco-friendly desalination technology because of its lesser energy utilization and working costs, deficient in secondary pollution and simply in regeneration and maintenance compared with other conventional techniques of desalination (Mezher et al., 2011; Wimalasiri and Zou 2013). CDI techniques are a combination of two words capacitive and deionization. Deionization represent the removal of ions which could be charged atoms or molecules. Capacitive deals with the truth of capacitor which assist in such removal. A capacitor is nothing but devices prepared from one or more couple of oppositely

charge electrode. Electrode produced a positive and negative pole by applying an electric potential. Salt solution contains the salt molecules are present in the form of ions having negative and positive charge poles. Cations (positive charge ions) and anions (negative charge ions) are attracted towards negative and positive electrodes, respectively because of the electrostatic force. Ions removal from water are carried out in this way.

Two main steps included in the CDI process first one is purification and the second one is regeneration. The Mechanism of purification or adsorption step is as shown in Fig. 2.5 (a). At purification steps potential difference is applied over the electrodes due that, ions are adsorbed or remove from water. The salt ions are passing through the inter particle pores to intra particle pores of porous electrode, where the electrosorption of ions occuring is called as electrical double layers. When the electrodes are getting saturated due to ions, there is need of desorption of ion from the electrode. Mechanism of regeneration steps is as shown in Fig. 2.5 (b). Removal of ions from the electrode by applying reversed potential difference or reduced to zero. Where the ions are desorbed from electrode pores and flow in steam, which is a highly concentrated solution.

(a)

(b)
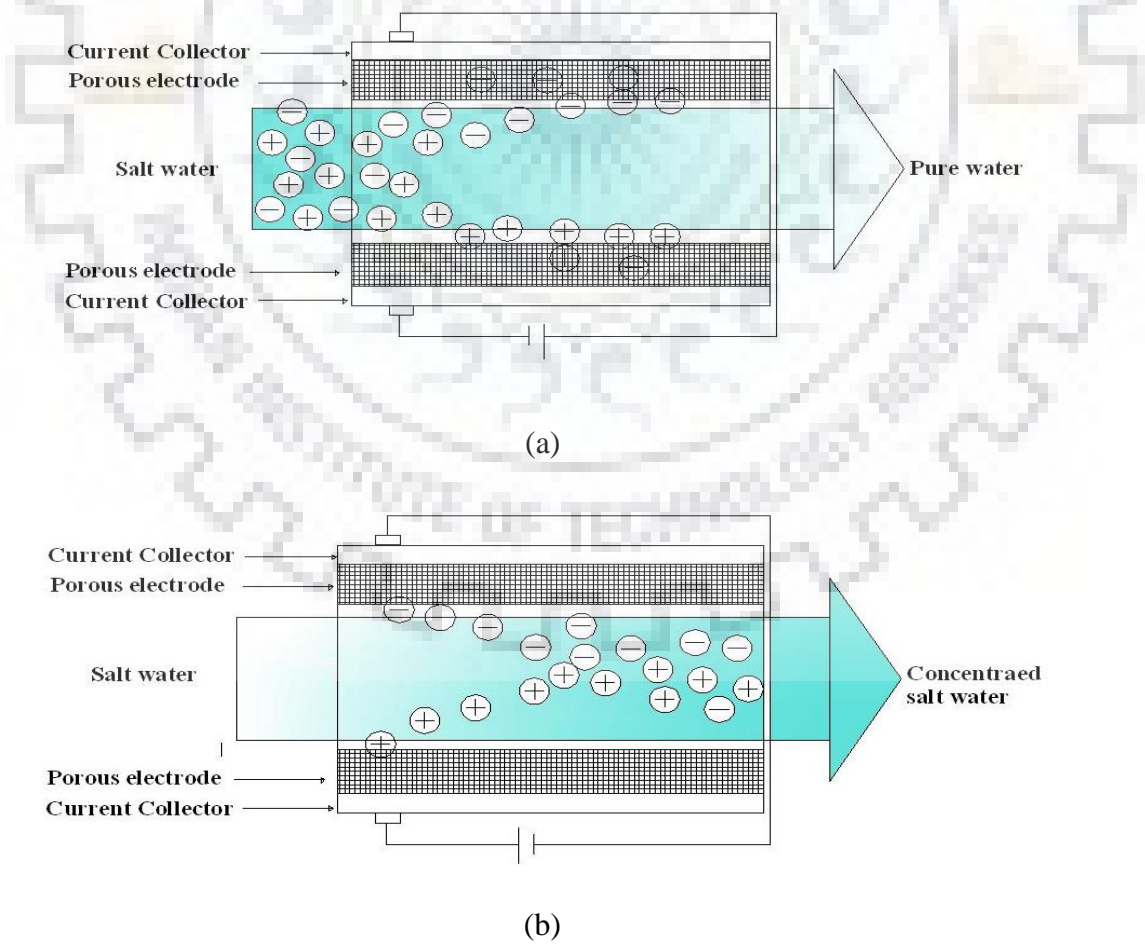
Fig. 2.5 Schematic of (a) CDI purification mechanism (b) CDI regeneration mechanism

2.5.2 Membrane capacitive deionization

The effective desalination technology is membrane capacitive deionization (MCDI) in which ion exchange membrane takes place in front of porous electrode operated by applying a potential difference (Lee et al., 2006; Li et al., 2008). MCDI is modified technology of CDI technology (Porada et al., 2013). Marc Andelman invented charge barrier flow through a capacitor and it is also termed as membrane capacitive deionization (Andelman and Walker, 2004), which solves the problem of the coulombic inefficiency (Andelman 2011). Mechanism of MCDI as shown in Fig. 2.6, in which ion exchange membrane- electrode separated by spacer section. cation and anion exchange membranes are positioned in front of negative and positively charged electrode respectively, because of membranes counter ions can transfer towards and out of electrode easily. Whereas co-ions transport is restricted. Feed solution is flowing through the spacer section where Ions are adsorbed on the surface of porous electrode, resulting in pure water at the outlet. In the CDI salt removal rate is reduced because of the effect of co-ions expulsion (Biesheuvel, 2009; Bazant et al., 2004) while in MCDI this effect does not happen. Another benefit of MCDI over CDI is during the regeneration steps when a reversal potential is applied, then the electrode areas get fully drain of the counter ions, in this manner capacity of ion-removal is increased.
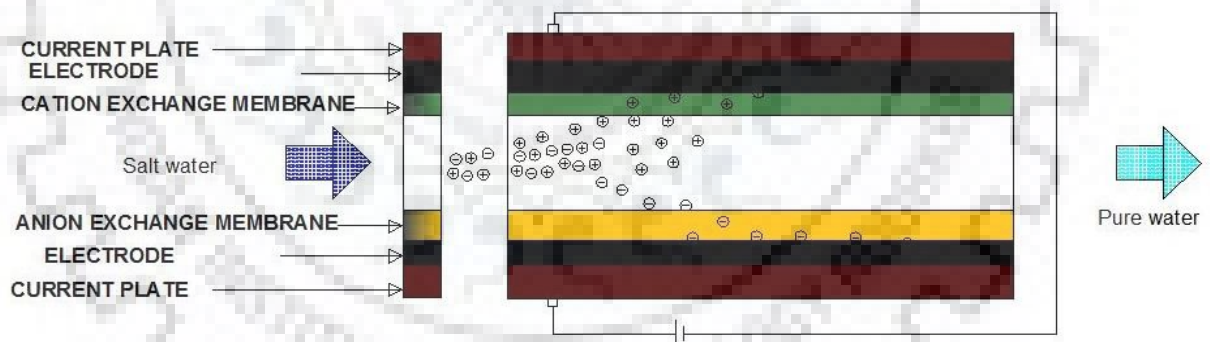
Fig. 2.6 Schematic of membrane capacitive deionization

2.5.3 Theory about capacitive deionization

The theoretical background of CDI is described as follows. The desalination technology with use of electric potential as a mean of salt separation. Hence, in CDI, ion transport is driven by electrostatic adsorption and not by oxidation and reduction reactions (Farmer et al., 1996). In CDI the separation mechanism is explained by the double layer models suggested independently by H. Helmholtz in 1883 (Helmholtz 1883) followed by J. Perrin in 1904 (Perrin, 1904). In 1861, G. Quincke first found this concept (Quincke,1861) having two layers of

opposite charge at the interface, but the term 'double layer' and else known as Parallel-Plate model (Bokris et al., 2000) was first used by H. Helmholtz later in 1883.

2.5.4 Main Parameters of Process (Huang et al., 2013).

2.5.4.1 Electrode material

2.5.4 1.1 Pore-size distribution

The porous material can be categorized as macroporous (pore dia. > 50 nm), mesoporous (2 nm < pore dia. < 50 nm) and microporous (pore dia. < 2 nm). As previously specified, it is problematic for ions to enter into micropores, while micropores cover maximum specific surface electrodes area. The use of very high surface area carbons might be not beneficial. Recent studies specified that CDI capacity prominently associated with the charge efficiency of EDL and that based on the volume of mesopore (Huang et al., 2012). The overlapping effect of EDL would be decreased in mesopores, leading to the increase of electrosorption capacity (Ying, 2002). There are numerous ways to develop the volume of mesopores of activated carbon. For example, microwave modification would open blind holes and increase entrances, which would be good for ion adsorption electrodes of activated carbon (Huang et al., 2013).

2.5.4.1.2 Surface properties

Several studies have presented that surface functional groups on carbon materials also prominently influenced the desalination of CDI process. Surface functional groups contain, carbonyl, phenol, carboxyl, lactone, etc. (Mattson and Mark, 1971). Surface functional groups could enhance surface wettability and thus improve the efficiency of surface utilization. Surface functional groups may lead to redox reactions to generate Faradaic pseudo capacitance in the process of charging and discharging, dramatically improving the specific capacitance (Bleda-Martinez et al., 2005).

In addition, it was found that carbonyl and the carboxyl groups in carbon-based materials are helpful for fast faradic reactions, because of their less charge transfer resistance than a hydroxyl group (Li and Li, 2011).

2.5.4.2 Voltage

The EDL theory described that, the thicker the EDL, stronger will be the adsorption of ions. Due to the higher the voltage on the electrodes. But, at high voltage electrolysis of a solution occurs. For example, if voltage is applied over 1.2 V then water is split in to hydroxide and hydrogen ions which would vary the pH of the solution and oxidize carbon electrodes and thus

negatively affects CDI process (Pan et al., 2009). When voltage is less than 1.0 V, solution pH rapidly improves until reached a constant as the increase of the potential, which is due to the reduction of dissolved oxygen. However, over 1.2 V, the pH rapidly reduced because of the oxidation of chloride at anodes (Lee et al., 2010). In addition, high voltage leads to enhanced energy consumption.

2.5.4.3 Flow rate

As increasing flow rate would reduce solution resistance and thus enhanced the current density, tends to the enhanced salt removal. However, on an increasing flow rate, which leads to reduce residence time, thus ions would have less contact time to adsorb on the surface of the electrode. Further, it is much more remarkable, leading to the flow rate that negatively affects salt removal in CDI process. (Kim and Choi, 2010a).

2.5.4.4 Ionic concentration in feed solution

In feed solution increased ionic concentration would reduces the solution resistance, hence there will be rise in adsorption velocity, and thus increase the capacitance and salt removal (Rasines et al., 2012). At a high ionic concentration, the increase would cease because of saturation limit.

2.5.4.5 Treatment time

Ionic concentration in solution reduces due to adsorption of ions on electrode with the time of treatment. At the starting, the concentration declined or reduced quickly, demonstrating a rapid adsorption of salts on the electrode due to availability of large sites on surface of electrode for electrosorption. Later on, due to reduction of the sites and ionic concentration, which tends to slow adsorption up to a dynamic equilibrium (Jia and Zou, 2012).

2.5.4.6 Temperature

In the CDI process removal of salt reduces with the increasing temperature, which has been established in the experiments through the electrode of carbon nanotubes, nanofibers and activated carbon (Mossad and Zou, 2012). The increasing temperature could effect in metallic ions to release into solution from surfaces of electrodes. Also, at lower temperature, hydrophobic–hydrophilic transition would be stronger in interfacial water. Leading the affinity between interfacial hydrated ions and activated carbon to be strengthened (Wang et al., 2008).

2.5.4.7 Other factors

There are several other factors, that effect on salt removal of CDI process such as number of electrode pairs and spacing between electrodes etc. The smaller the distance between electrodes leads the higher will be the ion adsorption and the smaller the treatment time (Huang et al., 2013).

2.5.5 Electrode materials (Huang et al., 2013)

The carbon-based materials are used in CDI electrodes fabrication for desalination because of their high adsorption capacity, extended specific surface area, special surface reactivity and reasonable microporous structure (Oren, 2008).

2.5.5.1 Activated carbon powder

The latest studies reported that activated carbon powder can be applied in the CDI process because of low cost, high specific surface area, high adsorption capacity and good electrochemical stability. Activated carbon powder might be one of the best potential electrode materials for the commercial industrialization of CDI technology (Park et al., 2011). It was reported that with activated carbon powder electrode in CDI process the desalination efficiency was found to be 89.25% (Hou and Huang, 2013). Usually the high surface area activated carbon powder used for attaining high specific capacitance and therefore high ion adsorption capacity (Oda and Nakagawa, 2003). The pore structure, pore size, also affected the desalination efficiency. For example mesopores percentage in activated carbon powder increased from 33% to 61% leads to adsorption capacity, improved from 90 to 180 mg/g (Sun et al., 2011).

2.5.5.2 Activated carbon fiber

Activated carbon fiber having microporous structure, narrow pore size distribution leading to promising ion adsorption and easy regeneration of electrode (Wang et al., 2012a). Activated carbon fiber contain traces of impurity such as O, H, N and S, which leads to an excellent adsorption performance (Brasquet et al., 2000). The activated carbon fiber as the electrode, an electrosorption capacity of 4.64 mg/g was achieved by a CDI process at 1.6V, which is relatively higher than that attained by activated carbon powder electrode (Wang et al., 2012a). But, the high price of activated carbon fiber because of the high production cost limits its commercial applications.

2.5.5.3 Carbon aerogels

Carbon aerogel is achieved from formaldehyde and resorcinol with the atmospheric pressure drying method. It has good conductivity, high specific surface area, wide density range, controllable pore structure, leading to an excellent performance in electrosorption (Ying et al., 2002). Carbon aerogel is considered as perfect electrode material for electric double layer capacitor (Xu et al., 2008). But, the high production cost and the difficulty in preparation limit the development of carbon aerogel as the electrodes in CDI process.

2.5.5.4 Nanomaterials

Nowadays, due to excellent property nanomaterial such as graphene used in synthesis of electrode of CDI, which show better response in desalination (Yang et al., 2014; Wen et al., 2013). Mostly graphene has been composite or modified with mesoporous carbon, carbon nanotubes, nanoparticles, which resulted in enhanced the wettability, surface area, hydrophobic ability (Jia and Zou, 2012). It has been reported that capacitance increased by merging metal oxides with nanostructure graphene (Myint and Dutta, 2012; Wang et al., 2013a; El-Deen et al., 2014a).

2.6 Review of literature for CDI

2.6.1 Comparison of nanomaterial CDI electrodes

CDI is a promising technology for desalination. A novel electrode synthesis from materials and composites aids in improvement of CDI technology with high efficiency (Biesheuvel et al., 2013). CDI electrodes have better electrical conductivity, a reasonable pore arrangement for electric double-layer formation, and high specific surface area and wettability to more efficiently capture ions in seawater (Hou et al., 2006; Jia and Zou 2012b). Carbon materials are used for the preparation of electrodes due to their high surface areas, good chemical stability, and eco-friendliness (Zou et al. 2008). Activated carbon (Gao et al., 2009), mesoporous carbon (Zou et al. 2008), and carbon aerogels (Lee, et al., 2010) have been used for carbon electrode synthesis. Graphene has been used for the fabrication of capacitive deionization electrodes because of their favorable properties for desalination (Wen et al. 2013; Yang et al. 2014). Graphene has been used as a composite or was modified with mesoporous carbon, carbon nanotubes, or nanoparticles to enhance the wettability, surface area, and hydrophobic ability (Jia and Zou 2012a). The capacitance was increased by merging metal oxides with nanostructure graphene (Myint and Dutta 2012; Wang et al. 2013a; El-Deen et al., 2014a). Comparison of nanomaterial electrodes for capacitive deionization is given in Table 2.6.

Table 2.6 Comparison of various nanomaterial electrodes for CDI.

Nanomaterials based electrode	Surface area (m^2/g)	Flow rate (ml/min)	Voltage (V)	Feed concentration (mg/L)	Salt adsorption (mg/g)	References
Oxide Nanoparticle						
Zinc oxide/Activated carbon	--	10	1.2	500	9.4	Liu et al., 2015a
Titanium dioxide coated carbon electrode	--	10	1.2	10[c]	17	kim et al., 2014
Graphene/Tin dioxide nanoparticles nanocomposite	--	--	1.4	61[d]	1.49	El-Deen et al., 2014b
Composite carbon electrode coated with Titanium dioxide nanoparticles	--	20	1.2	200	--	Lee and Choi, 2013
Oxide nanoparticles coated - Porous conducting carbon foam	300	--	1.2	(1 to10)[a,c]	15[e]	Han et al., 2013
Manganese dioxide / Activated carbon	558	20	1.2	--	16.9[e]	Yang et al., 2011
Titania / Activated carbon cloth	1890	--	1.0	0.1[c]	4.3	Ryoo and Seo, 2003
Manganese dioxide/Polystyrene Sodium Sulfonate / carbon nanotubes composite	191.8	20	1.2	128	80.4[e]	Yang et al., 2012

Zinc oxide nanorod/activated carbon cloth	687	3	1.6	1000	7.7	Laxman et al., 2015a
Titanium dioxide nanorod-intercalated reduced graphene oxide	658.6	20	1.2	300	16.4	El-Deen et al., 2015
Silicon dioxide coating on carbon fiber sheet	35.3	--	-1.5	$1.0^{b,c}$	--	Wouters et al., 2013
Carbon Nanotubes						
Ordered Mesoporous carbon–Carbon nanotubes	620.9	25	1.2	40	10.74^e	Peng et al., 2012
Single-walled Carbon Nanotubes	453	25	2.0	390^f	12.79^e	Li et al., 2011
Multi-walled Carbon nanotubes	129.36	10	1.2	~3000	1.734	Dai et al., 2005
Graphene						
Graphene composite microsphere	1128	20	1.8	800	33.52	Liu et al., 2015b
Graphene laminate electrodes	--	20	2	400	14.3	Wimalasiri et al., 2015
Graphene-carbon Nanotube	479.5	25	2.0	57^d	1.41	Zhang et al., 2012
Reduced graphene oxide-Activated carbon composite	407	25	1.2	~50	2.94	Li et al., 2012a

Graphene-like nanoflakes - Activated carbon	222.01	25	2.0	25	23.18[e]	Li et al., 2010b
Graphene	14.2	40	2.0	50[d]	1.8	Li et al., 2009
mesoporous graphene		10	1.6	300[d]	15.21	Gu et al., 2015a
Graphene by nitrogen doping	358.9	27	1.8	100[d]	4.81	Xu et al., 2015a
Three-dimensional porous graphene (Potassium hydroxide -activated graphene)	3513	10	2	~74	11.86	Li et al., 2015
Three-dimensional reduced graphene oxide–polypyrrole– Manganese dioxide composites	331	10	2	1000[d]	18.4	Gu et al., 2015b
graphene/carbon nanotubes hybrid sponge	498.2	27	1.2	~500	18.7	Xu et al., 2015b
Reduced graphite oxidate-resol	406.4	20	2.0	~65	3.229	Wang et al., 2012b
Sulphonated graphite nanosheet	464	25	2.0	250	8.6	Jia and Zou, 2012b
Three-Dimensional Graphene/Metal Oxide (TiO_2) Nanoparticle Hybrids	187.60	--	1.2	500 6000	15.1 24.2	Yin et al., 2013
Novel graphene sponge	356.0	--	1.2	~500	14.9	Xu et al., 2015c

Novel nitrogen doped graphene Sponge	526.7	--	1.2	~500	21	Xu et al., 2015d
Nonoporous activated carbon cloth / Nanofiber						
Activated carbon nanofiber webs	712	5	1.6	192[d]	4.64	Wang et al., 2012a
porous carbon nanofibers by electrospun polyacrylonitrile /dimethyl sulfone	212	10	1.2	500	8.1	Pan et al., 2015
Nitrogen-doped carbon nanorods	1557	50	1.2	500	17.62	Liu et al., 2015c
Carbon nanotubes-nanofibers composite	210.6	14	1.2	~119	56.8[e]	Wang et al., 2006

Note: All feed solution are sodium chloride, a-Feed solution is Potassium chloride, b -Feed solution Calcium chloride, c- Initial concentration in (mM), d-initial conductivity of feed solution in (µS/cm). e- Salt adsorption in (µmol/g), f- Initial concentration in (µmol/L).

2.6.1.1 Synthesis of nanomaterial-based CDI electrodes

The nanomaterials used for CDI have included nanoparticle oxides, carbon nanotubes, graphene, nanocomposite, nanoflakes, nanosheet, nonporous activated carbon cloth, and nanofibers.

2.6.1.1.1 Nanoparticle oxides

Fabrication of CDI electrodes using nanoparticle oxides has involved mechanical mixing, dip coating, and sol–gel spray processes. CDI electrodes have been prepared from activated carbon powder mixed with polyvinylidene fluoride as the binder in N,N,-dimethylacetamide. The electrode was coated by mixing solutions of titanium dioxide nanoparticles and sulfonated polystyrene. The efficiency was enhanced up to 30% using the titanium dioxide nanoparticles as reported by Lee and Choi (2013). Similarly, tetrahedrally coordinated titania decreased the physical adsorption of sodium chloride due to the reduction of polar groups on the surface of the activated carbon cloth. However, titania modification enhanced sodium chloride adsorption due to the increased sites for adsorption of ions in the presence of an electric field (Ryoo and Seo 2003). Composite electrodes were prepared from graphene oxide and tin dioxide with various proportions of the latter (10, 15, and 20%) using microwave irradiation. The electrosorption capacity was improved in the presence of tin dioxide nanoparticles. The 15% tin dioxide electrode offered favorable electrochemical performance, large specific capacitance, outstanding cycling stability, and good removal of ionic compounds (83%). An electrosorption capacity of 1.49 mg/g was reported by El-Deen et al. (2014b). Silicon dioxide-coated electrodes were prepared using pH 2.9 and pH 8.3 solutions of silicon dioxide. The removal efficiency of the coated electrode was higher (30%) than the uncoated carbon electrode. All electrodes removed more than 90% of Ca^{2+} after 30 min. In the regeneration process, the concentration of Ca^{2+} was 60 and 90% after 30 min for uncoated and coated electrodes (Wouters et al. 2013). A composite electrode was prepared by mechanical mixing of zinc oxide and activated carbon with superior electrochemical properties compared to an activated carbon electrode. Desalination was performed by arranging the asymmetric capacitor with the composite electrode (zinc oxide/activated carbon) as either positive or negative electrode. The capacitor (zinc oxide/activated carbon and activated carbon) efficiently achieved desalination with good reproducibility and cycling stability (Liu et al. 2015a). Zinc oxide nanorods improved the efficiency and increased the depth of electric field penetration. A reduction in energy consumption up to 30% was also reported (Laxman et al., 2015a). A manganese dioxide/polystyrene sodium sulfonate/ carbon nanotube composite electrode was synthesized by layer-by-layer deposition. Polystyrene sodium sulfonate was deposited on the

surface of carbon nanotubes, and manganese was attracted toward the anionic functional head and deposited on the carbon nanotubes. The small layer of manganese dioxide on the composite electrode provided the maximum surface area to accommodate ions. Outstanding desalination performance was reported by Yang et al., (2012). The manganese dioxide/activated carbon composite provided suitable pore size, high surface area, and suitable electrochemical properties (Yang et al. 2011). A titanium dioxide-coated carbon electrode was prepared by a sol–gel spray process. The sprayed solution was composed of 10% (v/v) titanium butoxide in isopropyl alcohol and dispersed on the electrode with a nozzle. The titanium dioxide-coated carbon electrode was heated at 250°C for 2 h. The electrosorption capacity of titanium dioxide-coated electrode provided twice the efficiency for desalination (17 mg/g carbon) compared to an uncoated carbon electrode (9 mg/g carbon). The higher efficiency of desalination was attributed to the wetting ability of the titanium coating (Kim et al. 2014). Titanium dioxide nanorod-intercalated, reduced graphene oxide has been shown to offer high wettability, delayed release of titanium dioxide, enhanced accessibility of water and ions through additional channels between graphene layers, and favorable electrochemical properties (El-Deen et al. 2015). The presence of nanoparticles increased the surface area and charge efficiency (Han et al. 2013).

2.6.1.1.2 Carbon nanotubes

CDI electrodes were synthesized from carbon nanotubes. A multiwalled carbon nanotubes CDI electrode was prepared from CH_4 with a La_2NiO_4 catalyst by chemical vapor deposition (Grujicic et al., 2002). Three electrodes were synthesized from unpurified and purified carbon nanotubes with 95% phenolic resin and 5% urotropine as the binder. The resulting electrodes provided excellent performance in salt removal, and the electrode was regenerated with good efficiency (Dai et al. 2005).

CDI electrodes were prepared using single-walled carbon nanotubes, double-walled carbon nanotubes, and graphene mixed with graphite as the conductive material and polytetrafluoroethylene as the binder for the fabrication of electrodes. Electrosorption capacities of 7.87, 12.79, and 9.35 µmol/g were obtained for graphene, single-walled carbon nanotubes, and double-walled carbon nanotubes, respectively. The surface groups, pore structure, specific surface area, and pore-size distribution of the carbon nanotubes and graphene affected the electrosorption capacity. The electrosorptive rate constant results showed that the carbon nanotubes were superior to graphene for capacitive deionization electrodes (Li et al. 2011). Graphene/carbon nanotube composites were prepared using 0, 5, 10, and 15% carbon nanotubes. The 10% graphene/carbon nanotube composite provided a higher surface area

compared to graphene. However, with further increases in the number of carbon nanotubes, the surface area decreased due to carbon nanotube aggregates on the graphene surface. Carbon nanotubes integrated into graphene may improve the accessible surface area and serve as a conductive network to reduce the resistance of composite electrodes. This property also indicates an enhancement in the capacity of electrosorption. The large accessible surface area and better electrical conductivity resulted into high capacitance values and reduced energy consumption (Zhang et al. 2012). Ordered mesopore carbon/ carbon nanotubes composites electrode were prepared using the inorganic–organic classic self-assembly route with soft templates. The resulting composite electrodes provided excellent performance in desalination due to the high specific surface area, ordered mesopores, and suitable electrical conductivity. (Pan et al. 2015).

2.6.1.1.3 Graphene

A CDI electrode was fabricated from graphene and tested for electrosorption. The results show that maximum salt removal was achieved at high voltage. The electrosorption capacity was 1.85 mg/g at 2V (Li et al. 2009). The effect on the specific area of graphene pretreated with acid at volume ratios of HNO_3 and H_2SO_4 of 0:1, 1:1, and 2:1. CDI electrode was fabricated from 72% graphene or activated carbon, 8% polytetrafluoroethylene as the binder, and 20% graphite powder as the conductive martial. The maximum surface area (222.01 m^2/g) was obtained with the 1:1 ratio as graphene-like nanoflakes. The surface area decreased with the increased acid concentration because excess HNO_3 diluted H_2SO_4. The graphene-like nanoflake electrode had a reduced surface area (222.01 m^2/g) than the activated carbon electrode (989.54 m^2/g) but had a high electrosorption capacity (23.18 µmol/g) than activated carbon (13.73 µmol/g) due to the nanoflakes providing more access to ions (Li et al. 2010b). A graphene nanosheet electrode was synthesized from graphene oxide by sulfonation. The CDI electrode was fabricated on graphite paper from 72% graphene, 8% graphite powder, and 20% polytetrafluoroethylene. The surface area of the sulfonated sample (464 m^2/g) was higher than for the unsulfonated material (299 m^2/g) because of less aggregation of the graphene nanosheet (Si and Samulski 2008). The results show that the sulfonated graphene nanosheet electrode provided superior salt removal efficiency (83.4%) and electrosorptive capacity (8.6 mg/g) than an unmodified electrode with the removal efficiency of 40% and an electrosorptive capacity of 4.1 mg/g (Jia and Zou 2012b).

Composite electrodes were prepared from reduced graphene oxide and activated carbon with 10, 20, 30, 40, and 50 wt% reduced graphene oxide. The electrodes were fabricated using graphene oxide and 70% activated carbon, 20% graphite as the conductor, and 10%

polytetrafluoroethylene as the binder. The 20 wt% composite electrode graphene oxide provided the most favorable electrochemical response (Li et al. 2012a). A novel functional graphene nanocomposite capacitive deionization electrode was prepared from reduced graphene oxide and resol-like martial. The surface area values were 406.4 m^2/g for reduced graphite oxidate and resol, 137.4 m^2/g for reduced graphite oxidate, and 836.0 m^2/g for activated carbon. The reduced graphite oxidate and resol nanocomposite electrode showed superior electrosorption compared to the other electrodes. Resol served to enhance the specific surface area of reduced graphite oxidate (Wang et al., 2012b). A simple-inverse suspension polymerization procedure was used to synthesize graphene oxide/resorcinol–formaldehyde microspheres with drying under ambient pressure. The graphene composite microspheres were obtained by carbonization in presence of nitrogen. The sample had low interfacial charge transfer resistance and high specific capacitance due to a porous structure with large surface area, leading to rapid ion diffusion and efficient charge transfer (Liu et al., 2015b). Graphene laminates with enhanced structural and electrochemical properties were used to remove sodium chloride from water by CDI (Wimalasiri et al., 2015). A high-density mesopores electrode was fabricated by etching Fe_3O_4 nanoparticles. This electrode provided higher specific capacitance, large specific surface area, and excellent desalination capacity, cycling stability, and regeneration performance (Gu, Hu et al. 2015a). Nitrogen-doped graphene was prepared by simple thermal treatment of graphene oxide with enhanced electrosorption performance. The higher pore volume and specific surface area provided enhanced specific capacitance using nitrogen doping with lower-chargetransfer resistance (Xu et al., 2015a). Graphene was activated by potassium hydroxide to synthesize the electrodes. After activation, the graphene forms a three dimensional network with nanopores in graphene planes. This electrode shows high electrical conductivity, excellent electrosorption capacity, high specific surface area, and better regeneration performance (Li et al. 2015). A three-dimensional reduced graphene oxide–polypyrrole–manganese dioxide composite electrode was synthesized by a two-step hydrothermal process. Pyrrole monomers were polymerized using potassium permanganate in the presence of graphene oxide. The manganese dioxide was introduced concurrently after a redox reaction between potassium permanganate and graphene to produce the composite electrode. The resulting electrode showed excellent microstructure, morphological, and electrode electrochemical properties (Gu et al., 2015b). Novel graphene/carbon nanotube hybrid sponge structures were prepared by directly freeze-drying a graphene oxide/carbon nanotube solution followed by annealing in nitrogen. The results showed that higher specific capacitance and specific surface area were obtained with excellent electrosorption capacity (Xu et al., 2015b). Recent studies showed that three-dimensional graphene was a promising

candidate for CDI. Yin et al. (2013) reported a novel, easy, and useful method of graphene preparation using aerogel/metal oxide hybrids with three-dimensional graphene/ metal oxide nanoparticle. These hybrids provided better performance for capacitive deionization. The graphene aerogel/ titanium dioxide hybrid gave significantly higher specific capacitance values and electroadsorption capacities than graphene aerogel and activated carbon. These electrodes also offered rapid electroadsorption and good reversibility due to their porous hybrid structure. A novel graphene sponge electrode for capacitive deionization was prepared by directly freeze-drying graphene oxide followed by annealing under nitrogen. The resulting electrode had a high accessible surface area, low-charge-transfer resistance, and good electrosorption due to the unique porous structure (Xu et al., 2015c). Novel nitrogen-doped graphene sponge electrodes for CDI were reported by Xu et al. (2015d). The electrode was synthesized by freeze-drying followed by annealing under an ammonia atmosphere. Nitrogen-doped graphene sponge electrode showed improved electrosorption with low-charge-transfer resistance, a large accessible surface area and pore volume, better specific capacitance, and superior pore structure due nitrogen doping.

2.6.1.1.4 Nanoporous activated carbon cloth and nanofibers

Carbon nanotube and nanofiber composite electrodes were prepared by chemical vapor deposition with acetylene and hydrogen. The carbon nanotube and nanofiber films were grown and kept on nickel plates as the catalyst at 550°C for 30 min. The surface area was 210.6 m^2/g. The carbon nanotube and nanofiber composite provided larger electrosorption capacities than carbon aerogel even with a reduced surface area (Wang et al. 2006). A polyacrylonitrile nanofiber CDI electrode was prepared from polyacrylonitrile and activated carbon nanofibers by electrospinning via oxidative stabilization and activation with carbon dioxide at 750, 800, and 900°C. The specific surface areas (335, 442, and 712 m^2/g) were enhanced with temperature (750, 800, and 900°C). Larger activation temperatures resulted in better capacitance and electrosorption capacity (Wang et al., 2012a). The preparation of porous carbon nanofibers was performed by electrospinning the polyacrylonitrile/dimethyl sulfone pristine fibers followed by preoxidation and carbonization. The nanopores were formed due to the removal of dimethyl sulfone during the preoxidation of nanofibers without additional chemical or physical activation. Electrochemical properties and desalination improved considerably by polyacrylonitrilebased carbon nanofibers electrodes because of the suitable micro/mesostructure contribution compared to pure polyacrylonitrile-based carbon nanofiber electrodes. This approach provided an efficient, economical, and simple method to produce porous carbon nanofiber electrodes without additional treatment (Pan et al. 2015). The sorption

capacity of the nanoporous activated carbon cloth electrode was characterized using a capacitive deionization cell. The thickness of the nanoporous activated carbon cloth was 1 mm, and the specific surface area was approximately 1200 m^2/g. The adsorption capacity was 10.5 mg/g, and the electrode was efficient with reduced electrode fouling in the regeneration process (Laxman et al., 2015b). Nitrogen-doped carbon nanorods were synthesized from nanocrystalline cellulose by simple freeze-drying followed by thermal treatment under an ammonia atmosphere at varying temperatures. The resulting material provided an extremely high electrosorption capacity. The nitrogen doping was shown to be effective for improving electrosorption performance (Liu et al. 2015c).

2.6.2 Progress of polymer coated CDI electrodes

The current progress of various polymer coated CDI electrodes is comparatively and systematically shown in Table 2.7.

Table 2.7 Comparison of various polymer coated CDI electrodes.

Polymer coated electrode	Coating thickness (mm)	Surface Area (m²/g)	Flow rate (ml/min)	Voltage (V)	Feed concentration (mg/L)	Salt adsorption (mg/g)	Percent removal (%)	References
Carbon electrode coated with an ion-exchange polymer (a mixture of poly (vinyl alcohol) and sulfosuccinic acid)	0.01	--	20	1.5	200	--	85	Kim and Choi, 2010a
Bromomethylated poly (2, 6-dimethyl-1, 4-phenylene oxide) ion exchanger layered electrodes	--	--	4	1.8	100	--	83.4	Lee et al., 2011
Ion selective polymer coating	0.0205		30	1.5	250	5.50	--	Nugrahenny et al., 2013
Anion exchange polymer (dimethyl diallyl ammonium chloride) and cation exchange (polyethyleneimine) polymer into carbon	--		50	1.2	50[a]	--	93	Liu et al., 2014

nanotubes (CNTs) electrodes								
Polyaniline-modified activated carbon electrodes	--	618.4	--	1.2	250	3.15	--	Yan et al., 2014
Polypyrrole/carbon nanotube composites		185.21	--	1.4	1000^a	43.99	--	Wang et al., 2014
Coating-type polypyrrole/carbon nanotube composite electrode	0.3	--	--	1.4	1000^a	93.68	--	Wang et al., 2015
Synthesized anion (aminated polysulfone) and cation (poly(phenylene oxide) exchange polymer coating on the electrodes	1-2	--	23	1.0	100	--	100	Kim et al., 2015

Note: all feed solutions are NaCl, a: Initial conductivity of feed solution (µS/cm).

2.6.2.1 Discussion of various polymer coated electrodes fabrication

Kim and Choi (Kim and Choi, 2010b) reported that MCDI a cation-exchange polymer coated electrode was prepared by simple and inexpensive way. A mixture of poly (vinyl alcohol) and sulfosuccinic acid mixture was used as coating solution to introduce negatively charged ion-exchange groups. Such electrode was prepared at various crosslinking temperatures and sulfosuccinic acid contents. Electrode performance shows that the specific capacitance and the electric resistance of the coated carbon electrodes were affected strongly by the crosslinking temperature. Despite this, when compared with commercial ion-exchange membranes, the area resistance of the coated layer was relatively low (Kim and Choi, 2010b). Multiplication of specific surface area carbon and double layer capacitance (Cdl) is known as specific capacitance (Cdl/F cm^{-2}) (Conway, 1999). Coating on carbon cloths was achieved by spraying with bromomethylated poly (2,6-dimethyl-1,4-phenylene oxide). Cation exchange and anion exchange layers are formed on the electrode by sulfonation and amination respectively. Such novel electrodes improve the weakness of MCDI by minimizing the interfacial resistance between the carbon electrode and ion exchanger layer (Lee et al., 2011). Salt removal efficiency was improved and contact resistances decreases by combined used of ion selective membrane and polymer in CDI cell (Nugrahenny et al., 2013). Application of polyethyleneimine (cation exchange polymer) and dimethyl diallyl ammonium chloride (anion exchange polymer) into carbon nanotube-based electrode shows better improvement in desalination due to decreased co-ion effect. It also enhanced the contact adhesion between electrodes and ion exchange polymers compared to contact adhesion between electrodes and commercial ion exchange membranes (Liu et al., 2014). A composite electrode reported by Yan et al. (2014), with conducting polymer polyaniline and activated carbon electrode was prepared by in situ polymerization. Results show that composite had a higher ion removal capacity and faster ion removal rate than original activated carbon electrode. A blend of two materials decreased the number of micropores and increased conductivity. Polyaniline made the conducting chains which connected microactivated carbon particles together and blocked most of the micropores (Yan et al., 2014). Carbon nanotube and a polypyrrole composite electrode was prepared by chemical oxidation method and sodium dodecyl benzene sulfonate was uesd as the dopant. The results prove that polypyrrole/carbon nanotube composites have specific capacitance enhanced three times compared to carbon nanotubes, they also indicated higher adsorption capacity (Wang et al., 2014). Same material, i.e. polypyrrole/carbon nanotube composite electrode fabricated by coating methodology was reported by (Wang et al., 2015). Performance of electrode shows that the coated electrode was significantly superior to the traditional compressed electrode in terms of the specific adsorption capacity and specific mass capacitance

(Wang et al., 2015). Coating of sulfonated poly (phenylene oxide) (cation exchange polymer) and aminated polysulfone (anion exchange polymer) on surface of commercial carbon electrodes is effective in reducing the "co-ion" effect (Kim et al., 2015).

Polymer coated CDI technology could be a capable technology for desalination. On the basis of reported literature the polymer coating improves the electrode performance, increases the specific capacitance and is effective in reducing the "co-ion" effect. Such electrodes improve the weakness of MCDI by minimizing the interfacial resistance between the carbon electrode and ion exchanger layer. Evidence is reported that the coated electrode was significantly superior to the traditional compressed electrode in terms of the specific adsorption capacity and specific mass capacitance. Contact adhesion between the electrodes and ion exchange polymers was enhanced compared to contact adhesion between electrodes and commercial ion exchange membranes. Thus, polymer coating is the promising method for the modification of CDI electrodes and great progress of such electrode in desalination application is expected.

2.6.3 Progress on MCDI

The ion exchange membrane resistance, mainly depends on the concentration of the solution. Membrane resistances increases with decreasing solution concentration (Długołecki et al., 2010). MCDI theory with the effect of the electrode pore space reported by P.M. Biesheuvel and co-workers (Biesheuvel et al., 2011). Energy related some studies in MCDI are depicted as follow. Studies on Energy consumption and constant current operation in MCDI reported by Zhao et al. (2012). The study of MCDI from charge efficiency reported by Li et al. (2012b). For treatment of brackish water MCDI is a more energy efficient technique compared to RO (Długołęcki and van der Wal, 2013). A similar kind of study reported on MCDI energy consumption for different water recoveries and flow rates, and comparison with RO reported by Zhao et al. (2013a). Wen et al. (2013) reported that the microbial desalination cell used as power supply for the MCDI show that high electrosorption capacity compared to potentiostat as a power supply (at 0.8V). Novel study reported on MCDI modified with flow electrode is newly designed and tested experimental performance show that successfully overcome the limitations of a typical CDI system for desalination of sea water (Jeon et al., 2013). Celine Huyskens et al. (2013) study evidently proves the technical feasibility of MCDI for process streams such as biomass hydrolysates. Cost evaluation study on Large-scale MCDI applied for biomass hydrolysate desalination carried out by Huyskens et al. (2015). MCDI used in cooling towers for water and chemical savings (van Limpt, and van der Wal, 2014).

2.6.3.1 Comparison of various MCDI literatures

The current progress of MCDI is comparatively and systematically presented in table 2.8.

Table 2.8 Comparison of various studies on MCDI.

Membranes used	Electrode material	Feed concentration (mg/l)	Voltage (V)	Flow rate (ml/min)	Removal efficiency	Salt adsorption (mg/g)	References
Commercial cation-exchange(CM-1) and anion-exchange membranes(AM-1)	Commercial activated carbon cloth electrode (CH900-10)	1000	1.2	40	92	--	Lee et al., 2006
Commercial cation-exchange membrane and anion-exchange membrane	Carbon nanotubes and nanofibres electrodes	50[b]	1.2	40	90.8	--	Li et al., 2008
Commercial cation-exchange membrane (Neosepta CMX, Tokuyama Soda Corp.)	Fabricated carbon electrodes	200	1.5	20	83	3.83	Kim and Choi, 2010c
The ion-exchange membranes (Shanghua Water Treatment Material Co. Ltd, Shanghai)	Carbon nanotube/ nanofiber electrodes	50[b]	1.2	40	--	0.3[e]	Nie et al., 2011
Cation-exchange membrane and anion-exchange membrane (MemBrain	Single walled carbon nanotubes electrode	110[b]	1.2	--	97	--	Li and Zou 2011

s.r.o.,Strazpod Ralskem , Czech) .							
The cation and anion exchange membranes were obtained from Membrain s.r.o. (Stráž pod Ralskem, Czech Republic).	MnO2 /PSS/CNTs composite electrodes	128	1.2	20	96.8	80.4[d]	Yang et al., 2012
Commercial ion-exchange membranes with high permselectivity. Neosepta AMX (Anion-exchange membrane) and CMX(cation-exchange mem-brane) membranes (Astom Co., Japan)	Carbon electrode	10	1.5	20	99.2	--	Lee and Choi, 2012
The cation-exchange membrane (CEM-DF-120) and anion-exchange membrane (AEM-DF-120) were purchased from Tianwei Company, China	Coupling ion-exchangers with inexpensive activated carbon fiber electrodes	~1000	1.2	~9	98	--	Liang et al., 2013

Ion exchange membranes (Beijing Tingrun Membrane Technology Development Co., LTD, JCM-II)	Graphite cloths electrode	400	3.0	37.5	--	5.62	Zhao et al., 2013b
Neosepta AMX (~0.15 mm thick) and CMX (~0.17 mm thick) ion exchange membranes	Pristine carbon xerogel (CX) electrodes	~5[c]	1.2	~16		~3.5	Omosebi et al., 2014
Commercial anion and cation exchange membranes	Ion-exchange polymers in carbon nanotubes electrodes	50[b]	1.2	50	93	--	Liu et al. 2014
Ion exchange membranes	Graphene/Polyaniline nanocomposite as electrode	500[b]	1.2	--	94	--	Yan et al., 2014
Cross-linked quaternised polyvinyl alcohol membrane	Activated carbon composite electrode	800	1.2	20	--	15.6	Tian et al., 2014
Ion exchange membranes	Synthesized Anion and Cation	100	1.0	23	100	--	Kim et al., 2015

	exchange Polymers coated carbon electrode						
An anion-exchange membrane (AMX,) and a cationexchange membrane(CMX) (Astom Co., Japan)	Activated carbon electrode	(10 to 0.63) [c]	1.4	20	~93.7	--	Choi, 2015
Neosepta AMX (~0.15 mm thick) and CMX (~0.17 mm thick) membranes were used as anionic and cationic membranes, respectively.	Pristine and nitric acid oxidized Zorflex (ZX) electrode	5 [c]	1.2	30	--	17	Omosebi et al., 2015
A cation exchange membrane (CEM-DF-120) and an anion exchange membrane (AEM-DF-120) Tianwei Membrane Technology Co., Ltd., Shandong, China).	Activated carbon fibers electrode (Granular activated carbon packed-MCDI)	100	1.2	13.5	--	(21.7 ± 0.2) [a]	Bian et al., 2015
Reduced graphene oxide/polyaniline	Electrode	--		--	~90	~1.5	Zhang et al., 2015

conductive anion exchange membranes							
Synthesized an aminated poly(vinylidene fluride-g-4-vinyl benzyl chloride) anion exchange membrane	Cathode and an anode plate	250	1.2	20	79.4	--	Jeong et al., 2015
Two commercial ion-exchange membranes (Neosepta AMX and CMX; Astom Co., Japan)	TiO2 nanorod-intercalated reduced graphene oxide electrode	~300	0.8	20	--	9.1	El-Deen et al., 2015

Note: a- desalination rate (mg/(L h)) , b: initial conductivity (μS/cm); c: initial concentration in (mM); d: Salt Adsorption in (μmol/g); e: Salt Adsorption in (mmol/lit)

2.6.3.2 Discussion on current progress of MCDI

A study reported by Lee et al. (2006) on the desalination performance of the MCDI process was checked for treatment of wastewater of power plant. Several MCDI experiments was carried for desalination capacity compared with CDI. It was found that salt removal rate was 19% higher in MCDI than CDI. A novel MCDI cell in that composite film of carbon nanotubes and carbon nanofibers with ion-exchange membrane are used reported by Li et al. (2008). Such process shows high removal efficiency, low cost and low energy consumption. MCDI comparative study with CDI shows better performance in desalination than CDI because of reduction in the desorption of ion during electrosorption.

In MCDI salt removal efficiency was higher than CDI. In capacitive deionization some ions were retained in pore of carbon electrode. These accumulated ions were getting re-adsorbed when potential was applied again at the electrode. Such accumulation of ions were not found, when ion-exchange membrane was used for the selective transport of ions (Kim and Choi 2010c). Various anion and cations electrosorption by MCDI study reported by Nie et al. (2011). Experimental outcomes were as multivalent ions are better adsorbed than monovalent ions. Combination of ion exchange membranes and single walled carbon nanotubes electrode shows higher efficiency than CDI without membranes. Here ion-exchange membranes improve the ion transfer rate in the electrosorption process because of low co-ions expulsion effect (Li and Zou 2011). Ion exchange membranes and composite electrode of polystyrene sodium sulfonate/ manganese dioxide/carbon nanotube shows 96.8% salt removal efficiency (Yang et al., 2012).

Lee and Choi (2012) reported study on the possibility of generating ultrapure water (UPW) through MCDI. Here anion- and cation-exchange membranes combined with the carbon electrode to carry out the desalination performance for various concentrations influent. The study proved experimentally the possibility of ultrapure water production by using membrane capacitive deionization technology. Application of ion-exchange membranes in capacitive deionization enhanced the rate of desalination, charge efficiency and salt removal efficiency. Further desalination performance was improved by using ion-exchange resin granules into the membrane capacitive deionization (Liang et al. 2013).

Comparative study on performance and energy consumption of capacitive deionization and MCDI was performed by Zhao et al. (2013b). Experimental outcome proved that application of ion exchange membrane could efficiently avoid the "co-ion" effect. MCDI indicate the higher adsorption capacity than CDI also specific energy consumption was reduced which reflects the complete economical advantage of MCDI technology. The asymmetric MCDI cell

with potential of zero charge (E_{PZC}) enhance the appropriate ion excess and the membrane in-place to reject expelled co-ions from accessing the bulk and mitigate electrochemical side reactions (Omosebi et al. 2014).

Liu et al. (2014) reported a modified MCDI by introducing the anion and cation exchange polymer modified carbon nanotubes electrodes. Such modified MCDI cell demonstrated much higher removal efficiency than that of conventional CDI cell with CNTs electrode. Yan et al. (2014) synthesized a novel graphene/polyaniline nanocomposite and used it as an electrode material in MCDI. Tian et al. (2014) study reported on a cross-linked quaternised polyvinyl alcohol (QPVA) membrane, modified by glycidyltrimethyl ammonium chloride and glutaraldehyde. Such membrane was applied as anion exchange membrane in MCDI shows highest adsorption capacity and short regeneration time. Kim et al. (2015) carried out a study on preventing the co-ion effect under the application of both anion and cation exchange polymers and 100% salt removal efficiency obtained with MCDI.

The comparative study was conducted on constant current and constant voltage modes of MCDI by Choi (2015). Result show that constant voltage modes indicate the maximum ions adsorbed compared to constant current. But charge efficiency was higher in constant current mode than in constant voltage mode. The energy consumption was found significantly lower when MCDI operated in constant current mode compared to constant voltage mode. Omosebi et al. (2015) reported that coupling of ion selective membranes with suitable potential of zerocharge (PZC) electrodes improves the desalination performance. A new study on design of membrane capacitive deionization was assembled by granular activated carbon packed in to flow chamber of the cell. Such design of MCDI shows greatest improvement in desalination rate compared to the regular MCDI (Bian et al., 2015). Zhang et al. (2015) reported a study on the preparation of a series of novel conductive anion exchange membranes via dry phase inversion method where the addition of additives (reduced graphene oxide/polyaniline) in polyvinylidene fluoride polymer matrix. The result of the study results indicated that sample LG 50, with low GO concentration, and 50% polyaniline / reduced graphene oxide composites in the membrane exhibited best performance among all the prepared membranes. Synthesized membranes indicated higher electrical conductivity also high ion exchange capacity. Study on preparation of a laminated poly (vinylidene fluoride-g-4-vinyl benzyl chloride) anion exchange membrane via casting method and heat treatment. Such membrane were used in MCDI process which show the excellent salt removal rate (Jeong et al. 2015). Nanocomposite introduce in MCDI cell indicate excellent cycling stability, high reversibility, distinguished electrosorptive capacity and full regeneration (El-Deen et al. 2015).

MCDI technique could be an effective technology for desalination. On the basis of reported literature, the MCDI improves desalination performance with preventing the "co-ion" effect. MCDI indicates the higher adsorption capacity than CDI, also specific energy consumption was reduced which reflects the complete economical advantage of MCDI technology. Thus, MCDI is the promising technique for desalination or water purification and great progress in this field is expected.

2.6.4. Current status of pollutants ion removal by CDI

The current state of CDI for removal of pollutants ion (arsenic, fluoride, boron, phosphate, lithium, copper, cadmium, ferric ion, and nitrate) is comparatively and systematically shown in Table 2.9.

Table 2.9 Current progress of CDI in removal of pollutants ion.

Pollutants ions	Electrode material	Electrode dimension W ×L ×T [mm³]	Surface area [m²/g]	Cell type	Initial ion concentration [mg/L]	Voltage [V]	Flow rate [ml/min]	Removal efficiency [%]	Electro-sorption capacity [mg/g]	References
Ferric ions	Graphene nano-flakes	70 × 140 × 0.3	2600	CDI	20	2.0	25	--	0.88	Li et al., 2010c
Boron	Activated carbon cloth	--× --× 0.26	1440	CDI	480	1.0	15	30	--	Avraham et al., 2011
Arsenic	Activated carbon	158 × 174 × 0.3	800	CDI Unit	0.04 0.1	1.5	3000	82.6 98.15	--	Zhang et al., 2016
Copper(II)	Activated carbon sheet	--× --× --	964	CDI	50	0.8	10	--	24.57	Huang et al., 2014a
Phosphate	Activated carbon	100× 100× --	--	CDI pilot plant	50 300	1.5	4800	86.5 77.4	--	Huang et al., 2014b
Lithium	Carbon electrodes	100× 100× 0.2	1260	MCDI	5 50 500	2.0 1.0 1.0	20	--	~ 0.5 ~ 1.9 ~ 3.7	Ryu et al., 2015
Cadmium(II)	Manganese oxide/acti	10× 20× 4	--	CDI	50	1.5	--	80.77	14.88	Chen et al., 2015

	ve carbon fiber									
Copper(II)	Manganese dioxide/ Carbon fiber	30× 20× --	--	CDI	6	0.8	--	90	172.88	Hu et al., 2015
Fluoride	Activated carbon	40 × 40 × --	--	CDI system	20	1.6	4600	~ 66.5	--	Tang et al., 2015
Nitrate	Activated carbon				300	1.6	4600	~ 91.6	--	Tang et al., 2015
As(V)	Activated carbon				0.1 0.2 50 100 200	1.2	5	1.16×10^{-2} 2.47×10^{-2} 5.52 7.08 10.31		Fan et al., 2016
As(III)	Activated carbon				0.1 0.2 50 100 200	1.2	5	0.77×10^{-2} 1.37×10^{-2} 2.85 5.03 7.57		Fan et al., 2016

2.6.4.1 Discussion on pollutant removal by CDI

A graphene nano-flakes electrode was fabricated for capacitive deionization because of better specific surface area and good electronic conductivity and this electrode was employed for ferric chloride electrosorption. An electrosorption capacity of 0.5 mg/g for an initial concentration of FeCl3 was reported. Electrosorption experiments were carried out for different ions and graphene nano-flakes electrode results were found in the order $Fe^{3+} > Ca^{2+} > Mg^{2+} > Na^+$ (Li et al., 2010c). Removal of boron present as boric acid form in water by CDI with activated carbon electrodes was reported by Avraham et al. (Avraham et al., 2011). It was removed in two steps. In the first step dissociation of boric acid proceeded done on the negative electrode due to local basic pH caused by polarizing the cell. Then electrosorption of borate ions was done at the positive electrode (Avraham et al., 2011). Zhang and coworkers reported that solar-powered CDI could be used for removal of arsenic from water. A Box–Behnken statistical experiment design was used to examine the effects of major process parameters. Experimental values and predicted values of arsenic removal were found in good agreement. Removal of arsenate ions by CDI favors lower salinity conditions and high pH (Zhang et al., 2016). Electrosorption of Cu^{2+} ions from aqueous solution by activated carbon electrodes was reported by Huang and coworkers (Huang et al., 2014a). At comparatively low voltage, electrodeposition of copper is restricted and Cu^{2+} ions removal on surface of electrode is due purely to electrostactic interaction in the electrical double-layer created in the nanoporous area. Further electrosorption experiments confirmed that Cu^{2+} ions were removed very selectively in a competitive environment over NaCl and NOM (Huang et al., 2014a). A study of a commercial CDI unit used for treatment of phosphate wastewater with various operating parameters was reported by Huang et al. (Huang et al., 2014b). Maximum removal (at flow rate 4.8 L/min and 50 mg P/L initial concentration) of phosphate was found to be 86.5%. The reported energy consumption was 7.01 kWh/kg P (removed) (or 1.65 kWh/m^3) (Huang et al., 2014b). Ryu et al. suggested a novel system for recovery of lithium with the help of electrostatic field assistance to improve the conventional adsorption process. They prepared a lithium-selective electrode with a lithium selective adsorbent and the hydrophilic PVA binder. A test set was fabricated by modifying the conventional MCDI technique. The adsorption performance for lithium by electrostatic field assistance was superior to that found with plain physisorption in the range of the initially tested lithium concentrations. The suggested system also showed good reproducibility and durability during repeated adsorption/desorption cycles (Ryu et al., 2015). A study of removal of Cd(II) ions from aqueous solution with a newly prepared manganese oxide/active carbon fiber (MO/ACF) electrode was reported by Chen et

68

al. (Chen et al., 2015). Results prove that the electrosorptive capacity of MO/ACF electrode was six times greater as compared to ACF. It has a greater adsorptive capacity compared to pure ACF because of more adsorptive sites and higher capacitance of MO/ACF. Hu et al. prepared of a manganese dioxide/carbon fiber (MnO_2/CF) electrode by anodic eletrodeposition and applied it for electrosoption of Cu^{2+} ions (Hu et al., 2015). Uniform distribution of MnO_2 nanoflowers with several "petals" was observed on the surface of the carbon fibers. MnO_2/CF electrode showed maximum adsorption capacity (172.88 mg/g) which was two times that of simple MnO2 absorbent without an electric field imposed (Hu et al., 2015). Work on removal of fluoride and nitrate removal by batch-mode CDI from brackish groundwaters was examined by Tang et al. (Tang et al., 2015). Removal experiments were carried out under different conditions such as feed concentration, flow rate and copresence of sodium chloride. At a constant concentration of sodium chloride, fluoride concentration was found to decline in the effluent with declining initial fluoride concentration. At higher initial concentration of chloride a higher equilibrium dissolved concentration of fluoride was found because of competitive electrosorption between fluoride and chloride for the limited pore surface sites. The authors have established a one-dimensional transport model for dual anions and found, that it consistently explains the dynamic process of removal of both fluoride and chloride ions in CDI cells at well-defined operating conditions. It was also used successfully for an explanation of nitrate removal from brackish ground waters (Tang et al., 2015). As(III) and As(V) removal by CDI with activated carbon electrodes was reported by Fan and coworkers (Fan et al., 2015). Result showed the sorption capacity is superior in the case of As(V) compared to As(III) because of the greater negative charge of the prevalent As(V) species. Results prove that electrosorption could be responsible for removal of As(V) whereas in case of As(III) the oxidation of As(III) to As(V) is involved, which could then be electrostatically adsorbed on the anode surface (Fan et al., 2015).

The CDI technology could be a promising technology in the field of pollutant ion removal due to its low energy consumption and ecofriendly regeneration of electrodes. According to literature reported, successive removal of pollutant ferric ions, boron, arsenic(III) and (V), copper(II), phosphate, lithium, cadmium (II), fluoride, nitrate, have been realized. Great progress in CDI technology for ground water and wastewater treatment is expected.

2.7 Isotherm modeling

The Langmuir, Freundlich (Chen et al., 2011; Li et al., 2010a) and Redlich Peterson isotherm models were used for single component system (Ozkaya 2006; Gupta et al. 2012a, 2013a). The multicomponent isotherm models, namely modified Langmuir, non modified Langmuir, extended Langmuir, extended Freundlich, modified Redlich Peterson and non modified Redlich Peterson were used for multicomponent system (Garg et al., 2004; Leitão and Serrão, 2005; Agarwal et al., 2013; Gupta, 2013b). The parameters in isotherms model were calculated by the nonlinear regression method in Microsoft excel 2013. All the equations of single and multicomponent isotherm models are mentioned bellow.

Single component isotherm model:

Langmuir

$$q_e = \frac{(Q_0 b C_e)}{(1 + b C_e)} \tag{2.27}$$

Freundlich

$$q_e = K_F C_e^{\frac{1}{n}} \tag{2.28}$$

Redlich–Peterson

$$q_e = \frac{K_{RP} \times C_{eq}}{1 + a_{RP} \times C_{eq}^{\beta}} \tag{2.29}$$

Multi component isotherm models:

Non modified Langmuir

$$Q_{e,i} = \frac{(Q_{0,i} b_i C_{e,i})}{(1 + \sum_{j=1}^{N} b_j C_{e,j})} \tag{2.30}$$

Modified Langmuir

$$Q_{e,i} = \frac{(\frac{Q_{0,i} b_i C_{e,i}}{\eta_i})}{(1 + \sum_{j=1}^{N} b_j (\frac{C_{e,j}}{\eta_j}))} \tag{2.31}$$

Extended Langmuir

$$Q_{e,i} = \frac{(Q_{0,i} b_i C_{e,i})}{(1 + \sum_{j=1}^{N} b_j C_{e,j})} \tag{2.32}$$

Extended Freundlich

$$Q_{e,i} = \frac{(K_{F,i} C_{e,i}^{\frac{1}{n,i+x,i}})}{(C_{e,i}^{x,i} + y_i C_{e,j}^{z,i})} \tag{2.33}$$

Non Modified R–P model

$$Q_{e,i} = \frac{K_{RP_i} C_{eq_i}}{1 + \sum_{j=1}^{N} a_{RP_j} (C_{eq_j})^{\beta_j}} \tag{2.34}$$

Modified R–P model

$$Q_{e,i} = \frac{K_{RP_i} \times (C_{eq_i} / \eta_{RP,i})}{1 + \sum_{j=1}^{N} a_{RP_j} (C_{eq_j} / \eta_{RP,j})^{\beta_j}} \tag{2.35}$$

MPSD was used to estimate the equilibrium adsorption data. To define the best isotherm model, MPSD may be produced as follows (Annadurai et al., 2000; Mall et al., 2006):

$$MPSD = 100 \sqrt{\frac{1}{N-P} \sum_{i=1}^{n} \left(\frac{Q_{e,i}^{exp} - Q_{e,i}^{cal}}{Q_{e,i}^{exp}} \right)^2} \tag{2.36}$$

2.8 Kinetic modeling

The nature of sorption process is generally checked by kinetic modeling. It is useful to find out equilibrium time and the mechanism of adsorption, such as physisorption and chemisorption. In the present study various kinetic models were used which are available in the literature (Gupta et al., 2012b; Wang et al., 2013b, Rakhshaee et al., 2006).

Pseudo first order model is

$$\log q_e - q_t = \log q_e - \frac{k_1}{2.303} t \tag{2.37}$$

Pseudo second orders is

$$\frac{t}{q_t} = \frac{1}{k_2 q_e^2} + \frac{t}{q_e} \tag{2.38}$$

ARE was calculated for the validation of kinetic model (Kumar et al., 2011).

$$ARE\% = \sqrt{\sum_{i=1}^{N} \left(\frac{Q_{e,i}^{exp} - Q_{e,i}^{cal}}{Q_{e,i}^{exp}} \right)^2} \times \frac{100}{N} \tag{2.39}$$

2.9 Detailed objectives

With use of an extensive literature review following detailed objectives have been formulated

1. Selection of NF and RO flat sheet membrane for the simultaneous removal of Cr(VI) and fluoride from binary synthetic solution of Cr(VI) and fluoride.

2. Preparation of synthetic single and multicompment solution of chromium (VI) and fluoride.

3. Characterization of flat sheet membranes (NF300, PN40, NF500 and RO) with different technique, namely, SEM, AFM, FTIR.

4. Estimation and identification of best flat sheet membrane for simultaneous removal of Cr(VI) and fluoride from binary synthetic solution by NF and RO.

5. Estimation of membrane transport parameters by membrane transport model such as CFSK model and CFSD model. Identification of best suitable membrane transport model.

6. Characterization of industrial wastewater with different wastewater analysis techniques.

7. Application of best flat sheet NF and RO membrane used for simultaneous removal of Cr(VI) and fluoride from actual industrial wastewater.

8. Selection of waste biomass/agriculture material for the preparation of activated carbon such as tea waste, limonia acidissima (wood apple) shell, rice husk.

9. Preparation of activated carbon from tea waste, wood apple shell, rice husk with acid treatment and thermal modification.

10. Analysis of activated carbon of tea waste, wood apple shell, rice husk with different characterization technique such as SEM, FTIR, TGA /DTA/DTG.

11. Preparation of porous activated carbon electrodes from different activated carbon such as commercial activated carbon, tea waste activated carbon, wood apple shell activated carbon, rice husk activated carbon.

12. Application of activated carbon electrodes from different activated carbon such as commercial activated carbon, tea waste activated carbon, wood apple shell activated carbon, rice husk activated carbon in the CDI process for treatment of Cr(VI) and fluoride.

13. To study the effect of different parameters such as voltage, flowrate, concentration on the simultaneous removal of Cr(VI) and fluoride by CDI.

14. Performance identification of best activated carbon electrode for simultaneous removal of Cr(VI) and fluoride from the binary synthetic solution of Cr(VI) and fluoride.

15. To study and parameters estimation of single component isotherms models namely Langmuir, Freundlich and Redlich Peterson model were applied for monocomponent system for experimental results for the removal of Cr(VI) and fluoride from binary synthetic solution by CDI.

16. To study and parameters estimation of the multicomponent isotherms model were used, namely, modified Langmuir, non-modified Langmuir, extended Langmuir, extended Freundlich, modified Redlich Peterson and non-modified Redlich Peterson.

17. Identification of best suitable isotherm model from single and multicomponent isotherm models for the simultaneous removal of Cr(VI) and fluoride from binary synthetic solution by CDI.

18. To study and parameters estimation of kinetic models, namely, pseudo first order, Pseudo second orders for experimental results for simultaneous removal of Cr(VI) and fluoride from binary synthetic solution by CDI.

19. Identification of best suitable kinetic model for simultaneous removal of Cr(VI) and fluoride from binary synthetic solution by CDI.

20. Application of best activated carbon electrode used for simultaneous removal of Cr(VI) and fluoride from actual industrial wastewater by CDI.

2.10 Conclusive Remarks

From above literature review it has been found that no studies has been reported on the simultaneous removal of Cr(VI) and fluoride from synthetic and industrial wastewater by CDI and membrane separation process.

EXPERIMENTAL SET UP AND INSTRUMENTATION

3.1 Motivation

This chapter deals with the experimental setup and instrument used for the present study on the simultaneous removal of Cr(VI) and fluoride from synthetic binary solution and actual industrial wastewater by membrane separation (NF and RO membrane) and CDI with different activated carbon electrode. Further the experimental design, range of experimental parameter, details of setup and analytical instruments used in the present study are described in this chapter.

3.2 Preparation of binary solution of Cr(VI) and fluoride

In this study potassium dichromate ($K_2Cr_2O_7$) and sodium fluoride (NaF) salts were used for the preparation of synthetic binary solution of Cr(VI) and fluoride (1:1)(V/V). All the chemicals were used of analytical grade. Deionized (DI) water (Millipore Crop.) was used for the preparation of sample and stock solution. The stock solution of Cr(VI) and fluoride was prepared by dissolving known amount of sodium fluoride and potassium dichromate in deionize water.

3.3 Analysis method for Cr(VI) and fluoride

Analysis of Cr(VI) and fluoride was performed out according to the American standard method [APHA](Clesceri et al., 1998). UV spectrophotometer made of HACH (model DR5000) was used for analysis Cr(VI) in filtrate. For Cr(VI) analysis, filtrate sample was reacted with a diphenyl carbazide solution and H_2SO_4 and let them stand for 10 min for full color development and its absorbance was taken at 540 nm. The residual concentration of fluoride was measured with ion chromatography.

3.4 Experimental set up of membrane separation

The experiments were carried out using a Perma®-pilot scale membrane system (Permionics, Vadodara, India) that utilizes cross flow filtration technique. A schematic diagram of the experimental setup is shown in Fig. 3.1 and actual digital photographs are shown in Fig. 3.2. The main components of the set-up can be separated into the following:

1) Feed tank (20 L)

2) Pipe network (SS 316)

3) Membrane module (flat plate module)

4) Pump with a damper (reciprocating pump with damper to stabilize pressure/flow of water)

5) Cooling water unit

The feed solution of different concentration was prepared by adding the appropriate amount of potassium dichromate and sodium fluoride to DI water. The experiments were performed with the commercial flat membrane NF and RO membranes (Permionics). The membrane housing cell is made of stainless steel (SS 316) of size (240mm (L) x 180mm (W) x 25mm thickness), with two halves fastened together with high bolts. The top half of the cell contained the flow distribution chamber and the bottom half was used as the membrane support system along with the passage for permeates to flow. The effective surface area of the membrane is 150 cm^2 (15cm (L) x 10cm (W)). To provide sufficient mechanical support to the test membrane Millipore filter was laid over the perforated stainless steel gauge. To avoid leakage, the upper half of the test cell was equipped with a rectangular boundary of gasket material.
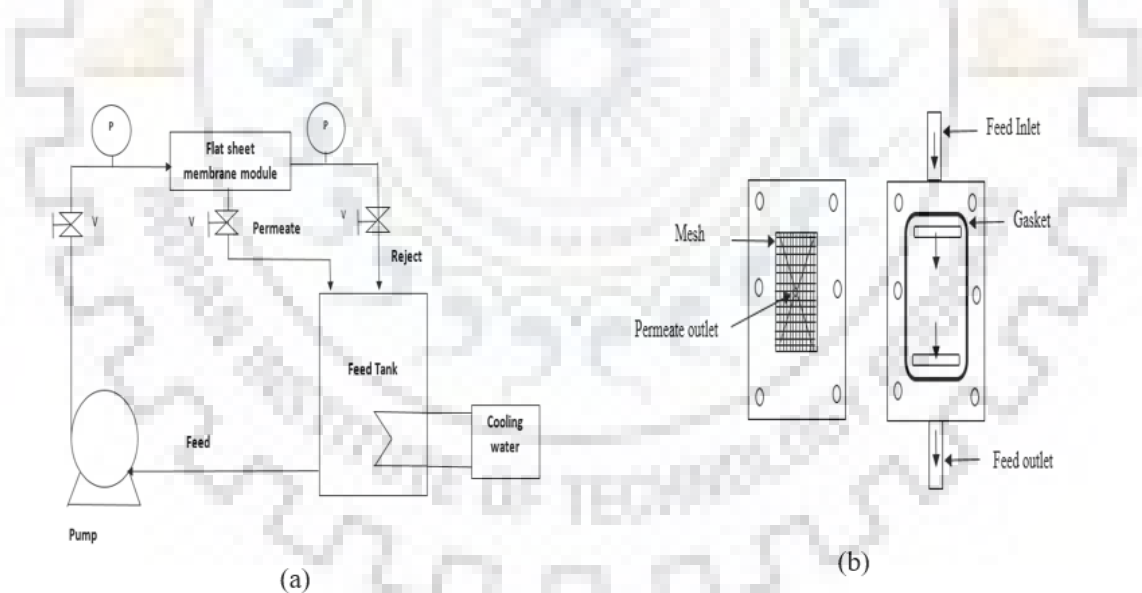
Fig. 3.1 Schematic of (a) Perma® -pilot scale membrane system (b) flat sheet membrane module.

Fig. 3.2 Perma® -pilot scale membrane system.

3.5 Experimental set up of CDI

3.5.1 Design and fabrication CDI Cell

The experimental lab scale set up in that CDI cell was fabricated from Plexiglas sheet. The Plexiglas sheet was cut in to two with the dimensions of 150 mm (L) x 150 mm (W). Another one thin Plexiglas sheet was cut in to the same dimensions (150 mm (L) x 150 mm (W)) which worked as separator frame. The separator frame having an inside cut of dimension (80mm (L) x 80mm (W)). Both sides of separator frame have 20 mm covered with a square boundary of gasket material (rubber gasket) to avoid leakage. Two supportive Plexiglas sheet and separator frame having holes on outer side for fastened together with nut and bolt. The effective surface area of the electrode is (80mm (L) x 80mm (W)). Detailed design of CDI cell is shown in the Fig.3.3.

3.5.2 Experimental CDI set up arrangements

The arrangement of the setup is schematically shown in Fig. 3.4 and actual digital photographs of CDI setup are shown in Fig. 3.5. Two activated carbon electrodes were assembled in CDI cell, these two electrodes were separated by nylon non conducting mesh and it was covered tightly with a Plexiglas sheet with screws. The experiments were carried out with batch mode lab scale CDI set up. Cr(VI) and fluoride mixed feed was supplied to CDI cell using peristaltic pump and circulated feed returned to feed the tank. The potential of 1.2 V was applied to the CDI cell by the DC power source at electrode terminals.

2 Plexiglas Sheet 2

150 mm

3 Separator Frame

100 mm
60 mm
80 mm
100 mm
150 mm

— Rubber Gasket
— Hole for nut and bolt
— Thin Plexiglas Sheet

1 Plexiglas Sheet 1

— Feed outlet
Feed Inlet —
150 mm

4 Nylon Mesh (Separator)

5 Activated Carbon Electrode

CDI Cell

6
Side view Front view
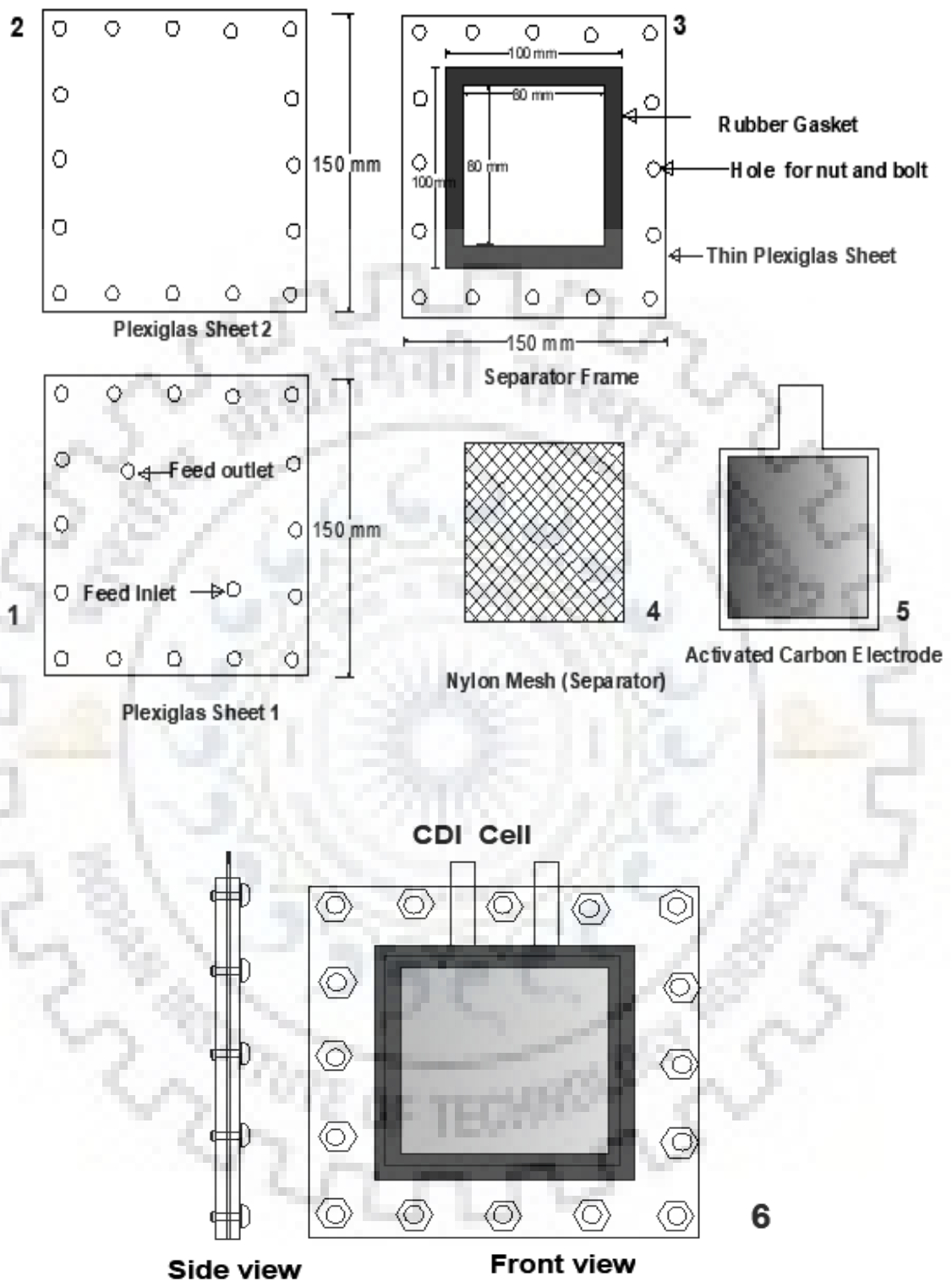
Fig. 3.3 CDI cell details design.
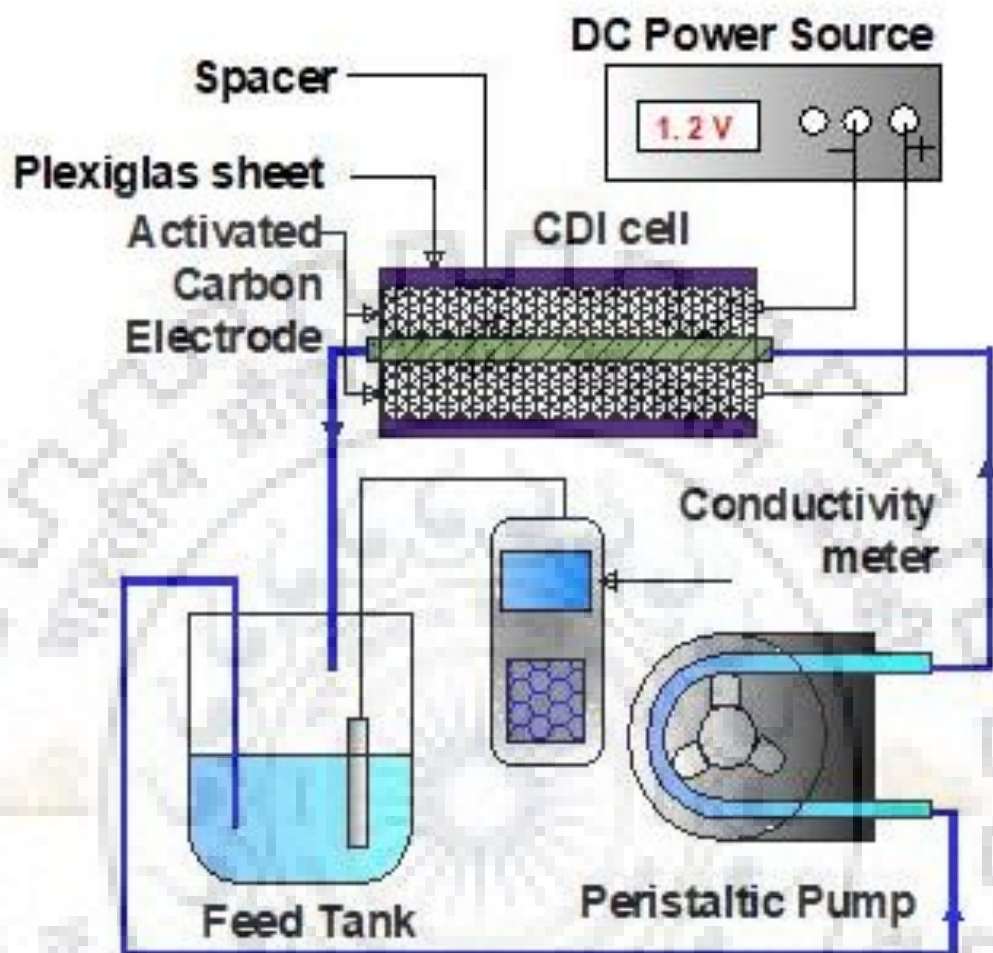
Fig. 3.4 Schematic of lab scale self-fabricated CDI set up.

(a) CDI experimental set up
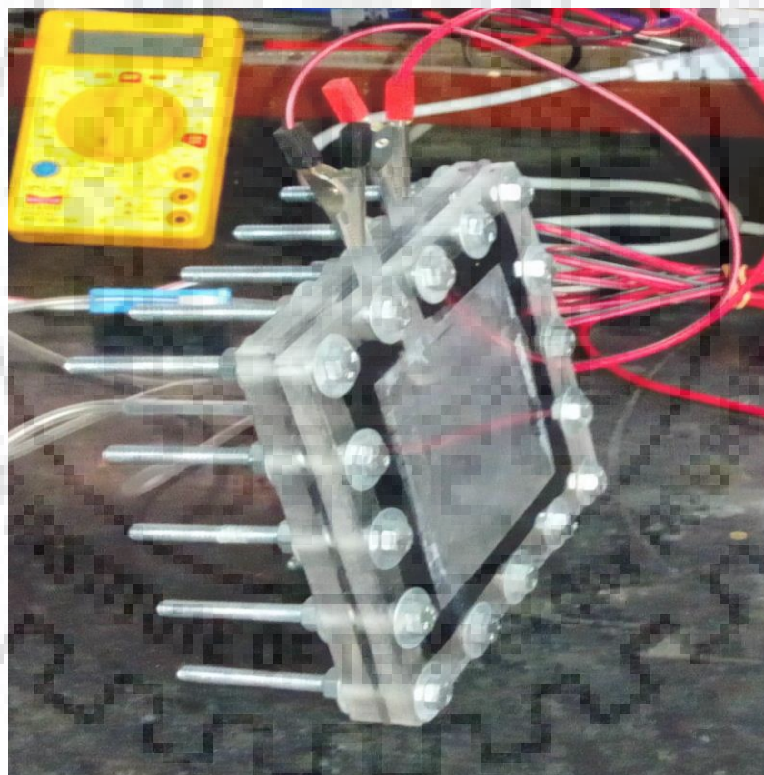
(b) CDI cell

Fig. 3.5 Digital photograph of lab scale self-fabricated CDI set up.

3.6 Analytical instruments used in the present study

Analytical instruments: UV-Vis Spectrophotometer, ion chromatography, cyclic voltammetry, Fourier Transform infrared spectrophotometer (FTIR), Fe- scanning electron microscope (SEM), Atomic force microscopy (AFM), Thermogravimetric analysis (TGA)/ Differential thermal analysis (DTA)/ derivative thermal gravimetric (DTG) analysis are used in the present study. The photographs of analytical instruments used in the present work are given in Fig. 3.6

3.7 Auxiliary equipments used in the present work

Auxiliary equipments used in the present work were hot air hoven, muffle furnace, magnetic stirrer, weighing balance, Milipore water system, pH meter, conductivity meter, TDS meter. The digital photographic images of all auxiliary equipments are mentioned in Fig. 3.7.

3.8 Calibration of equipment's

The instruments were calibrated with standard calibration process as mentioned by respected company manuals. The pH meter was calibrated with the standard buffer solution.

3.9 Summary of experiments conducted in the current study

In the present work various experimental runs of membrane separation and CDI process for treatment of Cr(VI) and fluoride were carried out and their details are systematically shown in Table 3.1.

(a) Ions Chromatography

(b) UV spectrophotometer

(c) SEM

(d) AFM

(e) FTIR

(f) TGA/DTA/DTG analysis

(g) ICP-MS
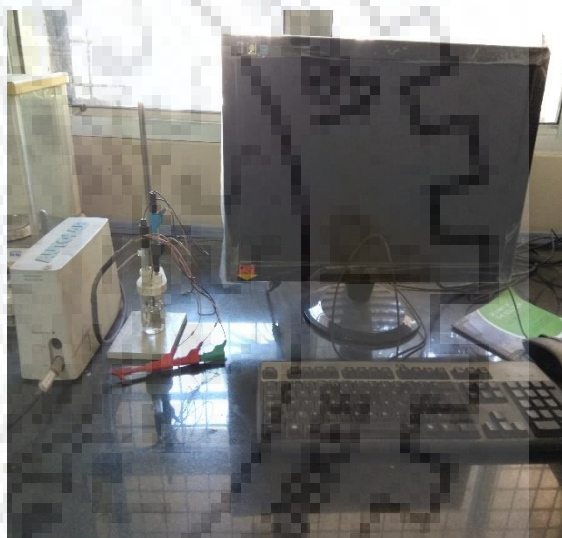
(h) Cyclic Voltammetry

Fig.3.6 Digital photograph of analytical instrument used in the present work.

(a) Muffle furnace

(b) Hot air oven

(c) Weighing Balance

(d) Millipore water

(e) Digital pH meter

(f) Digital conductivity meter

(g) TDS meter
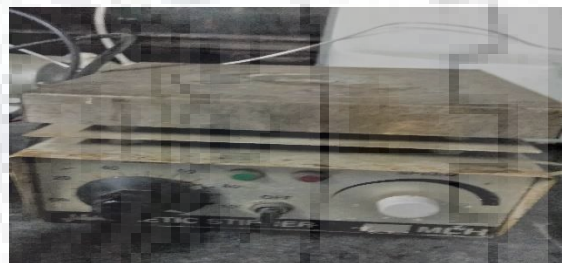
(h) Magnetic stirrer

Fig. 3.7 Digital photographic images of all auxiliary equipment's.

Table. 3.1 Summary of experiments conducted in the current study.

Experiments	Material used	Details study conducted	Synthetic wastewater	Industrial wastewater
Nanofiltration	Flatsheet NF300 membrane	Studies on effect of applied pressure effect on permeate flux with NF300.	1	24
		Studies on effect of applied pressure and feed concentration on percentage rejection of Cr(VI) and fluoride with NF300.	2	25
		Effect of pH on percentage rejection of Cr(VI) and fluoride with NF300.	3	-
	Flatsheet PN40 membrane	Studies on effect of applied pressure effect on permeate flux with PN40.	4	-
		Studies on effect of applied pressure and feed concentration on percentage rejection of Cr(VI) and fluoride with PN40.	5	-
		Effect of pH on percentage rejection of Cr(VI) and fluoride with PN40.	6	-
	Flatsheet NF500 membrane	Studies on effect of applied pressure effect on permeate flux with NF500.	7	-
		Studies on effect of applied pressure and feed concentration on percentage rejection of Cr(VI) and fluoride with NF500.	8	-
		Effect of pH on percentage rejection of Cr(VI) and fluoride with NF500.	9	-
Reverse osmosis	Flatsheet RO membrane	Studies on effect of applied pressure effect on permeate flux with RO membrane.	10	26
		Studies on effect of applied pressure and feed concentration on percentage rejection of Cr(VI) and fluoride with RO membrane.	11	27
		Effect of pH on percentage rejection of Cr(VI) and fluoride with RO membrane.	12	-

Capacitive deionization	CAC electrode	Studies on effect of applied voltage on conductivity change of binary feed of Cr(VI) and fluoride	13	-
		Studies on effect of flowrate on conductivity of binary feed of Cr(VI) and fluoride	14	-
		Studies on pH effect on removal of Cr(VI) and fluoride	15	-
		Studies on electrosorption of Cr(VI) and fluoride and regeneration of CAC electrode	16	-
		Studies on removal of Cr(VI) and fluoride with CAC electrodes	17	28
	TWBAC electrode	Studies on electrosorption of Cr(VI) and fluoride and regeneration of TWBAC electrode	18	-
		Studies on removal of Cr(VI) and fluoride with TWBAC electrodes	19	-
	RHAC electrode	Studies on electrosorption of Cr(VI) and fluoride and regeneration of RHAC electrode	20	-
		Studies on removal of Cr(VI) and fluoride with RHAC electrodes	21	-
	LASAC electrode	Studies on electrosorption of Cr(VI) and fluoride and regeneration of LASAC electrode	22	-
		Studies on removal of Cr(VI) and fluoride with LASAC electrodes	23	29

3.10 Concluding Remarks

This chapter gives brief description of the preparation of stock solutions, reagents and working solutions as well as provides an understanding of the designing of the experimental setup, summery of experimental runs, analytical instrumentals and auxiliary equipments and calibration of various instruments used in the present study.

EXPERIMENTAL PROGRAM

4.1 General

After thorough study of literature review, aims and objectives have been framed, and consequently an extensive research program on Cr(VI) and fluoride simultaneous removal from synthetic and actual electronic process industrial wastewater by using membrane separation, especially NF and RO pilot scale set up and CDI (lab scale set up) has been made. This chapter deals with the materials and methods, experimental procedures adopted to carry out the present work.

4.2 Experimental program

Experimental program was formulized to achieve the objectives of the research work. In the present study, a batch experiments were carried out for removing Cr(VI) and fluoride from both synthetic wastewater and industrial wastewater using various types of treatment methods, summarized in Fig. 4.1.

4.3 Membrane separation process

4.3.1 Chemical used

All the chemicals used in the experiments were of analytical reagent (AR) grade. Anhydrous potassium dichromate ($K_2Cr_2O_7$), sodium fluoride (NaF), Suphuric acid (H_2SO_4), were procured from HiMedia, Mumbai.

Commercial Nanofiltration NF300, PN40, NF500 and RO flatsheet membranes (Permionics, Vadodara, India) used for experimentation and detail specifications are systematically provided in table 4.1.
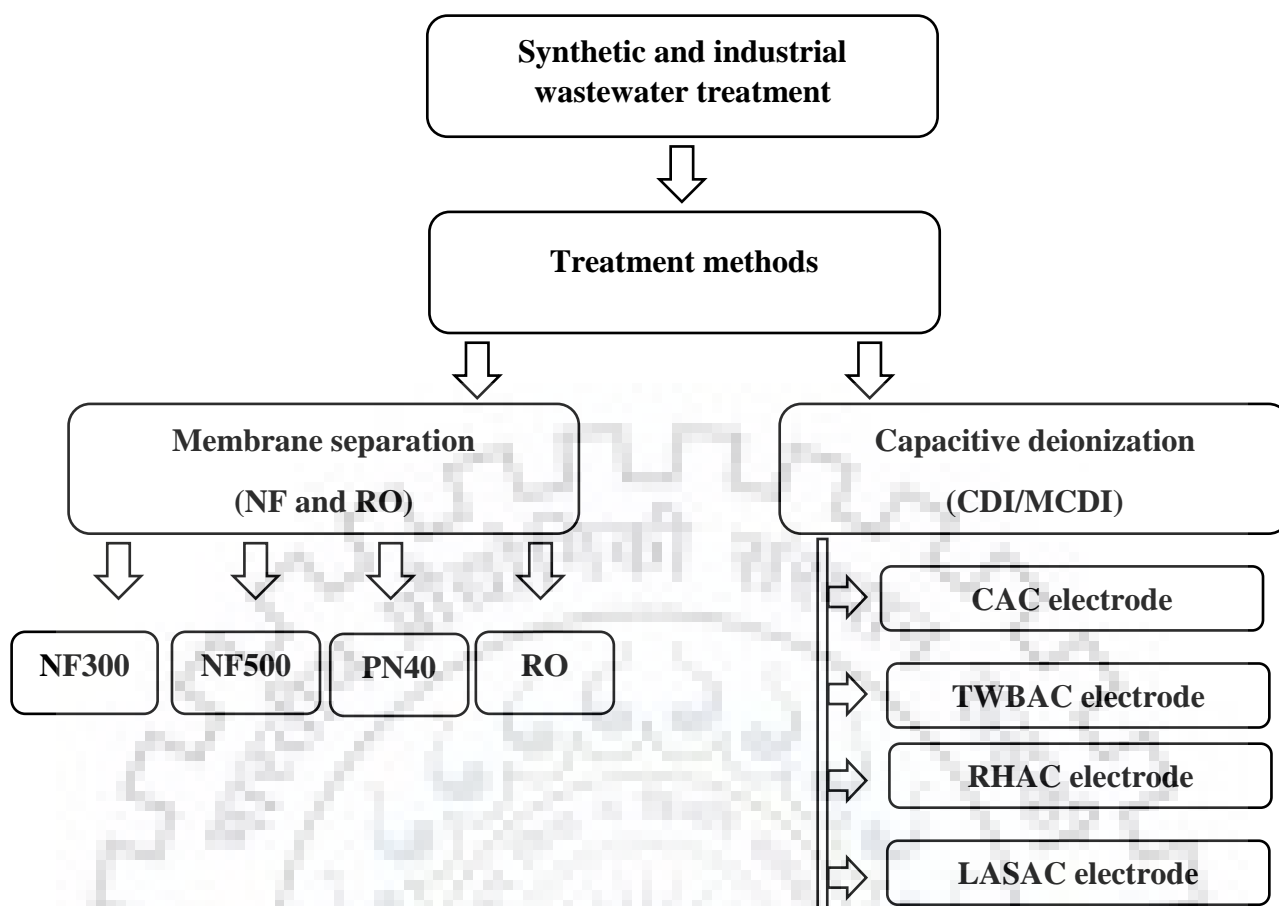
Fig. 4.1. Processes used for treatment of synthetic and industrial wastewater.

Table 4.1 Specifications of commercial membranes.

No.	Membrane Name	MWCO (Da)	Polymer material	pH range	Max. temp (°C)
1	NF 500 Membrane	500	Polyamide	2-11	40
2	NF 300 Membrane	300	Polyamide	2-11	40
3	NF Membrane (PN-40)	600	Polyamide	3-9	40
4	Membrane Sheet RO	*	Polyamide	3-9	40

Note: * Sodium chloride rejection 98%

4.3.2 Experimental program of membrane separation (NF/RO) study

In the present study, batch experiment has been carried for Cr(VI) and fluoride simultaneous removal from both synthetic wastewater and real industrial wastewater by the membrane separation process. Fig.4.2. Delineates the complete sequence of the experiments performed using commercial pilot scale Perma® membrane system (Permionics Membranes Pvt. Ltd., Vadodara, India).
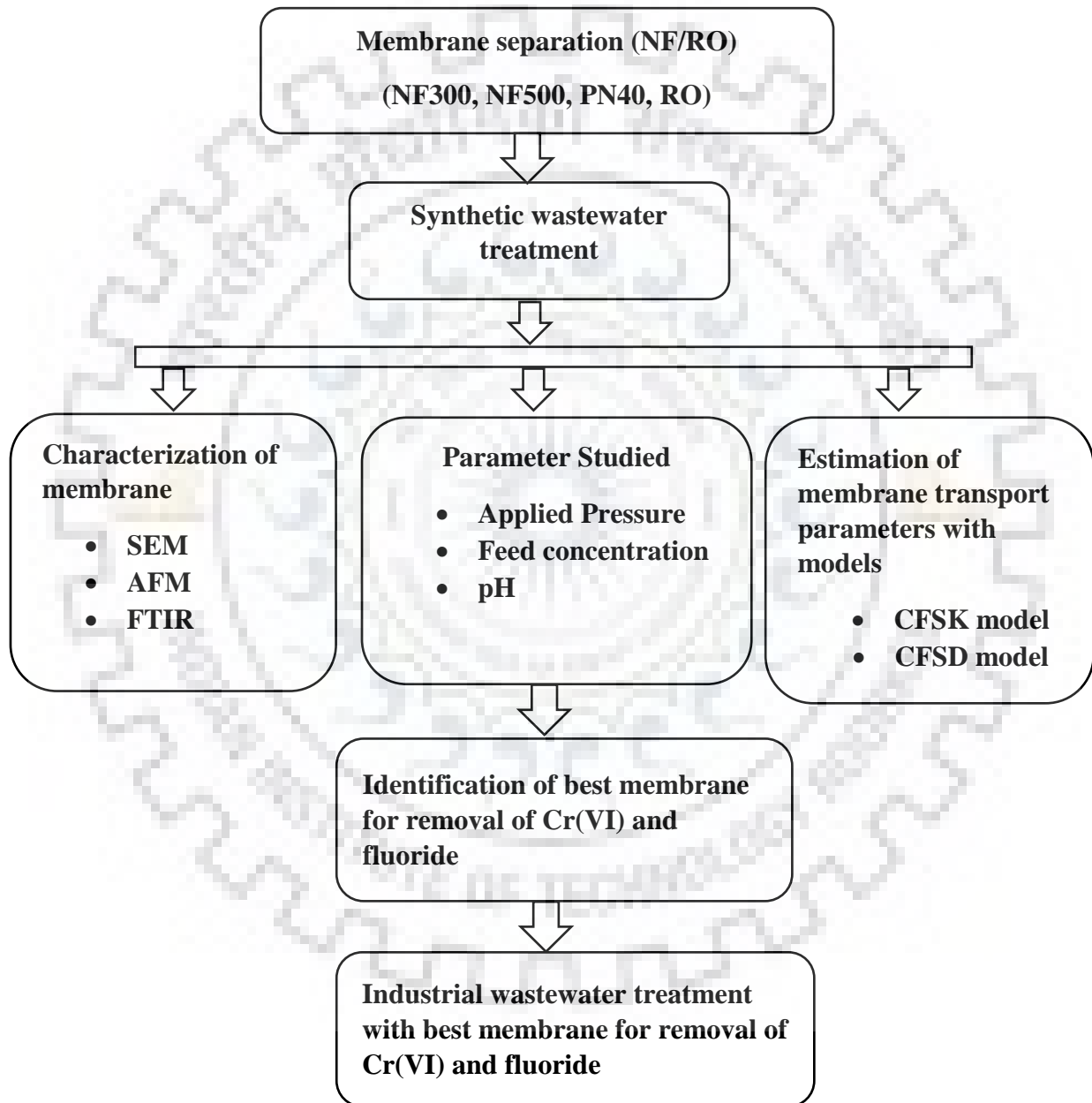
Fig. 4.2 Experimental programs for treatment of synthetic and industrial wastewater by membrane separation process.

4.3.3 Experimental procedure of membrane separation

Before starting the experiments, the membrane is conditioned by filtrating distilled water at experimentation pH (6-7) to reach the maximum permeability coefficient of the membrane. In order to avoid membrane compaction the membrane is stabilized for 2 hours at 10 bar (maximum pressure used in the experiments). After the above stabilization process, pure water permeability was measured at different pressures starting from high pressure to low pressure. The experiments were performed in the batch circulation mode and hence the sample of permeate. Permeate and retentate were recycled to the feed vessel in order to keep the constant feed concentration. The experiments were carried out for different feed concentration (5-100 mg/L), feed pressure (2-10 bar for NF and 4-20 bar for RO), and at different pH (2-10) and corresponding to it flux (J_v) and observed rejection (R_o) are measured. After each set of experiments for a given experimental condition, the set-up was rinsed with DI water for 30 min at 2 bar to clean the system.

Cleaning of membrane is usually essential to recover the flux reduced by fouling and reuse the same membrane for different experimental runs. Here, membrane fouling was not a major problem mainly due to the use of synthetic Cr(VI) and fluoride feed solution. Initially, only distilled water was used to find the flux of the membrane. A very small decrease in DI water flux was observed after each experimental run. This flux drop was recovered by cleaning the membrane with very dilute citric acid solution (1% strength). After every run feed, the feed tank was filled with DI water and citric acid solution and the membrane was cleaned by flushing at higher flow rate (16 L/min). After cleaning, distilled water was allowed to pass through the membrane in order to compare with initial distilled water flux. This test indicated whether the membrane had been cleaned properly or not.

4.3.4 Characterization and analysis

The permeate and feed samples collected containing Cr(VI) and fluoride during the course of experimentation. The analysis of Cr(VI) was done according to the standard diphenylcarbazide method (Clesceri et al., 1998) with a UV spectrophotometer (Hach DR-5000, HACH Co., USA). Fluoride analysis was done by ion chromatography (Metrohm compact IC, Switzerland). Morphological, surface roughness and chemical composition of NF300, NF500, PN40, TFC RO membranes were carried out with scanning electron microscopy (SEM) (FE-SEM Quanta 200 FEG), atomic force microscopy (AFM) (NT-MDT-INTEGRA) and Fourier transform infrared (FTIR) (Perkin Elmer spectrum GX range spectroscopy).

4.3.5 Studies on effect of applied pressure and feed concentration on percentage rejection

In this experiment influence of pressure on removal of Cr(VI) and Fluoride was studied by changing pressure like pressure (2-10 bar for NF and 4-20 bar for RO) with a concentration range of 5 -100 mg/L of Cr(VI) and fluoride each. All the experiments with using NF300, NF500, PN40 and RO flat sheet membranes were repeated thrice and average results have been presented in Annexure A-I.

4.3.6 Studies on effect of applied pressure effect on permeate flux

Pressure effect on permeate flux of binary mixture of Cr(VI) and fluoride feed at different feed concentration were studied. All the experiment with using NF300, NF500, PN40 and RO flat sheet membrane were repeated thrice and average results have been reported in Annexure A-I.

4.3.7 Effect of pH on percentage rejection

The effect of pH was investigated in the range of 2- 10 which is in the working range of NF300, NF500, PN40 and RO flat sheet membrane also the effect of pH on percent rejection with different feed concentration (5-100 mg/L) of Cr(VI) and fluoride were studied. All the experience with using NF300, NF500, PN40 and RO flat sheet membrane were repeated thrice and average results have been reported in Annexure A-I.

4.3.8 Estimation of membrane transport parameters

The membrane transport parameters estimation and membrane performance evaluation were carried out with two CFSK model and CFSD model. This is systemically described in the section 2.3.5. The mass transfer coefficient (k) and membrane transport parameters such as reflection coefficient (σ) and solute permeability (P_m) were simultaneously estimated by using CFSK model by providing the data of R_o and J_v at different pressures by maintaining constant flowrate and constant concentration of feed. Similarly $D_{AM}K/\delta$ and k can be evaluated with CFSD model using known Ro vs. Jv data, at constant feed concentration and different pressures.

4.4 Capacitive deionization

4.4.1 Chemical and membrane used

All the chemicals used in the experiments were of analytical reagent (AR) grade. Anhydrous potassium dichromate ($K_2Cr_2O_7$), sodium fluoride (NaF), Suphuric acid (H_2SO_4), were procured from HiMedia, Mumbai. Anion exchanged membrane (AMI-7001S) and cation exchanged membrane (CMI-7000S) (Membranes International Inc. USA), Graphite powder (Loba Chemie, Mumbai, India) and polyvinylidene fluoride (Hi Media laboratories Pvt. Ltd, Mumbai, India), N, N-dimethylacetamide (Loba Chemie, Mumbai, India).

4.4.2 Experimental program of CDI

In the present study, batch experiment has been carried for simultaneous removal of Cr(VI) and fluoride from both synthetic wastewater and industrial wastewater by CDI process. Fig. 4.3 indicate the complete sequence of the experiments of CDI with various types of electrode for removal of Cr(VI) and fluoride.

4.4.3 Activated carbon preparation

Steps of activated carbon preparation (refer Fig. 4.4) from waste biomass such as tea waste, rice husk, limonia acidissima shell were collected from different place. The details of activated carbon preparation process are discussed in this section. The chemically modified and thermal treated activated carbon were prepared and it was used for further work.

```
┌──────────────────────────────────────────────┐
│         CDI set up design and fabrication     │
└──────────────────────────────────────────────┘
                        ⇩
┌──────────────────────────────────────────────┐
│      Selection of waste biomass (TW, RH, LAS) │
└──────────────────────────────────────────────┘
                        ⇩
┌──────────────────────────────────────────────┐
│   Preparation of waste biomass activated carbon│
│                  (TW, RH, LAS)                 │
└──────────────────────────────────────────────┘
                        ⇩
┌──────────────────────────────────────────────┐
│  Fabrication of (CAC, TWBAC, RHAC, LASAC)     │
│                   electrodes                   │
└──────────────────────────────────────────────┘
                        ⇩
┌──────────────────────────────────────────────┐
│ Identification of best electrode for simultaneous removal of │
│      Cr(VI) and fluoride synthetic wastewater │
└──────────────────────────────────────────────┘
```

Characterization technique used	CDI experiment for synthetic wastewater treatment	Parameters Studied
• SEM • FTIR • TGA/DTA/DTG • CV	• CAC electrode • TWBAC electrode • RHAC electrode • LASAC electrode	• Voltage • Feed concentration • Flowrate

```
                        ⇩
┌──────────────────────────────────────────────┐
│  • Estimation of parameters with isotherm model│
│  • Estimation of parameters with kinetic model │
│  • Identification of best suitable isotherm and kinetic model │
└──────────────────────────────────────────────┘
                        ⇩
┌──────────────────────────────────────────────┐
│ Investigation of best electrode performance for removal of │
│   Cr(VI) and fluoride industrial wastewater with MCDI │
└──────────────────────────────────────────────┘
```

Fig. 4.3 Experimental programs for treatment of synthetic and industrial wastewater by CDI process.

```
┌─────────────────────────┐      ┌─────────────────────────┐      ┌─────────────────────────┐
│ Waste biomass collection│      │ Waste biomass           │      │ Waste biomass           │
│                         │      │ washed with hot         │      │ washed with DI          │
│  • Tea waste (TW)       │  ⇨   │ water to remove         │  ⇨   │ water to and            │
│  • Limonia acidissima   │      │ impurities dirt,        │      │ dried in hot air        │
│    (wood apple) shell   │      │ color etc.              │      │ oven                    │
│    (LAS)                │      │                         │      │                         │
│  • Rice husk (RH)       │      │                         │      │                         │
└─────────────────────────┘      └─────────────────────────┘      └─────────────────────────┘
                                                                              ⇩
┌─────────────────────────┐      ┌─────────────────────────┐      ┌─────────────────────────┐
│ Acid treated waste      │      │ Acid treated            │      │ Dried waste             │
│ biomass washed were kept│      │ waste biomass           │      │ biomass were            │
│ in muffle furnace for   │  ⇦   │ washed with DI          │  ⇦   │ put in                  │
│ thermal treatment       │      │ water to and            │      │ concentrated            │
│                         │      │ dried in hot air        │      │ sulfuric acid for       │
│                         │      │ oven                    │      │ 12 hours                │
└─────────────────────────┘      └─────────────────────────┘      └─────────────────────────┘
        ⇩
┌─────────────────────────┐
│    Activated Carbon     │
└─────────────────────────┘
```

Fig. 4.4 Steps of activated carbon preparation from waste biomass.

4.4.3.1 Preparation of tea waste activated carbon (TWBAC)

Tea waste biomass was collected from a local tea shop located in the campus of IIT Roorkee. Tea waste biomass was boiled for 15-20 min to remove impurities, color and sugar from that. Next, tea waste biomass was washed serval times with DI water and dried at 60 $^{\circ}$C in hot air oven for overnight. Further, the dried tea waste biomass was used for acid treatment study. Dry tea waste biomass was put in concentrated sulfuric acid for 12 h and washed with DI water and again dried in oven for overnight at 60 $^{\circ}$C. Then acid treated tea waste biomass was kept in a muffle furnace at the 450 $^{\circ}$C for 2 h for thermal treatment. Finally chemically modified and thermal treated TWBAC was prepared and it was used for further work.

4.4.3.2 Preparation of rice husk activated carbon (RHAC)

Rice husk were washed with DI water several times to remove dirt and impurities further it was dried at 60 $^{\circ}$C in hot air oven for overnight. Dried rice husk was kept in concentrated H_2SO_4 for 12 hours and wash with DI water and again dried in oven for overnight at 60°C. Then acid treated rice husk was kept in a muffle furnace at the 500 $^{\circ}$C for 3 hours for thermal treatment.

The chemically treated and thermal treated RHAC was changed to powder form and used for electrode fabrication.

4.4.3.3 Preparation of *Limonia acidissima* shells (wood apple) activated carbon (LASAC)

Limonia acidissima shells were broken into small pieces and several times washed with deionized water to remove dirt and impurities further it dried at $60^{\circ}C$ in hot air oven for overnight. Dried Limonia acidissima shells were kept in concentrated H_2SO_4 for 12 hours and washed with deionized waste and again dried in oven for overnight at $60^{\circ}C$. Then acid treated Limonia acidissima shells were kept in a muffle furnace at the $500^{\circ}C$ for 3 hours for thermal treatment. The chemically treated and thermal treated LASAC was changed to powder form and used for electrode fabrication.

4.4.4 Fabrication of electrodes

Steps of electrode preparation from activated carbon are schematically shown in Fig.4.5. The chemically modified and thermally treated activated carbon was converted into a fine powder. The activated carbon powder was mixed with graphite powder (Loba Chemie, Mumbai, India) and polyvinylidene fluoride (Hi Media laboratories Pvt. Ltd, Mumbai, India) and put into solvent N, N-dimethylacetamide (Loba Chemie, Mumbai, India). The blending solution was stirred for 6 h with magnetic stirrer to make homogeneous mixture. After the homogeneous mixing, the activated carbon casting mixture was cast on one side of the aluminum thin sheet and dried at $100^{\circ}C$ for 4h. Each activated carbon electrode has an effective surface area of 8 cm $\times$ 8 cm. The same procedure was applied for all waste biomass activated carbon electrode.

```
┌─────────────────────────────────────────────┐
│             Activated Carbon                 │
│     (CAC, TWBAC, RHAC, LASAC)                │
└─────────────────────────────────────────────┘
                      ⬇
┌─────────────────────────────────────────────┐
│          Convert in to fine powder           │
└─────────────────────────────────────────────┘
                      ⬇
┌─────────────────────────────────────────────┐
│  Activated carbon powder, graphite powder    │
│  and polyvinylidene fluoride (PVDF) were     │
│  put in N, N-dimethylacetamide solvent to    │
│     prepare electrode paste mixture          │
└─────────────────────────────────────────────┘
                      ⬇
┌─────────────────────────────────────────────┐
│  The electrode paste mixture was stirred     │
│  for 5 hours with magnetic stirrer to make   │
│          homogeneous mixture                 │
└─────────────────────────────────────────────┘
                      ⬇
┌─────────────────────────────────────────────┐
│  The homogeneous mixture was caste on one    │
│    side aluminum thin sheet and dried in     │
│                  oven                        │
└─────────────────────────────────────────────┘
                      ⬇
┌─────────────────────────────────────────────┐
│         Activated carbon electrode           │
└─────────────────────────────────────────────┘
```

Fig. 4.5 Steps of electrode preparation from activated carbon.

4.4.5 Experimental process of CDI

The meaning of CDI is a grouping of two words, first is capacitive and second is deionization. Deionization means the removal of ions which could be charged atoms or molecules. Capacitive deals with the act of capacitors supporting such removals. A capacitor, nothing but devices prepared from one or more couple of oppositely charge porous electrodes under the application of voltage to the electrodes creating a positive and negative pole. Salt solution pass through the space between two porous charged electrodes due to electrostatic force, cations (positive charge ions) and anions (negative charge ions) are attracted towards negative and positive electrode respectively. In this way removal of ions from water are carried out by using CDI process. In the CDI process, there are two main steps. The first one is purification and the second one is regeneration. The experimental parameters were set as feed concentrations (10, 25, 50 and 100 mg/L of Cr(VI) and fluoride) and voltage (0.4, 0.8 and 1.2 V) and time. The experimental setup consisted of CDI cell, peristaltic pump (M/S Ravel Hiteks Pvt. Ltd., Chennai, India), feed tank, DC power source (PS-3010), conductivity meter (HQ40d, HACH Co., USA). The experiments were carried out with batch mode lab scale CDI set up. Cr(VI) and fluoride mixed feed was supplied to CDI cell using peristaltic pump and circulated feed return to feed the tank. The potential 1.2 V was applied to the CDI cell by the DC power source at electrode terminals. The conductivity change of Cr(VI) and fluoride mix feed was measured with digital conductivity meter. The electrosorption capacity at equilibrium (q_e) was find using Eq. (4.1).

$$q_e = \frac{(C_o - C_e)V_f}{m} \qquad (4.1)$$

Where; V_f is volume (L) of feed in tank, m is mass (g) of activated carbon electrode, C_o and C_e represent the initial concentration and concentration at equilibrium stage respectively.

4.4.6 Characterization & analysis

The permeate and feed samples collected containing Cr(VI) and fluoride during the course of experimentation in that analysis of Cr(VI) was done according to the standard diphenylcarbazide method (Clesceri et al., 1998) with a UV spectrophotometer (Hach DR-5000, HACH Co., USA). Fluoride analysis was done by ion chromatography (Metrohm compact IC, Switzerland). The characterizations (Morphological, chemical composition) of activated carbon were carried out with scanning electron microscopy (SEM) (FE-SEM Quanta 200 FEG), and Fourier transform infrared (FTIR) (Perkin Elmer spectrum GX range

spectroscopy), TGA/DTA/DTG analysis of waste biomass was carried out using a thermal analysis instrument (PerkinElmer Pyris Diamond, USA).

4.4.7 Studies on effect of applied voltage on conductivity change of binary feed of Cr(VI) and fluoride

In the present study effect of voltage on conductive change of feed solution was investigated by changing voltage (0.4, 0.8 and 1.2 V) with electrode prepared from commercial activated carbon (CAC). The optimum voltage was set for further all experiments. All the experiments were repeated thrice and average results have been reported in Annexure A-I.

4.4.8 Studies on effect of flow rate on conductivity of binary feed of Cr(VI) and fluoride

In the present study effect of flowrate on conductive change of feed solution was carried out by changing flowrate (4, 8, 12, 16 and 20 mL/min) with electrode prepared from CAC. The optimum flow rate was set for further all experiments. All the experiment were repeated thrice and average results have been reported in Annexure A-I.

4.4.9 Studies on pH effect on removal of Cr(VI) and fluoride

The investigation study of pH effect on the removal of Cr(VI) and fluoride from feed solution was carried out by changing pH (3, 5, 7, 8, 9) with electrode prepared from CAC. The optimum pH was set for further all experiments. All the experiments were repeated thrice and average results have been reported in Annexure A-I.

4.4.10 Studies on electrosorption of Cr(VI) and fluoride and regeneration of electrode

The investigation of electrosorption of Cr(VI) and fluoride and regeneration of different electrode with 10 mg/L feed solution of Cr(VI) and fluoride was carried out. All the experiments were repeated thrice and average results have been reported in Annexure A-I.

4.4.11 Studies on removal of Cr(VI) and fluoride with different electrodes

The investigation of simultaneous removal of Cr(VI) and fluoride from feed solution of Cr(VI) and fluoride with different electrodes was carried out. All the experiments were repeated thrice and average results have been reported in Annexure A-I.

4.4.12 Studies on isotherm modeling

In the present work studies on mono and multicomponent isotherm models were carried out. The Langmuir, Freundlich and Redlich Peterson isotherm models were used for the single component system. The multicomponent isotherm models, namely modified Langmuir, non modified Langmuir, extended Langmuir, extended Freundlich, modified Redlich Peterson and non modified Redlich Peterson were used for multicomponent system. All the equations of single and multicomponent isotherm models are mentioned in section 2.7. The parameters in isotherms model were calculated by the nonlinear regression method in Microsoft excel 2013.

4.4.13 Kinetic study

The nature of sorption process is generally checked by kinetic modeling. It is useful to find out equilibrium time and the mechanism of adsorption, such as physisorption and chemisorption. In the present study various kinetic models are used which were available in the literature. All the equations of single and multicomponent isotherm models are mentioned in section 2.8.

4.5 Characteristics of industrial wastewater

For this study, water samples have been collected from the following locations: electronics process industry, Uttarakhand and the characteristics of industrial wastewater was analyzed through UV spectrophotometer, Ion chromatography, ICP-MS in the Institute Instrumentation Centre (IIC) and Department of Chemical Engineering, IIT Roorkee, India. Characterization of industrial wastewater is provided in Table 4.2. Synthetic wastewater was prepared based on electronics process effluent reported in literatures.

Table 4.2 Characterization of industrial wastewater (electronic process wastewater).

Parameter	Observed value
pH	8.01
TDS (mg/L)	1012
Conductivity (mS/cm)	1.310
Fluoride (mg/L)	35. 24
Chromium(VI) (mg/L)	11
Copper (mg/L)	0.06
Nickel (mg/L)	0.363
Cadmium (mg/L)	0.075
Mn (mg/L)	0.03
Fe (mg/L)	0.036
Pb (mg/L)	0.58
Zn (mg/L)	0.133
Phosphate(mg/L)	7.089

4.6 Concluding remarks

This section represents the experimental process and details procedure used for simultaneous removal of Cr(VI) and fluoride from synthetic solution and industrial wastewater. Moreover, details of experimental programs and procedures, adopted for Cr(VI) and fluoride removal by membrane separation (NF and RO) and CDI process have been described here.

RESULT AND DISCUSSION

5.1 Studies on Cr(VI) and fluoride removal by membrane separation (NF/RO)

In this study simultaneous removal of Cr(VI) and fluoride were carried out with different nanofiltration and reverse osmosis flat sheet membranes namely NF300, PN40, NF500, RO membranes.

5.1.1 Characterization of membranes

The characterizations of flat sheet commercial NF and RO membrane were carried with various techniques such as FTIR, SEM and AFM are described below.

5.1.1.1 FTIR analysis of membranes (NF300, PN40, NF500, RO)

The FTIR analysis of flat sheet commercial NF and RO membranes were carried which are systematically described as below.

FTIR analysis was done for NF300 and PN40 membranes. Fig.5.1 shows that the peak 3450 cm^{-1} and 3447 cm^{-1} which indicate the weak amide NH stretch. The 1646 cm^{-1} and 1640 cm^{-1} show the strong amide carbonyl (C$=$ O stretching). The presence of polyamide group was confirmed by bending vibration of amine group leading to NH_2 at 1646.06 cm^{-1}. The peaks at 1310 cm^{-1}, 1307 cm^{-1}, 1244 cm^{-1}, 1156 cm^{-1} and 1149 cm^{-1} indicate the sulfonic group with C─O bonding and the peak 1580 cm^{-1} is due to aromatic ring C─C stretching vibration and the being of strong absorption peak at 870 cm^{-1}, 861 cm^{-1}, 727 cm^{-1}, 723 cm^{-1} represent the polysulfone structure with aromatic C─H bending.

The chemical composition and vibration details of NF500 membrane has been made by FTIR analysis (Fig.5.2). Detailed description of peaks in FTIR graph are mentioned in Table 5.1.

The presence of the functional group, stretching and bending vibration details of polyamide RO membrane was carried out with FTIR analysis (Fig.5.3). Detailed information and explanations of FTIR peaks of RO membrane are presented in Table 5.2.
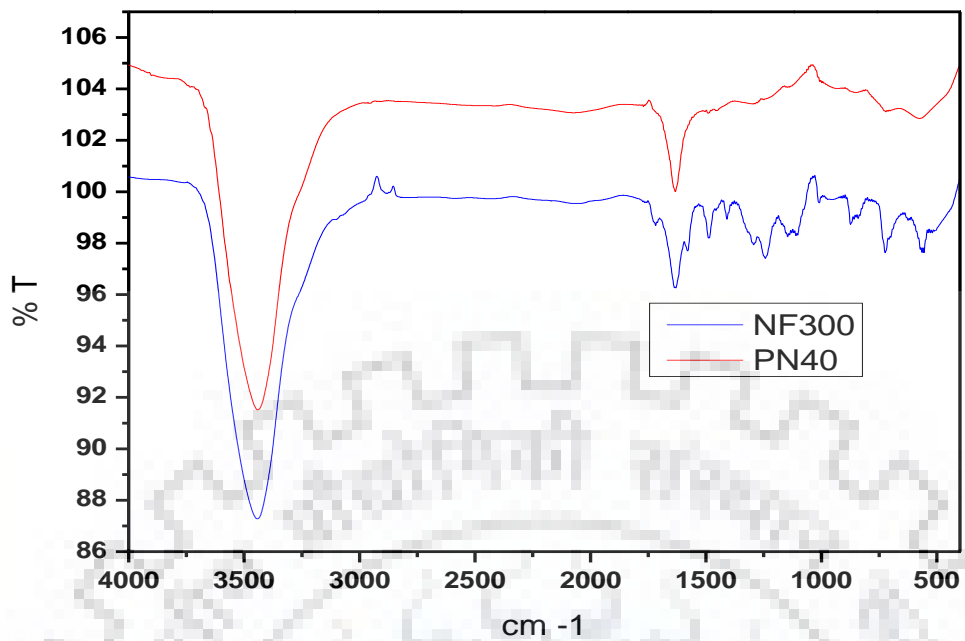
Fig. 5.1 FTIR image of NF300 and PN40 membranes.
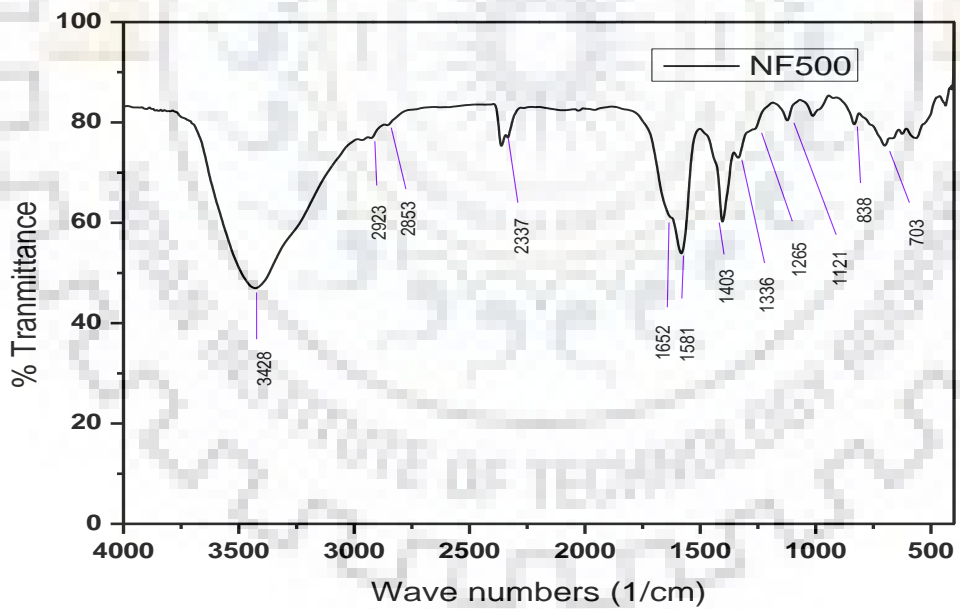
Fig. 5.2 FTIR image of NF500 membrane.

116

Table 5.1 FTIR analysis details of NF500 membrane.

Peak in FTIR graph	Vibration details	Chemical compositions details
3428 cm^{-1}	N−H stretching	Weak amides, primary and secondary amines
2923 cm^{-1}	CH$_2$ stretching	Anti-symmetric type aromatics
2853 cm^{-1}	C−H stretching	Alkane compounds
2337 cm^{-1}	C=N stretching	Nitrile group
1652 cm^{-1}	C=O stretching	Secondary amide
1575 cm^{-1}	C−C stretching vibration	aromatic ring compound
1403 cm^{-1}	OH bend stretching	-
1336 cm^{-1}, 1265 cm^{-1}, 1121 cm^{-1}	C−O stretching	presence of sulfonic group along
838 cm^{-1}, 703 cm^{-1}	Aromatic C−H bending	confirming polysulfone structure
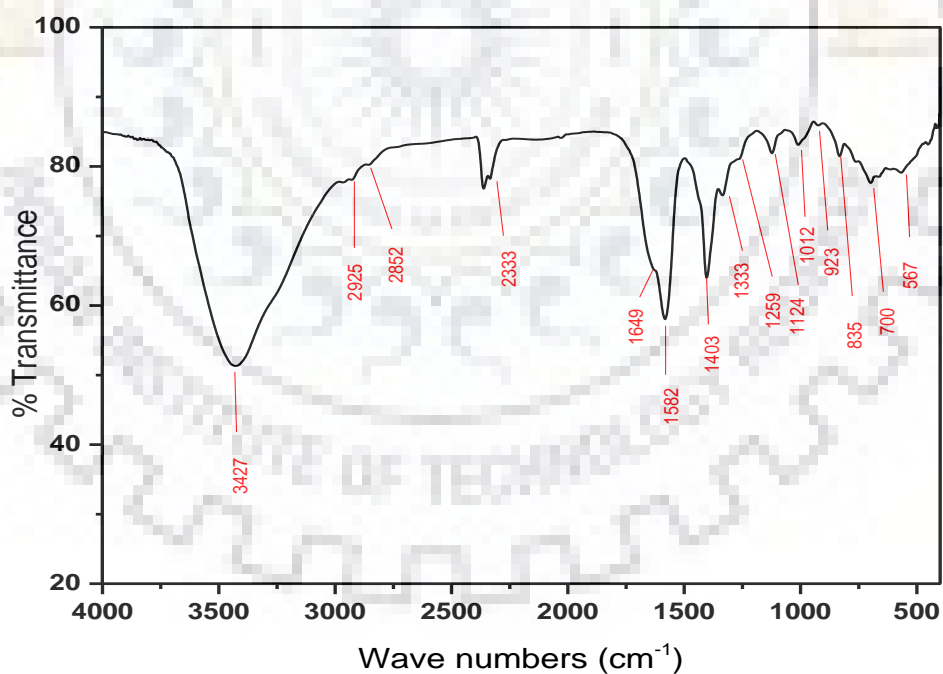
Fig. 5.3 FTIR image of polyamide RO membrane.

117

Table 5.2 FTIR analysis details of RO membrane.

FTIR Peak	Vibration and chemical compositions details
3427 cm^{-1}	N−H stretching Weak amides, primary and secondary amines
2925 cm^{-1}	CH$_2$ stretching Anti-symmetric type aromatics
2852 cm^{-1}	C−H stretching Alkane compounds
2333 cm^{-1}	C≡N stretching Nitrile group
1649 cm^{-1}	C=O stretching Secondary amide presence of polyamide group
1582 cm^{-1}	C−C stretching vibration aromatic ring compound
1403 cm^{-1}	OH bend stretching -
1333 cm^{-1}, 1259 cm^{-1}, 1124 cm^{-1}	C−O stretching presence of sulfonic group along
835 cm^{-1}, 700 cm^{-1}	Aromatic C−H bending confirming polysulfone structure

5.1.1.1.1 Conclusive Remark:

The presence of functional group, stretching and bending vibration details of NF300, PN40, NF500 and RO flat sheet membranes were confirmed with FTIR analysis.

5.1.1.2 SEM Analysis of membranes

The morphology of NF300 and PN40 membranes are presented in Fig.5.4. The images (Fig.5.4 (a) and (c)) shows top view of NF300 and PN40 membranes. It is observed that the asymmetric fiber structure on the top surface and fiber like structure is the active layer of polyamide of both membranes. Fig. 5.4 (b and d) show that, the cross sectional view of NF300 and PN40 membranes and three layers of this membrane are seen clearly. The first layer is polyamide polymer and this is the active layer where actual rejection of Cr(VI) and fluoride was done. The second layer and the third layer consist of polysulfone and polyester, respectively.

The morphological structures of NF500 are obtained by using SEM. Fig.5.5 (a-f) indicate the top surface morphology and cross sectional view of NF500 membrane at different magnifications. Top surface of NF500 represents asymmetric structure of active layer of polyamide polymeric material. Cross sectional view of NF500 membrane show the composite of three different layers of polymeric materials. The first layer is polyamide polymer layer structure of that layer has been shown at higher magnification in Fig. 5.5 (e). This is the active layer where actual rejection of Cr(VI) and fluoride was done. The second layer and third layer consist of polysulfone and polyester respectively.

Polyamide RO membrane morphological structures study was obtained with SEM. Fig.5.6 (a, c) show the top surface morphology and Fig.5.6 (b, d) indicates the cross sectional view of the polyamide RO membrane. The top surface of the polyamide RO membrane represents asymmetric structure active layer of polyamide polymeric material. Composite nature of polyamide RO membrane was observed in cross sectional view of polyamide RO membrane composite. There layers are polyamide, polysulfone and polyester respectively. The first layer is polyamide polymer layer. This is the active layer where actual rejections of fluoride and Cr(VI) were done.
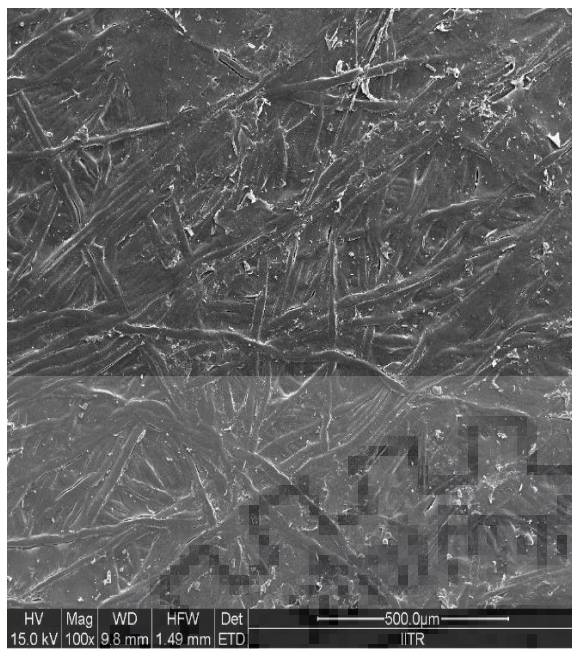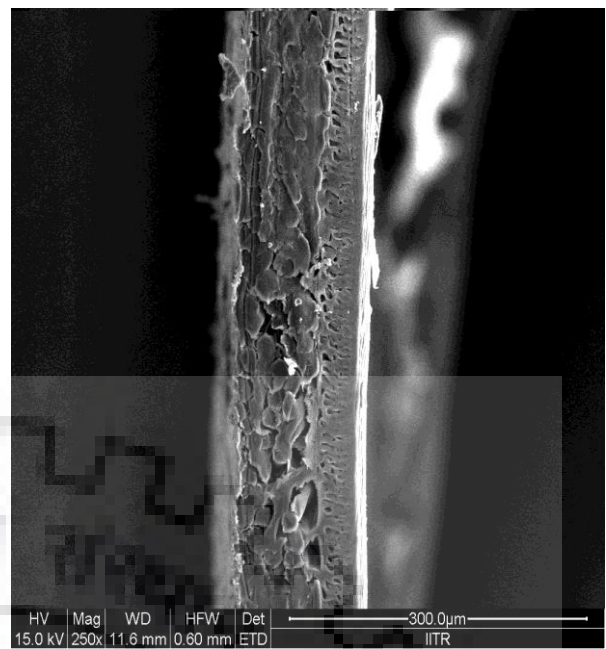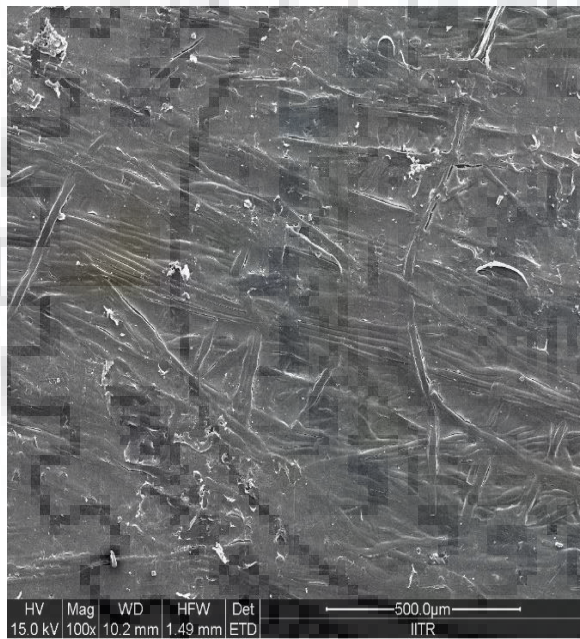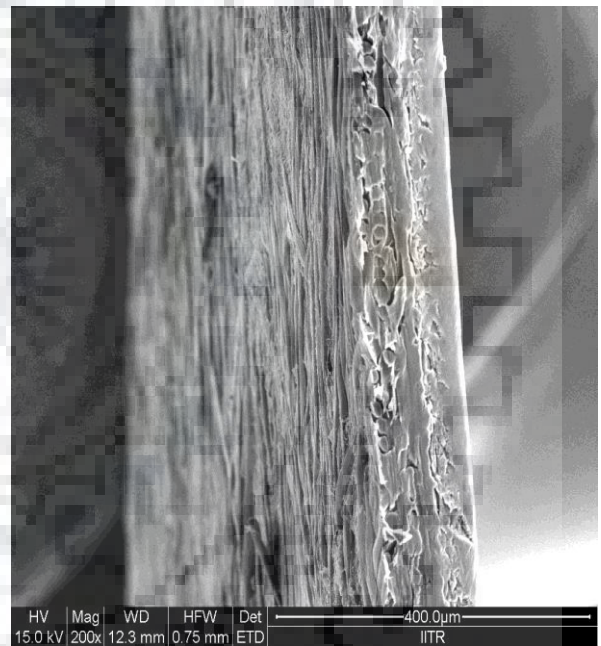
Fig. 5.4 SEM images of commercial NF membranes (a) Top view of NF300 (b) Cross sectional view of NF300 (c) Top view of PN40 (d) Cross sectional view of PN40.
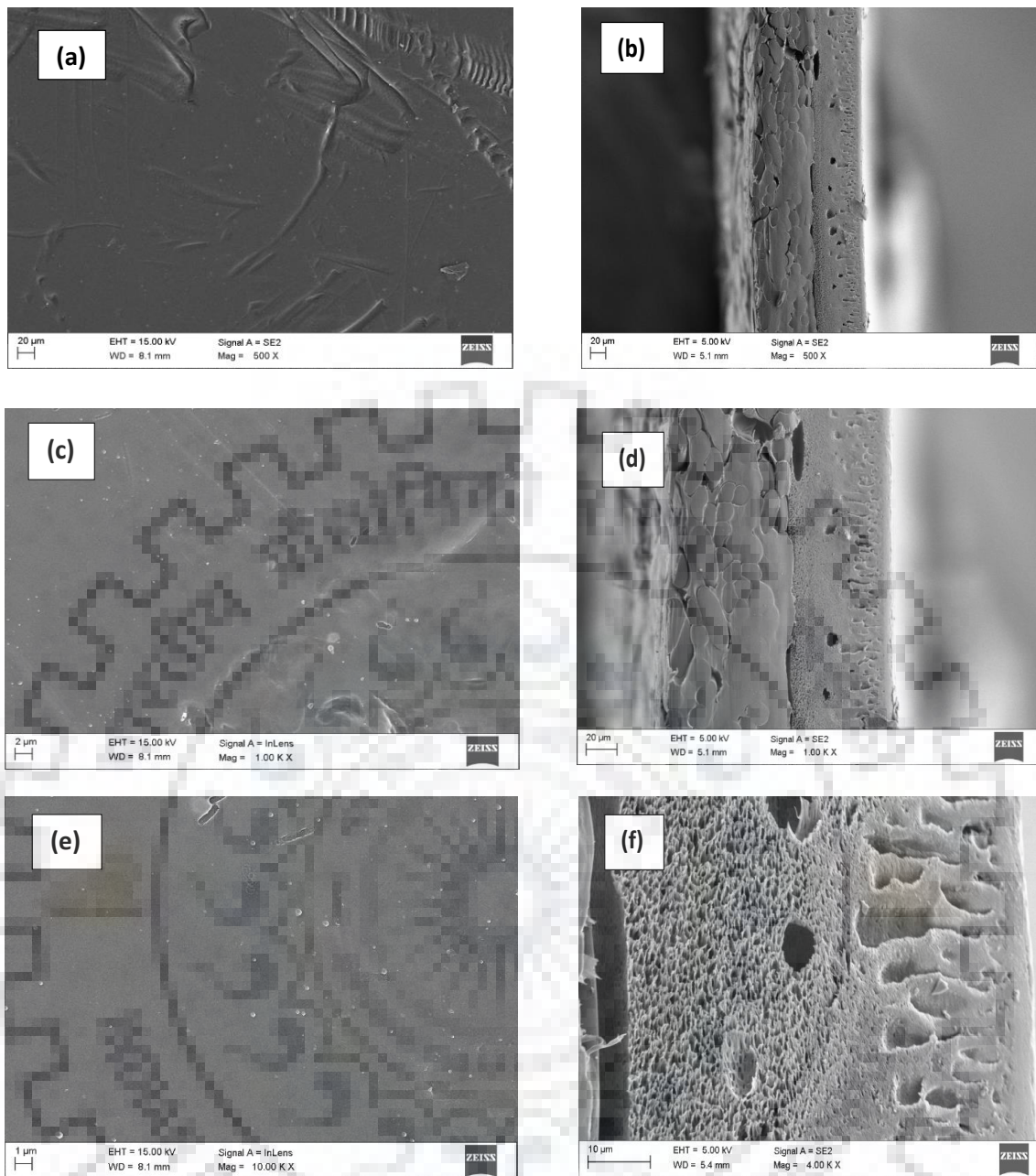
Fig. 5.5 SEM images of commercial NF500 membrane (a) Top view at 500X (b) Cross sectional view at 500X (c) Top view at 1.00KX (d) Cross sectional view at 1.00KX (e) Top view at 10.00 KX (f) Cross sectional view at 4.00KX.
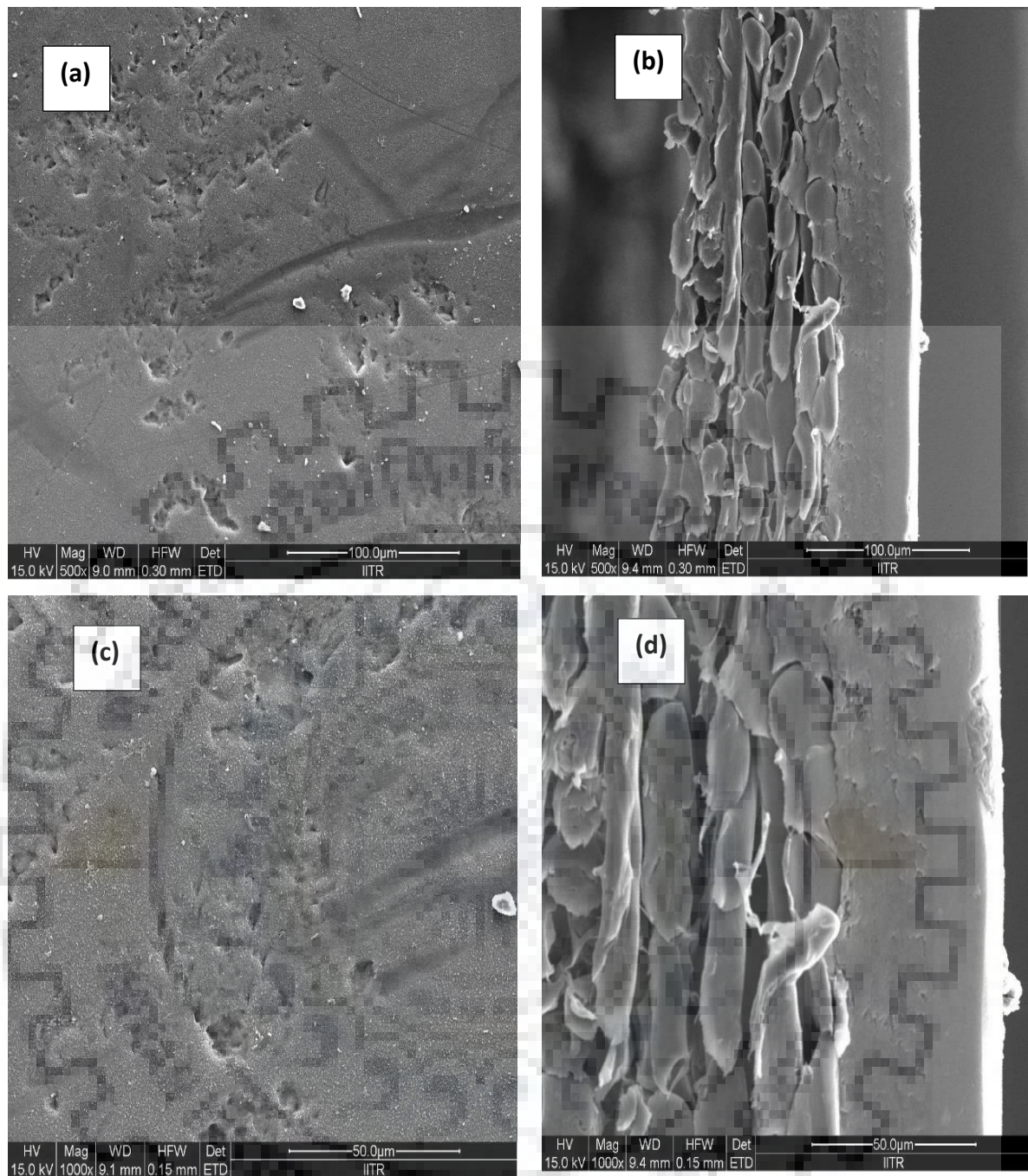
Fig. 5.6 SEM image of polyamide RO membrane (a) Top view at 500X (b) Cross sectional view at 500X (c) Top view at 1000X (d) Cross sectional view at 1000X.

5.1.1.2.1 Conclusive Remark

The morphological study was carried out for identification for these the composite structure of membranes (NF300, PN40, NF500 and RO) was made up from three different layers of polymeric materials namely polyamide, polysulfone and polyester respectively.

5.1.1.3 AFM Analysis of membranes

AFM image provides the surface morphology and roughness of polymeric membranes. AFM analysis has been done for a 5 µm × 5 µm projected surface area of NF300 and PN40 membrane. The average roughness and mean roughness values of virgin and used NF-300 and PN-40 values are mentioned in Table 5.3. The two dimensional and three dimensional plots of virgin and used NF300 and PN40 membranes are mentioned in Fig.5.7 (a1 to d6). Effect of feed solution pH on roughness of NF300 and PN40 membrane surface are shown in Fig. 5.7 (a1 to d6). The brighter area represents the peaks while the darker area indicates the valleys or depressions on the surface. Virgin membrane roughness value if higher may project to have comparatively high fouling on membrane surface due to particles accumulated in that valleys region of membrane because of high local flux (Hilal et al., 2005; Abu Seman et al., 2010, Elimelech et al., 1997; Al-Rashdi et al., 2013).

Surface roughness and morphology of NF500 were found with AFM. The two dimensional and three dimensional view of surface of NF500 membrane are clearly presented in Fig.5.8. The RMS roughness and average roughness values of NF500 were 4.82375 nm and 3.82525 nm by using NT-MDT SPM Software (Nova 1.0.26.1424) of selected area 5µm × 5µm of the membrane surface.

AFM analysis has been used to study the surface roughness and morphology of polyamide RO membrane. With the help of NT-MDT SPM Software (Nova 1.0.26.1424) RMS roughness and average roughness values of polyamide RO membrane were 16.1805 ± 1.36 nm and 12.8409 ± 1.0 nm evaluated for the selected area 5µm × 5µm of polyamide RO membrane surface. Fig. 5.9(a) and Fig.5.9 (b) indicate the two dimensional and three dimensional view of surface of polyamide RO membrane of selected area 5µm × 5µm of membrane surface.

Table 5.3 Root mean square and average roughness readings for commercial NF membranes.

No.	Membrane conditions	NF Membranes Types			
		NF300		PN40	
		RMS roughness(nm)	Average roughness(nm)	RMS roughness(nm)	Average roughness(nm)
1	Virgin	7.45	5.21	9.48	5.78
2	feed solution pH3	5.08	2.73	8.11	5.57
3	feed solution pH5	5.36	3.77	8.30	6.32
4	feed solution pH7	6.14	4.59	9.29	7.15
5	feed solution pH8	8.60	5.35	11.67	8.05
6	feed solution pH10	9.94	7.66	11.83	8.87

(a1) Virgin NF300　　**(b1) Virgin NF300**　　**(c1) Virgin PN40**　　**(d1) Virgin PN40**

(a2)pH3　　**(b2) pH3**　　**(c2) pH3**　　**(d2) pH3**

(a3) pH5　　**(b3) pH5**　　**(c3) pH5**　　**(d3) pH5**

(a4) pH7　　**(b4) pH7**　　**(c4) pH7**　　**(d4) pH7**

(a5) pH8　　**(b5) pH8**　　**(c5) pH8**　　**(d5) pH8**

(a6) pH10　　**(b6) pH10**　　**(c6) pH10**　　**(d6) pH10**
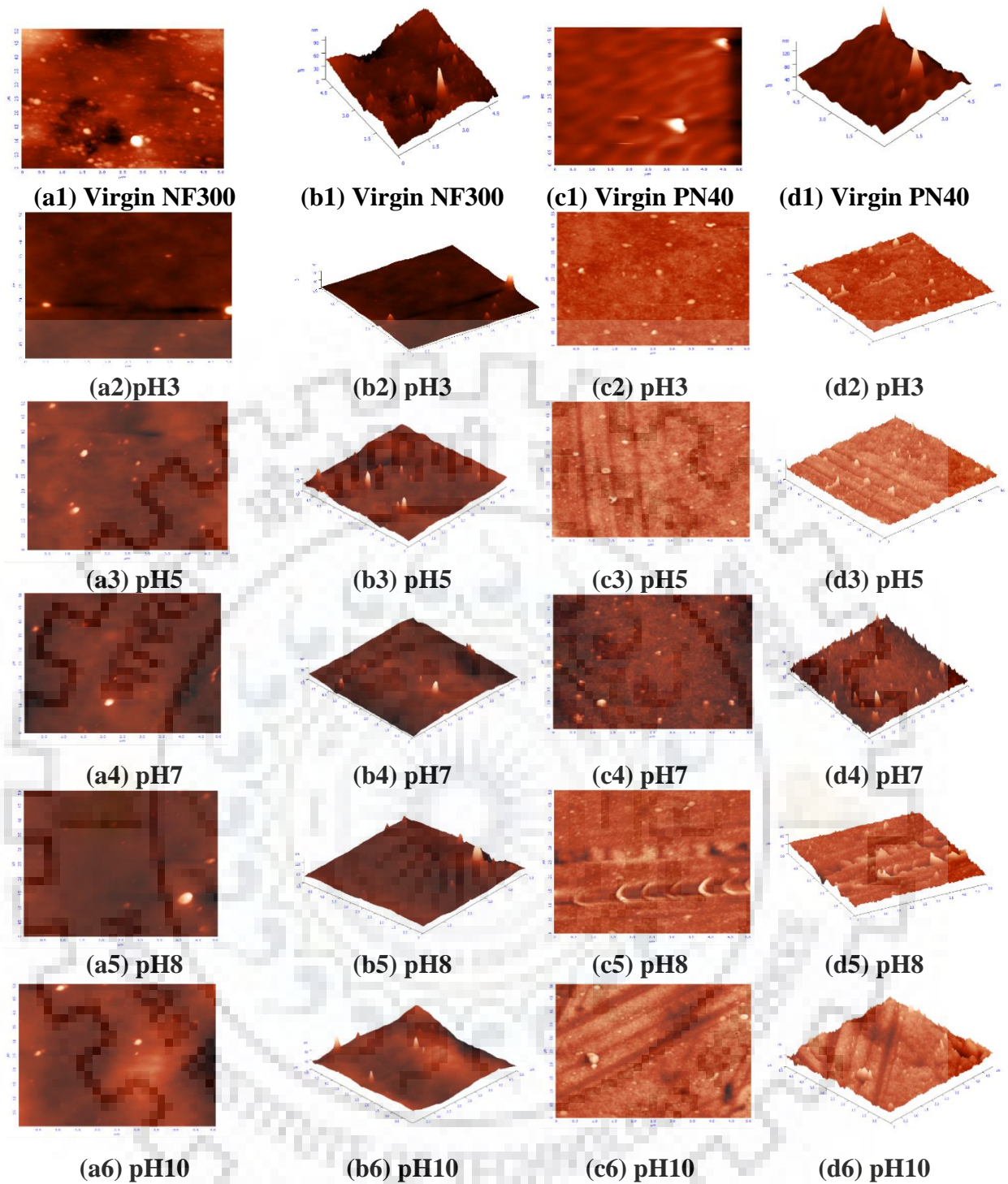
Fig. 5.7 AFM image of commercial NF membranes (virgin and different pH): 2D view of NF300 [(a1) to (a6)] and PN40 [(c1) to (c6)] 3D view of NF300 [(b1) to (b6)] and PN40 [(d1) to (d6)].

129
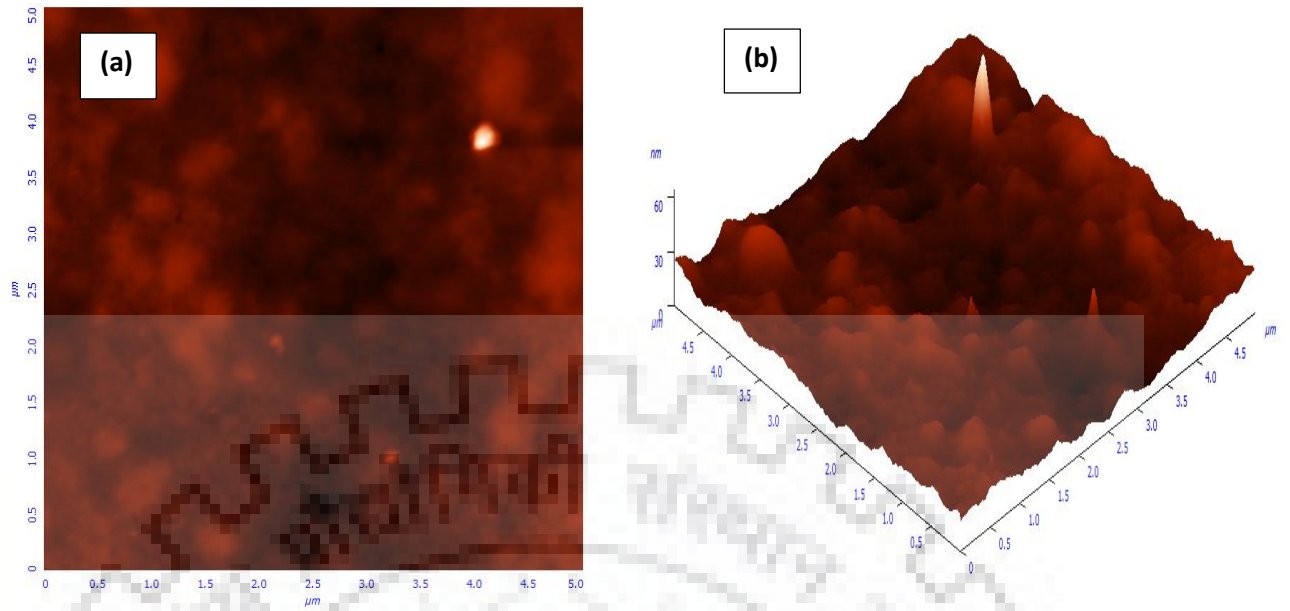
Fig. 5.8 AFM images of commercial NF500 membrane (a) 2D view (b) 3D view.
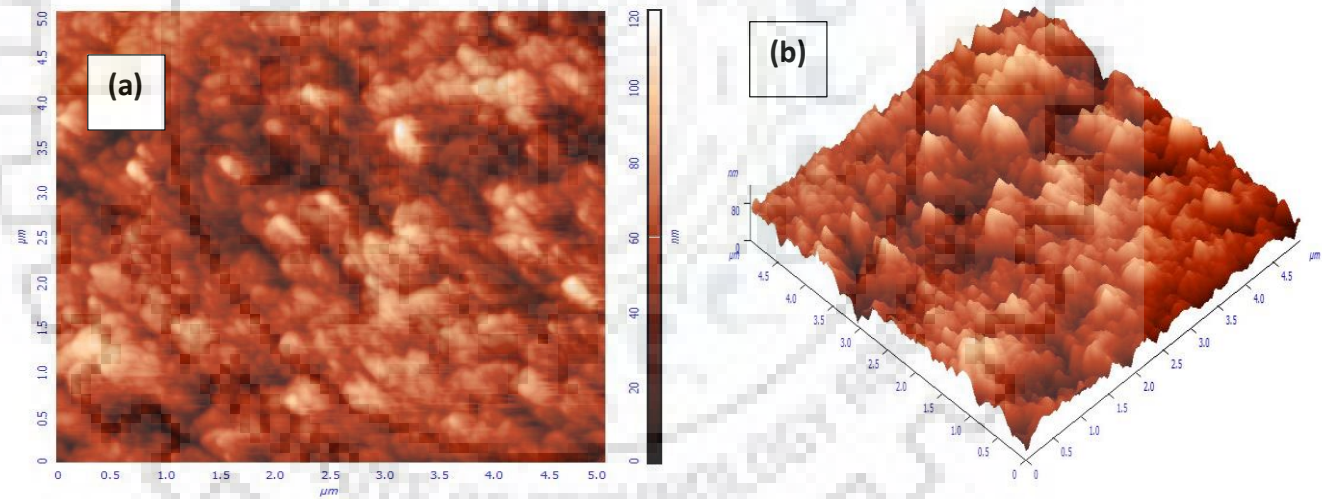
Fig. 5.9 AFM image of polyamide RO membrane (a) 2D view (b) 3D view.

5.1.1.3.1 Conclusive Remark:

Identification roughness values of different membrane (NF300, PN40, NF500 and RO) with AFM analysis were carried out. The present study confirms that pH of feed solution influence on the roughness values of membrane.

5.1.2 Pure water permeability (PWP) of membranes

PWP of NF300 and PN40 membranes was found out at room temperature of 30±2 °C before the start of experiments. The PWP coefficient (Lp) value was found by plotting PWP versus applied pressure. Lp value was determined from the slope of that graph. The PWP coefficients were found to be 8.14 L/m²hbar for NF300 and 14.8 L/m²hbar for PN40, which are in the range of nanofiltration membranes (Ballet et al., 2004; Mehiguene et al., 1999). The PWP coefficient was found to be 13.5 L/m²hbar for NF500 which was in the range of NF membranes (Ballet et al., 2004; Mehiguene et al., 1999). Polyamide RO membrane PWP was measured with using simply running DI water through the experimental set up at different pressure. The PWP coefficient was found to be 4.85 L/m²hbar for polyamide RO membrane which was in the range of RO membranes (Kim et al., 2005; Xu et al., 2006).

5.1.3. Effect of applied pressure and feed concentration

5.1.3.1 NF300 and PN40

In this experiment operating pressure was changed from 2-10 bar with a concentration range of 5 -100 mg/L of Cr(VI) and fluoride. Fig. 5.10 (a) and Fig. 5.10 (b) illustrate the effects on permeate flux and the percent rejection of Cr(VI) and fluoride with NF300 membrane and similarly Fig.5.11 (a) and Fig.5.11(b) for PN40 membrane respectively. Highest percent rejection of Cr(VI) and fluoride were found to be 97% and 92% with NF300 and 88% and 82% with PN40 membranes for 5 mg/L feed respectively. Fig.5.10 (a) and Fig. 5.11(a) indicate that as pressure increases the permeate flux linearly increases as represented by Eq. (5.1). This implies that on the surface of the membrane, there is insignificant or no concentration polarization.

$$J_v = L_p \ (\Delta P - \Delta \Pi) \ \text{-------------------------------} \ (5.1)$$

Here ΔP and $\Delta \Pi$ signify trans-membrane pressure and osmotic pressure difference respectively.

Solvent flux was enhanced without corresponding enhancement in solute flux at increasing pressure. This is resulted due to solute and solvent flux separation in solution–diffusion

mechanism of NF membrane transport mechanism (Kumar et al., 2011). The flux of pure water increases while no any changes in the flux of solute (Cr(VI) and fluoride) at increasing pressure because of the permeate contains less concentration of Cr(VI) and fluoride. This suggests the rejection of Cr(VI) and fluoride solutes enhancement with increasing pressure (refer Fig. 5.10(b) and Fig. 5.11(b)). In size exclusion mechanism pore size of the membrane and dimension of solute has a significant part in finding degree of separation. Negatively charged ions and negatively charged membrane enhanced the Cr(VI) and fluoride rejection from binary solution due to the electrostatic charge repulsion mechanism.

5.1.3.2 NF500

Pressure and feed concentration effect on rejection of Cr(VI) and fluoride were presented in Fig. 5.12. The effect of pressure study was carried with the range 2 to 10 bar and concentration of Cr(VI) and fluoride was varied from 5 mg/L to 100 mg/L at a constant feed flow rate 16 L/min. Fig. 5.12(a) represents the effects of pressure on the permeate flux of Cr(VI) and fluoride with NF500 membrane. Fig. 5.12(a) clearly represents that as pressure increases then permeate flux linearly increases (Eq. 5.1). This signifies no concentration polarization on surface membrane. Solvent flux was enhanced without corresponding enhancement in solute flux at increasing pressure are resulted due to solute and solvent flux separation in solution–diffusion mechanism of NF membrane transport mechanism (Kumar et al., 2011). The flux of pure water increases while there is no any change or remains constant flux of solute (Cr(VI) and fluoride) at increasing pressure because of this permeate contains less concentration of Cr(VI) and fluoride. This proposed that rejection Cr(VI) and fluoride (solute) are enhanced with increasing pressure (refer Fig. 5.12(b)). In size exclusion mechanism pore size of membrane and dimension of solute having significant part in finding degree of separation. Negatively charge ions and negatively charge membrane enhanced the Cr(VI) and fluoride rejection from binary solution due to the electrostatic charge repulsion mechanism.
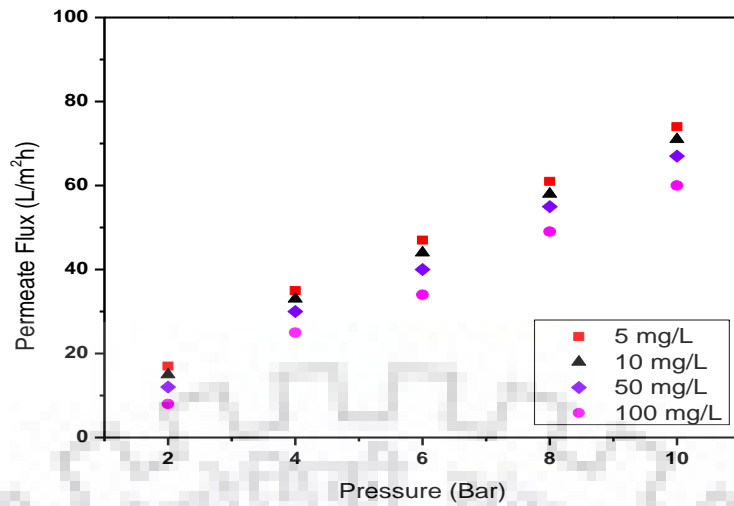
(a)
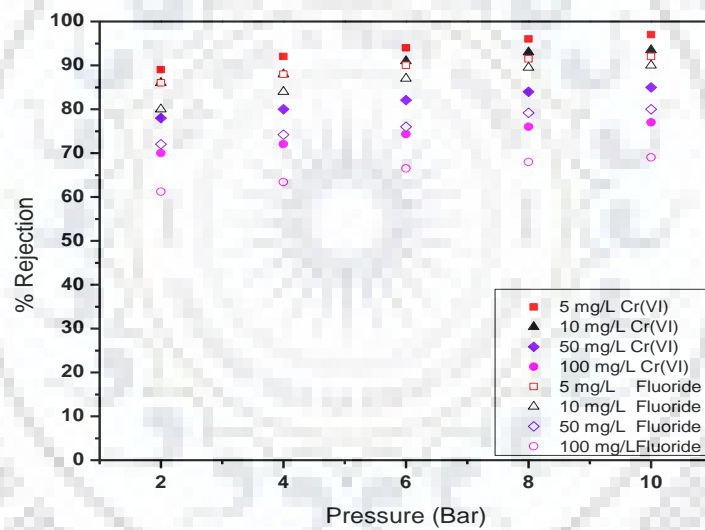
(b)

Fig. 5.10 (a) Effect of pressure on permeate flux of binary mixture of Cr(VI) and fluoride with different feed concentration by using NF300 membrane. (b) Effect of applied pressure on percentage rejection of Cr(VI) and fluoride with different feed concentration by using NF300 membrane at pH 8.
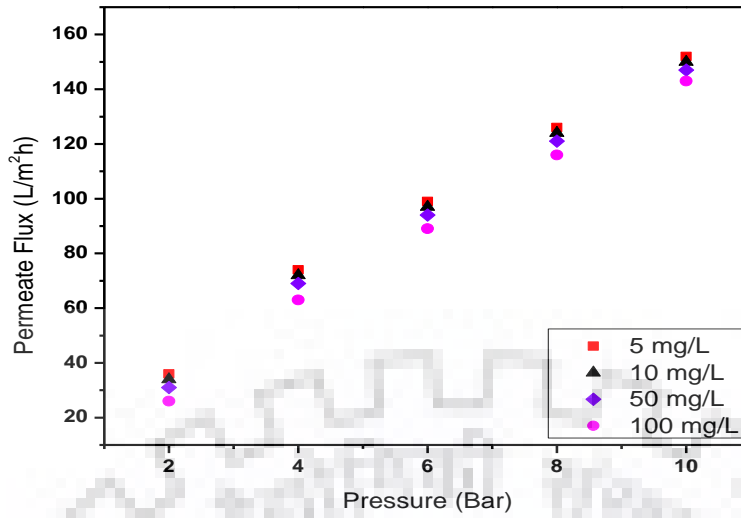
(a)
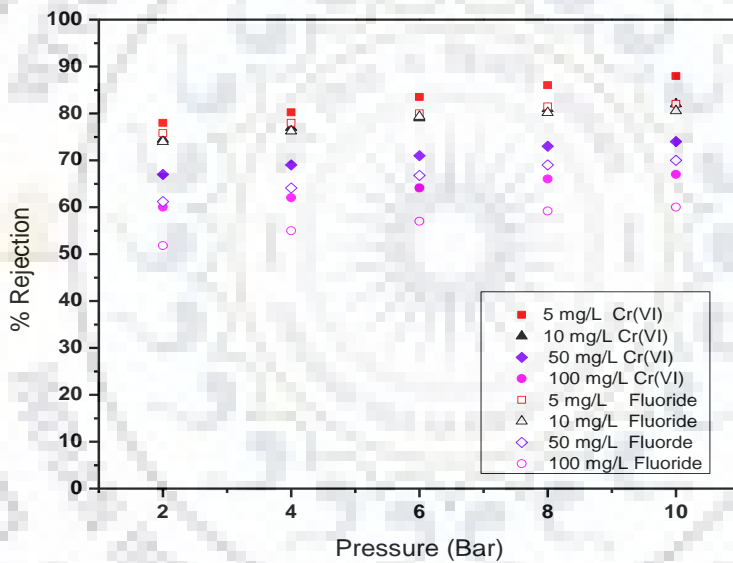
(b)

Fig. 5.11 (a) Effect of pressure on permeate flux of binary mixture of Cr(VI) and fluoride with different feed concentration by using PN40 membrane. (b) Effect of applied pressure on percentage rejection of Cr(VI) and fluoride with different feed concentration by using PN40 membrane at pH 8.

136
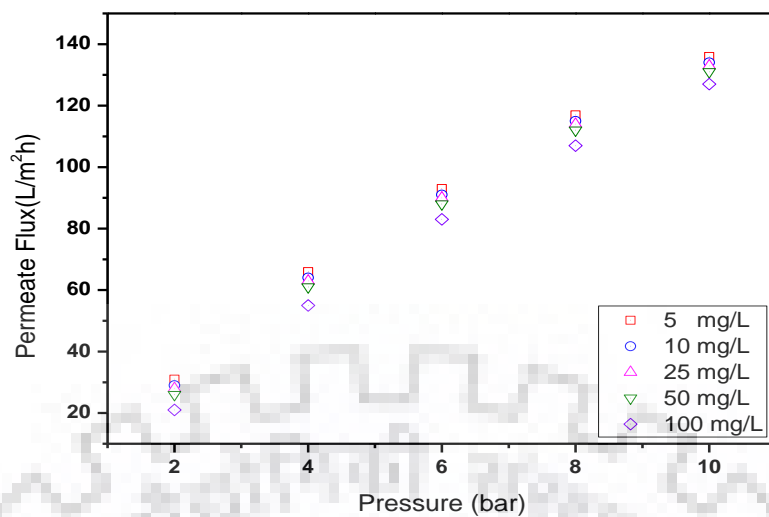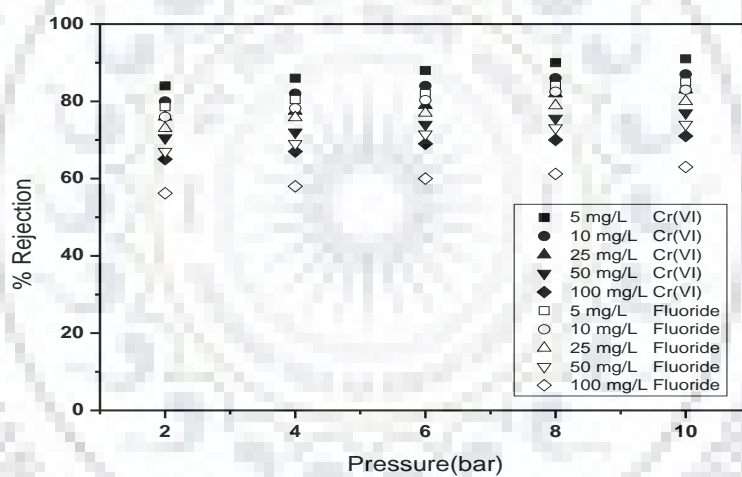
Fig. 5.12 (a) Effect of pressure on permeate flux of binary mixture of Cr(VI) and fluoride with different feed concentration by using NF500 membrane. (b) Effect of applied pressure on percentage rejection of Cr(VI) and fluoride with different feed concentration by using NF500 membrane at pH 8.

5.1.3.3 RO membrane

Effect on simultaneous rejection of Cr(VI) and fluoride achieved with different pressure and different feed concentration are presented in Fig. 5.13(a). The applied pressure range used in the experiment are 4, 8, 12, 16 and 20 bar. Feed concentration (both fluoride and Cr(VI)) range like 5, 50, 100 and 400 mg/L was used for experimental study. Effects of pressure on the permeate flux of fluoride and Cr(VI) feed for polyamide RO membrane are presented in Fig. 5.13(b). It shows that as pressure increases then permeate flux linearly increases (Eq. 5.1). This signifies that on surface membrane, there is insignificant or no concentration polarization. This is as per solution–diffusion mechanism which comes under the transport mechanism of NF/RO membranes. Solute flux and solvent flux are separated which resulted in to solvent flux enhanced without corresponding enhancement in solute flux at increasing pressure (Kumar et al., 2011; Chianese et al., 1999). There is no any change or remains constant flux of solute (fluoride and Cr(VI)) with increase in flux of pure water at increasing pressure. Permeate contains less concentration of fluoride and Cr(VI) suggested that the rejection of fluoride and Cr(VI) (solute) is enhanced with the increasing pressure (refer Fig. 5.13(a)). In size exclusion mechanism pore size of membrane and dimension of solute have significant part in finding degree of separation.

5.1.3.4 Conclusive remarks

This study suggests that permeate flux and rejection of Cr(VI) and fluoride are enhanced with increasing pressure and decreased with increasing feed concentration with different(NF300, NF500, PN40 and RO) flat sheet membranes.
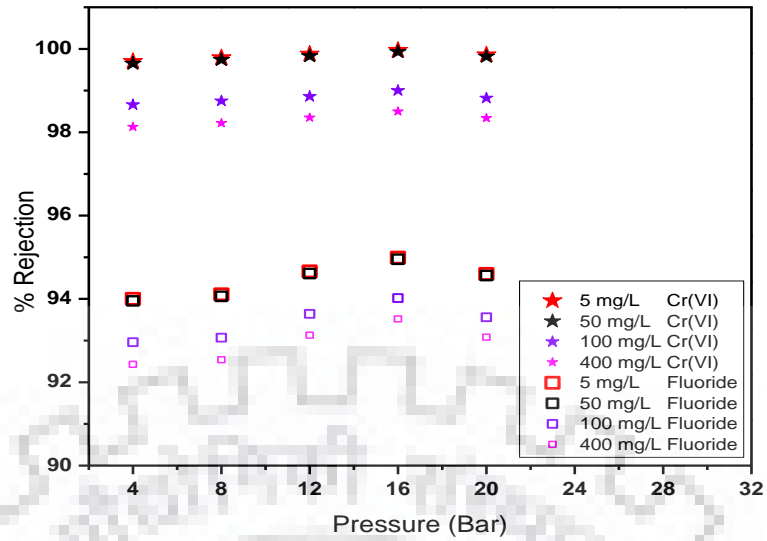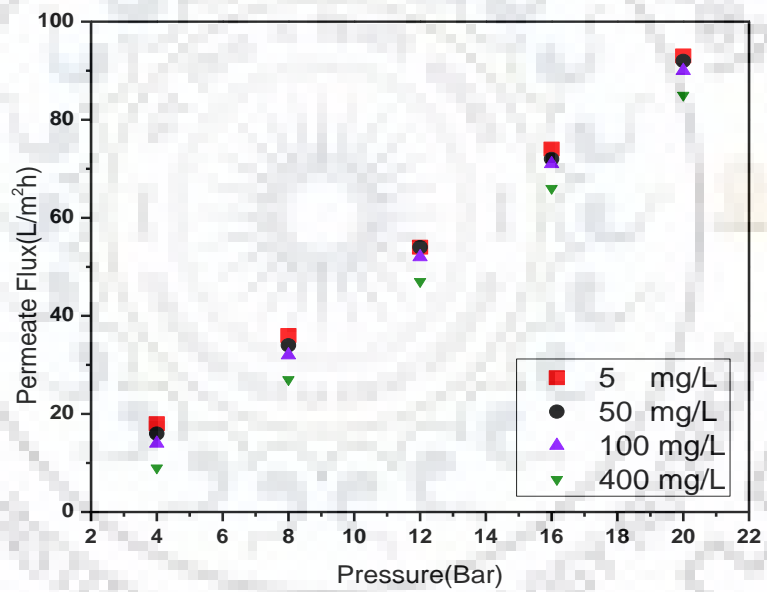
Fig. 5.13 (a) Effect of pressure on percentage rejection of fluoride and Cr(VI) at different feed concentration by using polyamide RO membrane at pH 8. (b) Effect of pressure on permeate volume flux of binary mixture of fluoride and Cr(VI) at different feed concentration by using polyamide RO membrane.

5.1.4 pH effect on rejection

5.1.4.1 NF300 and PN40

Feed solution of Cr(VI) was prepared form potassium dichromate ($K_2Cr_2O_7$). Cr(VI) compounds are usually highly soluble, mobile and bioavailable compared to sparingly soluble trivalent Cr species (Kotas and Stasicka, 2000). Similarly fluoride solution was prepared from sodium fluoride (NaF) which is also soluble in water (Haynes, 2010). Fluoride is the earth's crust common element and is highly soluble in water (Yang et al., 2015). Cr(VI) is occured in various ionic forms ($HCrO_4^-$, CrO_4^{2-}, $Cr_2O_7^{2-}$) that depends on the pH and the concentration of Cr(VI) solution. The Cr(VI) equilibrium reactions and related equilibrium constants (pK) at 25°C are mentioned in Eqs. (5.2) – (5.4) (Cabatingan et al., 2001; Ren et al., 2010).

$$H_2CrO_4 \rightarrow H^+ + HCrO_4^- \qquad\qquad pK = -0.08 \qquad\qquad (5.2)$$

$$HCrO_4^- \rightarrow H^+ + CrO_4^{2-} \qquad\qquad pK = 6.5 \qquad\qquad (5.3)$$

$$2HCrO_4^- \rightarrow CrO_7^{2-} + H_2O \qquad\qquad pK = -1.55 \qquad\qquad (5.4)$$
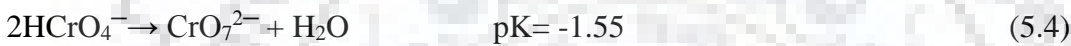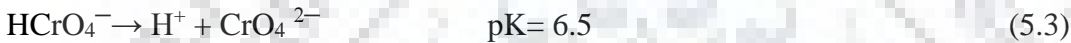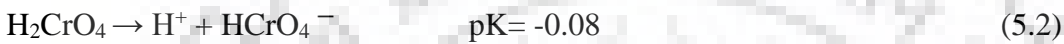
As per Eqs. (5.2) – (5.4) and their pK values, $HCrO_4^-$ monovalent species was dominant when pH was set below 6.5. When pH was set higher than 6.5, the rejection of solute was enhanced due to that conversion of 50% of $HCrO_4^-$ to CrO_4^{2-}. When pH was adjusted up to 8, all the chromium species are converted to CrO_4^{2-} (Ren et al., 2010). Thus, maximum removal was obtained at pH 8 due to Donnan effect for the negatively charged membrane and negatively charge ions. Some studies reported that NF membranes have lower isoelectric points (i.e. in the range of pH 3 to pH 4). At the high pH membrane gain, the more negative charge and at low pH membrane surface charge is positive (Childress et al., 1996; Zahrim et al., 2013). When pH higher than isoelectric points, then polyamide NF membrane net surface charge is negative (H_2N – polyamide – COO–) while when pH less than isoelectric point, then polyamide NF membrane the net surface charge is positive (H_3N^+ – polyamide – COOH). At nearer to isoelectric point the negative surface charge becomes weak (Zahrim et al., 2013).

For pH effect on rejection of Cr(VI) and fluoride, the experiments were done with a pH (3 to 9) which is operating ranges of NF300 and PN40 membranes. Fig. 5.14(a) and Fig. 5.14(b) represent the effect of pH on rejection of Cr(VI) and fluoride by NF300 and PN40 membranes respectively. It found that minimum percent rejection (45% with NF300 and 34% with PN40) at pH 3 which was happening due to Donnan effect for the negatively charged membrane which is result in to minor rejection to the monovalent anion $HCrO_4^-$. When pH was changed to 7, some of the $HCrO_4^-$ anions converted in to CrO_4^{2-} and removal was increased. When pH was

adjusted to 8 and above, maximum removal (97% with NF300 and 88% with PN40) was observed. The same kind of trend was observed for fluoride, lower rejection (37% with NF300 and 28% with PN40) was obtained at pH 3. Highest rejection (92% with NF300 and 82% with PN40) was found when the pH was adjusted to 8 and above. Similar effect of pH on rejection of fluoride by NF membrane was found in previously reported literatures (Wei-fang et al., 2009; Richards et al., 2010; Chakrabortty et al., 2013). Therefore, it concludes that the NF300 and PN40 membranes can be efficiently employed in the removal of Cr(VI) and fluoride when pH was adjusted above 8.0.
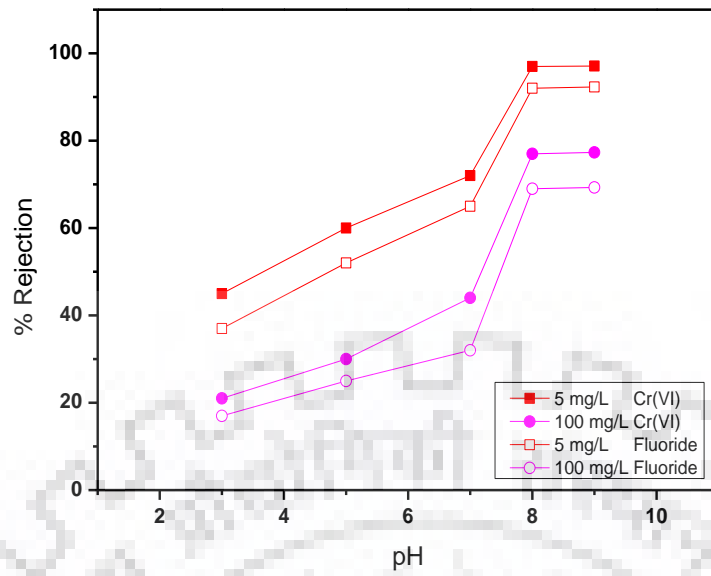
(a)
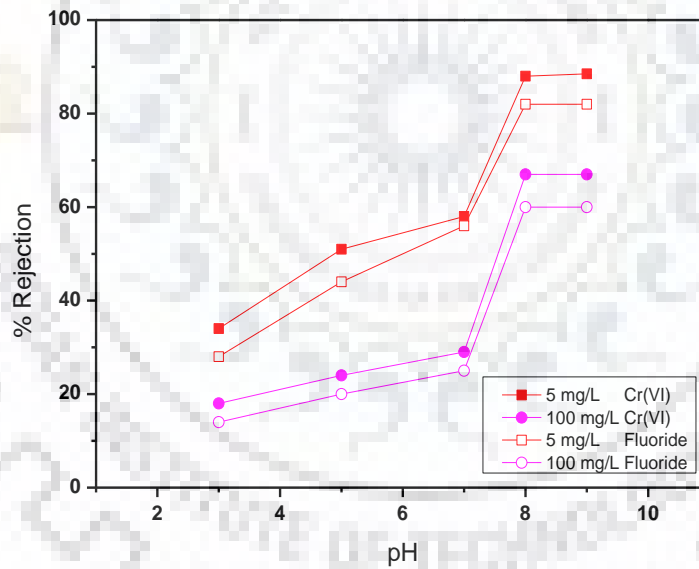
(b)

Fig. 5.14 pH effect on percentage rejection of Cr(VI) and fluoride for 5 mg/L and 100 mg/L feed concentration at 10 bar applied pressure using (a) NF300 membrane (b) PN40 membrane.

5.1.4.2 NF500

The pH effect on rejection of Cr(VI) and fluoride are mentioned in Fig. 5.15. In pH effect study, pH varied from 2,4,6,8 and 10 which is in the working range of NF500 and the effect of pH on percent rejection with different feed concentration (5, 25, and 100) of Cr(VI) and fluoride are studied. In aqueous solution Cr(VI) is existed in various ionic forms ($HCrO_4^-$, CrO_4^{2-}, $Cr_2O_7^{2-}$) due to Cr(VI) concentration and solution pH. From Fig.5.15 we conclude that less rejection was observed in acidic condition at pH 2 due to Donnan effect for the negatively charged membrane result in to minor rejection to the monovalent anion $HCrO_4^-$. When pH was set to 7, some of $HCrO_4^-$ anions converted in to CrO_4^{2-} and removal of chromium was increased. When pH was adjusted to 8 and above, maximum rejection was observed. In case of fluoride same trend has been found. Less rejection was found at pH 2 and higher rejection was observed at pH 8 and above. Similar effect of pH on rejection of fluoride by NF membrane was found in earlier reported literatures (Wei-fang et al., 2009; Richards et al., 2010; Chakrabortty et al., 2013). Hence, we can conclude that the NF500 membranes work efficiently in the removal of Cr(VI) and fluoride when pH was adjusted above 8.0.

5.1.4.3 RO membrane

Rejections of fluoride and Cr(VI) were changed due to the effect of pH of feed solution (Fig. 5.16). pH range (3 to 9) was used for the experiment which is in the working range of polyamide RO membrane and the effect of pH on percent rejection with different feed concentration (5, 50, 100 and 400) of fluoride and Cr(VI). In aqueous solution Cr(VI) is existed in various ionic forms ($HCrO_4^-$, CrO_4^{2-}, $Cr_2O_7^{2-}$) due to Cr(VI) concentration and solution pH. Fig. 5.16. indicated that slightly less rejection was found at acidic condition at pH 3 it appears due to Donnan effect for the negatively charged membrane to minor rejection to the monovalent anion $HCrO_4^-$. At pH 7 some of $HCrO_4^-$ anions converted in to CrO_4^{2-} and removal of chromium was increases. Maximum removal was found when pH was adjusted to 8. For the case of fluoride similar kind of trend has been observed. Less rejection was found at pH 3 and higher rejection was observed at pH 8 and above. A similar trend was found in earlier reported literatures (Wei-fang et al., 2009; Richards et al., 2010; Chakrabortty et al., 2013). Hence, it can conclude that the polyamide RO membranes can be efficiently working at pH 8 for the removal of fluoride and Cr(VI).
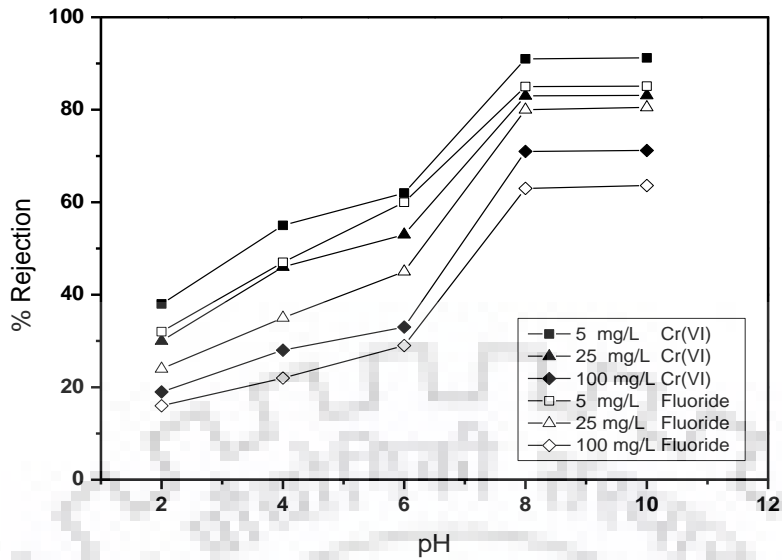
Fig. 5.15 Effect of pH on percentage rejection of Cr(VI) and fluoride for 5 mg/L, 25 mg/L and 100 mg/L feed concentration at 10 bar applied pressure using NF500 membrane.
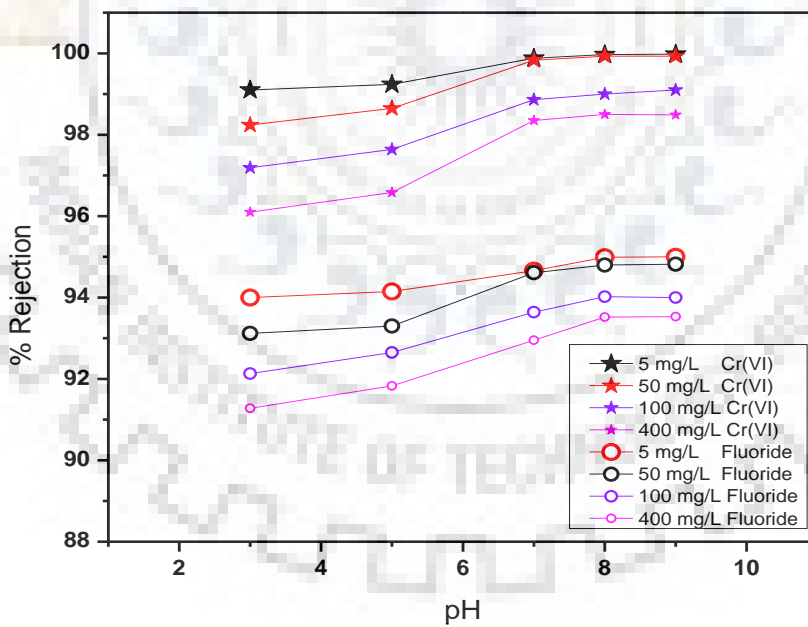
Fig. 5.16 Effect of pH on percentage rejection of fluoride and Cr(VI) at 16 bar applied pressure using polyamide RO membrane.

144

5.1.4.4 Conclusive remarks

The present study suggested that pH of feed solution significantly influence on rejection of Cr(VI) and fluoride. The higher rejection was observed at pH 8 and above.

5.1.5 Estimation of membrane transport parameters

5.1.5.1 Estimation of NF300 and PN40 membranes performance by CFSK model

The CFSK model Eq.(2.17) was used for simultaneous estimation of the membrane parameters σ and P_m and the mass transfer coefficient, k, with the help of a nonlinear parameter calculation method by using known parameters R_o and J_v at various pressures. MTPs and MTC for NF300 and PN40 membrane are shown in Table 5.4 and Table 5.5 respectively. It indicates that solute permeability P_m and reflection coefficient σ are dependent on the feed concentration. σ slightly decreases due to low solute rejection and P_m increases with increasing feed concentration due to more solute is passing through the membrane. The same kind of trend was observed for NF membranes by Murthy and his co-workers (Murthy and Chaudhari, 2008; Murthy and Gupta, 1998). The values of k shown in Tables 5.4 and 5.5 are then used in Eq. (2.17) along with the previous data R_o and J_v to determine true rejection R. Simultaneous rejection of Cr(VI) and fluoride by NF300 and PN40 membranes are compared with true rejection estimated by CFSK model (Fig. 5.17 (a) and Fig. 5.17 (b)). It indicates good agreement for experimental rejection and true rejection for Cr(VI) and fluoride by NF300 and PN40 membranes, respectively.

5.1.5.2 Estimation of NF300 and PN40 membranes performance by CFSD Model

The mass transfer coefficient, (k) and membrane transport parameter, ($D_{AM}K/\delta$) are simultaneously estimated for the removal of Cr(VI) and fluoride with for NF300 and PN40 membrane by using CFSD model by providing the data of R_o and J_v at different pressures with maintaining constant flowrate and constant concentration of feed. Estimated mass transfer coefficient and membrane transport parameter NF300 and PN40 membrane by CFSD model are shown in Table 5.6 and Table 5.7. Simultaneous observed rejection Cr(VI) and fluoride by NF300 and PN40 membrane are compared with true rejection estimated by CFSD model (Fig. 5.18 (a) and Fig. 5.18 (b)). A reasonably well agreement for experimental rejection and true rejection for Cr(VI) and fluoride is estimated by CFSD model.

Table 5.4 Parameter estimated using CFSK model for removal Cr(VI) and fluoride by NF300.

Cr(VI and Fluoride feed concentration (mg/L)	Chromium (VI)			Fluoride		
	σ	$P_m \times 10^5$ (cm/s)	$K \times 10^4$ (cm/s)	σ	$P_m \times 10^5$ (cm/s)	$k \times 10^4$ (cm/s)
5	0.9688	4.03	6.88	0.9223	6.23	5.74
10	0.9433	4.63	6.81	0.8911	6.83	5.71
50	0.8644	5.43	6.77	0.8023	7.44	5.68
100	0.7874	5.61	6.72	0.7121	8.08	5.61

Table 5.5 Parameter estimated using CFSK model for removal Cr(VI) and fluoride by PN40.

Cr(VI) and Fluoride feed concentration (mg/L)	Chromium (VI)			Fluoride		
	σ	$P_m \times 10^5$ (cm/s)	$K \times 10^4$ (cm/s)	σ	$P_m \times 10^5$ (cm/s)	$k \times 10^4$ (cm/s)
5	0.8894	5.21	3.76	0.8324	7.31	2.84
10	0.8214	5.54	3.71	0.8114	7.94	2.81
50	0.7555	6.31	3.68	0.7046	8.54	2.78
100	0.6817	6.94	3.61	0.6178	9.12	2.71
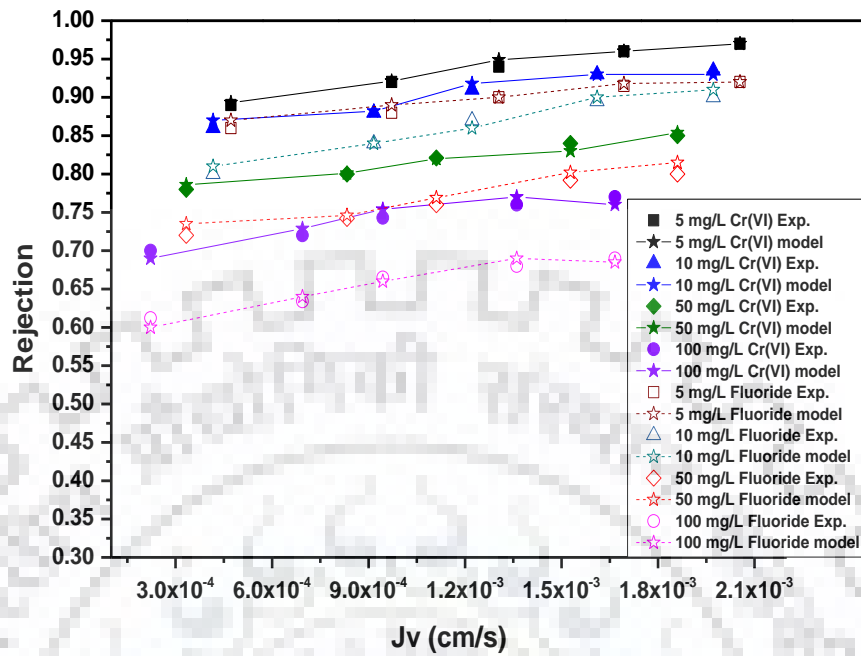
(a)
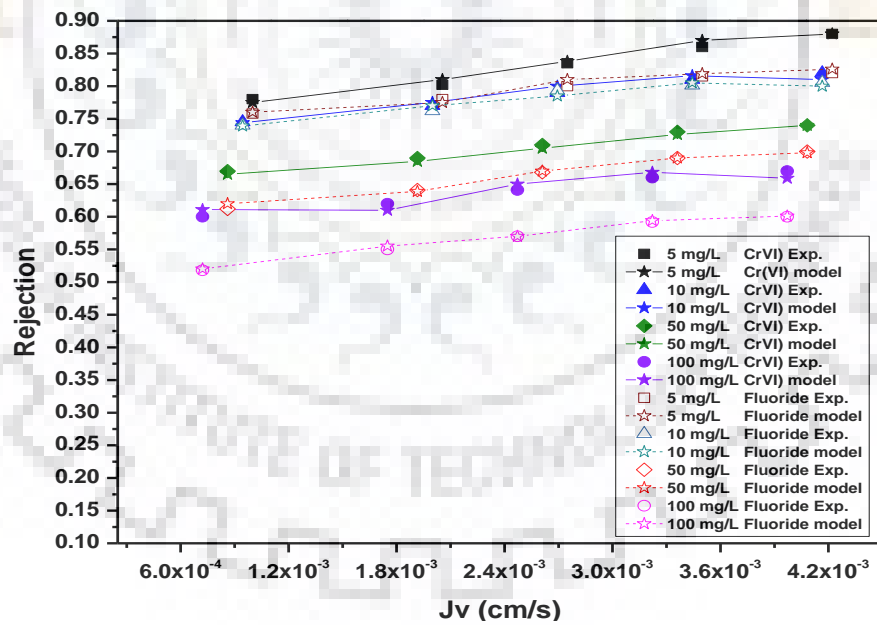
(b)

Fig. 5.17 Experimental and predicted comparison for rejection of Cr(VI) and fluoride as function of flux by CFSK model for (a)NF300 membrane (b) PN40 membrane.

Table 5.6 Estimated parameter with CFSD model for removal Cr(VI) and fluoride by NF300.

Cr(VI and Fluoride feed concentration (mg/L)	Cr(VI)		Fluoride	
	$(D_{AM}K/\delta) \times 10^4$ (cm/s)	$k \times 10^3$ (cm/s)	$D_{AM}K/\delta) \times 10^4$ (cm/s)	$k \times 10^3$ (cm/s)
5	1.332	3.90	1.536	2.81
10	1.336	3.88	1.545	2.75
50	1.396	3.38	1.565	2.53
100	1.438	3.10	1.584	2.11

Table 5.7 Estimated parameter with CFSD model for removal Cr(VI) and fluoride by PN40.

Cr(VI and Fluoride feed concentration (mg/L)	Cr(VI)		Fluoride	
	$(D_{AM}K/\delta) \times 10^4$ (cm/s)	$k \times 10^3$ (cm/s)	$D_{AM}K/\delta) \times 10^4$ (cm/s)	$k \times 10^3$ (cm/s)
5	1.465	2.65	1.646	1.52
10	1.471	2.63	1.658	1.50
50	1.511	2.32	1.716	1.38
100	1.554	2.18	1.759	1.14
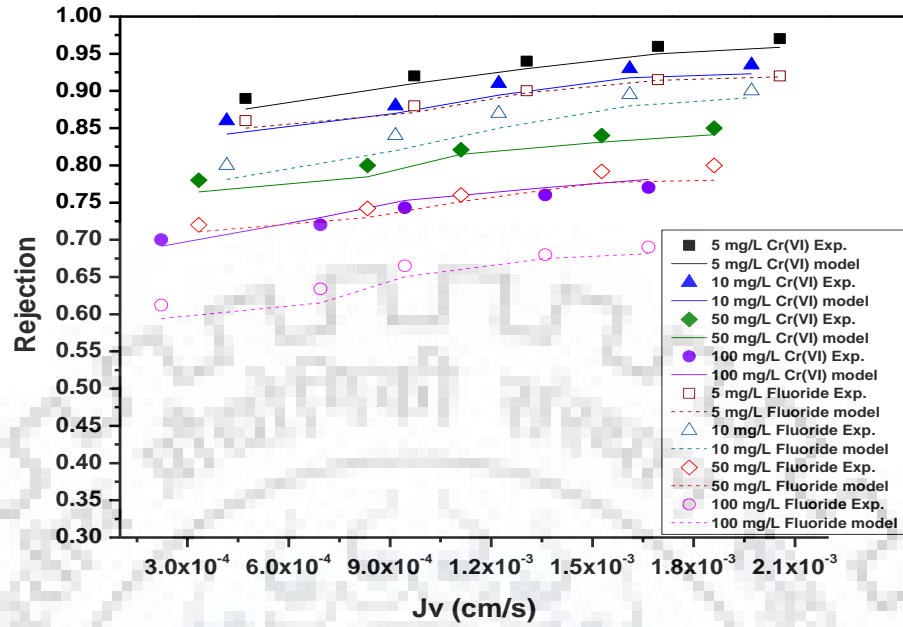
(a)
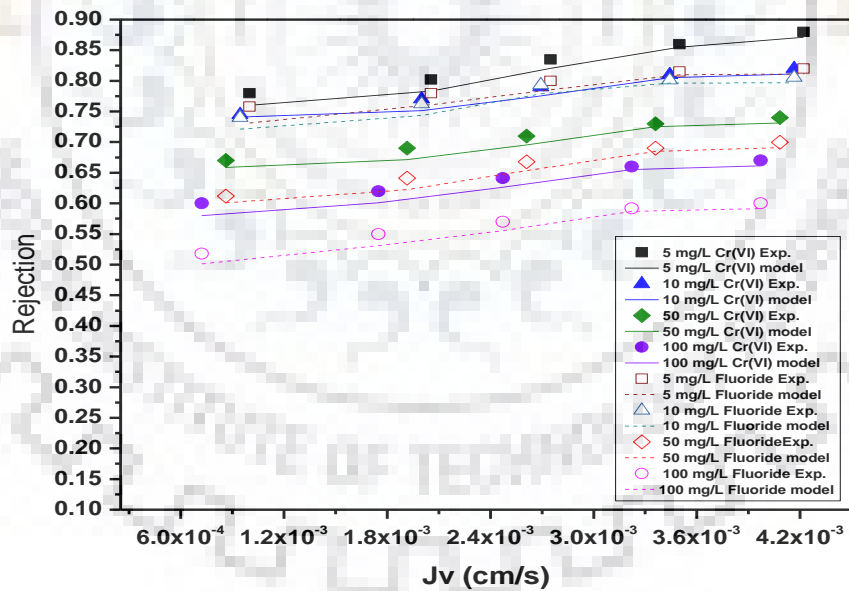
(b)

Fig. 5.18 Experimental and predicted comparison for rejection of Cr(VI) and fluoride as function of flux by CFSD model for (a) NF300 membrane (b) PN40 membrane.

5.1.5.3 Estimation of NF500 membrane performance by CFSK and CFSD models

The MTC (k) and MTPs (σ and P_m) are simultaneously evaluated by using CFSK model (with the help of nonlinear parameter evaluation process) with given data of R_o and J_v at different pressures and constant feed rate by keeping constant feed concentration. MTC and MTPs of NF500 membrane are shown in Table 5.8 where solute permeability P_m and reflection coefficient σ are dependent on the feed concentration. σ slightly decreases due to the reduction in solute rejection and P_m increases with feed concentration due to the high amount of solute passing through the membrane, The same kind of trend for NF membranes was observed by Murthy and co-workers (Murthy and Chaudhari, 2008; Murthy and Gupta, 1998). The values of k shown in Table 5.8 are used in Eq. (2.17) along with the previous data R_o and J_v to determine true rejection R. Simultaneous observed rejection of Cr(VI) and fluoride by NF500 membrane are compared with true rejection and is estimated by CFSK model (Fig. 5.19). Fig. 5.19 indicated good agreement for experimental rejection and true rejection for Cr(VI) and fluoride by NF500 membrane.

The mass transfer coefficient (k) and membrane transport parameter ($D_{AM}K/\delta$) are simultaneously estimated for NF500 membrane to remove Cr(VI) and fluoride using CFSD model by providing the data of R_o and J_v at different pressures by maintaining constant flowrate and constant concentration of feed. Estimated mass transfer coefficient and membrane transport parameter NF500 membrane by CFSD model are shown in Table 5.9. Simultaneous observed rejection of Cr(VI) and fluoride by NF500 membrane are compared with true rejection estimated by CFSD model (Fig. 5.20). A reasonably well agreement for experimental rejection and true rejection for Cr(VI) and fluoride is observed by CFSD model.

Table 5.8 MTC and MTPs parameter estimated of NF500 membrane for removal Cr(VI) and fluoride by CFSK model.

Feed concentration (mg/L)	Cr(VI)			Fluoride		
	Reflection Coefficient σ	Solute permeability $P_m \times 10^5$ (cm/s)	Mass Transfer Coefficient $k \times 10^3$ (cm/s)	Reflection Coefficient σ	Solute permeability $P_m \times 10^5$ (cm/s)	Mass Transfer Coefficient $k \times 10^3$ (cm/s)
5	0.9112	4.84	57.80	0.8513	6.81	47.88
10	0.8810	5.12	57.40	0.8366	7.31	47.58
25	0.8348	5.44	56.71	0.8012	7.51	47.37
50	0.7713	5.76	56.20	0.7441	7.98	47.07
100	0.7189	6.28	55.98	0.6388	8.51	46.72
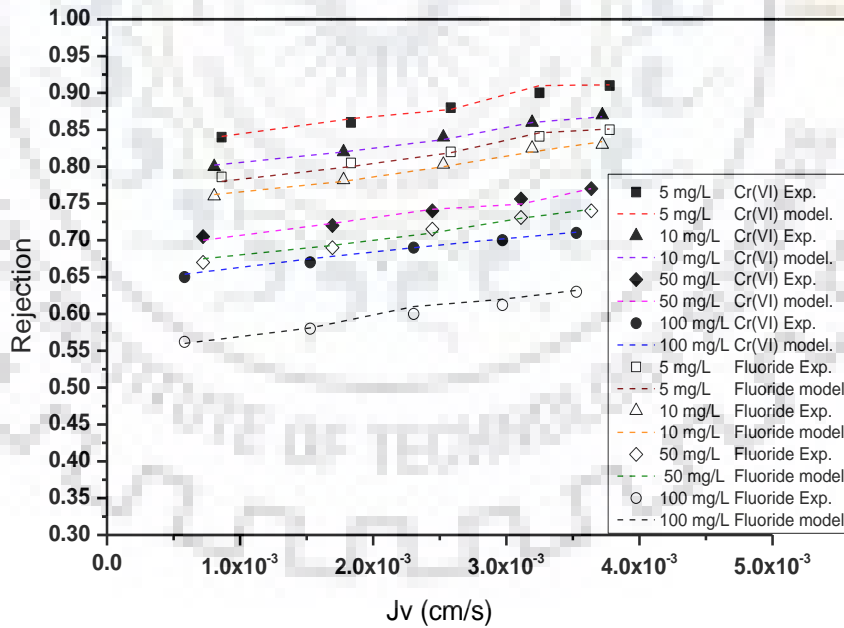
Fig. 5.19 Experimental and estimated rejection (by CFSK model) of Cr(VI) and fluoride as function of permeate flux with NF500 membrane.

Table 5.9 Estimated parameter with CFSD model for removal Cr(VI) and fluoride by NF500.

Cr(VI and Fluoride feed concentration (mg/L)	Cr(VI)		Fluoride	
	$(D_{AM}K/\delta) \times 10^4$ (cm/s)	$k \times 10^3$ (cm/s)	$(D_{AM}K/\delta) \times 10^4$ (cm/s)	$k \times 10^3$ (cm/s)
5	1.451	2.82	1.626	1.76
10	1.455	2.80	1.635	1.71
50	1.495	2.58	1.668	1.60
100	1.527	2.22	1.689	1.18
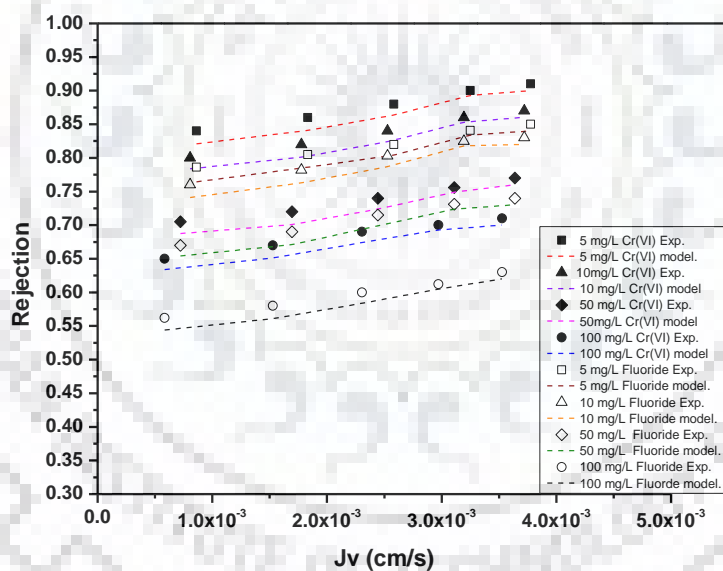
Fig. 5.20 Cr(VI) and fluoride experimental and estimated rejection (by CFSD model) of as function of permeate flux with NF500 membrane.

152

5.1.5.4 Estimation of RO membrane performance by CFSK and CFSD models

The MTC (k) and membrane TPs (σ and P_m) are simultaneously estimated using CFSK model by providing data of R_o and J_v at different pressures by maintaining constant flowrate and constant concentration of feed. Similarly $D_{AM}K/\delta$ and k can be evaluated with CFSD model using known Ro vs. Jv data, taken at constant feed concentration and different pressures. Estimated mass transfer coefficient and membrane transport parameter polyamide RO membrane by CFSK model are shown in Table 5.10. Table 5.10 indicated that P_m and σ are solute permeability and reflection coefficient respectively and that are dependent on the feed concentration. σ slightly decreases due to solute rejection was declined and high amount of solute passing through membrane which resulted in to P_m increased, The same kind of trend was observed in work reported by Murthy and co-workers (Ballet et al., 2004; Mehiguene et al., 1999; Murthy and Gupta, 1999). The parameters estimated by using CFSD model are systematically provided in Table 5.11. Simultaneous observed rejection fluoride and Cr(VI) by polyamide RO membrane are compared with true rejection estimated by CFSK model are shown in Fig. 5.21(a). Similarly simultaneous observed rejection of fluoride and Cr(VI) by polyamide RO membrane are compared with true rejection estimated by CFSD model are shown in Fig.5.21(b). From Fig. 5.21(a) and Fig. 5.21(b) it is observed that a reasonably well agreement for experimental rejection and true rejection for fluoride and Cr(VI) is observed by CFSK model and CFSD model, respectively. The CFSK model predicted values are more accurate compared to CFSD model which may be due to of reflection coefficient existence in the model.

Table 5.10 Parameter estimated using CFSK model for removal Cr(VI and fluoride by polyamide RO membrane.

Cr(VI and Fluoride feed concentration (mg/L)	Chromium (VI)			Fluoride		
	σ	$P_m \times 10^5$ (cm/s)	$k \times 10^4$ (cm/s)	σ	$P_m \times 10^5$ (cm/s)	$k \times 10^4$ (cm/s)
5	0.9998	1.428	26.97	0.9510	1.618	25.84
50	0.9993	1.450	26.92	0.9495	1.658	25.80
100	0.9911	1.490	26.86	0.9411	1.696	25.76
400	0.9866	1.588	26.72	0.9356	1.792	25.61

Table 5.11 Parameter estimated using CFSD model for removal Cr(VI and Fluoride by polyamide RO membrane.

Cr(VI and Fluoride feed concentration (mg/L)	Chromium (VI)		Fluoride	
	$(D_{AM}K/\delta) \times 10^5$ (cm/s)	$k \times 10^4$ (cm/s)	$(D_{AM}K/\delta) \times 10^5$ (cm/s)	$k \times 10^4$ (cm/s)
5	1.511	9.92	1.726	8.98
50	1.529	9.84	1.755	8.90
100	1.589	9.45	1.785	8.58
400	1.628	9.10	1.834	8.11
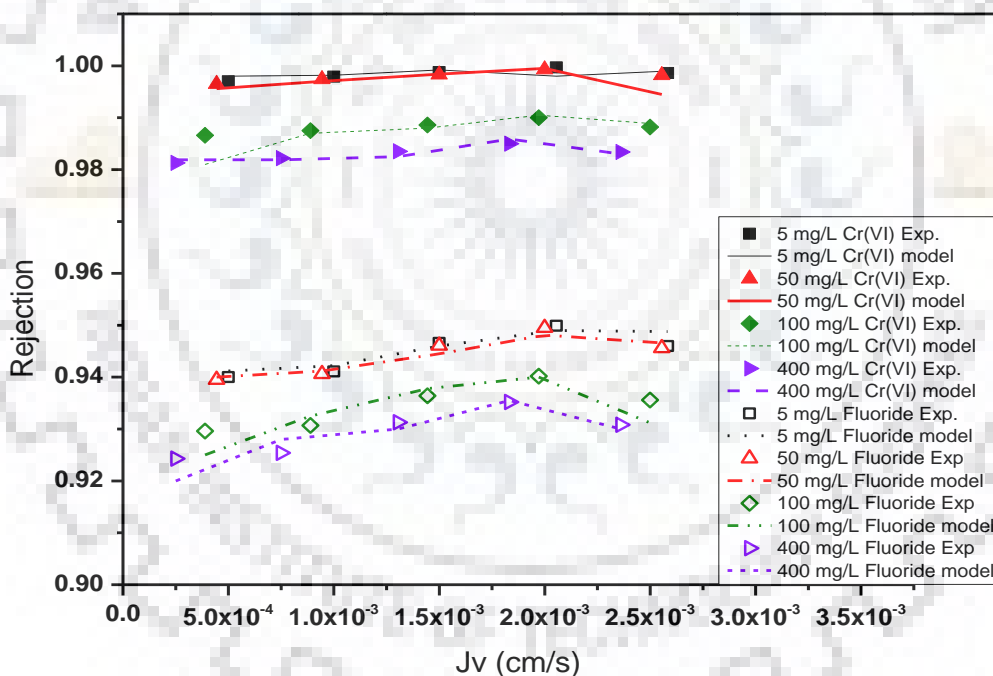
(a)
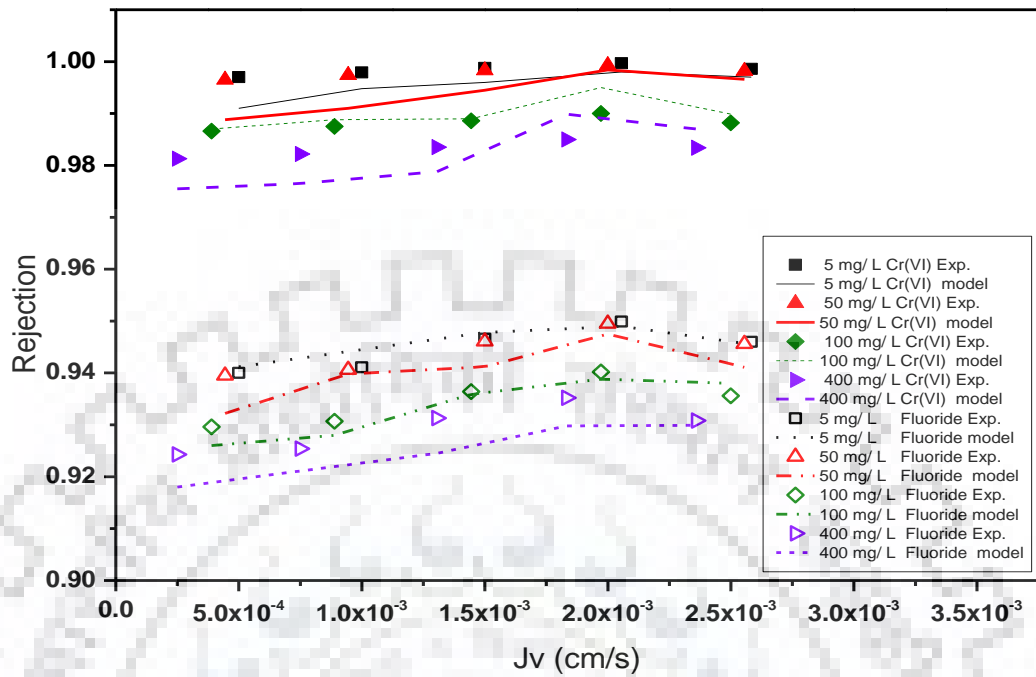
(b)

Fig. 5.21 (a) Experimental and predicted comparison for rejection of Cr(VI and Fluoride as function of flux (a) by CFSK model (b) by CFSD model for polyamide RO membrane.

5.1.5.5 Conclusive remarks

In the present study it was observed that CFSK model indicated a good agreement compared to CFSD model for experimental rejection and true rejection for Cr(VI) and fluoride.

5.2 Studies on Cr(VI) and fluoride removal by capacitive deionization

In this study simultaneous removal of Cr(VI) and fluoride were carried out with different activated carbon electrodes namely CAC electrode, TWBAC electrode, RHAC electrode and LASAC electrode.

5.2.1. Studies on CDI with CAC electrode

5.2.1.1 Characterization of electrode

5.2.1.1.1 SEM and EDX

The electrodes were disassembled from CDI set up after the treatment of binary solution containing Cr(VI) and fluoride. CAC electrodes were then dried in the oven. The dried electrodes were further used for SEM analysis. The morphological study of CAC electrode before and after treatment of Cr(VI) and fluoride binary feed solution was carried with SEM and shown in Fig. 5.22 (a-h). The virgin CAC electrodes show uniform distribution of casting layer at different magnification (100X, 500X, 1000X and 2000X) images are presented in Fig.5.22 (a-d). Fig.5.22 (e-h) indicated that used CAC electrode images at different magnification (100X, 500X, 1000X and 2000X). After treatment solute are adsorbed on the surface of electrode and surface become roughs. Element composition change on surface of virgin AC electrode, anode, and cathode are shown in Fig.5.23 (a-c).

5.2.1.1.2 Cyclic voltammograms

Cyclic voltammograms of CAC electrode is presented in Fig. 5.24. The area under CV curve represent the energy storage capability of electrode material (Hu et al., 2015). Cyclic voltammograms of CAC electrode were carried with 1M sodium chloride solution at scan rate 5 mV/s, 10 mV/s, and 20 mV/s. Shapes of CV curves are almost rectangular scan rate at 5 mV/s, 10 mV/s, and 20 mV/s. Rectangular shape of CV curve almost same after increasing scan rate from 5 mV/s to 20 mV/s.
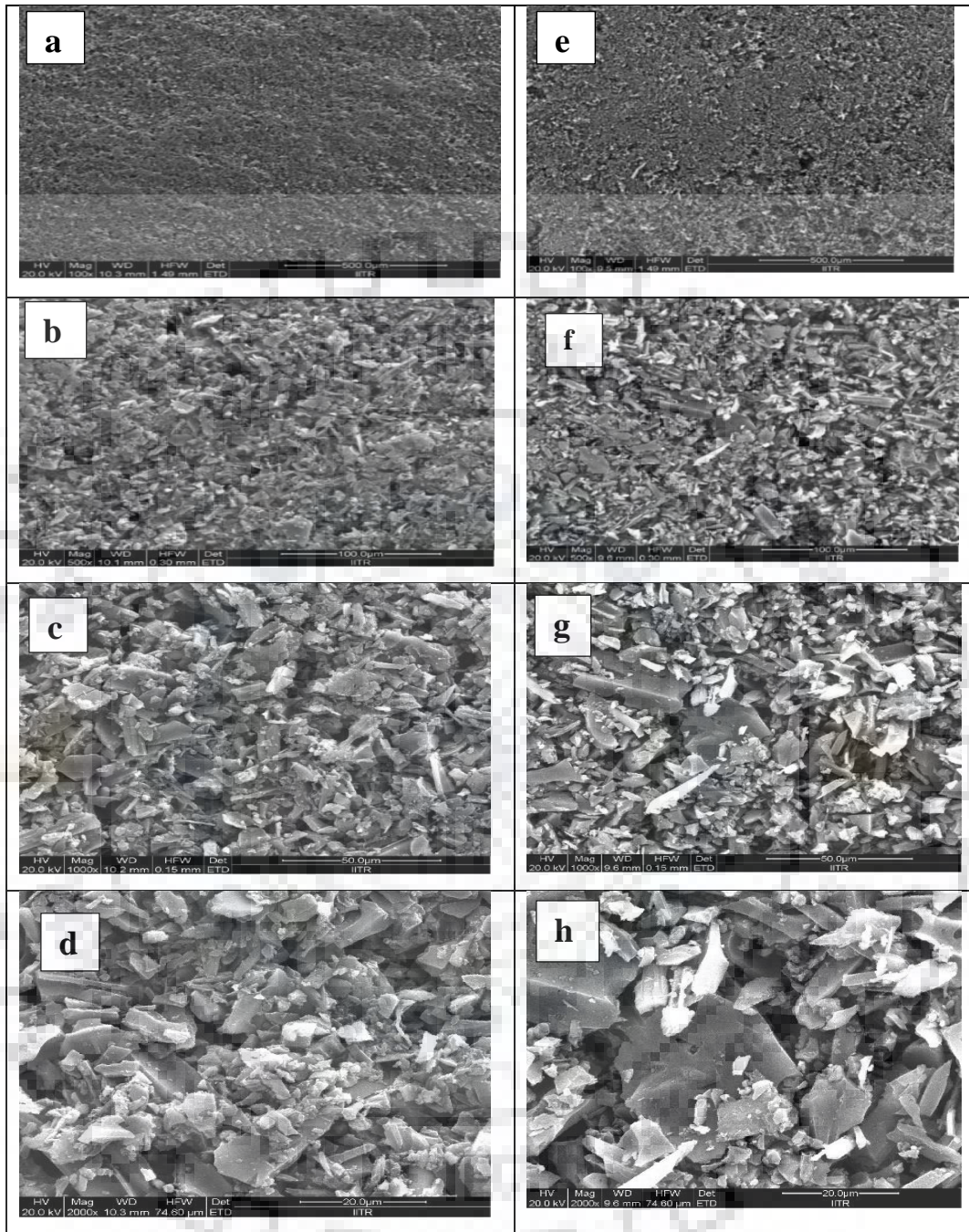
Fig. 5.22 SEM images of virgin CAC electrode (a) at 100X(b)at 500X(c)at 1000X (d) 2000X and used CAC electrode (e)at 100X (f)at 500X (g) at 1000X (h) 2000X.
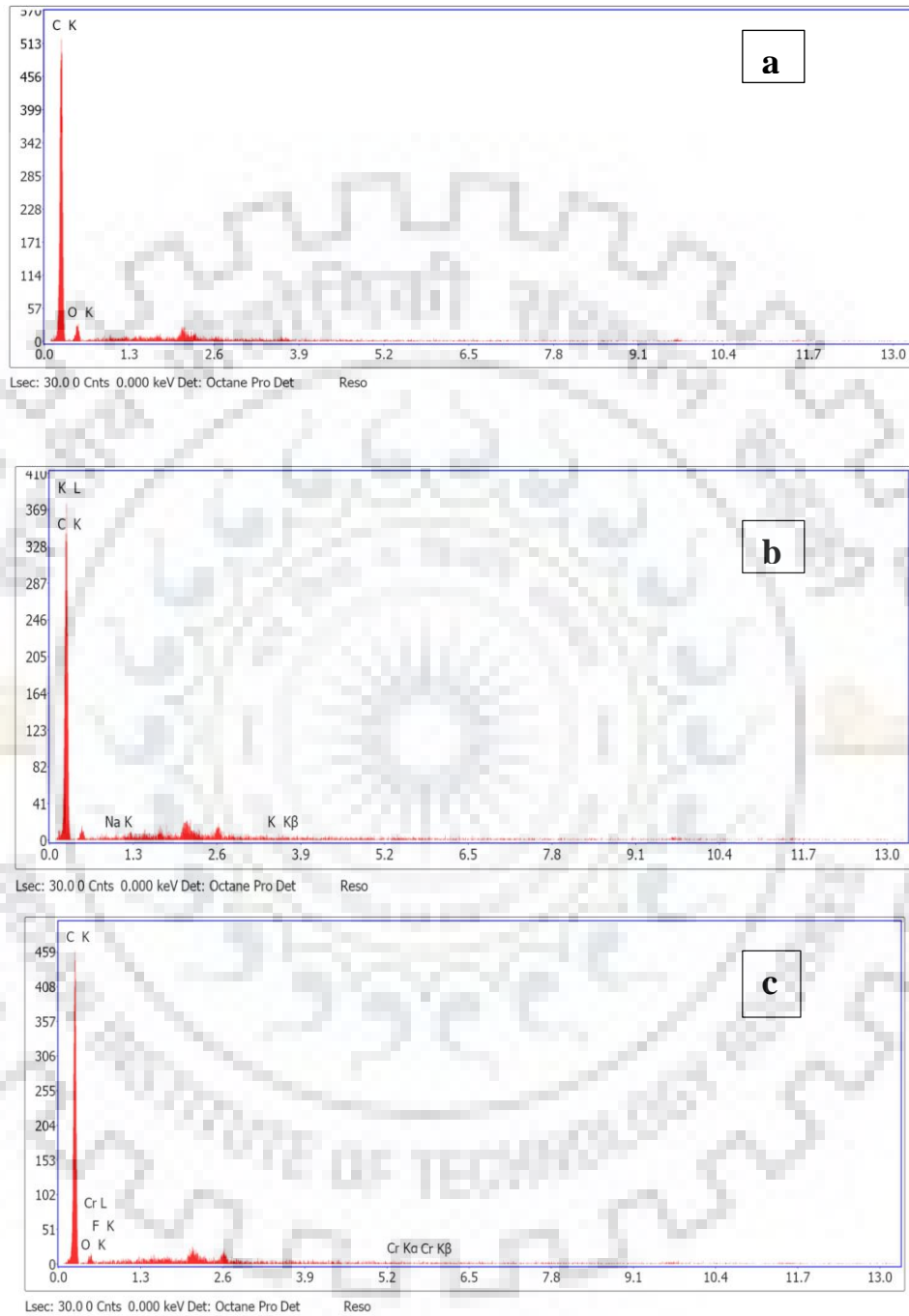
Fig. 5.23 EDX images of (a) virgin CAC electrode (b) Used CAC electrode [cathode] (c) Used AC electrode [anode].
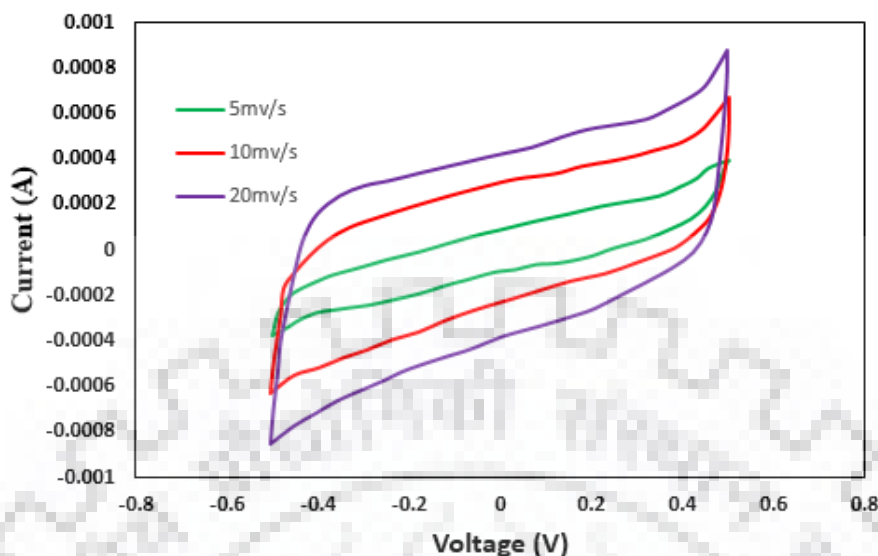
Fig. 5.24 CV curve of CAC electrode in 1M NaCl at different sweep rate.

5.2.1.2 Effect of flowrate and applied voltage on conductivity of binary feed of Cr(VI) and fluoride

The change in conductivity of Cr(VI) and fluoride binary solution with time at different flow rates is shown in Fig. 5.25. The conductivity of the binary solution decreases as the flow rate increases up to 16 mL/min and less changes in conductivity was observed as the flow rate increased beyond 16 mL/min. Maximum conductivity change was observed at 16 mL/min due to highest electrosorption of ions. At high flow rate, low electrosorption efficiency was observed due to low residence time in the CDI cell resulting in a high Cr(VI) fluoride concentration in the effluent water. For low flow rates, the feed flow rate is the limiting step to decrease the bulk concentration of Cr(VI)-fluoride binary feed solution. Hence, low electrosorption efficiency was observed. Therefore, the optimal flow rate for the highest electrosorption efficiency was obtained at 16 mL/min. The electrosorptive removal of Cr(VI) and fluoride was carried out with CAC electrodes at different range of various voltages (0.4–1.2 V). Fig. 5.26 indicates that the change in conductivity of Cr(VI) and fluoride binary feed solution with time. Effect of voltage on conductivity change was carried out with 10 mg/L Cr(VI) and fluoride binary feed solution with an initial conductivity of 75.54 μS/cm and pH 7.2 $\pm$ 0.2. It was observed that as voltage increases conductivity was decreases with time. 1.2 V was found better removal performance. Thus it was set for all experiments.
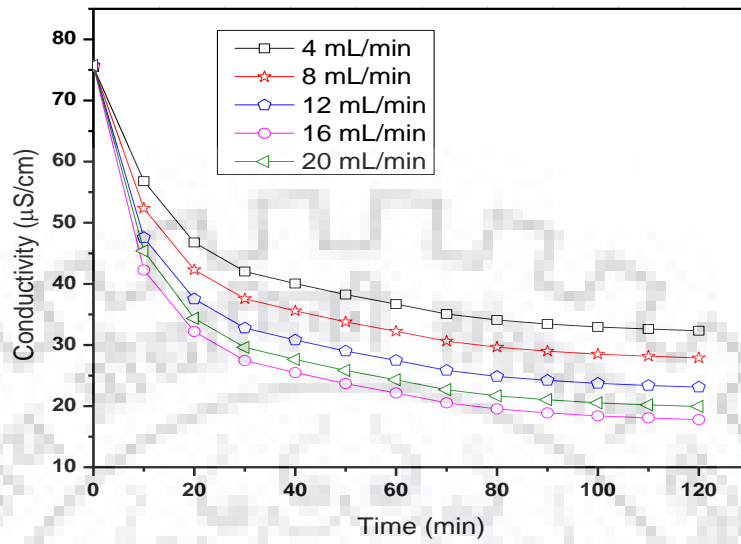
(b)

Fig. 5.25 Cr(VI) and fluoride binary feed conductivity change with time at different flow rates with CAC electrode.
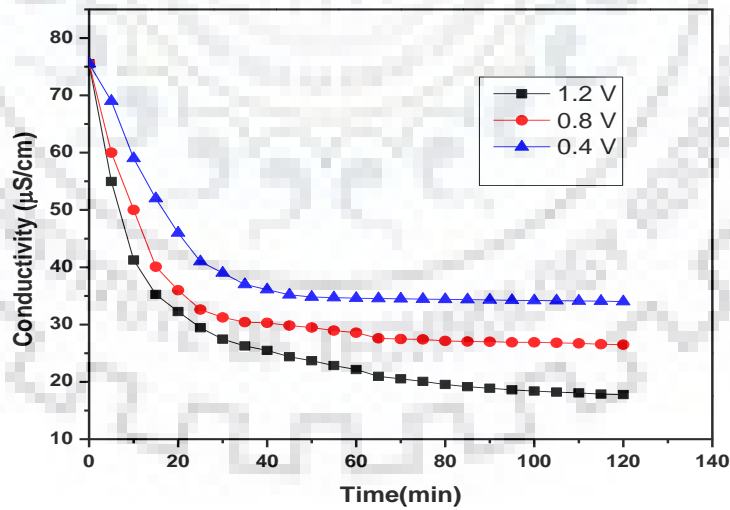
Fig. 5.26 Effect of voltage on conductivity change of Cr(VI) and fluoride binary feed with CAC electrode.

5.2.1.3 Studies on electrosorption of Cr(VI) and fluoride and regeneration of electrode

The electrosorptive removal experiments were carried out with different concentration from 10 mg/L to 100 mg/L. The electrosorption capacity with respect to time was shown in Fig. 5.27. Maximum electrosorption of Cr(VI) and fluoride were found as 0.85 mg/g and 0.82 mg/g for 10 mg/L; 2.023 mg/g and 1.88 mg/g for 25 mg/L; 2.79 mg/g and 2.44 mg/g for 50 mg/L; 3.67 mg/g and 3.22 mg/g for 100 mg/L respectively of binary feed Cr(VI) and fluoride. In simultaneous removal experiment sorption capacity of Cr(VI) was found higher than fluoride ions with CAC electrode. Hydrated radius of Fluoride (3.52 Å) (Nightingale, E.R., 1959) which was smaller than hydrated radius of CrO_4^{2-} (3.75Å) (Nightingale, E.R., 1959). The electrosorption selectivity of the divalent CrO_4^{2-} is higher than that of the monovalent F^-. This has occurred due to electrostatic attraction of divalent ion is strong than monovalent ions (Li et al. 2016). Li et al. reported similar kind of observation for the case of SO_4^{2-} and NO_3^- (Li et al. 2016).
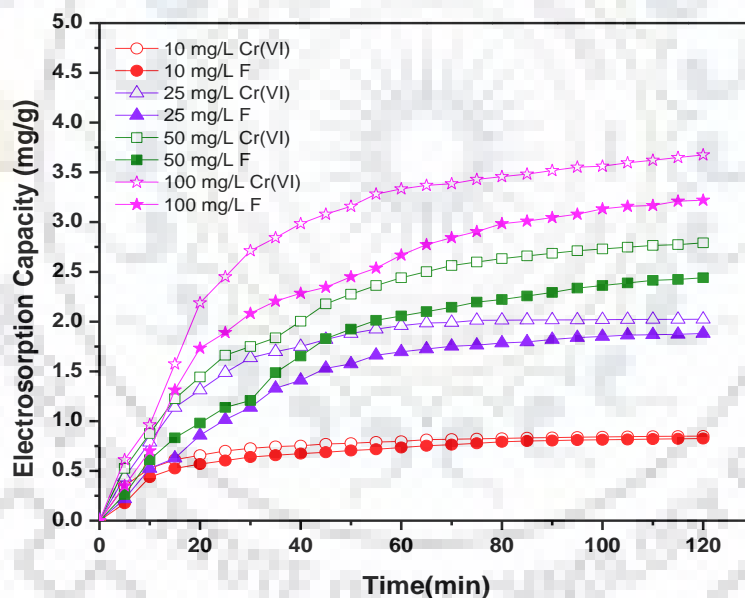
Fig. 5.27 Electrosorption capacity with time for different concentration.

Profile of maximum removal percentage at different feed concentration is shown in Fig. 5.28. Maximum removal of Cr(VI) and fluoride were found to 97.1% and 94.20% for 10 mg/L and 42% and 36.8% for 100 mg/L respectively from binary feed solution of Cr(VI) and fluoride. Purification and regeneration of electrodes are important steps in CDI. Study on regeneration of electrode was carried out. Purification and regeneration of profile with 10 mg/l Cr(VI) and fluoride binary mixture was shown in Fig. 5.29. The purification step was carried out until the conductivity of inlet feed solution was close to the CDI cell outlet stream conductivity, signifying that the electrodes were saturated by ions. Then, regeneration step was carried by removing the external voltage of electrodes. Three purification and regeneration cycle studies were conducted. The effective performance of CAC electrode was found for electrosorption of Cr(VI) and fluoride and regeneration of electrode.
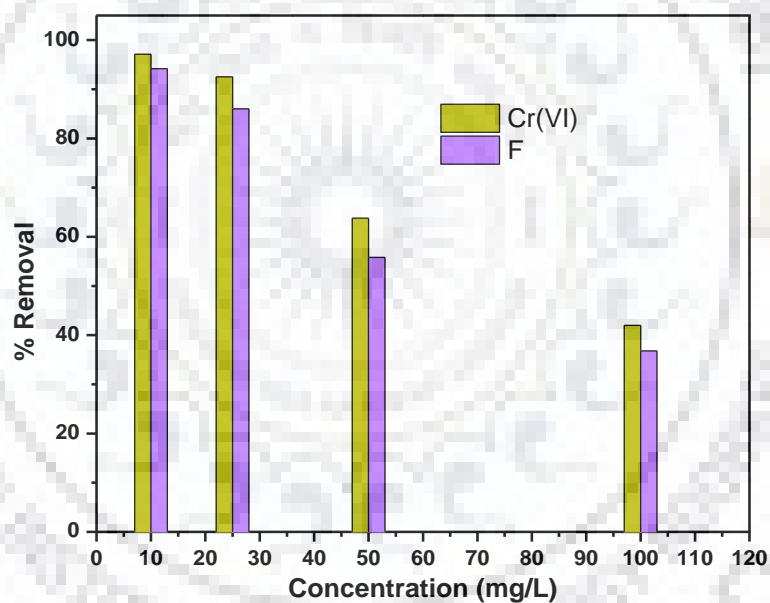
Fig. 5.28 Effect of concentration on removal percentage of Cr(VI) and fluoride with CAC electrode.
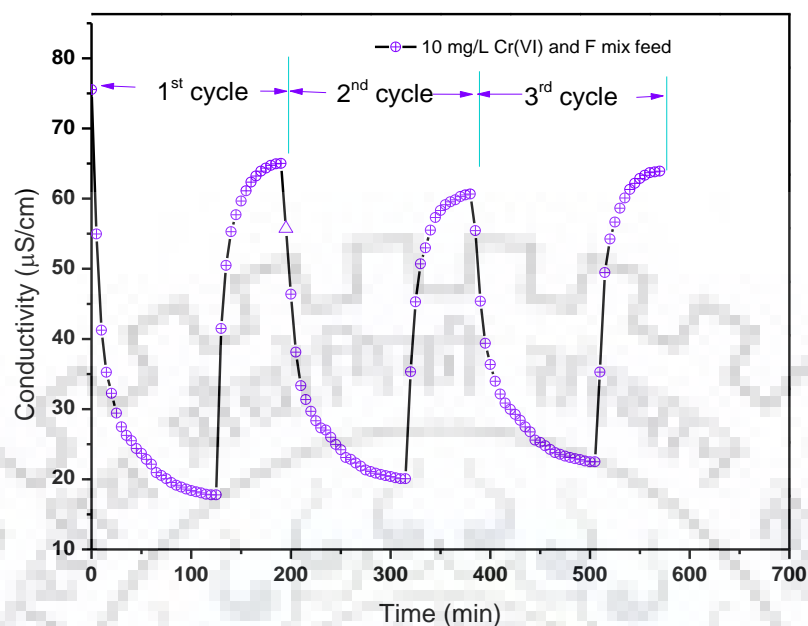
Fig. 5.29 Purification and regeneration profile of CAC electrode performance in Cr(VI) and fluoride binary feed.

5.2.1.4 Effect of pH on removal of Cr(VI) and fluoride

In the present study effect of pH was carried out with change in pH from 3 to 9 (Fig.5.30). Cr(VI) occurs in various ionic forms ($HCrO_4^-$, CrO_4^{2-}, $Cr_2O_7^{2-}$) that depend on the solution pH. It was found that minimum percent removal was observed at pH 3 because in the acidic condition Cr (VI) occurs in the monovalent form and fluoride was present in the form of HF. When pH was changed to 7 some of $HCrO_4^-$ anions converted to CrO_4^{2-} and removal was increased. When pH was adjusted to 8 and above, maximum removal (97.58 % Cr(VI) and 94.74% fluoride) was observed. In acidic medium $HCrO_4^-$, CrO_4^{2-} and H_2CrO_4 are the predominant species when pH range is 2-6. In basic medium chromium exists in the form of CrO_4^{2-} (Sahu et al., 2008). In case of fluoride, the pH between 6-9 is good for fluoride electrosorption (Wu et al., 2016). Highest removal of Cr(VI) and fluoride was found when the pH was adjusted to up to 8 and above.
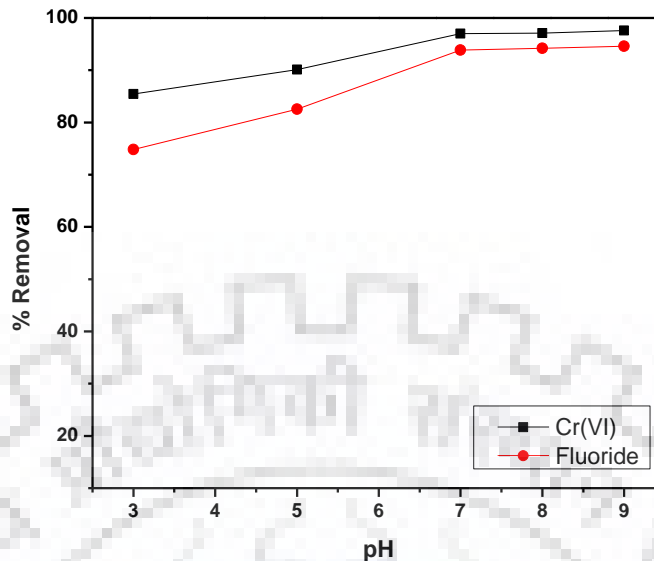
Fig. 5.30 Effect of pH on removal percentage of Cr(VI) and fluoride with CAC electrode.

5.2.1.5 Isotherm modeling

Monocomponent modeling was carried out for identification of best fit model and estimation of parameters for calculation of multicomponent equilibrium isotherm parameters. Table 5.12 shows the estimated parameters of mono and multicomponent isotherm model. In mono component modeling Redlich Peterson model and Freundlich isotherm model were found in good agreement (Fig.5.31 (a and b)) for both Cr(VI) and fluoride which is confirmed by higher R^2 value and lower value of MPSD. The value of the constant b suggested the interaction of Cr(VI): carbon interaction more stable than that of F: carbon interaction thus the value of Q_o (mg/g) for Cr(VI) was higher than fluoride. The value of constant n in Freundlich isotherm model for both Cr (VI) and fluoride is greater than 1 and lies in the range of 2–10 signifying more favorable adsorption. The β value in R-P model lies in 0-1 range suggesting good adsorption. In multicomponent isotherm modeling, Extended Freundlich and Non Modified R–P model were best agreed with experimental data having lower MPSD and higher R^2 values for both Cr(VI) and fluoride than other multicomponent isotherm models (refer Table 5.12). It is clear from Fig. 5.32 (a and b) that the Extended Freundlich and Non Modified R–P model for both Cr(VI) and fluoride agreed well with experimental data for binary sorption of Cr(VI) and fluoride.

Table 5.12 Estimated parameter of mono and multicomponent isotherms modelling for electrosorption of Cr(VI) and fluoride with CAC electrode.

Name of model	Parameters	Cr(VI)	Fluoride
Single component			
Langmuir	Q_0 (mg g^{-1})	3.136	2.922
	b (L mg^{-1})	2.183	0.840
	MPSD	18.72	15.87
	R^2	0.445	0.5193
Freundlich	K_F(mg g^{-1}) / (mg L^{-1})$^{1/n}$	1.485	1.132
	n	4.002	3.578
	MPSD	17.30	14.86
	R^2	0.8615	0.8873
Redlich–Peterson	K_{RP}(L g^{-1})	11.01	3.728
	a_{RP}(L mg^{-1})	5.047	1.968
	β	0.867	0.863
	MPSD	7.899	7.704
	R^2	0.7146	0.7397
Multicomponent			
Non modified Langmuir	MPSD	37.330	75.71
	R^2	0.5697	0.5787
Modified Langmuir	η_i	0.979	0.641
	MPSD	48.63	61.76
	R^2	0.6112	0.6565
Extended Langmuir	$Q_{0,i}$ (mg g^{-1})	49.07	2.740
	b_i (L mg^{-1})	0.080	0.876
	MPSD	19.76	18.18
	R^2	0.711	0.4749
Extended Freundlich	x_i	0.001	0.001
	y_i	0.109	0.078
	z_i	0.001	0.001
	MPSD	19.49	16.43
	R^2	0.871	0.8911
Non Modified R–P model			
	MPSD	28.60	16.15
	R^2	0.7401	0.7488
Modified R–P model	$\eta_{i,j}$	0.185	0.112
	MPSD	32.02	51.77
	R^2	0.828	0.6293
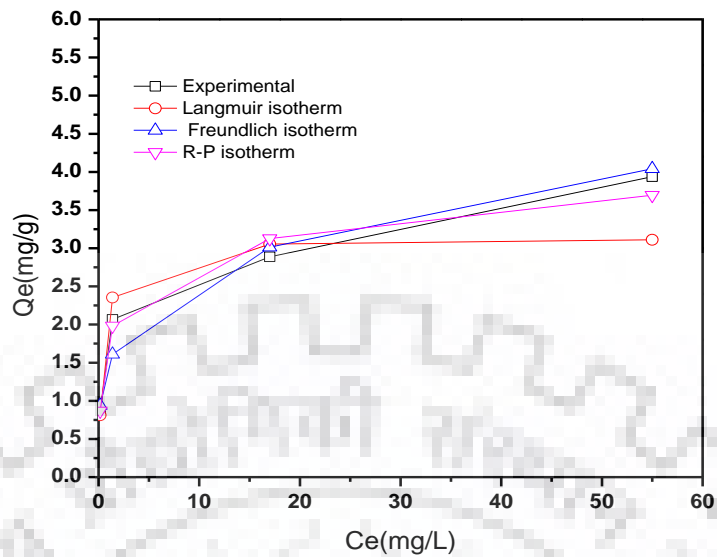
(a)
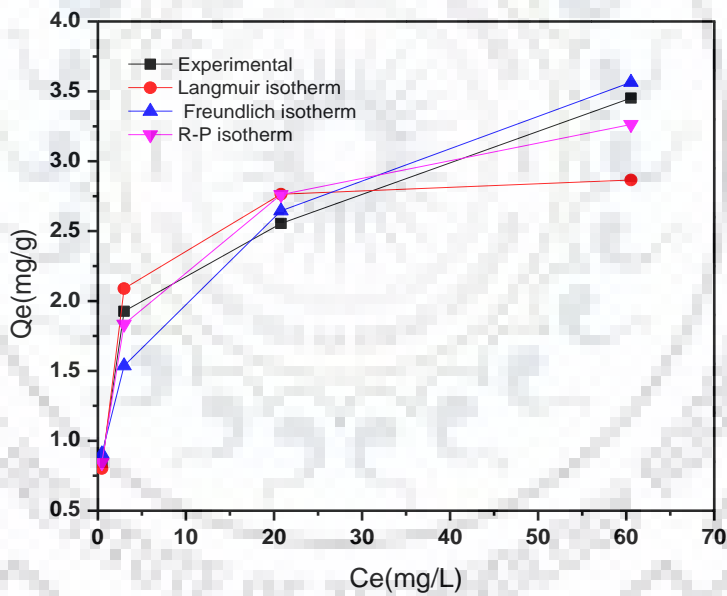
(b)

Fig. 5.31 Comparison of monocomponent isotherm models for electro sorption of (a) Cr(VI) and (b) Fluoride with CAC electrode.
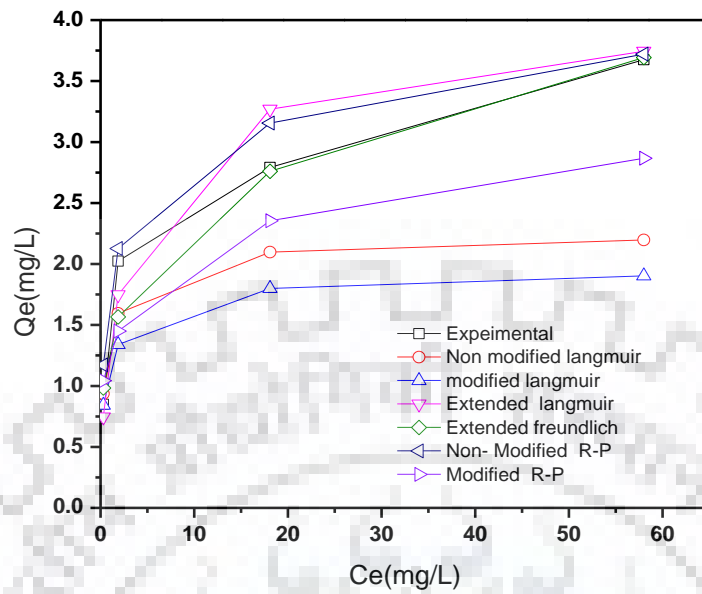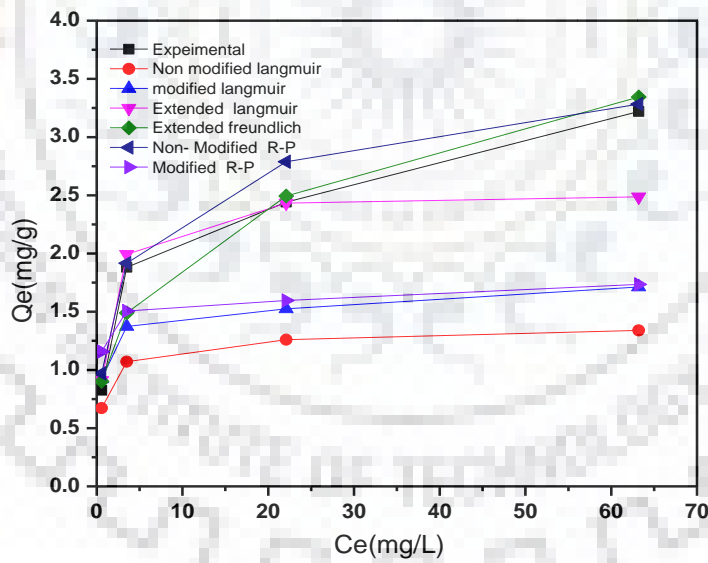
Fig. 5.32 Comparison of multicomponent isotherm models for electrosorption of (a) Cr(VI) and (b) Fluoride with CAC electrode.

5.2.1.6 Kinetic modeling

The experimental data for the dual sorption of Cr(VI) and fluoride were applied to the pseudo first order, pseudo second order kinetic model. The kinetic model: pseudo first order and pseudo second order model for Cr(VI) and fluoride is shown in Fig. 5.33 (a and b) respectively. The value of parameters of kinetic model for Cr(VI) and fluoride is depicted in Table 5.13, respectively. In both the cases the kinetic data are well agreed with the Pseudo first order model which is further confirmed by lower ARE values and higher R^2 compared to Pseudo second order kinetic model. A comparative graph of experimental and calculated value of the elctrosorption capacity Qt (mg/g) for both Cr(VI) and fluoride is shown in Fig. 5.33 (a and b) respectively. It is clear that experimental value for both Cr(VI) and fluoride is in good agreement with the pseudo first order model. This suggested that the electrosorption is because of electrostatic interaction between ions on the electrode and in solution (Li et al., 2009).
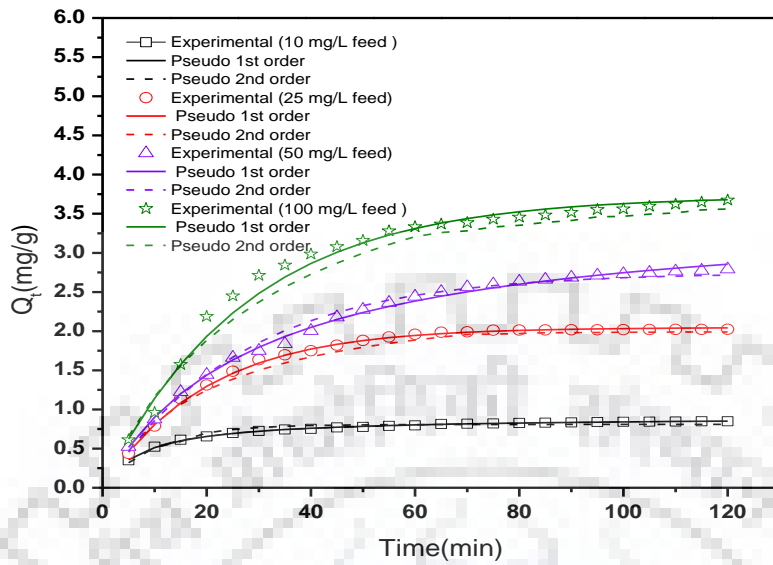
(a)
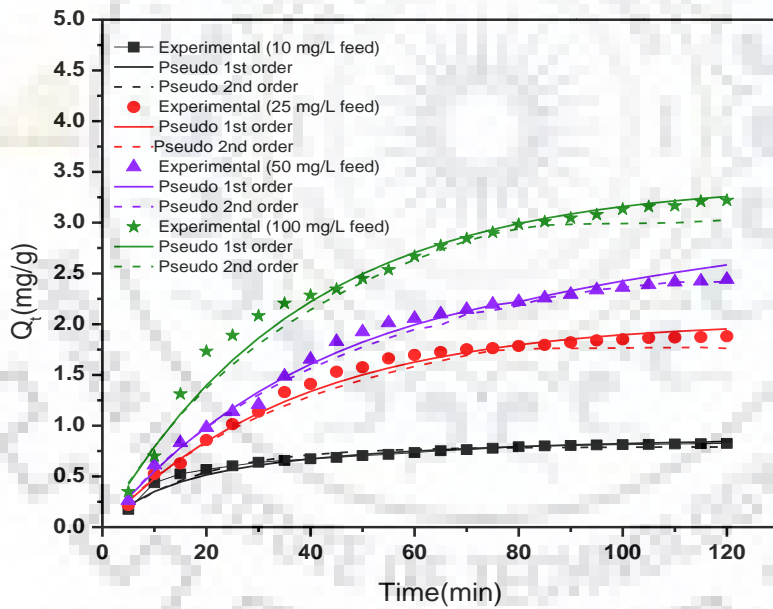
(b)

Fig. 5.33 Comparison of kinetic models for electrosorption of (a) Cr(VI) and (b) Fluoride with CAC electrode.

Table 5.13 Estimated parameter of kinetic modelling for electrosorption of Cr(VI) and fluoride with CAC electrode.

Kinetic models	Parameters	Concentration			
		Cr(VI)			
		10 mg L^{-1}	25 mg L^{-1}	50 mg L^{-1}	100 mg L^{-1}
Pseudo first order					
	$q_{e,cal}$ (mg g^{-1})	0.9669	2.8917	3.8347	4.9420
	k_1(min^{-1})	0.1448	0.0190	0.0095	0.0062
	ARE	0.1864	0.3320	0.4154	1.1156
	R^2	0.6718	0.7155	0.8546	0.7913
Pseudo second order					
	$q_{e,cal}$ (mg g^{-1})	0.8088	2.0465	2.7471	3.7248
	k_2(g mg^{-1} min^{-1})	0.1006	0.0501	0.0374	0.0366
	ARE	0.8736	1.0920	0.7658	1.5932
	R^2	0.4326	0.6732	0.7728	0.7798
		Fluoride			
Pseudo first order					
	$q_{e,cal}$(mg g^{-1})	0.9051	2.5369	3.5537	4.8861
	k_1(min^{-1})	0.0589	0.0069	0.0044	0.0039
	ARE	1.3629	1.0861	0.9298	1.6387
	R^2	0.7867	0.8627	0.9094	0.8650
Pseudo second order					
	$q_{e,cal}$(mg g^{-1})	0.7900	2.0350	2.6441	3.3992
	k_2(g mg^{-1} min^{-1})	0.0580	0.0267	0.0233	0.0264
	ARE	1.5070	1.5256	1.1679	1.9356
	R^2	0.6192	0.8111	0.8978	0.8330

5.2.1.7 Conclusive remarks

The present study includes the characterization of electrode, performance of electrode, isotherms and kinetic study for simultaneous removal of Cr(V) and fluoride for mix feed of Cr(VI) and fluoride. It is observed in the present study that better optimized flow rate 16 mL/min, optimized voltage 1.2 V which was set for all further experiments. Maximum removal of Cr(VI) and fluoride were found to be 97.1% and 94.20% for 10 mg/L mix feed of Cr(VI) and fluoride. Effective purification and regeneration of electrode were found for the case of binary feed solution of Cr(VI) and fluoride. Freundlich isotherm model and Redlich Peterson model was found in good agreement for both Cr(VI) and fluoride in mono component models. Extended Freundlich model and Non Modified R–P model among six applied multicomponent isotherm models were found to fit well with the experimental data for both Cr(VI) and fluoride Electrosorption performance . Pseudo first order kinetic model was found to be in good agreement with experimental data for both Cr(VI) and fluoride.

5.2.2 Studies on CDI with tea waste activated carbon electrode

5.2.2.1 Characterization

5.2.2.1.1 SEM

TWBAC morphology was studied by using SEM analysis. TWBAC surface morphology at different magnifications is shown in Fig. 5.34 (a-d). The morphological images indicated that TWBAC was highly microporous in nature. The shape and size of pores were clearly observed at 5.00 KX magnifications. The irregular pore structure was observed in Fig. 5.34 (d).

5.2.2.1.2 TGA/DTA/DTG Analysis

TGA/DTA/DTG analysis of tea waste biomass was carried out using a thermal analysis instrument (PerkinElmer Pyris Diamond, USA) in a nitrogen atmosphere with a flow rate 200 ml min^{-1}. Thermal stability of tea waste biomass is directly dependent on the decomposition temperature of its various functional groups and oxides. The TGA, DTA and DTG profiles of tea waste biomass are shown in Fig. 5.35. The TGA curve shows three main zones, in which the first zone is from 29 to 200 ºC and it indicates the loss in weight of tea waste biomass due to moisture and light volatile compounds with moderate rate. The second zone is from 200 to 560 ºC in which weight loss of tea waste biomass increases due to evolution of CO_2 and CO with high rate. The third zone is from 560 to 1000 ºC where weight loss slightly declined or became nearly constant. The maximum degradation rates are found to be 0.70 mg min^{-1} at 327 ºC for tea waste biomass in DTG curve. A significant amount of heat (-2.68 J mg^{-1}) was released due to oxidation of tea waste biomass at a temperature of 510 ºC.
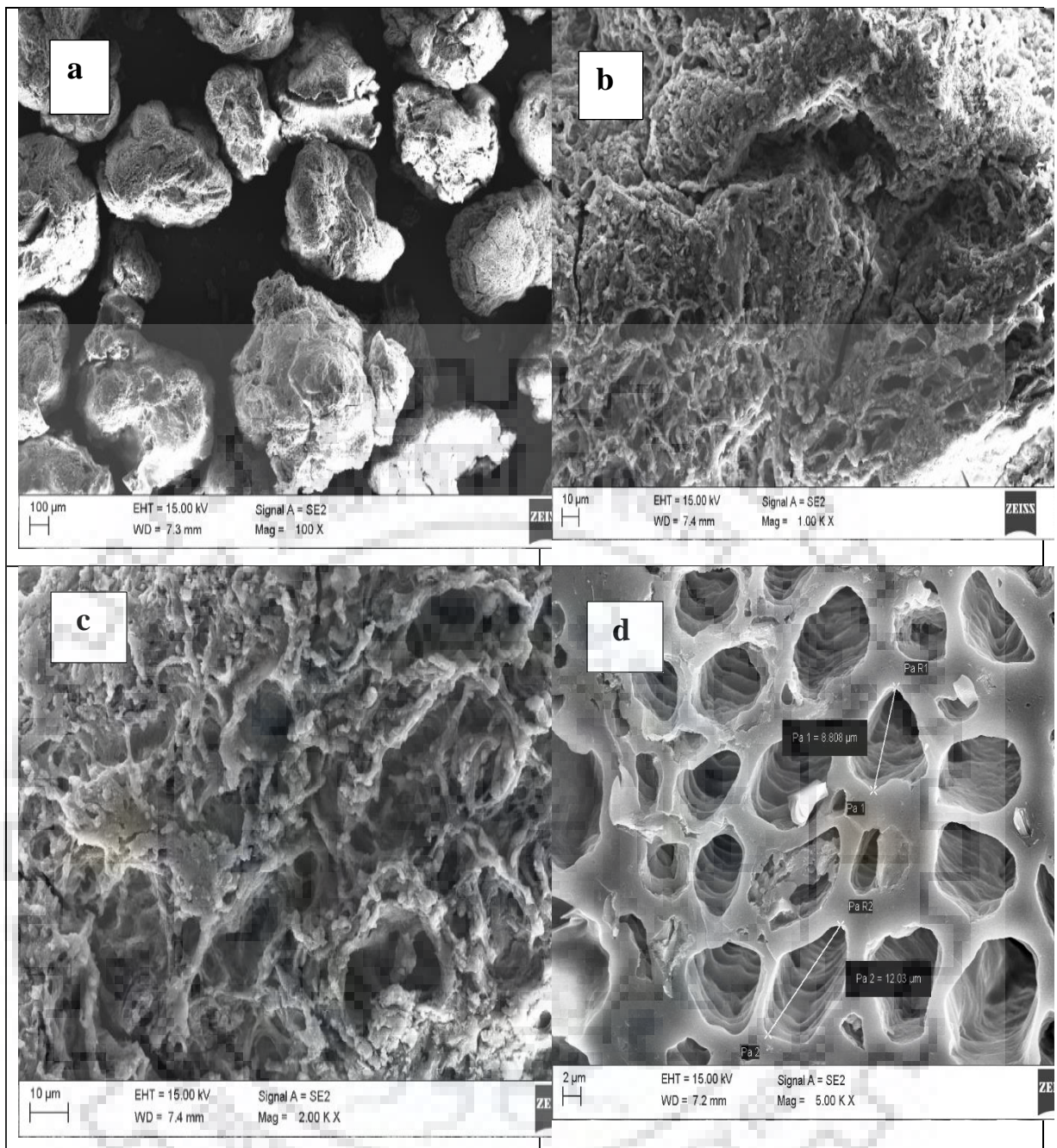
Fig. 5.34 SEM micrographs of TWBAC (a) at 100X (b) 1.00 KX(c) 2.00KX (d) 5.00 KX.
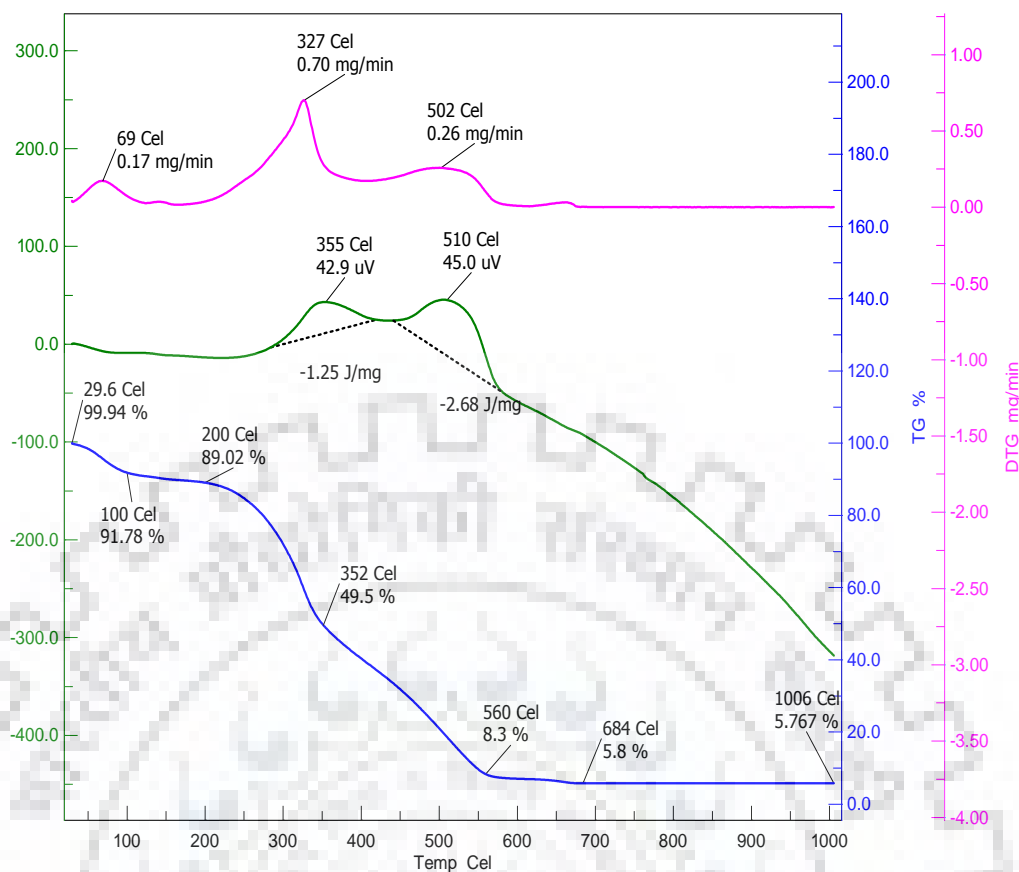
Fig. 5.35 TGA/DTA/DTG analysis graphs of tea waste biomass

5.2.2.1.3 FTIR

FTIR graph of TWBAC was shown in Fig. 5.36. The FTIR graph indicates sharp peaks in the range of 3800–3200 cm^{-1} which shows the presence of water molecules in the lattice structure of a crystalline compound due to O–H stretching. The long stretch bandwidth around 3500–3200 cm^{-1} suggests the existence of O−H and N−H functional groups, although located at different bandwidths. The peak 3465 cm^{-1} indicate that TWBAC has its O−H bandwidth. The TWBAC has peaks in between 2342 − 2226 cm^{-1} representing C−H stretching. The peak position located between 1599.41 and 1400 cm^{-1} indicates saturated CH$_3$, CH$_2$ and CH, functional groups such as C═O, C−O and C═C. Some inorganic sulfates and silica Si−O−Si asymmetric stretch were found in the wavenumber range between 1120–603 cm^{-1}. The peak range between 700–600 cm^{-1} indicates C–S stretching, which confirms the presence of sulfur compound.
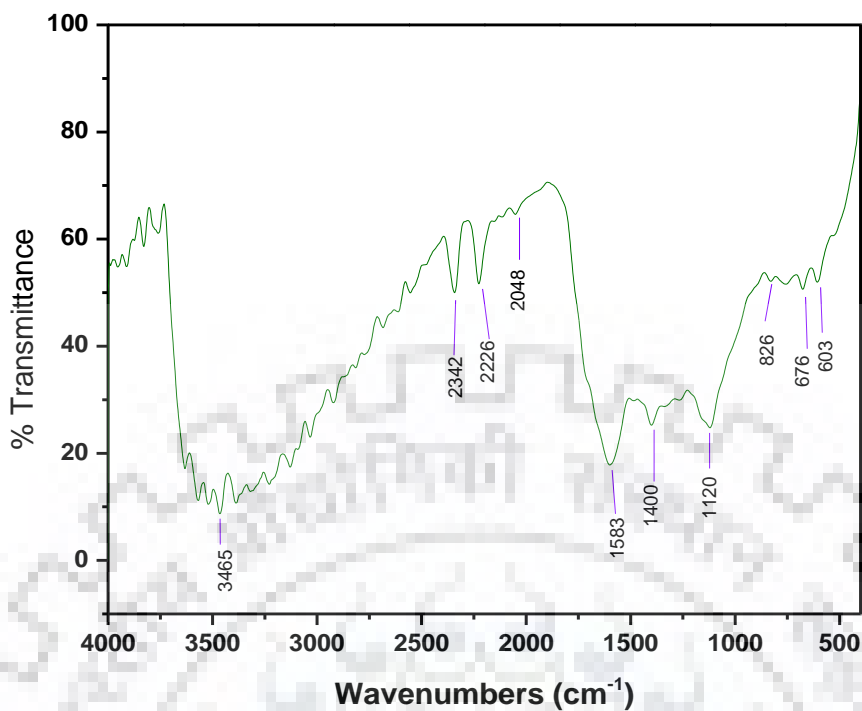
Fig. 5.36 FTIR spectra of TWBAC.

5.2.2.2 Effect on conductivity change

The electrosorptive removal of Cr(VI) and fluoride was carried out with TWBAC electrodes at an initial conductivity of 75.54 μS cm^{-1} and pH 7.1 $\pm$ 0.25. It was observed that as voltage increased, conductivity was decreased with time. The 1.2V showed better removal performance, thus it was set for all experiments. Fig. 5.37 indicates the change in conductivity of Cr(VI) and fluoride binary feed solution with time at different feed concentration. Conductivity of feed solution was decreased with respect to time due to sorption of Cr(VI) and fluoride by TWBAC porous electrode. At the start, the conductivity of feed solution of Cr (VI) and fluoride was decreased drastically and after some time it was found declining slowly.

178
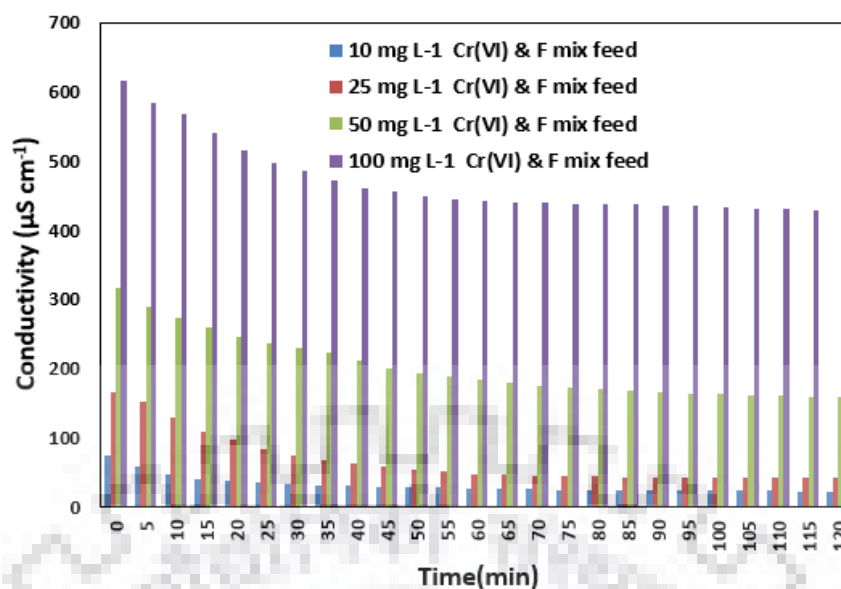
Fig. 5.37 Conductivity change vs. time at different feed concentration with TWBAC electrode.

5.2.2.3 Electrosorption and desorption study with TWBAC electrode

In this study 1.2 V was applied to terminals of TWBAC electrodes to create a positive and negative pole. Feed solution was passed through the space between these two charged porous electrodes. Due to electrostatic force, cations (Na^+ and K^+ ions) and anions ($HCrO_4^-/CrO_4^{2-}/CrO_7^{2-}$ and F^- ions) are attracted towards negative and positive TWBAC electrodes respectively. Here the electrodes act as a capacitor, which store the ions into the pores and surface of electrodes. The electrosorptive removal experiments were carried out with different feed concentrations (10, 25, 50 and 100 mg L^{-1}). Electrosorption capacity with respect to time is shown in Fig. 5.38. Maximum electrosoption capacity of Cr(VI) and fluoride were found to be 0.77 and 0.74 mg g^{-1} for 10 mg L^{-1}; 2.83 and 2.49 mg g^{-1} for 100 mg L^{-1} respectively. In simultaneous removal experiment, sorption capacity of Cr(VI) was found higher than fluoride ions with TWBAC electrode. Hydrated radius of F (3.52 Å) (Nightingale, E.R., 1959) was smaller than the hydrated radius of CrO_4^{2-} (3.75Å) (Nightingale, E.R., 1959). Cr(VI) occurs in various ionic forms ($HCrO_4^-$, CrO_4^{2-}, $Cr_2O_7^{2-}$) that depend on the solution pH. In acidic medium $HCrO_4^-$, CrO_4^{2-} and H_2CrO_4 are the predominant species. $HCrO_4^-$ and $Cr_2O_7^{2-}$ are predominant in equilibrium when pH range is 2-6. In basic medium chromium exists in the form of CrO_4^{2-} (Sahu et al., 2008). In case of fluoride, the pH between 6-9 is good for fluoride electrosorption (Wu et al., 2016). The electrosorption selectivity of the divalent CrO_4^{2-} is higher than that of the monovalent F^-. This occurs due to electrostatic attraction of divalent ion

179

which is stronger than monovalent ions (Li et al. 2016). Li et al. reported similar kind of observation in the case of SO_4^{2-} and NO_3^- (Li et al. 2016). The profile of maximum percentage removal at different feed concentration is shown in Fig. 5.39. The maximum removal of Cr(VI) and fluoride were found to be 88.5% and 85.20% for 10 mg L^{-1} and 32.45% and 28.52% for 100 mg L^{-1} respectively from the mix feed solution of Cr (VI) and fluoride. Study on regeneration of electrode was carried out. Electrosorption and desorption profile of TWBAC electrode with 10 mg L^{-1} mix feed solution of Cr(VI) and Fluoride was shown in Fig. 5.40. Effective regeneration of TWBAC electrode was found after simultaneous electrosorption of Cr(VI) and fluoride.
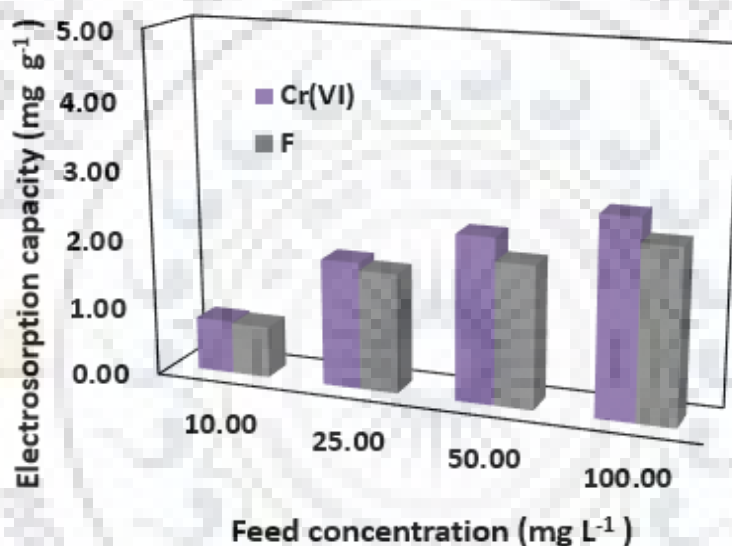
Fig. 5.38 Effect of initial Cr(VI) and fluoride mix feed concentration on electrosorption capacity with TWBAC electrode.
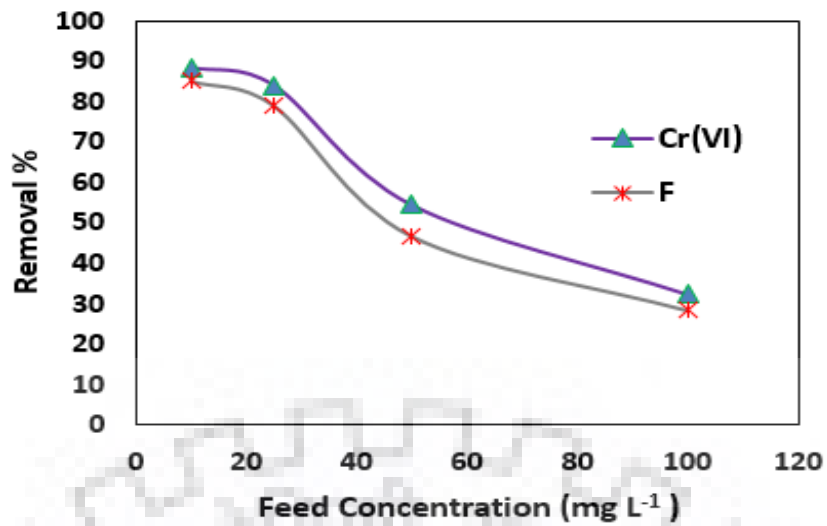
Fig. 5.39 Effect of initial Cr(VI) and fluoride mix feed concentration on removal percentage with TWBAC electrode.
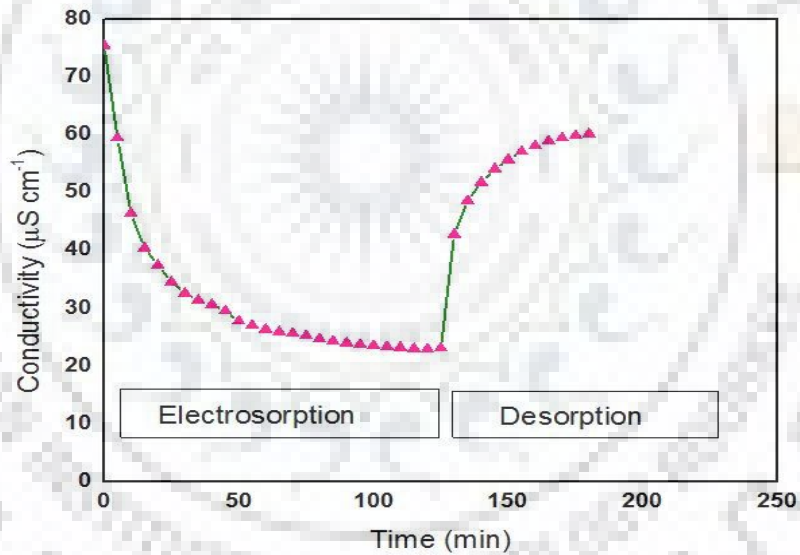
Fig. 5.40 Electrosorption and desorption performance of TWBAC electrode with Cr(VI) and fluoride mix feed.

5.2.2.4 Isotherm modeling

Single component modeling was done to find out the best fit model and for estimation of parameters used to evaluate the multicomponent equilibrium isotherm parameters. In single component modeling, Langmuir isotherm model and Redlich Peterson model were founded in best agreement (Fig.5.41 a and b) for both Cr (VI) and fluoride which is confirmed by the lower value of MPSD. The value of the constant b suggests that the interaction of Cr (VI): carbon interaction more stable than that of fluoride: carbon interaction, thus the value of Q_o (mg g^{-1}) for Cr(VI) is higher than fluoride. In multicomponent isotherm modeling, Extended Langmuir and Non modified Redlich Peterson were best agreed with experimental data having lower MPSD for both Cr(VI) and fluoride than other multicomponent isotherm models (Table 5.14). It is clear from Fig. 5.42 (a and b) that Extended Langmuir and Non modified Redlich Peterson for both Cr(VI) and fluoride agreed well with experimental data for binary sorption of Cr(VI) and fluoride. The predicted parameter of single and multicomponent isotherm model was systematically shown in Table 5.14.

5.2.2.5 Kinetic modeling

The experimental data of simultaneous sorption of Cr(VI) and fluoride were used in the pseudo first order and pseudo second order kinetic model to estimate the parameters of kinetic models. The value of parameters of kinetic models for Cr (VI) and fluoride is systematically shown in Table 5.15. The comparison of experimental data and kinetic models for Cr(VI) and fluoride were represented in Fig. 5.43 (a and b). In both cases the experimental data are well agreed with the Pseudo first order model which is confirmed by lower ARE values compared to Pseudo second order kinetic model. The experimental and calculated value of the electrosorption capacity Qt (mg g^{-1}) for both Cr(VI) and fluoride were represented systematically in Fig. 5.43 (a and b), respectively. It is clear that experimental value for both Cr(VI) and fluoride is in good agreement with the pseudo first order model. This suggested that the electrosorption is because of electrostatic interactions between ions on the electrode and in solution (Li et al., 2009).
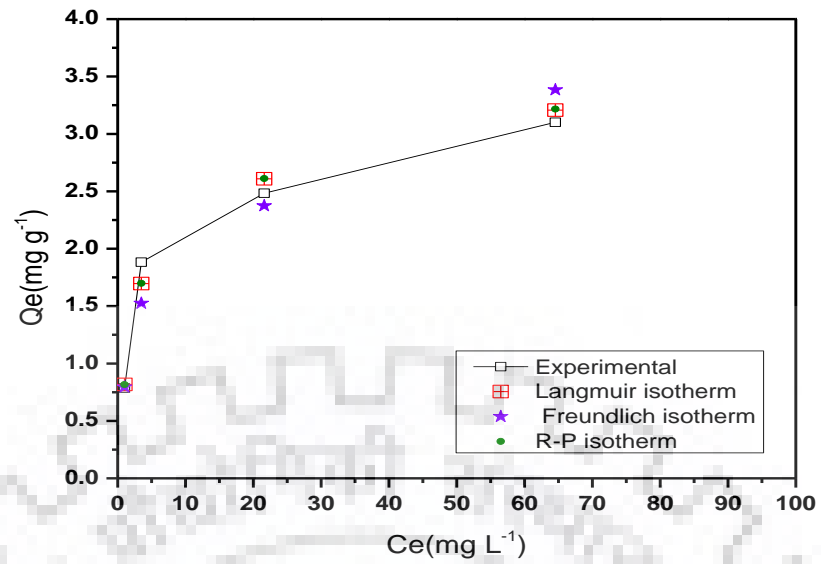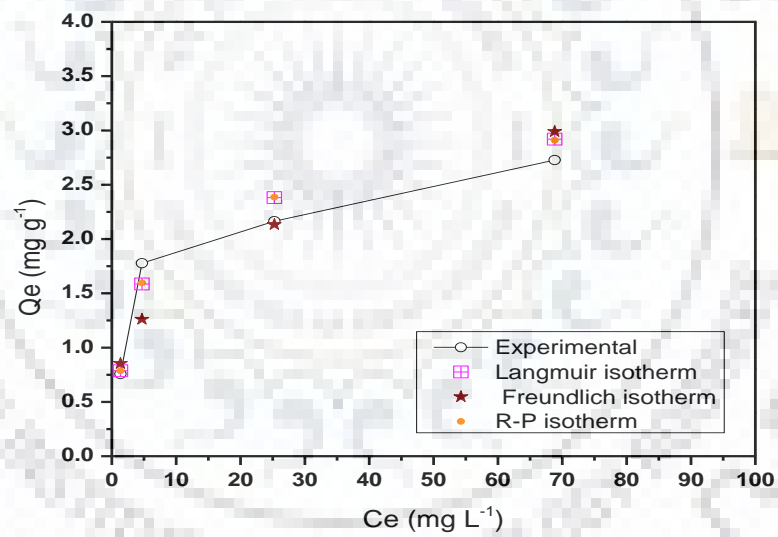
Fig. 5.41 Comparisons of single component isotherms for electrosorption of (a) Cr(VI) (b) fluoride with TWBAC electrode.
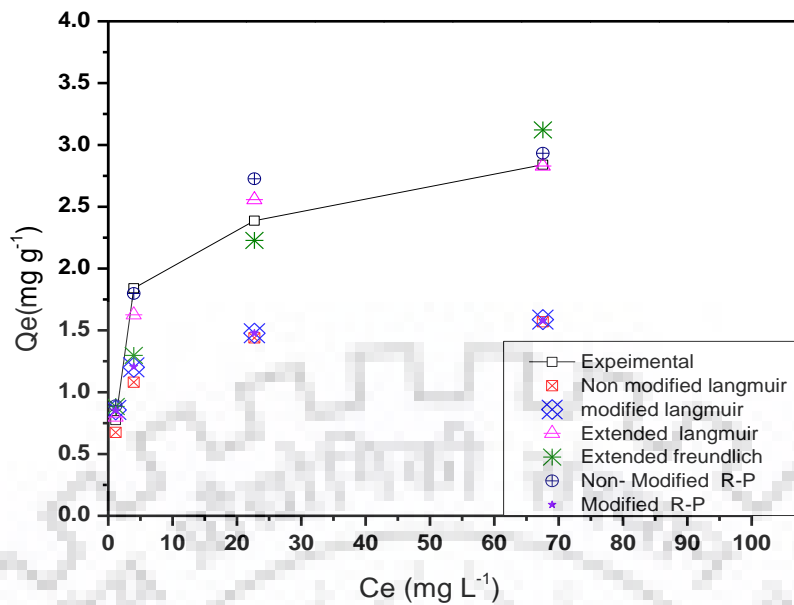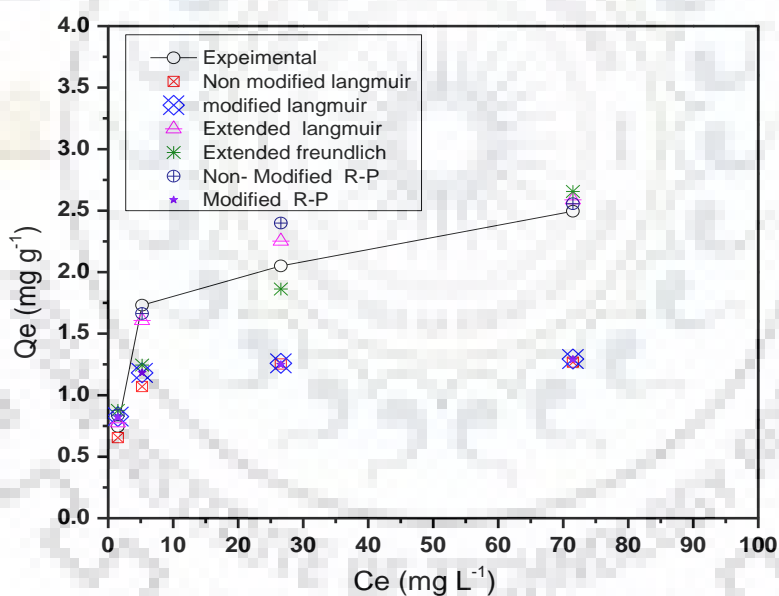
Fig. 5.42 Comparisons of multicomponent component isotherms for electrosorption of (a) Cr(VI) (b) fluoride with TWBAC electrode.

Table 5.14 Estimated parameter of mono and multicomponent isotherms modelling for electrosorption of Cr(VI) and fluoride with TWBAC electrode.

Name of model	Parameters	Cr(VI)	Fluoride
Single component			
Langmuir	Q_0 (mg g^{-1})	3.0597	2.6885
	b (L mg^{-1})	0.3573	0.3066
	MPSD	10.661	11.540
Freundlich	K_F(mg g^{-1}) / (mg L^{-1})$^{1/n}$	0.8891	0.7772
	n	3.1299	3.1971
	MPSD	24.136	23.035
Redlich–Peterson	K_{RP}(L g^{-1})	1.0880	0.8110
	a_{RP}(L mg^{-1})	0.3516	0.2908
	β	1.0030	1.0098
	MPSD	10.659	11.525
Multicomponent			
Non modified Langmuir	MPSD	52.184	52.680
Modified Langmuir	η_i	0.6061	0.6099
	MPSD	48.546	49.722
Extended Langmuir	$Q_{0,i}$ (mg g^{-1})	11.2741	3.7385
	b_i (L mg^{-1})	0.2590	0.0647
	MPSD	9.9374	11.317
Extended Freundlich	x_i	0.0092	0.0000
	y_i	0.0504	0.4430
	z_i	0.0000	0.0000
	MPSD	24.629	23.746
Non Modified R–P model	MPSD	14.899	15.225
Modified R–P model	$\eta_{i,j}$	0.6275	0.6259
	MPSD	48.574	49.903

Table 5.15 Estimated parameter of kinetic modelling for electrosorption of Cr(VI) and fluoride with TWBAC electrode.

Kinetic models	Parameters	Concentration			
		Cr(VI)			
		10 mg L^{-1}	25 mg L^{-1}	50 mg L^{-1}	100 mg L^{-1}
Pseudo first order					
	$q_{e,cal}$ (mg g^{-1})	0.8427	2.6126	3.1360	3.7121
	k_1 (min^{-1})	0.0868	0.0113	0.0090	0.0089
	ARE	0.3738	1.6354	0.8629	0.8435
Pseudo second order	$q_{e,cal}$ (mg g^{-1})	0.7392	1.9477	2.3804	2.8474
	k_2 (g mg^{-1} min^{-1})	0.1250	0.0367	0.0320	0.0379
	ARE	0.7696	2.2428	1.2164	1.2573
	Fluoride				
Pseudo first order					
	$q_{e,cal}$ (mg g^{-1})	0.7235	2.3024	2.8256	3.4253
	k_1 (min^{-1})	0.0488	0.0201	0.0250	0.0076
	ARE	1.5517	1.8947	0.7516	1.9457
Pseudo second order					
	$q_{e,cal}$ (mg g^{-1})	0.6149	1.7560	2.1047	2.5446
	k_2 (g mg^{-1} min^{-1})	0.0868	0.0540	0.0043	0.0082
	ARE	1.7781	3.1247	1.0110	3.6478
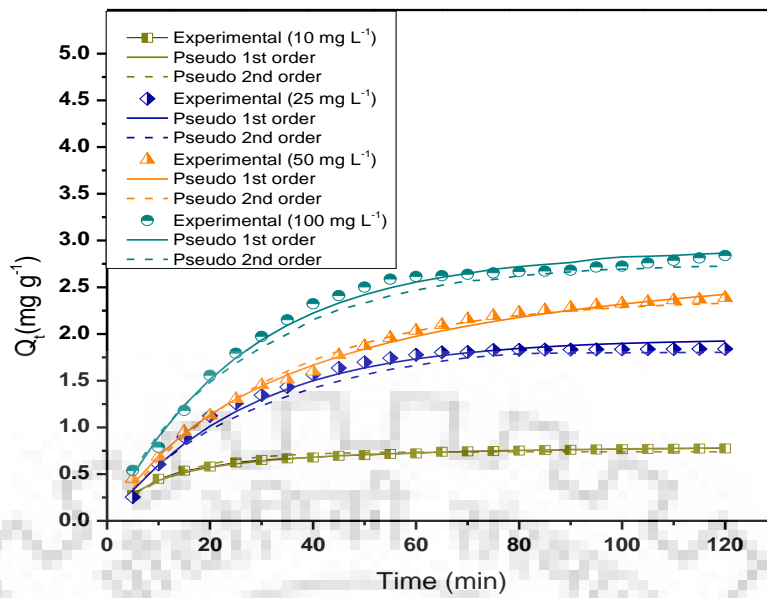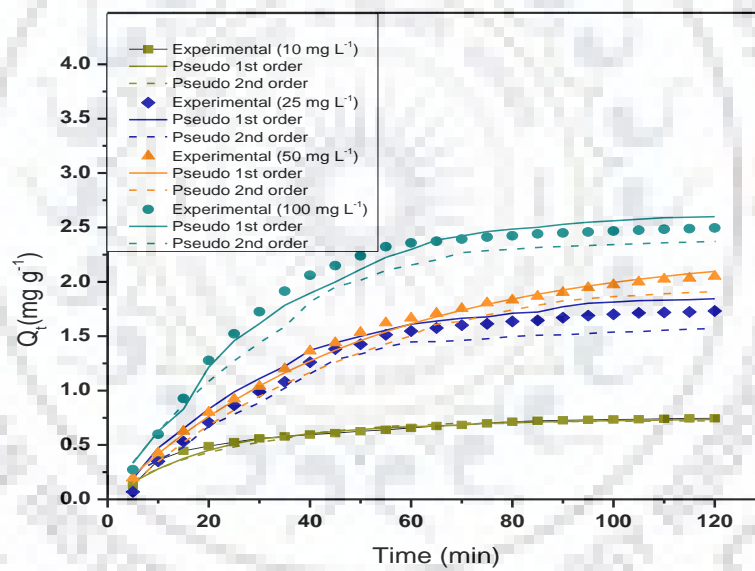
Fig. 5.43 Comparisons of kinetic models for electrosorption of (a) Cr(VI) (b) fluoride with TWBAC electrode.

5.2.2.6 Conclusive Remark

The TWBAC was successfully prepared from tea waste biomass and it was implemented for electrode preparation. The TWBAC electrode was applied in CDI application for simultaneous removal of Cr (VI) and fluoride from the mix feed solution of Cr (VI) and fluoride. The percent removal of Cr(VI) and fluoride were found to be 88.5% and 85.20% for 10 mg L-1 mix feed solution respectively. The effective electrosorption and desorption with TWBAC electrode were observed. In single component isotherm modeling, Langmuir isotherm model and Redlich Peterson model were found in best agreement for both Cr(VI) and fluoride removal. Among the six applied multicomponent isotherm models, Extended Langmuir model and Non modified Redlich Peterson were found in good correlation with the experimental data for both Cr(VI) and fluoride removal. In the kinetic study, Pseudo first order kinetic model was found in good fit with experimental data for both Cr(VI) and fluoride.

5.2.3. Studies on CDI with RHAC electrode

5.2.3.1 Characterization

5.2.3.1.1 SEM

RHAC morphology was studied by using SEM analysis. RHAC surface morphology at different magnifications were shown in Fig. 5.44 (a-c). The morphological images indicated that RHAC was highly microporous in nature. The shape and size of pores were clearly observed at 3.00 KX magnifications. The irregular pore structure was observed in Fig. 5.44 (c).

5.2.3.1.2 TGA/DTA/DTG analysis

TGA/DTA/DTG analysis of rice husk waste biomass was carried out using a thermal analysis instrument (PerkinElmer Pyris Diamond, USA) in a nitrogen atmosphere with a flow rate 200 ml min^{-1}. Thermal stability of rice husk waste biomass is directly dependent on the decomposition temperature of its various functional groups and oxides. The TGA, DTA and DTG profiles of rice husk waste biomass are shown in Fig. 5.45. The TGA curve shows three main zones, in which the first zone is from 31.2 to 200 $^{\circ}$C which indicates the loss in weight of rice husk waste biomass due to moisture and light volatile compounds with moderate rate. The second zone is from 200 to 580 $^{\circ}$C in which weight loss of rice husk waste biomass increases due to evolution of CO_2 and CO with high rate. The third zone is from 580 to 1000 $^{\circ}$C where weight loss was slightly declined or became nearly constant. The maximum degradation rates are found to 394 μg min^{-1} at 282 $^{\circ}$C for rice husk waste biomass in DTG curve. A significant amount of heat (-1.70 J mg^{-1}) was released due to oxidation of rice husk waste biomass at a temperature of 508 $^{\circ}$C.

5.2.3.1.3 FTIR

FTIR graph of RHAC was shown in Fig. 5.46. The FTIR graph indicates sharp peaks in the range of 3800–3200 cm^{-1} which shows the presence of water molecules in the lattice structure of a crystalline compound due to O–H stretching. The long stretch bandwidth around 3500–3200 cm^{-1} suggests the existence of O−H and N−H functional groups, although located at different bandwidths. The peak 3411 cm^{-1} indicates that RHAC has its O−H bandwidth. The 2920 cm^{-1} showed absorption bands due to aliphatic C-H. The RHAC has peak position located between 1600 and 1400 cm^{-1} indicates saturated CH_3, CH_2 and CH, functional groups such as C=O, C−O and C=C. Some inorganic sulfates and silica Si−O−Si asymmetric stretch were found in the wavenumber range between 1115–600 cm^{-1}. The broad peak at about 1115 cm^{-1} and sharp peaks at 805 and 474 cm-1 indicate the presence of silica, in parallel with peaks from

commercial grade silica (Liou, T-H., 2004). The peak range between 700–600 cm^{-1} indicates C–S stretching, which confirms the presence of sulfur compound.
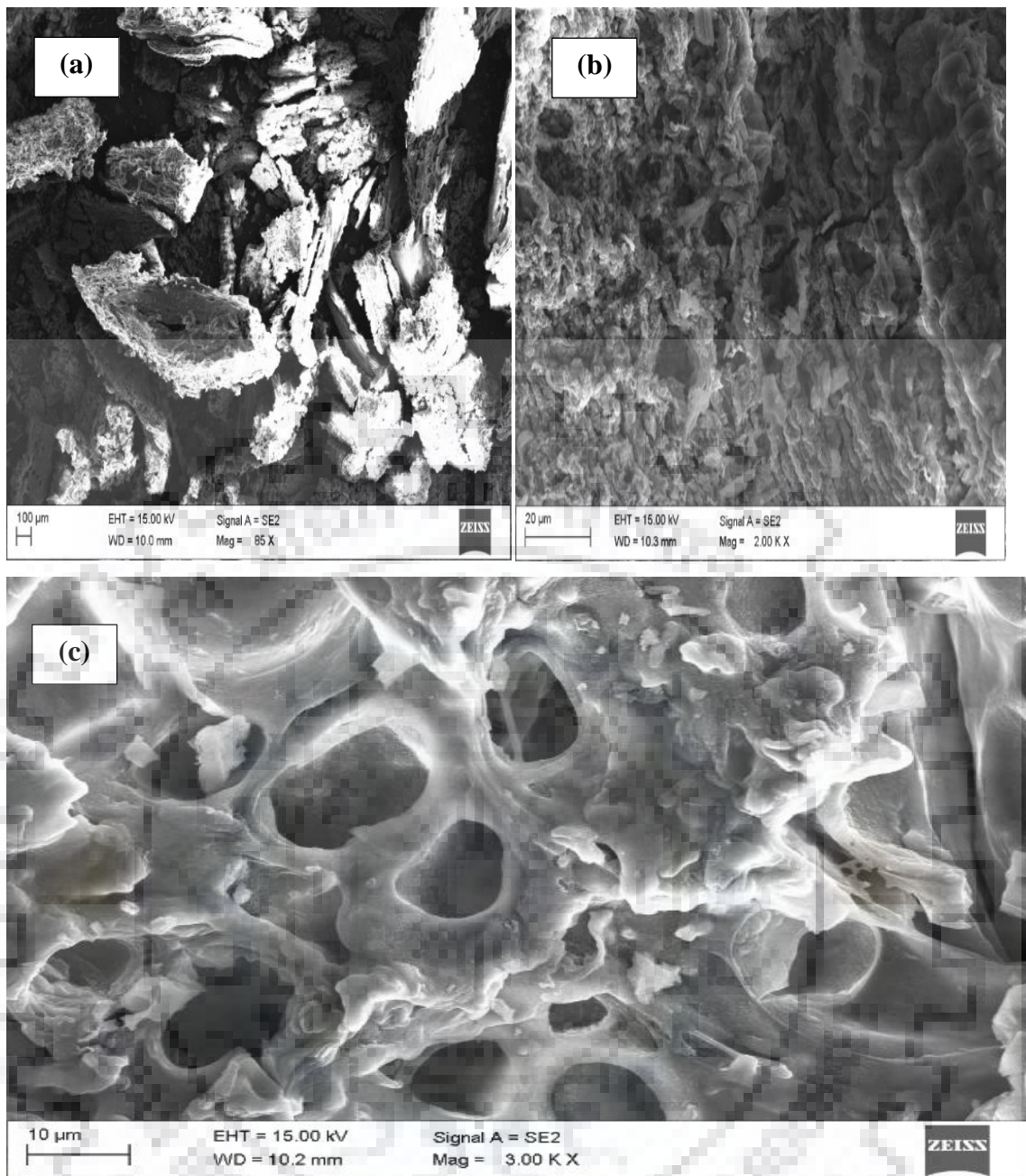
Fig. 5.44 SEM micrographs of RHAC (a) at 85X (b) 2.00 KX (c) 3.00 KX.
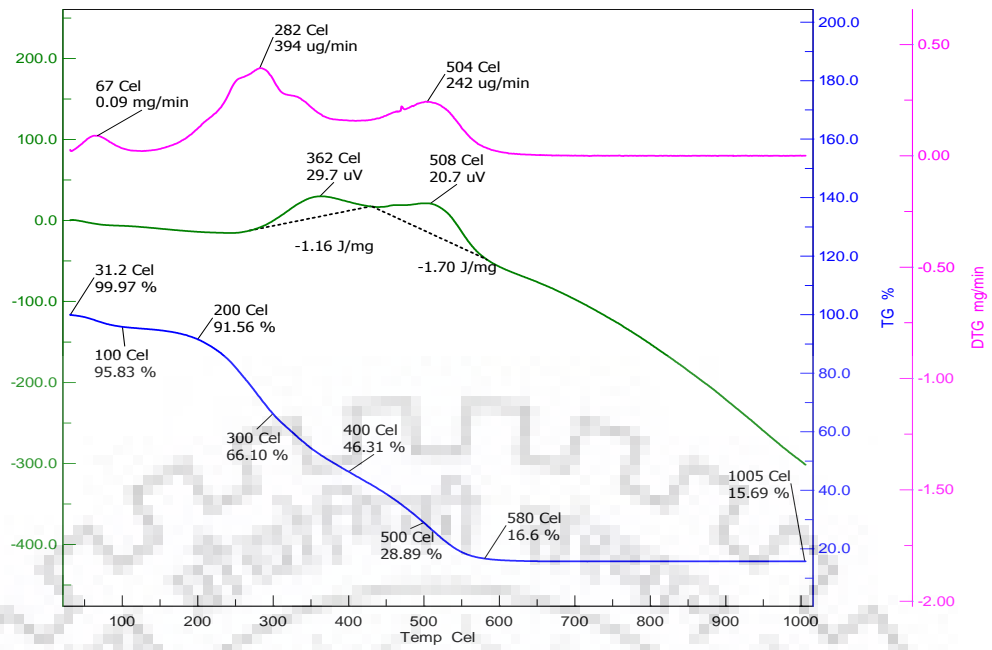
Fig. 5.45 TGA/DTA/DTG analysis graphs of rice husk biomass.
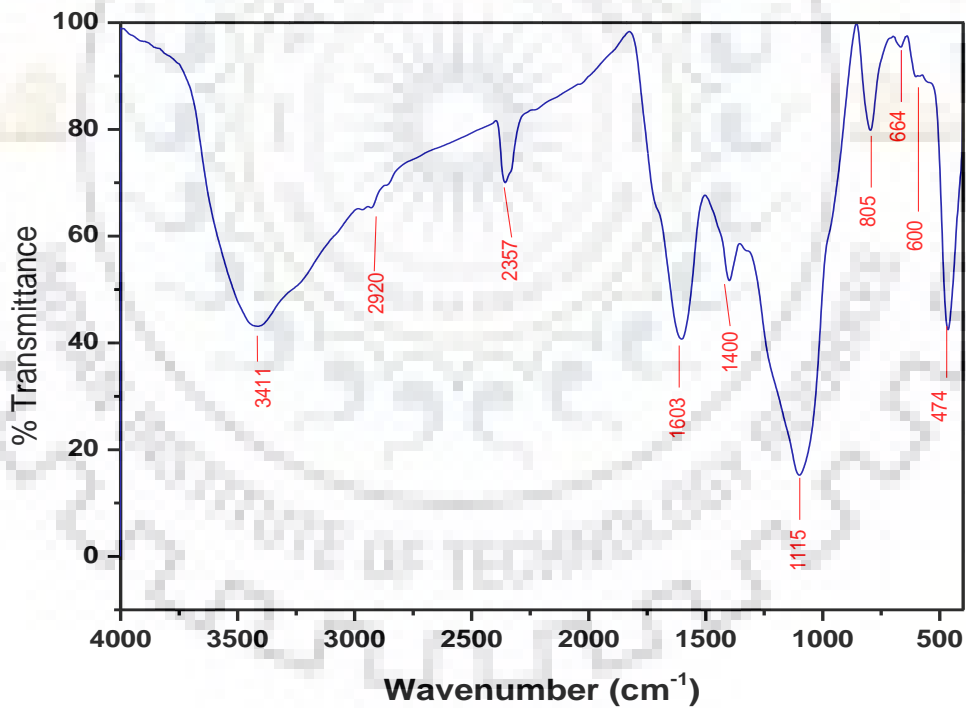
Fig. 5.46 FTIR spectra of RHAC.

5.2.3.2 Effect on conductivity change

The effect on conductivity change was carried out with 10 mg L^{-1} -100 mg L^{-1} Cr(VI) and fluoride of mix feed solution having an initial conductivity of 75.54 μS cm^{-1} and pH 7.1 $\pm$ 0.25. Fig. 5.47 shows the change in conductivity of Cr(VI) and fluoride binary feed solution with time at different feed concentration. Conductivity of feed solution was decreased with respect to time due to sorption of Cr(VI) and fluoride by RHAC porous electrode (refer Fig. 5.47). At starting, the conductivity of feed solution of Cr (VI) and fluoride was decreased drastically and after some time it was found declining slowly.
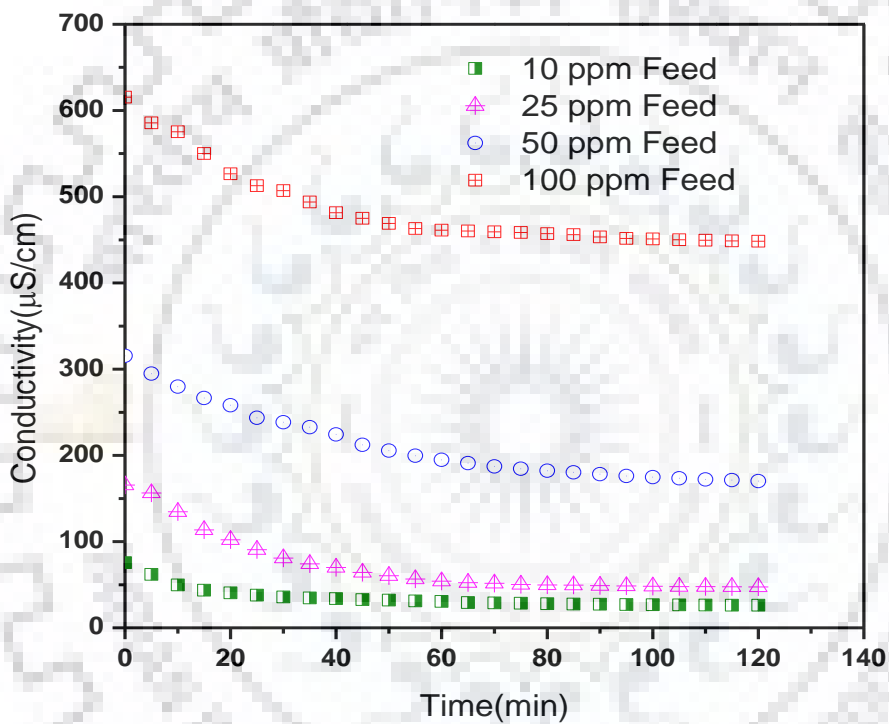
Fig. 5.47 Conductivity change vs. time at different feed concentration with RHAC electrode.

5.2.3.3 Electrosorption and desorption study with RHAC electrode

In this study 1.2 V was applied to terminals of RHAC electrodes to create a positive and negative pole. Feed solution was passed through the space between these two charged porous electrodes. Due to electrostatic force, cations (Na^+ and K^+ ions) and anions ($HCrO_4^-$ /CrO_4^{2-} / CrO_7^{2-} and F^- ions) attracted towards negative and positive RHAC electrodes respectively. Here the electrodes act as a capacitor. That ions store into the pores and surface of electrodes. The electrosorptive removal experiments were carried out with different feed concentrations (10, 25, 50 and 100 mg L^{-1}). Electrosorption capacity with respect to time is shown in Fig. 5.48. The maximum electrosoption capacity of Cr(VI) and fluoride were found 0.72 and 0.70 mg g-1 for 10 mg L^{-1}; 2.47 and 2.34 mg g^{-1} for 100 mg L^{-1} respectively. In simultaneous removal experiment sorption capacity of Cr(VI) was found higher than fluoride ions with RHAC electrode. Hydrated radius of F (3.52 Å) (Nightingale, E.R., 1959) which was smaller than the hydrated radius of CrO_4^{2-} (3.75Å) (Nightingale, E.R., 1959). Cr(VI) occurs in various ionic forms ($HCrO_4^-$, CrO_4^{2-}, $Cr_2O_7^{2-}$) that depend on the solution pH. In acidic medium $HCrO_4^-$, CrO_4^{2-} and H_2CrO_4 are the predominant species. $HCrO_4^-$ and $Cr_2O_7^{2-}$ are predominant in equilibrium when pH range is 2-6. In basic medium chromium exists in the form of CrO_4^{2-} (Sahu et al., 2008). In case of fluoride, the pH between 6-9 is good for fluoride electrosorption (Wu et al., 2016). The electrosorption selectivity of the divalent CrO_4^{2-} is higher than that of the monovalent F^-. This occurs due electrostatic attraction of divalent ion is stronger than monovalent ions (Li et al. 2016). Li et al. reported similar kind of observation in the case of SO_4^{2-} and NO_3^- (Li et al. 2016). The profile of maximum removal percentage at different feed concentration is shown in Fig. 5.49. The maximum removal of Cr(VI) and fluoride were found to be 83.1% and 80.4 % for 10 mg L^{-1} and 28.28% and 26.75% for 100 mg L^{-1} respectively from the mix feed solution of Cr (VI) and fluoride. Study on regeneration of electrode was carried out. Electrosorption and desorption profile of RHAC electrode with 10 mg L^{-1} mix feed solution of Cr(VI) and fluoride was shown in Fig.5.50. Effective regeneration of RHAC electrode was found after simultaneous electrosorption of Cr(VI) and fluoride.
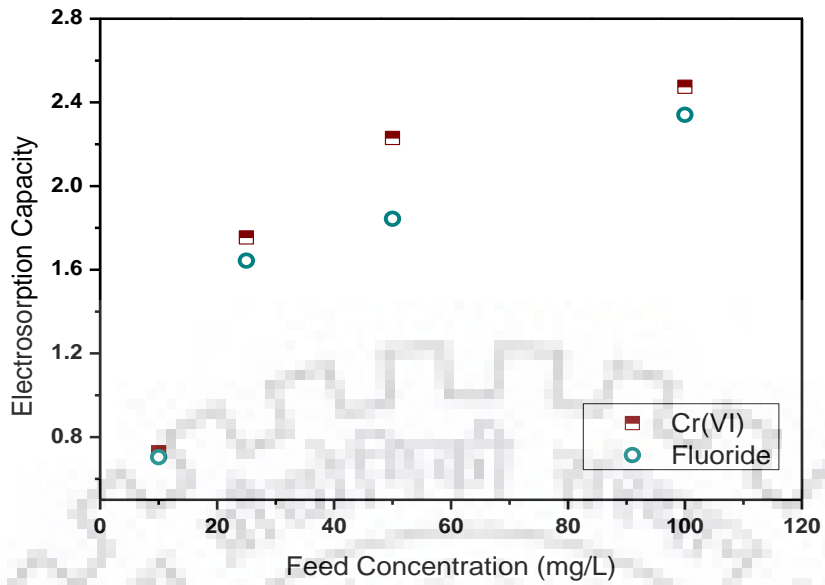
Fig. 5.48 Effect of initial Cr(VI) and fluoride mix feed concentration on electrosorption capacity with RHAC electrode.
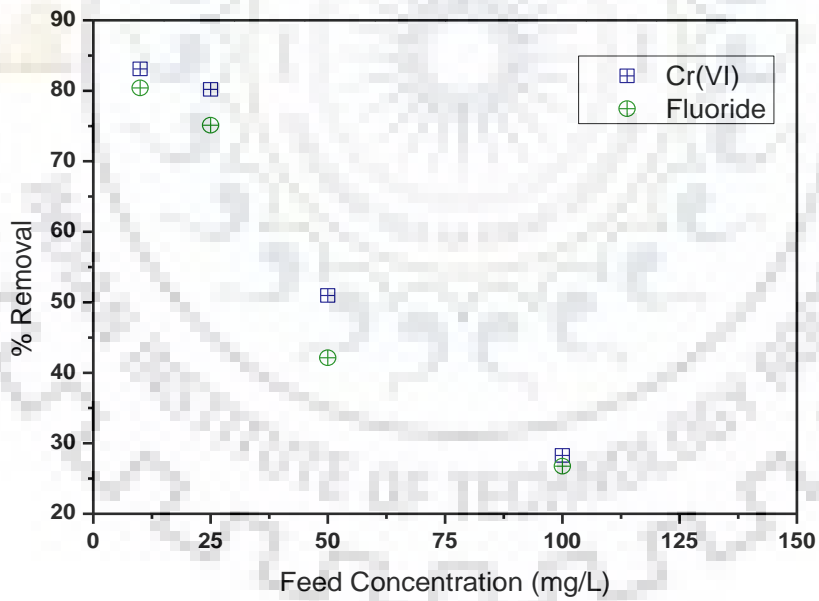
Fig. 5.49 Effect of initial feed concentration on removal percentage of Cr(VI) and fluoride with RHAC electrode.

196
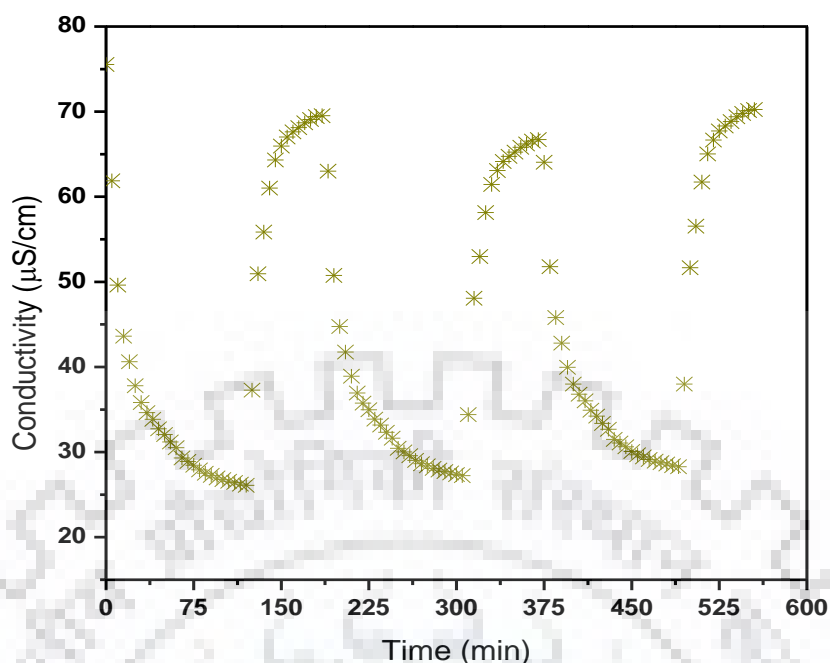
Fig. 5.50 Electrosorption and desorption performance of RHAC electrode of Cr(VI) and fluoride mix feed concentration.

5.2.3.4 Isotherm modeling

Single component modeling was done to find out the best fit model and for estimation of parameters used to evaluate the multicomponent equilibrium isotherm parameters. In single component modeling, Langmuir isotherm model and Redlich Peterson model were found in best agreement (refer Fig.5.51 (a and b)) for both Cr (VI) and fluoride which is confirmed by the lower value of MPSD. The value of the constant b suggests that the interaction of Cr (VI): carbon interaction more stable than that of F: carbon interaction, thus the value of Q_o (mg g^{-1}) for Cr(VI) is higher than fluoride. In multicomponent isotherm modeling, Extended Langmuir and Non modified Redlich Peterson were best agreed with experimental data having lower MPSD for both Cr(VI) and fluoride than other multicomponent isotherm models (refer Table 5.16). It is clear from Fig. 5.52 (a and b) that Extended Langmuir and Non modified Redlich Peterson for both Cr(VI) and fluoride agreed well with experimental data for binary sorption of Cr(VI) and fluoride. The predicted parameter of single and multicomponent isotherm model was systematically shown in Table 5.16.
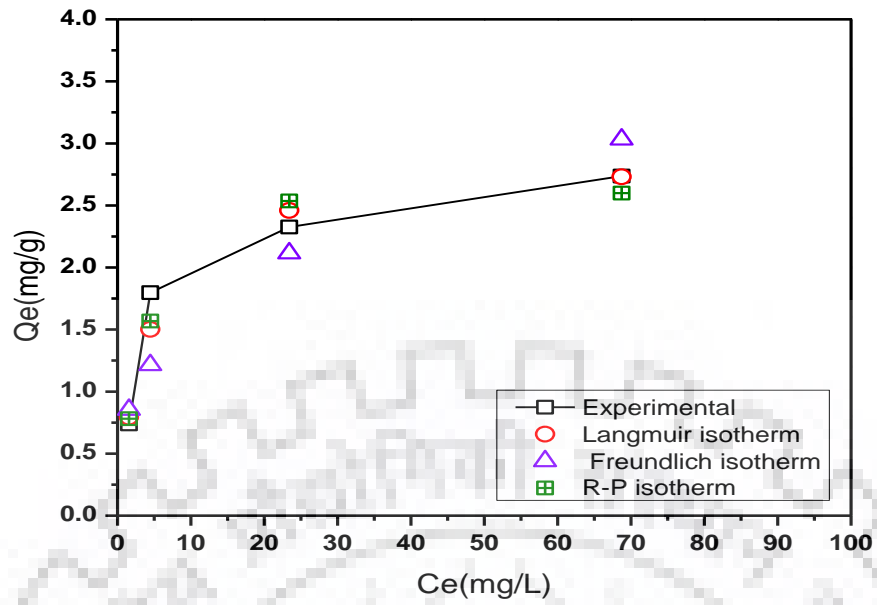
(a)
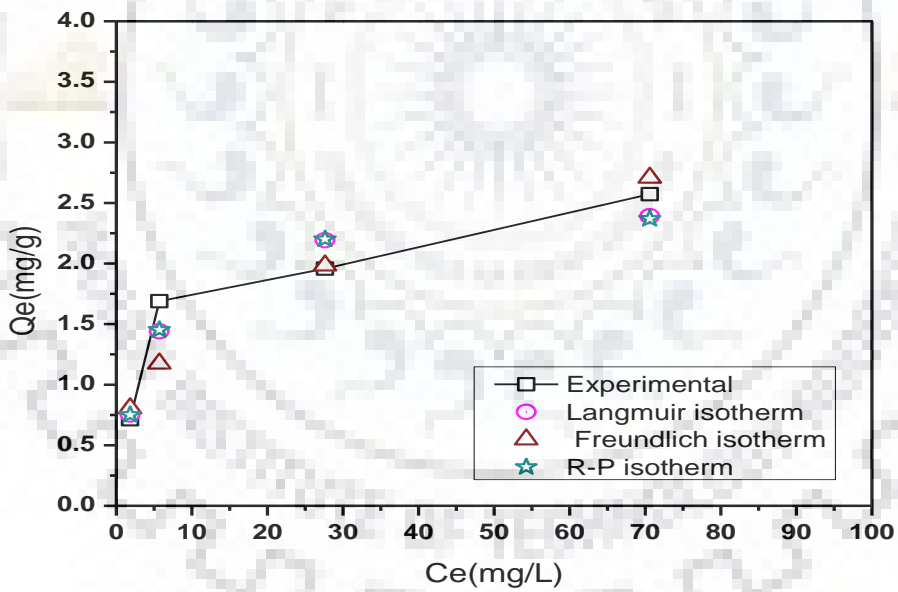
(b)

Fig. 5.51 Comparisons of single component isotherms for electrosorption of (a) Cr(VI)

(b) fluoride with RHAC electrode.
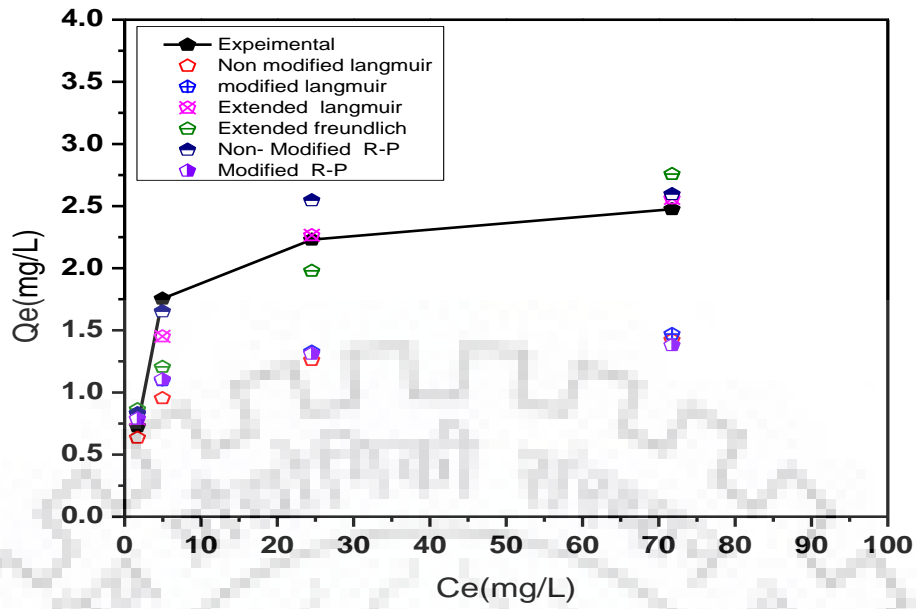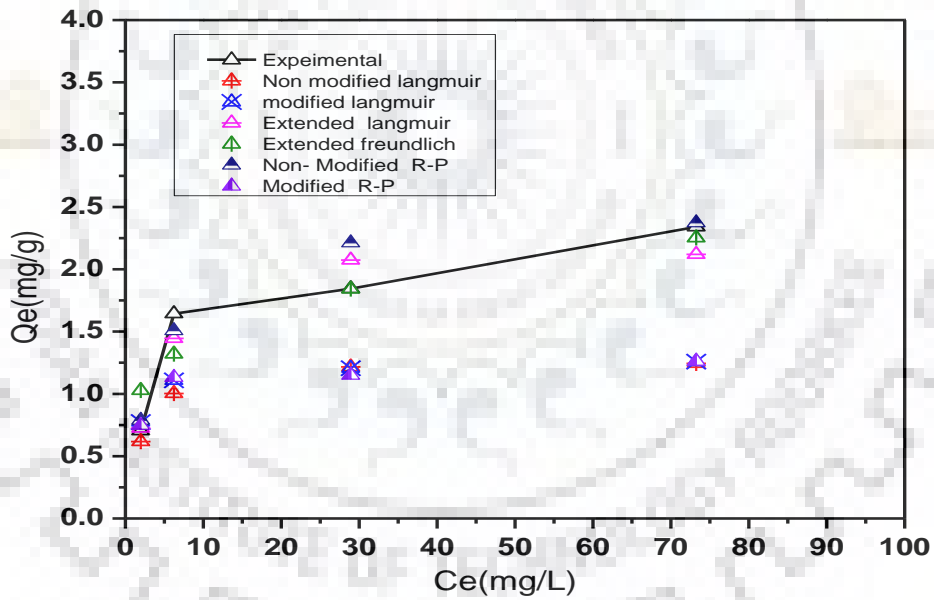
Fig. 5.52 Comparisons of multicomponent component isotherms for electrosorption of (a) Cr(VI) (b) fluoride with RHAC electrode.

Table 5.16 Estimated parameter of mono and multicomponent isotherms modelling for electrosorption of Cr(VI) and fluoride with RHAC electrode.

Name of model	Parameters	Cr(VI)	Fluoride
Single component			
Langmuir	Q_0 (mg g^{-1})	2.89493	2.53676
	b (L mg^{-1})	0.24166	0.23072
	MPSD	13.3712	14.8110
Freundlich	K_F(mg g^{-1}) / (mg L^{-1})$^{1/n}$	0.73633	0.65883
	n	2.98836	3.01112
	MPSD	27.3573	23.6377
Redlich–Peterson	K_{RP}(L g^{-1})	0.62235	0.57095
	a_{RP}(L mg^{-1})	0.14954	0.21140
	β	1.09644	1.01651
	MPSD	12.3040	14.7871
Multicomponent			
Non modified Langmuir	MPSD	54.4507	50.1630
Modified Langmuir	η_i	0.57938	0.60337
	MPSD	49.4362	47.5259
Extended Langmuir	$Q_{0,i}$ (mg g^{-1})	11.7928	3.32541
	b_i (L mg^{-1})	0.19988	0.04469
	MPSD	13.8590	15.914
Extended Freundlich	x_i	0.00013	0.07823
	y_i	0.42755	0.00738
	z_i	0.0000	0.0000
	MPSD	28.2280	35.5136
Non Modified R–P model	MPSD	15.2234	17.5598
Modified R–P model	$\eta_{i,j}$	0.68176	0.76711
	MPSD	50.4579	47.9001

5.2.3.5 Kinetic modeling

The experimental data of simultaneous sorption of Cr(VI) and fluoride by RHAC electrode were used in the pseudo first order and pseudo second order kinetic model to estimate the parameters of kinetic models. The value of parameters of kinetic models for Cr (VI) and fluoride is systematically shown in Table 5.17. The comparison of experimental data and kinetic models for Cr(VI) and fluoride were represented in Fig. 5.53 (a and b). In both the cases the experimental data are well agreed with the Pseudo first order model which is confirmed by lower ARE values compared to Pseudo second order kinetic model. The experimental and calculated value of the electrosorption capacity Q_t (mg g^{-1}) for both Cr(VI) and fluoride were represented systematically in Fig. 5.53 (a and b), respectively. It is clear that experimental value for both Cr(VI) and fluoride is in good agreement with the pseudo first order model. This suggested that the electrosorption is because of electrostatic interactions between ions on the electrode and in solution (Li et al., 2009).

Table 5.17 Estimated parameter of kinetic modelling for electrosorption of Cr(VI) and fluoride with RHAC electrode

Kinetic models	Parameters	Concentration			
		Cr(VI)			
		10 mg L^{-1}	25 mg L^{-1}	50 mg L^{-1}	100 mg L^{-1}
Pseudo first order					
	$q_{e,cal}$ (mg g^{-1})	0.8552	3.1627	3.3371	4.1892
	k_1(min^{-1})	0.0528	0.0037	0.0035	0.0034
	ARE	0.5808	1.0654	0.9666	1.1327
Pseudo second order					
	$q_{e,cal}$ (mg g^{-1})	0.6968	2.0155	2.3013	2.7655
	k_2(g mg^{-1} min^{-1})	0.0776	0.0380	0.0271	0.0367
	ARE	0.6997	1.7169	1.1705	1.3154
		Fluoride			
Pseudo first order					
	$q_{e,cal}$(mg g^{-1})	0.8073	2.4242	3.1409	3.2629
	k_1(min^{-1})	0.1103	0.0132	0.0071	0.0099
	ARE	1.2907	1.9554	1.5105	2.4389
Pseudo second order					
	$q_{e,cal}$(mg g^{-1})	0.6784	1.8379	2.1473	2.500
	k_2(g mg^{-1} min^{-1})	0.0486	0.0180	0.0180	0.0214
	ARE	1.4214	2.2550	1.7163	2.7861
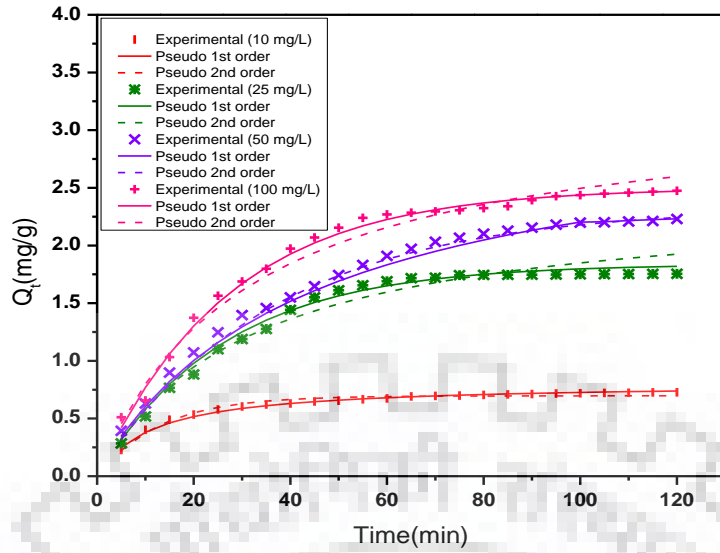
(a)
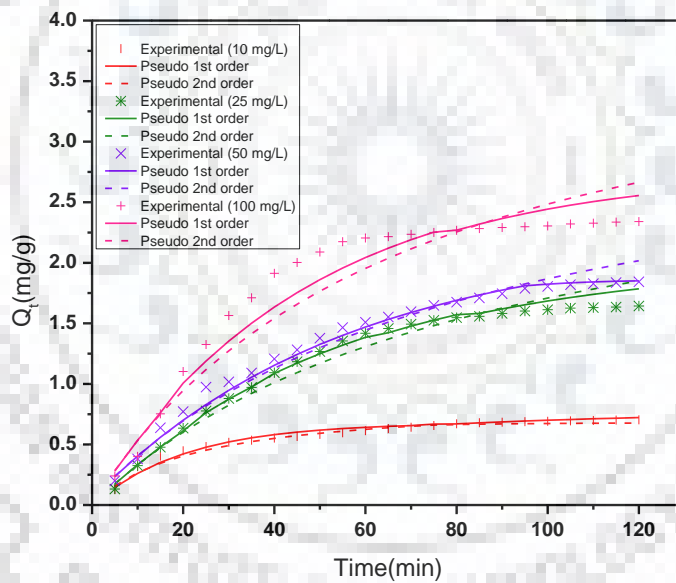
(b)

Fig. 5.53 Comparisons of kinetic models for electrosorption of (a) Cr(VI) (b) fluoride with RHAC electrode.

5.2.3.6 Conclusive Remarks

The section includes that preparation of RHAC electrode from rice husk activated carbon and implemented for simultaneous removal of Cr(VI) and fluoride from binary feed solution. The maximum removal of Cr(VI) and fluoride were found to be 83.1% and 80.4 % for 10 mg L^{-1}, respectively from the mix feed solution of Cr (VI) and fluoride. The Study on regeneration of electrode was carried out. The effective regeneration of RHAC electrode was found after simultaneous electrosorption of Cr(VI) and fluoride.

5.2.4. Studies on CDI with LASAC electrode

5.2.4.1 Characterization

5.2.4.1.1 SEM of LASAC and ion exchange membrane

LASAC morphology studied by using SEM analysis. LASAC surface morphology at different magnifications were shown in Fig. 5.54 (a-c). The morphological images indicated that LASAC was highly nanoporous and microporous in nature. Micropore contains a number of nanopores and pores irregular in shape and structured were clearly observed in Fig. 5.54 (c). The morphological images of cation exchange membrane and anion exchange membrane were shown in Fig. 5.54 (d-e.) The membrane surface was found to be rough in nature.

5.2.4.1.2. TGA/DTA/DTG Analysis

Limonia acidissima (wood apple) shells TGA/DTA/DTG analysis was done with thermal analysis (TA) instrument (PerkinElmer Pyris Diamond, USA) in a nitrogen atmosphere with a flow rate 200 ml/min. The TGA, DTA and DTG profile of Limonia acidissima shell was shown in Fig. 5.55. Limonia acidissima shell thermal stability are directly dependent on the decomposition temperature of its various functional groups and oxides. The TGA curve of Limonia acidissima (wood apple) shells indicates the three main zones, in which first zone was from 30.2 to 242 $^{\circ}$C shows the loss in weight of Limonia acidissima shell due to moisture and light volatile compounds with moderate rate. From 242 to 561 $^{\circ}$C is the second zone where weight loss of Limonia acidissima shell increases due to evolution of CO_2 and CO with high rate. In the third zone from temperature range beyond 561 $^{\circ}$C and up to 1005°C weight loss was slightly declined or became nearly constant. The maximum degradation rates are 0.70 mg/min at 332° C for Limonia acidissima shell was observed in DTG curve. A significant amount of heat (-7.16 J/mg) is released due to oxidation of Limonia acidissima shell at temperature 502 $^{\circ}$C.
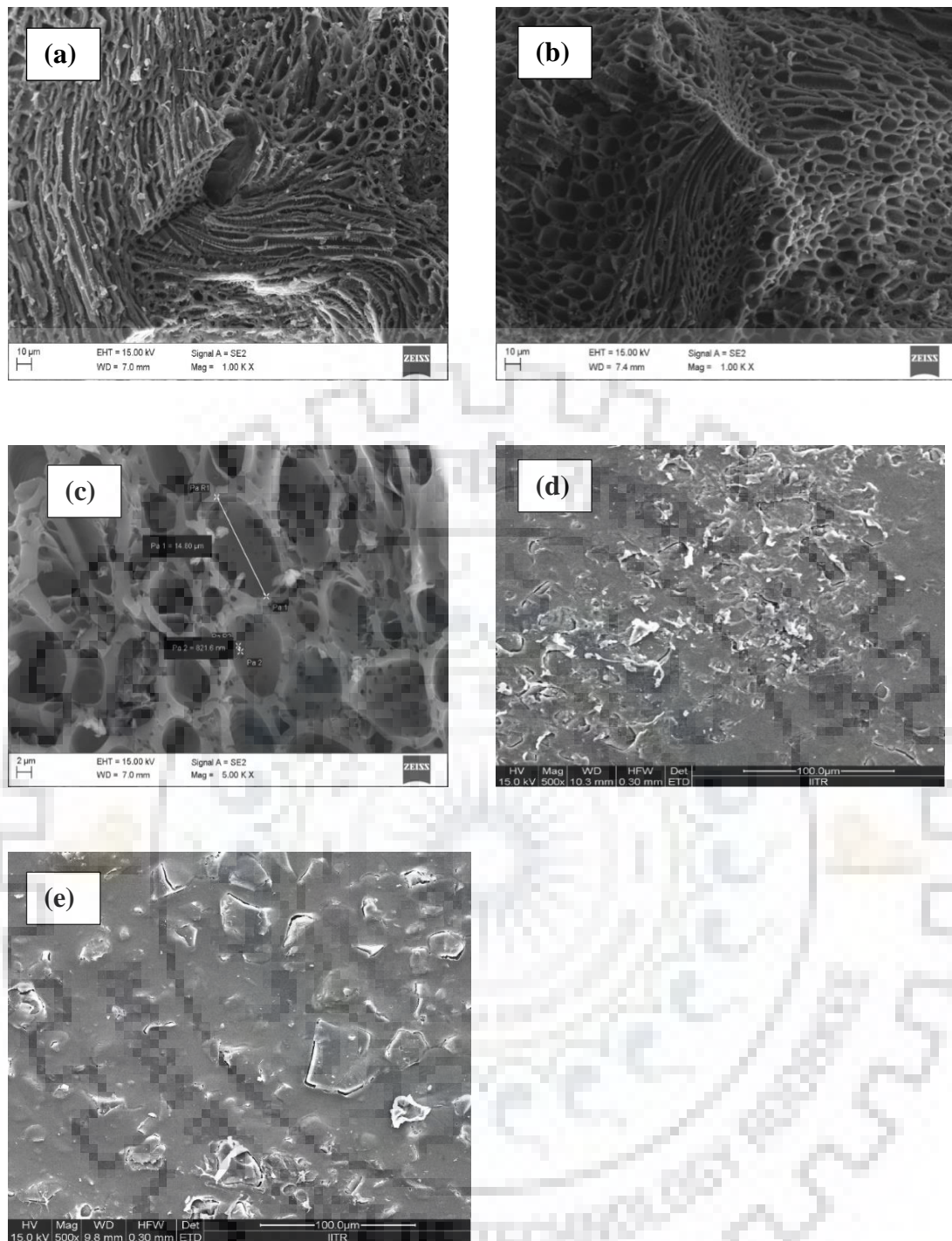
**Fig. 5.54 SEM images of Limonia acidissima (wood apple) shells activated carbon (a),
(b) at 1.0 KX magnification (c) 5.0 KX magnification. SEM images of ion exchange
membrane (d) anion exchange membrane (e) cation exchange membrane.**
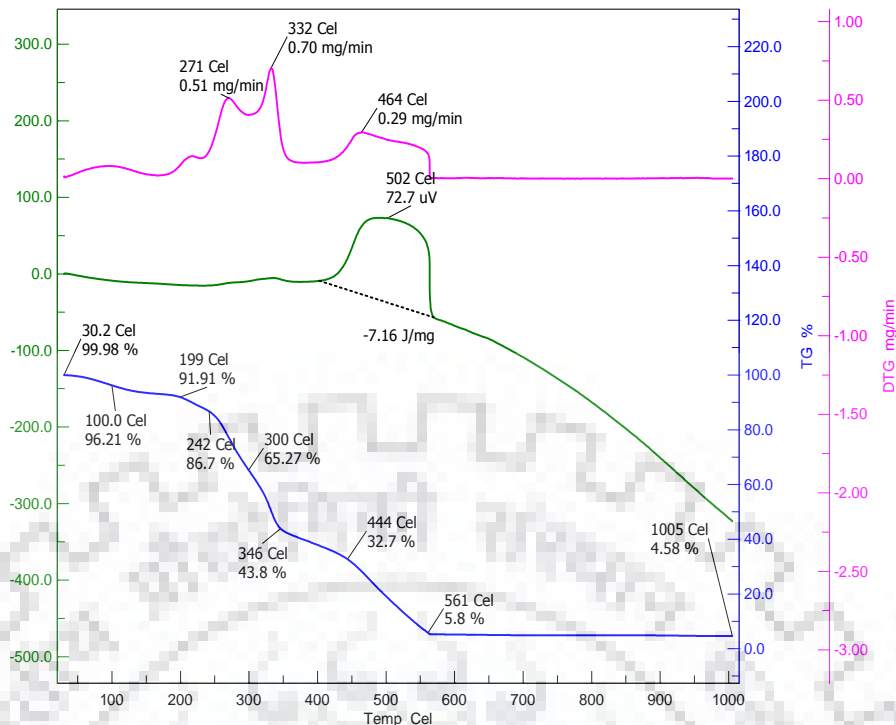
Fig. 5.55 TGA/DTA/DTG analysis of Limonia acidissima (wood apple) shells.

5.2.4.2 Electrosorption study with LASAC electrode

The LASAC electrode feasibility for electrosorption of Cr(VI) and fluoride was carried out in MCDI self-made lab scale setup at 1.2 V at 10 mg/L-100 mg/L binary feed. The Cr(VI) and fluoride binary feed solution pass was through the space between two porous LASAC charged electrode with external 1.2 V supply. The positive ions (Na^+ and K^+ ions) and negative ions ($HCrO_4^-$ /CrO_4^{2-} / CrO_7^{2-} and F^- ions) are attracted due to electrostatic force towards negative and positive LASAC electrode respectively. Thus conductivity of feed solution was decreased due to electrosorption of ions. The feed solution pH was 7.2 ± 0.20. The solution pH dependent various forms of Cr(VI) are $HCrO_4^-$, CrO_4^{2-}, $Cr_2O_7^{2-}$. The $HCrO_4^-$, CrO_4^{2-} and H_2CrO_4 in acidic medium, are the predominant species. The $HCrO_4^-$ and $Cr_2O_7^{2-}$ in equilibrium are predominant mostly in 2-6 pH range. The CrO_4^{2-} ion form exists in the basic medium (Sahu et al., 2008). The good electrosorption of fluoride was for the case of fluoride was reported at 6-9 pH range (Wu et al., 2016). The Electrosorption capacity performance of LASAC electrode with respect to time profile was shown in Fig. 5.56. The Cr(VI) and fluoride maximum electrosoption were found to be 0.8086 mg/g and 0.7805 mg/g for 10 mg/L; 3.227 mg/g and 2.7554 mg/g for 100 mg/L respectively. The Cr(VI) sorption capacity was found higher than fluoride ions with LASAC electrode. Gabelich et al. reported that ion selectivity was dependent

on ionic hydrated radius and monovalent ions with smaller hydrated radii were preferentially removed compared to multivalent ions from solution (Gabelich et al., 2002). The Hydrated radius of F^- (3.52 Å) is slightly smaller than CrO_4^{2-} (3.75 Å) (Nightingale, E.R., 1959) but here the divalent CrO_4^{2-} electrosorption selectivity is higher than the monovalent F^-. The reason behind this is the electrostatic attraction of divalent ion is stronger than monovalent ions (Li et al. 2016). Similar type of investigation was reported by Li et al. for the case of SO_4^{2-} and NO_3^- (Li et al. 2016).   The profile of maximum percentage removal of Cr(VI) and fluoride by LASAC electrode at different feed concentration is shown in Fig. 5.56. The maximum removal of Cr(VI) and fluoride were found to be 92.2 % and 89.23% for 10 mg/L and 36.88 % and 31.49 % for 100 mg/L, respectively from the binary feed solution of Cr(VI) and fluoride by LASAC electrode.
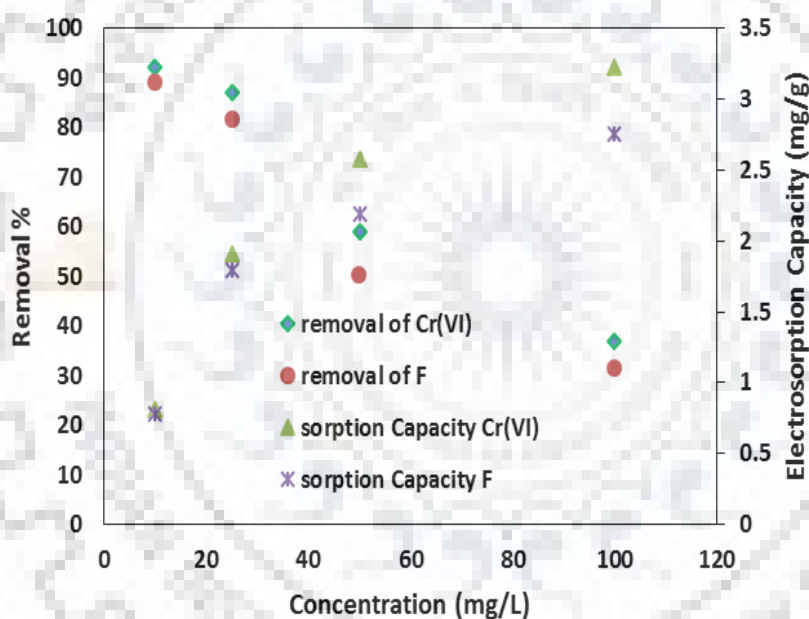
Fig. 5.56 Removal percentage Cr(VI) and fluoride profile and electrosorption capacity profile at a different feed concentration by LASAC electrode with MCDI.

5.2.4.3 Regeneration of electrode

The study on regeneration of LASAC electrode was carried out. When electrode gets saturated, there is need of regeneration of electrode. The regeneration step was carried out when the conductivity of the inlet feed solution was close to the MCDI cell outlet stream conductivity, signifying that the electrodes were saturated by ions. Then, regeneration step was carried out by changing the terminal of electrode means applying a reverse voltage. In the regeneration process due to reverse potential anions and cations coming out from the electrode and not attracted toward the oppositely charged electrode due to ion exchange membranes directly come into a water stream. Electrosorption and desorption profile of LASAC electrode with 10 mg/L Cr(VI) and fluoride binary mixture is shown in Fig. 5.57. Three purification and regeneration cycle studies was conducted and effective regeneration of LASAC electrode was found after simultaneous electrosorption of Cr(VI) and fluoride.
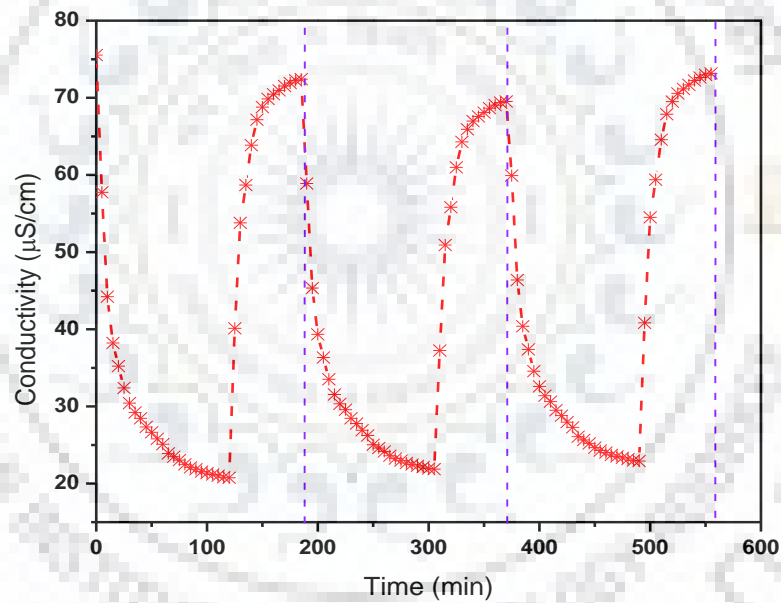
Fig. 5.57 Cr(VI) and fluoride electrosorption and desorption profile of LASAC electrode in MCDI study.

5.2.4.4 Parameter estimation of isotherm models

Mono and multicomponent isotherm modeling were carried out in the present study to identify the best fit model with experimental results. The Fig. 5.58 (a-b) indicated that the mono component isotherm modeling comparison with experimental results. The isotherm model, namely Langmuir isotherm model and Redlich Peterson model having lower value of MPSD and found best fitting to the experimental values. The parameter estimated in mono component isotherm modeling was used for estimation of multicomponent isothermal modeling. The Fig. 5.59 (a-b) show the comparisons of the fitting of multicomponent isothermal modeling with experimental results. The model Extended Langmuir and Non modified Redlich Peterson from multicomponent isotherm modeling were found best fitting with experimental for both Cr(VI) and fluoride. The multicomponent isotherm modeling estimated parameters is presented in Table 5.18. The constant b value represents that Cr(VI): carbon interaction more stable than that of F: carbon interaction. Therefore the value of Qo(mg/g) for Cr(VI) was higher compared to fluoride. The mono and multicomponent isotherm modeling estimated parameters are systematically shown in Table 5.18.

5.2.4.5 Parameter estimation of kinetic models

The kinetic modeling study was carried out for identification of categories of the sorption process such as chemisorption and physisorption. Here two kinetic model were used, namely pseudo first order and pseudo second order model for estimation of kinetic model parameters for simultaneous sorption Cr(VI) and fluoride by LASAC electrode. The kinetic model parameters estimated values for Cr(VI) and fluoride are presented in Table 5.19. Fig. 5.60 (a-b) show that comparison of kinetic model with experimental results for the removal of Cr(VI) and fluoride. In both model pseudo first order is a good fit with experimental results for Cr(VI) and fluoride. It is also confirmed by lower ARE values which is shown in Table 5.19.
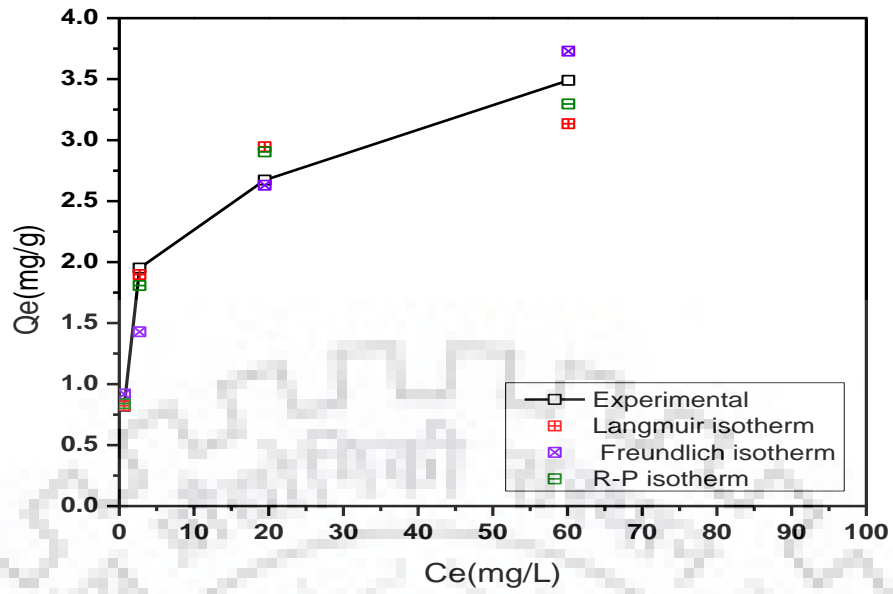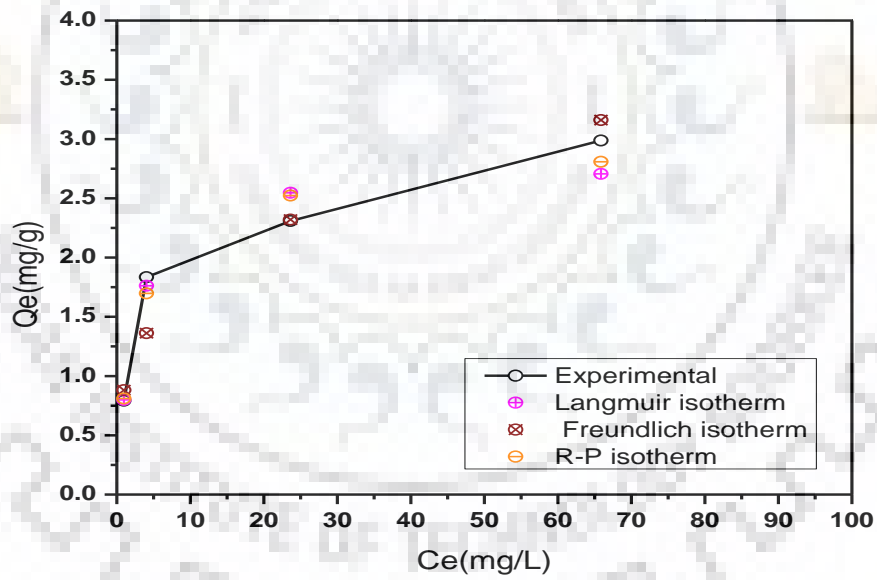
Fig. 5.58 Comparisons of single component isotherms for electrosorption of (a) Cr(VI) (b) fluoride with LASAC electrode.
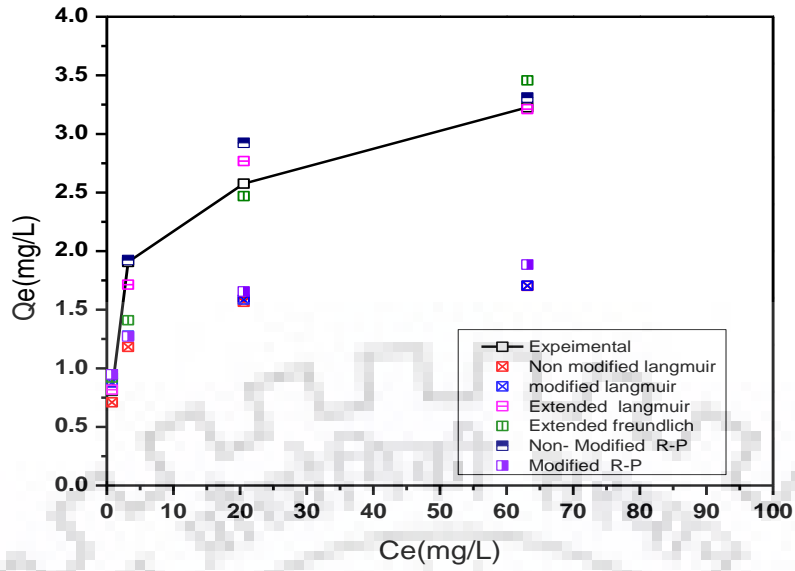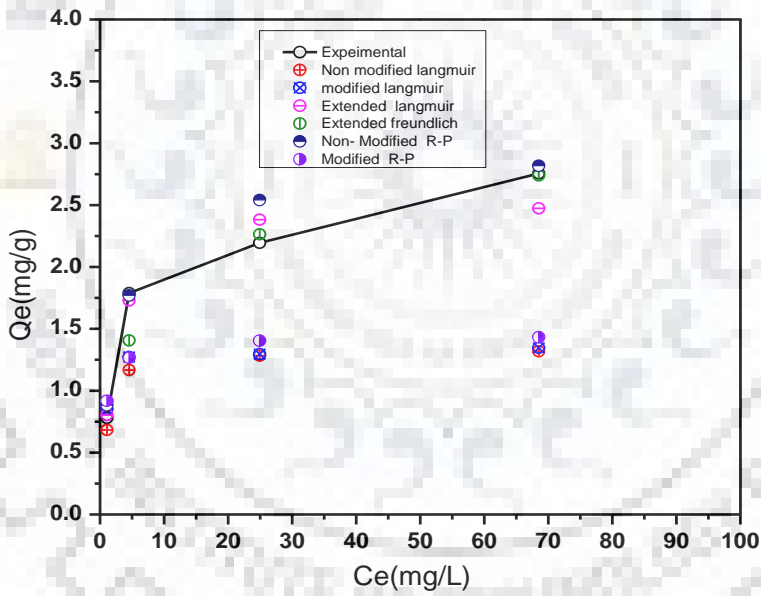
Fig. 5.59 Comparisons of multicomponent component isotherms for electrosorption of (a) Cr(VI) (b) fluoride with LASAC electrode.

Table 5.18 Estimated parameter of mono and multicomponent isotherms modelling for electrosorption of Cr(VI) and fluoride with LASAC electrode.

Name of model	Parameters	Cr(VI)	Fluoride
Monocomponent isotherm models			
Langmuir	Q_0	3.11413	2.80382
	b	0.52423	0.41967
	MPSD	10.3753	10.3006
Freundlich	K_F	1.04963	0.89452
	n	3.23125	3.31771
	MPSD	21.3906	20.3147
Redlich–Peterson	K_{RP}	1.94216	1.31522
	a_{RP}	0.75391	0.56803
	β	0.93286	0.94608
	MPSD	9.08154	9.60901
Multicomponent isotherm models			
Non modified Langmuir	MPSD	51.7178	53.9243
Modified Langmuir	η_i	0.63968	0.63385
	MPSD	49.3188	51.0421
Extended Langmuir	$Q_{0,i}$	16.0714	3.22849
	b_i	0.09318	0.32923
	MPSD	8.97865	9.93640
Extended Freundlich	x_i	0.0000	0.0000
	y_i	0.05503	0.00096
	z_i	0.12907	1.24375
	MPSD	21.7698	29.2606
Non Modified R–P model	MPSD	15.7685	14.5401
Modified R–P model	$\eta_{i,j}$	0.43045	0.41632
	MPSD	47.0408	48.8445

Table 5.19 Estimated parameter of kinetic modelling for electrosorption of Cr(VI) and fluoride with LASAC electrode.

Kinetic models	Parameters	Concentration			
		Cr(VI)			
		10 mg L^{-1}	25 mg L^{-1}	50 mg L^{-1}	100 mg L^{-1}
Pseudo first order					
	$q_{e,cal}$ (mg g^{-1})	0.8936	2.7166	3.4643	4.4728
	k_1(min^{-1})	0.0487	0.0033	0.0047	0.0042
	ARE	0.2758	0.9868	0.6090	0.7711
Pseudo second order					
	$q_{e,cal}$ (mg g^{-1})	0.7578	1.9847	2.5794	3.2433
	k_2(g mg^{-1} min^{-1})	0.0504	0.0182	0.0224	0.0264
	ARE	0.8191	1.6807	0.9650	1.1812
		Fluoride			
Pseudo first order					
	$q_{e,cal}$(mg g^{-1})	0.8689	2.4502	3.3496	4.2746
	k_1(min^{-1})	0.1340	0.0144	0.0090	0.0073
	ARE	1.6311	2.8733	0.6047	2.2789
Pseudo second order					
	$q_{e,cal}$(mg g^{-1})	0.7190	1.9027	2.5589	3.0847
	k_2(g mg^{-1} min^{-1})	0.0928	0.0422	0.0340	0.0367
	ARE	1.8798	3.1405	0.8226	2.7356
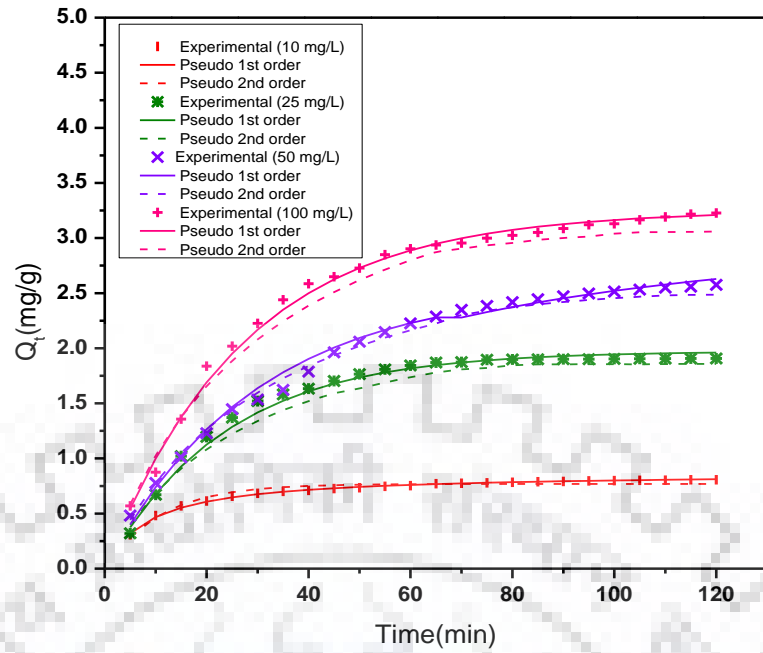
(**a**)
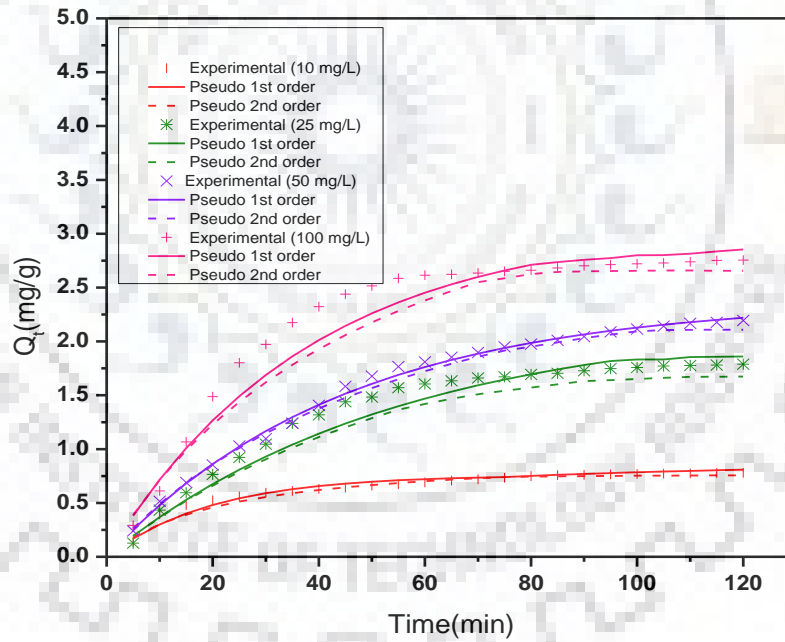
(**b**)

Fig. 5.60 Comparisons of kinetic models for electrosorption of (a) Cr(VI) (b) fluoride with LASAC electrode.

215

5.2.4.6 Conclusive Remark

The present work includes the preparation of LASAC electrode from activated carbon Limmonia acidissima, characterization and application in membrane capacitive deionization for treatment of Cr(VI) and fluoride simultaneous removal from binary feed. The effective performance was found in electrosorption of Cr(VI) and fluoride and regeneration of electrode. The maximum removal of Cr(VI) and fluoride were found to be 92.2 % and 89.23% for 10 mg/L respectively from the binary feed solution of Cr(VI) and fluoride by LASAC electrode with MCDI.

5.3 Studies on Industrial wastewater treatment by membrane separation and capacitive deionization

In the present study treatment of wastewater from electroplating (electronic process) industry was carried out by membrane separation (with NF300 and RO flat sheet membrane) and capacitive deionization (with CAC electrode and LASAC electrode) techniques. Detail experimental results are systematically described below.

5.3.1 Simultaneous removal of Cr(VI) and fluoride from industrial wastewater treatment by membrane separation (NF/RO) technique

The electronic process wastewater which contains Cr(VI) and fluoride [11 mg/L Cr(VI) and 35.24 mg/L fluoride] was treated by using NF300 with an operating pressure range 2-10 bar. Fig. 5.61 (a) and Fig. 5.61 (b) illustrate the effects on permeate flux and the percent rejection of Cr(VI) and fluoride with NF300 membrane respectively. Effect on simultaneous rejection of Cr(VI) and fluoride achieved with different pressure from electronic process wastewater which contains Cr(VI) and fluoride [11 mg/L Cr(VI) and 35.24 mg/L fluoride] were carried out by RO flat sheet membrane. The applied pressure range used in the experiment are 4-20 bar. Effects of pressure on the permeate flux of fluoride and Cr(VI) feed for polyamide RO membrane are presented in Fig. 5.62(a). Fig. 5.61 (a) and Fig. 5.62(a) indicate that as pressure increase the permeate flux linearly increases as represented by Eq. (5.1). This implies that on the surface of the membrane, there is insignificant or no concentration polarization. Solvent flux was enhanced without corresponding enhancement in solute flux at increasing pressure are resulted due to solute and solvent flux separation in solution–diffusion mechanism of NF membrane transport mechanism (Kumar et al., 2011). The flux of pure water increases while there is no changes in the flux of solute (Cr(VI) and fluoride) at increasing pressure because of the permeate contains less concentration of Cr(VI) and fluoride. This suggests the rejection of Cr(VI) and fluoride solutes enhancement with increasing pressure (refer Fig. 5.61(b) and Fig. 5.62(b)). In size exclusion mechanism pore size of the membrane and dimension of solute has a significant part in finding degree of separation. Negatively charge ions and negatively charge membrane enhanced the Cr(VI) and fluoride rejection from industrial wastewater due to the electrostatic charge repulsion mechanism. Highest percent rejection of Cr(VI) and fluoride were found to be 92.2% and 83% with NF300; 99.96% and 94.97% from industrial wastewater concentration [11 mg/L Cr(VI) and 35.24 mg/L fluoride], respectively.
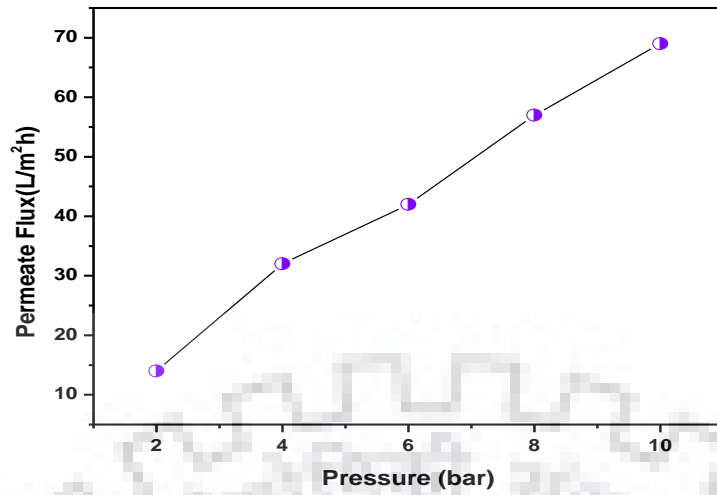
(a)
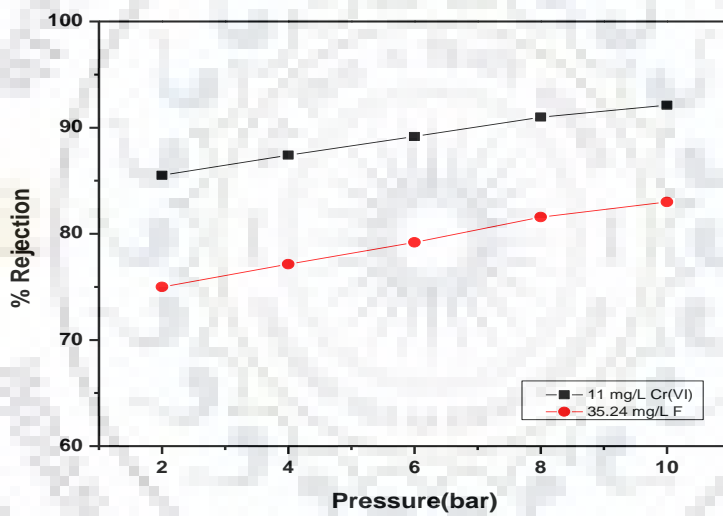
(b)

Fig. 5.61 (a) Effect of pressure on permeate flux of electronic process wastewater by using NF300 membrane [wastewater contains Cr(VI) 11 mg/L and fluoride 35.24 mg/L]. (b) Effect of applied pressure on percentage rejection of electronic process wastewater by using NF300 membrane [wastewater contains Cr(VI) 11 mg/L and fluoride 35.24 mg/L].
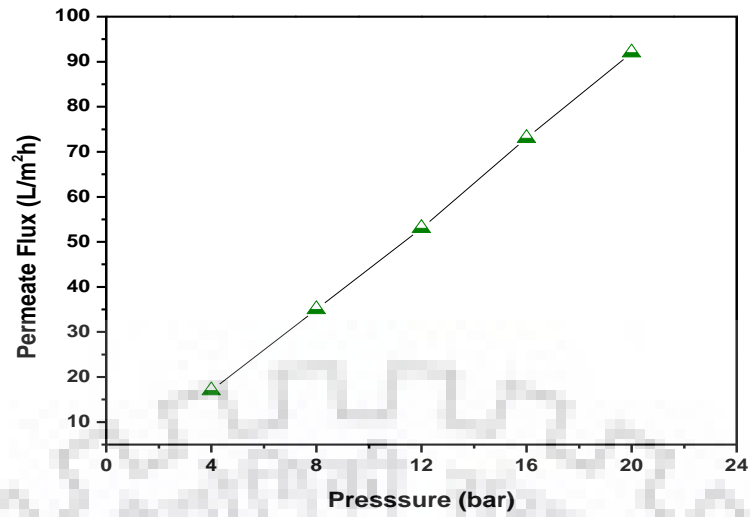
(a)
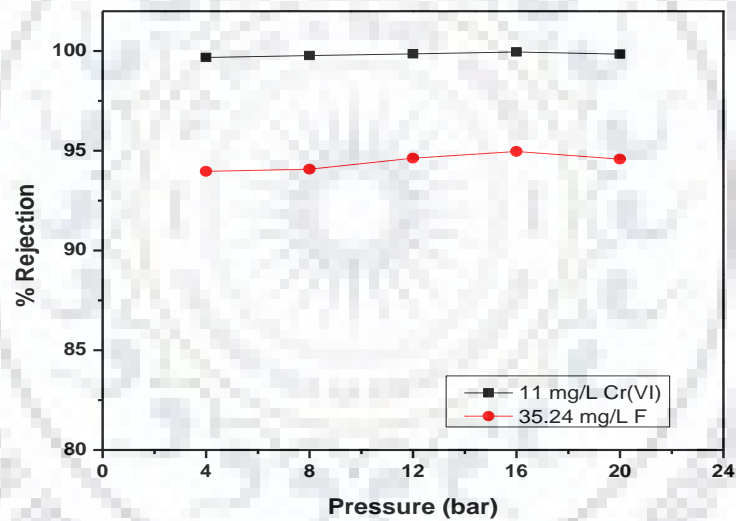
(b)

Fig. 5.62 (a) Effect of pressure on permeate flux of electronic process wastewater by using RO membrane [wastewater contains Cr(VI) 11 mg/L and fluoride 35.24 mg/L].
(b) Effect of applied pressure on percentage rejection of electronic process wastewater by using RO membrane [wastewater contains Cr(VI) 11 mg/L and fluoride 35.24 mg/L].

5.3.2 Simultaneous removal of Cr(VI) and fluoride from industrial wastewater treatment by MCDI

The feasibility CAC electrode and LASAC electrode separately for electrosorption of Cr(VI) and fluoride from electronic process wastewater which contains Cr(VI) and fluoride [11 mg/L Cr(VI) and 35.24 mg/L fluoride] was carried out in MCDI self-made lab scale setup. The electronic process wastewater was passed through the space between two porous charged electrodes (CAC electrode and LASAC electrode separately studied) with an external 1.2 V supply. The positive ions and negative ions ($HCrO_4^-$ /CrO_4^{2-} / CrO_7^{2-} and F^- ions) are attracted due to electrostatic force towards negative and positive electrode respectively. The feed solution pH was 7.2 ± 0.20. The solution pH dependent various forms of Cr(VI) are $HCrO_4^-$, CrO_4^{2-}, $Cr_2O_7^{2-}$. The $HCrO_4^-$, CrO_4^{2-} and H_2CrO_4 in acidic medium, are the predominant species. The $HCrO_4^-$ and $Cr_2O_7^{2-}$ in equilibrium are predominant mostly in 2-6 pH range. The CrO_4^{2-} ion exists in the basic medium (Sahu et al., 2008). The good electrosorption in the case of fluoride was reported at 6-9 pH range (Wu et al., 2016). The profile of maximum percentage removal of Cr(VI) and fluoride by CAC and LASAC electrode is shown in Fig. 5.63. The maximum removal of Cr(VI) and fluoride by CAC electrode were found to be 94.35 % and 80.00 %; LASAC electrode were found to be 90.2 % and 76.00 % from electronic process wastewater which contains Cr(VI) and fluoride [11 mg/L Cr(VI) and 35.24 mg/L fluoride]. The Cr(VI) sorption capacity was found higher than fluoride ions with LASAC electrode. Gabelich et al. reported that ion selectivity depends on ionic hydrated radius and monovalent ions with smaller hydrated radii were preferentially removed compared to multivalent ions from solution (Gabelich et al., 2002). The Hydrated radius of F^- (3.52 Å) is slightly smaller than CrO_4^{2-} (3.75 Å) (Nightingale, E.R., 1959) but here the divalent CrO_4^{2-} electrosorption selectivity is higher than the monovalent F^-. The reason behind this is the electrostatic attraction of divalent ion is stronger than monovalent ions (Li et al. 2016). Similar type of investigation was reported by Li et al. for the case of SO_4^{2-} and NO_3^- (Li et al. 2016).
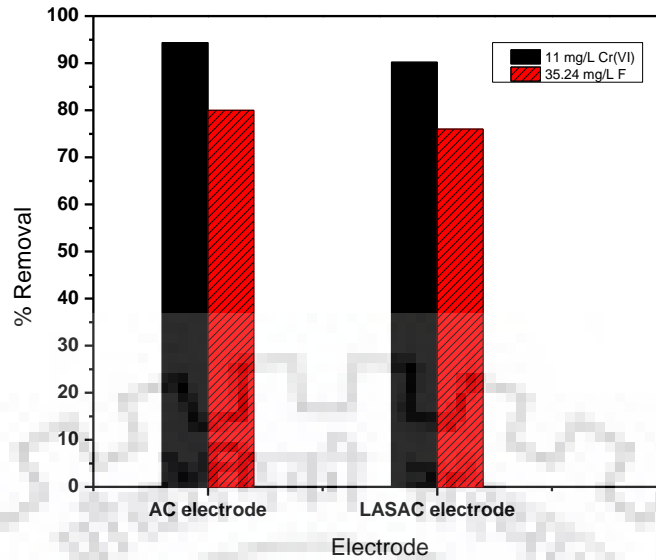
Fig. 5.63 Profile of maximum removal of Cr(VI) and fluoride by CAC electrode and LASAC electrode at 1.2 V and flowrate 16 mL/min.

5.3.3 Conclusive remarks

This study suggests that permeate flux and rejection of Cr(VI) and fluoride enhances with the increasing pressure with NF300 and RO flat sheet membrane. Highest percent rejection of Cr(VI) and fluoride were found 92.2% and 83% with NF300; 99.96% and 94.97% with RO flat sheet membrane from industrial wastewater [11 mg/L Cr(VI) and 35.24 mg/L fluoride] respectively.

The investigation of CAC electrode and LASAC electrode separately for electrosorption of Cr(VI) and fluoride from electronic process wastewater which contains Cr(VI) and fluoride [11 mg/L Cr(VI) and 35.24 mg/L fluoride] was carried out in MCDI self-made lab scale setup. The maximum removal of Cr(VI) and fluoride by CAC electrode were found 94.35 % and 80.00 %; LASAC electrode were found 90.2 % and 76.00 % at 1.2 V and flowrate 16 mL/min from industrial wastewater which contains Cr(VI) and fluoride [11 mg/L Cr(VI) and 35.24 mg/L fluoride].

SUMMARY OF PRESENT WORK, CONCLUSION AND SCOPE OF FUTURE WORK

6.1 Summary of present work

Membrane separation technology has been widely used to separate metal ions from dilute solutions. The present study provide information about the influence of various operating variables to separate Cr(VI) and fluoride from feed synthetic and real industrial wastewater with different NF and RO flat sheet membrane. The simultaneous rejection of Cr(VI) and fluoride ions from synthetic binary solution by NF300, NF500, PN40 and RO flat sheet membranes as a function of feed concentration, applied pressure, feed pH was examined. It was observed that the simultaneous rejection of Cr(VI) and fluoride ions increases with the increase in feed pressure and decreases with the increase in feed concentration. Simultaneous rejection of Cr(VI) and fluoride ions were significantly influenced by the pH of feed solution.

The Maximum removal was found at pH 8. The highest percent rejection of Cr(VI) and fluoride were found to be 97% and 92% with NF300; 91% and 84% with NF500 and 88% and 82% with PN40 membranes for lower concentration 5 mg/L feed respectively. The highest removal of Cr(VI) and fluoride by RO flatsheet membrane were found to be 99.98% and 95.1% for 5 mg/L feed respectively at 16 bar pressure. The highest percent rejection of Cr(VI) and fluoride were found to be 77% and 70% with NF300; 71% and 64% with NF500 and 68% and 61% with PN40 membranes for higher concentration 100 mg/L feed respectively. The highest removal of Cr(VI) and fluoride by RO flatsheet membrane were found to be 99.10% and 94% for 100 mg/L feed, respectively at 16 bar pressure. The rejection performances of membranes were found in the sequence as RO > NF300 > NF500 > PN40.

Two membrane transport model, namely CFSK and CFSD model were used to estimate true membrane transport parameters. The values of flux and rejection estimated using membrane transport parameters are in good agreement with the experimental results. Reasonably well agreement for experimental rejection and true rejection for fluoride and Cr(VI) estimated by CFSK model and CFSD model, respectively, but CFSK model predicted values are more accurate compared to CFSD model.

The flat sheet membranes NF 300 and RO were found best performance for synthetic wastewater. Further these were used for the treatment of simultaneous removal of Cr(VI) and fluoride from real industrial wastewater. The maximum percent rejection of Cr(VI) and fluoride were found 92.2% and 83% with NF300; 99.96% and 94.97% with RO flat sheet membrane from industrial wastewater concentration [11 mg/L Cr(VI) and 35.24 mg/L fluoride], respectively.

The capacitive deionization (CDI) process is recently developing and worldwide attracted techniques, eco-friendly, having less energy consumption and simplicity in regeneration. In the present study different activated carbon electrodes were prepared from commercial activated carbon, tea waste activated carbon, rice husk activated carbon, and limonia acidissma activated carbon.

The CAC electrode has been fabricated from commercial activated carbon and successfully applied for investigation of performance in CDI for simultaneous electrosorptive treatment of Cr(VI) and fluoride binary water system. The result shows that maximum electrosorption capacity for Cr(VI) and fluoride were found to be 0.85 mg/g and 0.82 mg/g for 10 mg/L; 3.67 mg/g and 3.22 mg/g for 100 mg/L Cr(VI) and fluoride binary feed solution respectively from the binary feed solution of Cr(VI) and fluoride at 1.2 V. Effective purification and regeneration of electrode were found in the case of binary feed solution of Cr(VI) and fluoride. Freundlich isotherm model and Redlich Peterson model were found in best agreement for both Cr(VI) and fluoride in mono component models. Extended Freundlich model and Non Modified R–P model, among six applied multicomponent isotherm models were found to fit well with the experimental data for both Cr(VI) and fluoride electropsorption performance . Pseudo first order kinetic model was found good in agreement with experimental data for both Cr(VI) and fluoride. Thus CDI with CAC electrode could be a promising treatment for simultaneous electrosorptive removal of low concentrated Cr(VI) and fluoride synthetic binary water system.

The TWBAC was successfully prepared from tea waste biomass and it was implemented for electrode preparation. The TWBAC electrode was applied in CDI application for simultaneous removal of Cr (VI) and fluoride from the mix feed solution of Cr (VI) and fluoride. The TWBAC electrode has an effective removal performance at low concentration of feed. The percent removal of Cr(VI) and fluoride were found to be 88.5% and 85.20% for 10 mg L^{-1} mix feed solution respectively. Effective electrosorption and desorption with TWBAC electrode were found. In single component isotherm modeling, Langmuir isotherm model and Redlich Peterson model were found in best agreement for both Cr(VI) and fluoride removal. Among the six applied multicomponent isotherm models Extended Langmuir model and Non modified

Redlich Peterson were found in good correlation with the experimental data for both Cr(VI) and fluoride removal. In the kinetic study, Pseudo first order kinetic model was found in good fit with experimental data for both Cr(VI) and fluoride removal.

The RHAC was derived from rice husk used and further it was used in electrode preparation. The RHAC electrode was applied in CDI application for simultaneous removal of Cr (VI) and fluoride from the mix feed solution of Cr (VI) and fluoride. The RHAC electrode has an effective removal performance at low concentration of feed. The percent removal of Cr(VI) and fluoride were found 83.1 % and 80.4 % for 10 mg L^{-1} mix feed solution respectively. Effective electrosorption and desorption with RHAC electrode were found. In single component isotherm modeling, Langmuir isotherm model and Redlich Peterson model were found in best agreement for both Cr(VI) and fluoride removal. Among the six applied multicomponent isotherm models Extended Langmuir model and Non modified Redlich Peterson were found in good correlation with the experimental data for both Cr(VI) and fluoride removal. In the kinetic study, Pseudo first order kinetic model was found in good fit with experimental data for both Cr(VI) and fluoride removal.

The LASAC electrode was prepared from Limonia acidissima (wood apple) shells activated carbon. The LASAC electrode was assembled in the MCDI system for simultaneous removal of Cr(VI) and fluoride from feed solution. The LASAC electrode effective performance was observed for electrosorption and desorption of Cr(VI) and fluoride. The ion sorption process follows Langmuir isotherm model and Redlich Peterson model for mono component; Extended Langmuir and Non modified Redlich Peterson for multicomponent isotherm modeling. Pseudo first order kinetic model was found in good fit with experimental data for both Cr(VI) and fluoride. The percent removal of Cr(VI) and fluoride were found to be 92.2 % and 89.23% for 10 mg/L concentration. Thus LASAC electrode could be promising electrode for MCDI.

LASAC electrode was found to have better performance than TWBAC and RHAC electrode for electrosorption and desorption of Cr(VI) and fluoride. The electrodes sorption performances were found in the sequence as CAC electrode > LASAC electrode > TWBAC electrode > RHAC electrode.

The removal of Cr(VI) and fluoride from real industrial wastewater by membrane separation with NF 300 flat sheet membrane, RO flat sheet membrane were found effective. The capacitive deionization with CAC electrode and LASAC electrode was found promising for removal of Cr(VI) and fluoride from low concentrated wastewater.

6.2 Conclusions

- In this work simultaneous removal of Cr(VI) and Fluoride were carried out by membrane separation and capacitive deionization techniques.

- The present study provide information about the influence of various operating variables to separate Cr(VI) and fluoride from feed synthetic and real industrial wastewater with different NF and RO flat sheet membrane.

- The simultaneous rejection of Cr(VI) and fluoride ions from synthetic binary solution by NF300, NF500, PN40 and RO flat sheet membranes as a function of feed concentration, applied pressure, feed pH was examined.

- The rejection performances of membranes were found in the sequence as RO > NF300 > NF500 > PN40.

- Reasonably well agreement for experimental rejection and true rejection for Cr(VI) and fluoride estimated by CFSK model and CFSD model, respectively, but CFSK model predicted values are more accurate compared to CFSD model.

- The maximum percent rejection of Cr(VI) and fluoride were found 92.2% and 83% with NF300; 99.96% and 94.97% with RO flat sheet membrane from industrial wastewater [11 mg/L Cr(VI) and 35.24 mg/L fluoride], respectively.

- Capacitive deionization lab scale design and fabrication were done.

- In the present study different activated carbon electrodes were prepared from commercial activated carbon, tea waste activated carbon, rice husk activated carbon, and limonia acidissma activated carbon.

- Effective purification and regeneration of electrode were found in the case of binary feed solution of Cr(VI) and fluoride.

- The electrodes sorption performances were found in the sequence as CAC electrode > LASAC electrode > TWBAC electrode > RHAC electrode.

- In the CDI study with CAC electrode: Redlich Peterson model and Freundlich isotherm model; In CDI study with LASAC electrode: Redlich Peterson model and Langmuir isotherm model were found best agreement for both Cr(VI) and fluoride in mono component models.

- In the CDI study with CAC electrode: Non Modified R–P model and Extended Freundlich model; In CDI study with LASAC electrode: Extended Langmuir model and Non modified Redlich Peterson were found best agreement for both Cr(VI) and fluoride in multicomponent isotherm models.

- Electrosorption of Cr(VI) and fluoride process follows Pseudo first order kinetic model.

- The maximum removal of Cr(VI) and fluoride by CAC electrode were found 94.35 % and 80.00 %; LASAC electrode were found 90.2 % and 76.00 % at 1.2 V and flowrate 16 mL/min from industrial wastewater which contains Cr(VI) and fluoride [Cr(VI) 11 mg/L and fluoride 35.24 mg/L].

- The simultaneous removal of Cr(VI) and fluoride from real industrial wastewater by membrane separation with NF 300 flat sheet membrane, RO flat sheet membrane were found effective.

- The capacitive deionization with CAC electrode and LASAC electrode was found promising for simultaneous removal of Cr(VI) and fluoride from low concentrated wastewater.

6.3 Scope for future work

There is scope of the present work for the future. These have been given below.

1) Testing of others NF and RO membranes can be used to see the effectiveness of Cr(VI) and fluoride removal.

2) Testing of various modules such as spiral wound and tubular can be tested in order to operate such a unit on an industrial scale.

3) Experiment with various NF/RO membranes with various real wastewater will give more reliable data that can be used for real world applications.

4) Different modeling techniques could be applied to best fit the data, which further enables better understanding of the separation mechanisms.

5) Preparation and investigation of other different biochar electrode for water treatment application.

6) Application and investigation of number of electrode pair for treatment of wastewater.

7) Study the different arrangement of CDI cell pattern and investigating the performance for waste water treatment.

8) Developing the large scale CDI system for water treatment.

PUBLICATION LIST

1) **Mahendra S. Gaikwad**, Chandrajit Balomajumder, Tea waste biomass activated carbon electrode for simultaneous removal of Cr(VI) and fluoride by capacitive deionization, **Chemosphere,** 2017, 184, 1141–1149 (Elsevier Publisher, Netherlands) **(IF: 4.208).**

2) **Mahendra S. Gaikwad**, Chandrajit Balomajumder, Simultaneous rejection of fluoride and Cr(VI) from synthetic fluoride-Cr(VI) binary water system by polyamide flat sheet reverse osmosis membrane and prediction of membrane performance by CFSK and CFSD models, **Journal of Molecular Liquids,** 2017, 234, 194–200 (Elsevier Scientific Publication, Netherlands) **(IF: 3.648).**

3) **Mahendra S. Gaikwad**, Chandrajit Balomajumder, Simultaneous electrosorptive removal of chromium(VI) and fluoride ions by capacitive deionization(CDI): multicomponent isotherm modeling and kinetic study, **Separation and Purification Technology,** 2017,186, 272–281 (Elsevier Science Publisher B.V., Netherlands) **(IF: 3.359).**

4) **Mahendra S. Gaikwad**, Chandrajit Balomajumder, Removal of Cr(VI) and fluoride by membrane capacitive deionization with nanoporous and microporous Limonia acidissima (wood apple) shell activated carbon electrode, **Separation and Purification Technology,** 2018,195, 305-313. (Elsevier Science Publisher B.V., Netherlands) **(IF: 3.359).**

5) **Mahendra S. Gaikwad**, Chandrajit Balomajumder, Capacitive Deionization for Desalination Using Nanostructured Electrodes, **Analytical Letters,** 2016, 49(11), 1641-1655 (Taylor & Francis Group Publication, USA) **(IF: 1.150).**

6) **Mahendra S. Gaikwad**, Chandrajit Balomajumder, TFC polyamide NF membrane: characterization, application and evaluation of MTPs and MTC for simultaneous removal of hexavalent chromium and fluoride, **e-Polymer,** 2017, 17(2), 129–136. (Walter de Gruyter GmbH, Germany) **(IF: 0.949)**

7) **Mahendra S. Gaikwad**, Chandrajit Balomajumder, Simultaneous rejection of chromium(VI) and fluoride [Cr(VI) and F] by nanofiltration: Membranes characterizations and estimations of membrane transport parameters by CFSK model, **Journal of Environmental Chemical Engineering,** 2017,5,45-53. (Elsevier publication, UK).

8) **Mahendra S. Gaikwad**, Chandrajit Balomajumder**, Current Progress of Capacitive Deionization in Removal of Pollutant ions, **Electrochemical Energy Technology,** 2016, 2, 17-23. (De Gruyter Open, Poland)**.**

9) **Mahendra S. Gaikwad**, Chandrajit Balomajumder, Polymer coated Capacitive Deionization Electrode for Desalination: A mini review, **Electrochemical Energy Technology**, 2016, 2, 1-5. **(De Gruyter Open, Poland**).

10) **Mahendra S. Gaikwad**, Chandrajit Balomajumder, Multicomponent isotherm modeling and kinetic study for simultaneous electrsorption of chromium(VI) and fluoride ions by acid treated activated carbon electrode (Under Review).

Conference Papers

1. **Mahendra S. Gaikwad**, Chandrajit Balomajumder "Removal of hexavalent chromium from aqueous solution by capacitive deionization with rice husk activated carbon electrode" at **ICOEST 2017, Budapest, Hungary**. (19th-23rd Oct. 2017).

2. **Mahendra S. Gaikwad**, Chandrajit Balomajumder "Characterization, separation and membrane transport parameters estimation of NF300 membrane for Cr(VI) and fluoride by CFSD model" at CHEMCON 2016 (69th Annual Session of the Indian Institute of Chemical Engineers) Chennai Regional Centre of IIChE, Chennai, Tamilnadu, India (27th-30th Dec.2016).

REFERENCES

1. Abe, I., Iwasaki, S.; Tokimoto, T.; Kawasaki, N.; Nakamura, T.; Tanada, S. Adsorption of fluoride ions onto carbonaceous materials. Journal of Colloid and Interface Science 275, 35–39, (2004).

2. Abu Seman, M.N.; Khayet, M.; Bin Ali, Z.I.; Hilal, N.; Reduction of nanofiltration membrane fouling by UV-initiated graft polymerization technique. Journal of Membrane Science 355, 133–141, (2010).

3. Agarwal, B.; Balomajumder, C.; Thakur, P.K. Simultaneous co-adsorptive removal of phenol and cyanide from binary solution using granular activated carbon. Chemical Engineering Journal 228, 655–664, (2013).

4. AlMarzooqi, F.A.; Al Ghaferi, A.A.; Saadat, I.; Hilal, N. Application of Capacitive Deionisation in water desalination: A review. Desalination 342, 3–15, (2014).

5. Al-Rashdi, B.A.M.; Johnson, D.J.; Hilal, N. Removal of heavy metal ions by nanofiltration. Desalination 315, 2–17, (2013).

6. Andelman, M.D. Flow through capacitor basics. Separation and Purification Technology 80, 262–269, (2011).

7. Andelman, M.D.; Walker, G.S., Charge Barrier Flow Through Capacitor, Patent US 6709560 (2004).

8. Annadurai, G.; Babu, S.R.; Mahesh, K.P.O.; Murugesan, T. Adsorption and biodegradation of phenol by chitosan-immobilized Pseudomonas putida (NICM 2174). Bioprocess Engineering 2, 493–501, (2000).

9. Apambire, W.B.; Boyle, D.R.; Michel, F.A. Geochemistry, genesis, and health implications of fluoriferous ground waters in the upper regions of Ghana. Environmental Geology 33, 13–24, (1997).

10. Avraham, E.; Noked, M.; Soffer, A.; Aurbach, D. The feasibility of boron removal from water by capacitive deionization. Electrochimica Acta 56, 6312–6317, (2011).

11. Baker, R. Membrane Technology and Applications, Wiley, (2004).

12. Ballet, G.T.; Gzara, L.; Hafiane, A.; Dhahbi, M. Transport coefficients and cadmium salt rejection in nanofiltration membrane. Desalination 167, 369–376, (2004).

13. Banks, D.; Reimann, C.; Røyset, O.; Skarphagen, H. Sæther, O.M. Natural concentrations of major and trace elements in some Norwegian bedrock ground waters. Applied Geochemistry 10, 1–16, (1995).

14. Bazant, M.Z.; Thornton, K.; Ajdari, A. Diffuse-charge dynamics in electrochemical systems. Physical Review E 70, 021506-24, (2004).

15. Bellona, C.; Drewes, J.E. The role of membrane surface charge and solute physico-chemical properties in the rejection of organic acids by NF membranes. Journal of Membrane Science 249, 227-234, (2005).

16. Bhore, N.; Gould, R.; Jakob, S.; Staffeld, P.; McNally, D.; Smiley, P.; Wildemuth, G. New membrane process debottlenecks solvent dewaxing unit. Oil Gas Journal 97, 67-74, (1999).

17. Bian, Y.; Yang, X.; Liang, P.; Jiang, Y.; Zhang, C.; Huang, X. Enhanced desalination performance of membrane capacitive deionization cells by packing the flow chamber with granular activated carbon. Water Research 85, 371-376, (2015).

18. Biesheuvel, P.M. Thermodynamic cycle analysis for capacitive deionization. Journal of Colloid and Interface Science 332, 258-264, (2009).

19. Biesheuvel, P.M.; Porada, S.; Presser, V. Comment on "Carbon nanotube/graphene composite for enhanced capacitive deionization performance" by Y. Wimalasiri and L. Zou. Carbon 63, 562–592, (2013).

20. Biesheuvel, P.M.; Zhao, R.; Porada, S.; van der Wal, A. Theory of membrane capacitive deionization including the effect of the electrode pore space. Journal of Colloid and Interface Science 360, 239–248, (2011).

21. Bleda-Martinez, M.J.; Macia-Agullo, J.A.; Lozano-Castello, D.; Morallon, E.; Cazorla-Amoros, D.; Linares-Solano, A. Role of surface chemistry on electric double layer capacitance of carbon materials. Carbon 43, 2677–2684, (2005).

22. Bokris, J.O.M.; Reddy, A.K.N.; Gamboa-Aldeco M. Modern electrochemistry: fundamentals of electrodics. Kluwer, New York, (2000).

23. Bontha, R.; Pintauro, P.N. Water orientation and ion solvation effects during multicomponent salt partitioning in a nafion cation exchange membrane. Chemical Engineering Science 49, 3835-3851, (1994).

24. Brasquet, C.; Rousseau, B.; Estrade-Szwarck, H.; Cloirec, P.L. Observation of activated carbon fibres with SEM and AFM correlation with adsorption data in aqueous solution. Carbon 38, 407–422, (2000).

25. Bungay, P.M.; Lonsdale, H.K.; Pinlo, M.N. Synthetic membrane: science, engineering and application, NATO ASI series, Vol.181, D. Reidel publishing co., Netherlands, (1986).

26. Burnouf, T.; Radosevich, M. Nanofiltration of plasma-derived biopharmaceutical products. Haemophilia 9, 24–28, (2003).

27. Butchermaker, B. Membrane technology benefits the food processing industry. Filtration & Separation 10, 32-33, (2004).

28. Cabatingan, L.K.; Agapay, R.C.; Rakels, J.L.L.; Ottens, M.; van der Wielen, L.A.M. Potential of biosorption for the recovery of chromate in industrial wastewaters. Industrial & Engineering Chemistry Research 40, 2302– 2309, (2001).

29. California Department of Public Health, Maximum Contaminant Levels and Regulatory Dates for Drinking Water. Retrieved 2013-12-05, (2013).

30. California Department of Public Health, State Adoption of a Hexavalent Chromium MCL. Retrieved 2014-10-08, (2014).

31. Camargo, J.A. Fluoride toxicity to aquatic organisms: a review. Chemosphere 50, 251-264, (2003).

32. Cameselle, C.; Reddy, K.R. Effects of periodic electric potential and electrolyte recirculation on integrated electrochemical remediation of contaminant mixtures. Water, Air, & Soil Pollution 224, 1-13, (2013).

33. Canadian Environmental Protection Act. Priority Substances List Supporting Document for Inorganic Fluorides. Prepared by Eco-Health Branch & Environment Canada, Ottawa (Ontario), (1994).

34. Cao, H.; Jin, W. Industrial Cr(VI) pollution analysis and control strategies in China, The 5th International Symposium on Metallomics, Guangxi, China, (2015).

35. Capelle, N.; Moulin, P.; Charbit, F.; Gallo, R. Purification of heterocyclic drug derivates from concentrated saline solution by nanofiltration. Journal of Membrane Science 196, 125-141, (2002).

36. Cavaco, S.A.; Fernandes, S.; Quina, M.M.; Ferreira, L.M. Removal of chromium from electroplating industry effluents by ion exchange resins. Journal of Hazardous Materials144, 634-638, (2007).

37. Central Pollution Control Board (CPCB), Proposed Standards for Emission or Discharge of Environmental Pollutants. New Delhi, India, (2012).

38. Cervantes, C.; Campos-García, J.; Devars, S.; Gutiérrez-Corona, F.; Loza-Tavera, H.; Torres-Guzmán, J.C.; Moreno-Sánchez, R. Interactions of chromium with microorganisms and plants. FEMS Microbiology Reviews 25, 335-347, (2001).

39. Chakrabortty, S.; Roy, M.; Pal, P. Removal of fluoride from contaminated groundwater by cross flow nanofiltration: transport modeling and economic evaluation. Desalination 313, 115–124, (2013).

40. Chaudhari, L.B.; Murthy, Z.V.P. Separation of Cd and Ni from multicomponent aqueous solutions by nanofiltration and characterization of membrane using IT model. Journal of Hazardous Materials 180, 309-315, (2010).

41. Chen, S.S.; Taylor, J.S.; Mulford, L.A.; Norris, C.D. Influences of molecular weight, molecular size, flux, and recovery for aromatic pesticide removal by nanofiltration membranes. Desalination 160, 103-111, (2004).

42. Chen, Y.; Gu, G. Preliminary studies on continuous chromium (VI) biological removal from wastewater by anaerobic–aerobic activated sludge process. Bioresource Technology 96, 1713-1721, (2005).

43. Chen, Y.; Peng, L.; Zeng, Q.; Yang, Y.; Lei, M.; Song, H.; Chai, L.; Gu, J. Removal of trace Cd(II) from water with the manganese oxides/ACF composite electrode. Clean Technologies and Environmental Policy 17, 49–57, (2015).

44. Chen, Z.; Song, C.; Sun, X.; Guo, H.; Zhu, G. Kinetic and isotherm studies on the electrosorption of NaCl from aqueous solutions by activated carbon electrodes. Desalination 267, 239–243, (2011).

45. Cheryan, M. Ultrafiltration and Microfiltration Handbook, Technomic Pulishing Company, Lancaster, (1998).

46. Chianese, A.; Ranauro, R.; Verdone, N. Treatment of landfill leachate by reverse osmosis. Water Research 33, 647–652, (1999).

47. Childress, A.E.; Elimelech, M. Effect of solution chemistry on the surface charge of polymeric reverse osmosis and nanofiltration membranes. Journal of Membrane Science 119, 253-268, (1996).

48. Chilekar, S.N. Environmental application of filtration/membrane processes. Chemical Industry Digest, 3rd quarter 128-130, (1993).

49. Chilyumova, E.; Thöming, J. Nanofiltration of bivalent nickel cations—model parameter determination and process simulation. Desalination 224, 12-17, (2008).

50. Chitry, F.; Garcia, R.; Nicod, L.; Gass, J.L.; Madic, C.; Lemaire, M. Separation of gadolinium (III) and lanthanum (III) by nanofiltration-complexation in aqueous medium. Journal of Radioanalytical and Nuclear Chemistry 240, 931-934, (1999).

51. Chitry, F.; Pellet-Rostaing, S.; Gozzi, C.; Lemaire, M. Separation of lanthanides (III) by nanofiltration-complexation in aqueous medium. Separation Science and Technology 36, 605-618, (2001).

52. Choi, J-H. Comparison of constant voltage (CV) and constant current (CC) operation in the membrane capacitive deionisation process. Desalination and Water Treatment 56, 921–928, (2015).

53. Clesceri, L.S.; Greenberg, A.E.; Eaton, A.D. Standard Methods for the Examination of Water and Wastewater. American Public Health Association, Washington, (1998).

54. Conway, B.E. Electrochemical Supercapacitors: Scientific Fundamentals and Technological Applications, Kluwer Academic/ Plenum Publishers, New York, (1999).

55. Dai, K.; Shi, L.; Fang, J.; Zhang, D.; Yu, B. NaCl adsorption in multi-walled carbon nanotubes. Materials Letters 59, 1989–1992, (2005).

56. Dakiky, M.; Khamis, M.; Manassra, A.; Mer'eb, M. Selective adsorption of chromium (VI) in industrial wastewater using low-cost abundantly available adsorbents. Advances in Environmental Research 6, 533-540, (2002).

57. Das, T.K.; Mitra, A. Economic Utilisation of Cow-Dung and Cattle Urine Through Bio-Gas Plant: A Case Study in Labpur Block of Birbhum District, West Bengal. Economic Affairs (Calcutta) 40(1), 62, (1995).

58. De, M.; Azargohar, R.; Dalai, A.K.; Shewchuk, S.R. Mercury removal by bio-char based modified activated carbons. Fuel 103, 570-578, (2013).

59. Dhabhai, R.; Ahmadifeijani, E.; Dalai, A.K.; Reaney, M. Purification of crude glycerol using a sequential physico-chemical treatment, membrane filtration, and activated charcoal adsorption. Separation and Purification Technology 168, 101-106, (2016).

60. Długołecki, P.; Anet, B.; Metz, S. J.; Nijmeijer, K.; Wessling, M. Transport limitations in ion exchange membranes at low salt concentrations, Journal of Membrane Science 346, 163–171, (2010).

61. Długołęcki, P.; van der Wal, A. Energy Recovery in Membrane Capacitive Deionization. Environmental Science & Technology 47, 4904−4910, (2013).

62. Duranceau, S.J.; Taylor, J.S.; Mulford, L.A. SOC removal in a membrane softening process. Journal-American Water Works Association 84, 68-78, (1992).

63. Edigaryan, A.A.; Safonov, V.A.; Lubnin, E.N.; Vykhodtseva, L.N.; Chusova, G.E.; Polukarov, Y.M. Properties and preparation of amorphous chromium carbide electroplates. Electrochimica Acta 47, 2775-2786, (2002).

64. Edmunds, M.; Smedley, P. Fluoride in natural waters. In Essentials of Medical Geology, Impacts of Natural Environment on Public Health, Elsevier Academic Press, (2005).

65. El-Deen, A.G.; Barakat, N.A.M.; Khalil, K.A.; Motlak, M.; Yong Kim, H.; Graphene/SnO2 nanocomposite as an effective electrode material for saline water

desalination using capacitive deionization. Ceramics International 40, 14627–14634, (2014b).

66. El-Deen, A.G.; Barakat, N.A.M.; Kim, H.Y. Graphene wrapped MnO2-nanostructures as effective and stable electrode materials for capacitive deionization desalination technology. Desalination 344, 289–298, (2014a).

67. El-Deen, A.G.; Choi, J.-H.; Kim, C.S.; Khalil, K.A.; Almajid, A.A.; Barakat, N.A.M. TiO2 nanorod-intercalated reduced graphene oxide as high performance electrode material for membrane capacitive deionization. Desalination 361, 53–64, (2015).

68. Elimelech, M.; Phillip, W. A. The future of seawater desalination: Energy, technology, and the environment. Science 333,712–17, (2011).

69. Elimelech, M.; Xiaohua, Z.; Childress, A.E.; Seungkwan, H. Role of membrane surface morphology in colloidal fouling of cellulose acetate and composite aromatic polyamide reverse osmosis membranes. Journal of Membrane Science 127, 101–109, (1997).

70. Eriksson, P.K. Nanofilration extends the range of membrane filtration. Environmental Progress 7, 58-62, (1998).

71. Fan, C.-S.; Tseng, S.-C.; Li, K.-C.; Hou, C.-H. Electro-removal of arsenic(III) and arsenic(V) from aqueous solutions by capacitive deionization. Journal of Hazardous Materials 312, 208–215, (2016).

72. Farmer, J.C.; Fix, D.V.; Mack, G. V.; Pekala, R.W.; Poco, J.F. Capacitive deionization of NaCl and NaNO3 solutions with carbon aerogel electrodes. Journal of The Electrochemical Society 143, 159–169, (1996).

73. Farooqi, A.; Masuda, H.; Siddiqui, R.; Naseem, M. Sources of arsenic and fluoride in highly contaminated soils causing groundwater contamination in Punjab. Archives of Environmental Contamination and Toxicology 21, 693-706, (2008).

74. Feng, C.J.; Hou, C.; Chen, S.H.; Yu, C.P. A microbial fuel cell driven capacitive deionization technology for removal of low level dissolved ions. Chemosphere 91, 623–28, (2013).

75. Foo, K.Y.; Hameed, B.H. A short review of activated carbon assisted electrosorption process: an overview, current stage and future prospects. Journal of Hazardous Materials 170, 552-559, (2009).

76. Freeman, S.D.; Stocker, T.F. Comparison of two thin-film composite membranes: low pressure FT-30 to very low pressure NF40HF. Desalination 62, 183-191, (1987).

77. Gabelich, C.J.; Tran, T.D.; Suffet, I.H. Electrosorption of inorganic salts from aqueous solution using carbon aerogels. Environmental Science & Technology 36, 3010–3019, (2002).

78. Gandhi, P.J.; Murthy, Z.V.P. Transmission of p-anisic acid through nanofiltration and goat membranes. Desalination 315, 46-60, (2013).

79. Gao, Y.; Pan, L.; Li, H.; Zhang, Y.; Zhang, Z.; Chen, Y. Electrosorption behavior of cations with carbon nanotubes and carbon nanofibres composite film electrodes. Thin Solid Films 517, 1616–1619, (2009).

80. Garg, V.K.; Gupta, R.; Kumar, R.; Gupta, R.K. Adsorption of chromium from aqueous solution on treated sawdust. Bioresource Technology 92, 79–81, (2004).

81. Geraldes, V.; de Pinho, M. Process water recovery from pulp bleaching effluents by an NF/ED hybrid process. Journal of Membrane Science 102, 209-221, (1995).

82. Gillespie, R.J.; Humphries, D.A.; Baird, N.C.; Robinson, E.A. Chemistry, second ed. Allyn and Bacon, Boston, (1989).

83. Glueckauf, E. The distribution of electrolytes between cellulose acetate membranes and aqueous solutions. Desalination 18, 155-172, (1976).

84. Gonzalez, A.R.; Ndung'u, K.; Flegal, A.R. Natural occurrence of hexavalent chromium in the Aromas Red Sands Aquifer, California, Environmental Science & Technology 39, 5505-5511, (2005).

85. Greenwood, N.N.; Earnshaw, A. Chemistry of the Elements. Pergamon Press, Toronto, (1984).

86. Grujicic, M.; Cao, G.; Gersten, B. Optimization of the chemical vapor deposition process for carbon nanotubes fabrication. Applied Surface Science 199, 90-106, (2002).

87. Gu, X.; Hu, M., Du, Z.; Huang, J.; Wang, C. Fabrication of mesoporous graphene electrodes with enhanced capacitive deionization. Electrochimica Acta 182, 183–191, (2015a).

88. Gu, X.; Yang, Y.; Hu, Y.; Hu, M.; Huang, J.; Wang, C. Facile fabrication of graphene–polypyrrole–Mn composites as high-performance electrodes for capacitive deionization. Journal of Materials Chemistry A 3, 5866-5874, (2015b).

89. Gunda, N.S.K.; Choi, H.W.; Berson, A.; Kenney, B.; Karan, K.; Pharoah, J.G.; Mitra, S.K. Focused ion beam-scanning electron microscopy on solid-oxide fuel-cell electrode: Image analysis and computing effective transport properties. Journal of Power Sources 19, 3592-3603, (2011).

90. Gupta, N.; Balomajumder, C.; Agarwal, V.K. Adsorption of cyanide ion on pressmud surface: a modeling approach. Chemical Engineering Journal 191, 548–556, (2012b).

91. Gupta, V.K.; Ali, I.; Saleh, T.A.; Nayak, A.; Agarwal, S. Chemical treatment technologies for waste-water recycling – an overview. RSC Advances 2, 6380–6388, (2012a).

92. Gupta, V.K.; Kumar, R.; Nayak, A.; Saleh, T.A.; Barakat, M.A. Adsorptive removal of dyes from aqueous solution onto carbon nanotubes: a review. Advances in Colloid and Interface Science 193–194, 24–34, (2013a).

93. Gupta, V.K.; Saleh, T.A. Sorption of pollutants by porous carbon, carbon nanotubes and fullerene – an overview. Environmental Science and Pollution Research International 20, 2828–2843, (2013b).

94. Hamad, F.; Khulbe, K.C.; Matsuura, T. Comparison of gas separation performance and morphology of homogeneous and composite PPO membranes. Journal of Membrane Science 256, 29–37, (2005).

95. Han, L.; Karthikeyan, K.G.; Anderson, M.A.; Wouters, J.J.; Gregory, K.B. Mechanistic insights into the use of oxide nanoparticles coated asymmetric electrodes for capacitive deionization. Electrochimica Acta 90, 573–581, (2013).

96. Haynes, W.M. CRC Handbook of Chemistry and Physics, 91st ed., CRC Press, Taylor & Francis Group, (2010).

97. Heberer, T.; Feldmann, D.; Reddersen, K.; Altmann, H.; Zimmermann, T. Production of drinking water from highly contaminated surface waters: removal of organic, inorganic and microbial contaminants applying mobile membrane filtration units. Acta hydrochimica et hydrobiologica 30, 24-33, (2002).

98. Helmholtz, H.V. Helmholtz's theory of double electric layers. Journal of The Franklin Institute 115, 310, (1883).

99. Hickey, P.J.; Goading, C.H. Mass transfer in spiral wound pervaporation modules. Journal of Membrane Science 92, 59-74, (1994).

100. Hilal, N.; Al-Zoubi, H.; Darwish, N.A.; Mohammad, A.W. Characterisation of nanofiltration membranes using atomic force microscopy. Desalination 177, 187–199, (2005).

101. Horitsu, H.; Nishida, H.; Kato, H.; Tomoyeda, M. Isolation of potassium chromate-tolerant bacterium and chromate uptake by the bacterium. Agricultural and Biological Chemistry 42, 2037-2043, (1978).

102. Hou, C.H.; Huang, C.Y. A comparative study of electrosorption selectivity of ions by activated carbon electrodes in capacitive deionization. Desalination 314, 124–129, (2013).

103. Hou, C.H.; Liang, C.; Yiacoumi, S.; Dai, S.; Tsouris, C. Electrosorption capacitance of nanostructured carbon-based materials. Journal of Colloid and Interface Science 302, 54–61, (2006).

104. Hu, C.; Liu, F.; Lan, H.; Liu, H.; Qu, J. Preparation of a manganese dioxide/carbon fiber electrode for electrosorptive removal of copper ions from water. Journal of Colloid and Interface Science 446, 359– 365, (2015).

105. Huang, G.-H.; Chen, T.-C.; Hsu, S.-F.; Huang, Y.-H.; Chuangd, S.-H. Capacitive deionization (CDI) for removal of phosphate from aqueous solution. Desalination and Water Treatment 52, 759–765, (2014b).

106. Huang, S.-Y.; Fan, C.-S.; Hou, C.-H. Electro-enhanced removal of copper ions from aqueous solutions by capacitive deionization. Journal of Hazardous Materials 278, 8–15, (2014a).

107. Huang, W.; Zhang, Y.; Bao, S.; Song, S. Desalination by capacitive deionization with carbon-based materials as electrode: a review. Surface Review and Letters 20, 1330003-10, (2013).

108. Huang, Z.-H.; Wang, M.; Wang, L.; Kang, F. Relation between the charge efficiency of activated carbon fiber and its desalination performance. Langmuir 28, 5079–5084, (2012).

109. Huyskens, C.; Helsen, J.; Groot, W.J.; de Haan, A.B. Cost evaluation of large-scale membrane capacitive deionization for biomass hydrolysate desalination. Separation and Purification Technology 146, 294–300, (2015).

110. Huyskens, C.; Helsen, J.; Groot, W.J.; de Haan, A.B. Membrane capacitive deionization for biomass hydrolysate desalination. Separation and Purification Technology 118, 33–39, (2013).

111. Ishibashi, Y.; Cervantes, C.; Silver, S. Chromium reduction in Pseudomonas putida. Applied and Environmental Microbiology 56, 2268-2270, (1990).

112. Ito, E.; Mozia, S.; Okuda, M.; Nakano, T.; Toyoda, M.; Inagaki, M. Nanoporous carbons from cypress II. Application to electric double layer capacitors. New Carbon Mater. 22, 321-326, (2007).

113. Jain, M.; Garg, V.K.; Kadirvelu, K. Chromium (VI) removal from aqueous system using Helianthus annuus (sunflower) stem waste. Journal of Hazardous Materials 162, 365-372, (2009).

114. Jana, S.; Saikia, A.; Purkait, M. K.; Mohanty, K. Chitosan based ceramic ultrafiltration membrane: Preparation, characterization and application to remove Hg(II) and As(III) using polymer enhanced ultrafiltration. Chemical Engineering Journal 170, 209-219, (2011).

115. Jeon, S.-I.; Park, H.-R.; Yeo, J.-G.; Yang, S.; Cho, C. H.; Han, M. H.; Kim, D. K. Desalination via a new membrane capacitive deionization process utilizing flow-electrodes. Energy & Environmental Science 6, 1471–1475, (2013).

116. Jeong, K. S.; Hwang, W. C.; Hwang, T. S. Synthesis of an aminated poly(vinylidene fluride-g-4-vinyl benzyl chloride) anion exchange membrane for membrane capacitive deionization(MCDI). Journal of Membrane Science 495, 316–321, (2015).

117. Jia, B.; Zou, L. Graphene nanosheets reduced by a multi-step process as highperformance electrode material for capacitive deionization. Carbon 50, 2315–2321, (2012a).

118. Jia, B.; Zou, L. Wettability and its influence on graphene nanosheets as electrode material for capacitive deionization. Chemical Physics Letters 548, 23–28, (2012b).

119. Jin, W.; Moats, M.S.; Zheng, S.; Du, H.; Zhang, Y.; Miller, J.D. Modulated Cr (III) oxidation in KOH solutions at a gold electrode: Competition between disproportionation and stepwise electron transfer. Electrochimica Acta 56, 8311–8318, (2011).

120. Jin, W.; Zheng, S.; Du, H.; Xu, H.; Zhang, Y. Isopiestic Study of the Na_2CrO_4 − H_2O System at 353.15 K: Prediction of the Solubility of Na_2CrO_4 in Aqueous NaOH Solutions. Industrial & Engineering Chemistry Research 49, 8244–8247, (2010).

121. Jo, S.W.; Sherif, S.A.; Lear, W.E. Numerical simulation of saturated flow boiling heat transfer of ammonia/water mixture in bubble pumps for absorption–diffusion refrigerators. Journal of Thermal Science and Engineering Applications 6, 011007, (2014).

122. Joshi, T.; Iyengar, L.; Singh, K.; Garg, S. Isolation, identification and application of novel bacterial consortium TJ-1 for the decolourization of structurally different azo dyes. Bioresource Technology 99, 7115-7121, (2008).

123. Jung, S.M.; Choi, J.H., Kim, J.H. Application of capacitive deionization (CDI) technology to insulin purification process. Separation and Purification Technology 98, 31–35, (2012).

124. Kalsi, A.S. Srivastava, A. K. Biological Phosphorous removal by Acinetobacter bacteria, CHEMCON 98 (Indian Chemical Engineering Congress 1998) at Visakhapatnam (Andhra Pradesh), (1998).

125. Kim J.-S.; Choi J.-H. Fabrication and characterization of a carbon electrode coated with cation-exchange polymer for the membrane capacitive deionization applications. Journal of Membrane Science 355, 85–90, (2010b).

126. Kim, C.; Lee, J.; Kim, S.; Yoon, J. TiO2 sol–gel spray method for carbon electrode fabrication to enhance desalination efficiency of capacitive deionization. Desalination 342, 70 –74, (2014).

127. Kim, J. S.; Kim, C. S.; Shin, H. S.; Rhim, J. W. Application of Synthesized Anion and Cation Exchange Polymers to Membrane Capacitive Deionization (MCDI). Macromolecular Research 23, 360-366, (2015).

128. Kim, J.S.; Kim, C. S.; Shin, H. S.; Rhim, J.W. Application of Synthesized Anion and Cation Exchange Polymers to Membrane Capacitive Deionization (MCDI). Macromolecular Research 23, 360– 366, (2015).

129. Kim, T.-U.; Amy, G.; Drewes, J.E. Rejection of trace organic compounds by high-pressure membranes. Water Science and Technology 51, 335–344, (2005).

130. Kim, Y. J.; Choi, J. H. Improvement of desalination efficiency in capacitive deionization using a carbon electrode coated with an ion-exchange polymer. Water Research 44, 990–996, (2010a).

131. Kim, Y.-J.; Choi, J.-H. Enhanced desalination efficiency in capacitive deionization with an ion-selective membrane. Separation and Purification Technology 71, 70-75, (2010c).

132. Kimura, K.; Amy, G.; Drewes, J.E., Heberer, T.; Kim, T.U.; Watanabe, Y. Rejection of organic micropollutants (disinfection by-products, endocrine disrupting compounds, and pharmaceutically active compounds) by NF/RO membranes. Journal of Membrane Science 227, 113–121, (2003b).

133. Kotas, J.; Stasicka, Z. Chromium occurrence in the environment and methods of its speciation. Environmental Pollution 107, 263–283, (2000).

134. Koter, S. Determination of the parameter of the Spiegler-Kedem-Katchalsky model, Desalination 198, 335-345, (2006).

135. Kozlowski, C.A.; Walkowiak, W. Removal of chromium (VI) from aqueous solutions by polymer inclusion membranes. Water Research 36, 4870-4876, (2002).

136. Ku, Y.; Chen, S.W.; Wang, W.Y. Effect of solution composition on the removal of copper ions by nanofiltration. Separation and Purification Technology 43, 135-142, (2005).

137. Kumar, P.; Headley, J.; Peru, K.; Bailey, J.; Dalai, A. Removal of dicyclohexyl acetic acid from aqueous solution using ultrasound, ozone and their combination. Journal of Environmental Science and Health, Part A 49, 1512-1519, (2014).

138. Kumar, R.; Bhakta, P.; Chakrabortty, S.; Pal, P. Separating cyanide from coke wastewater by cross flow nanofiltration. Separation Science and Technology 46, 2119–2127, (2011).

139. Kumar, S.; Zafar, M.; Prajapati, J.K.; Kumar, S.; Kannepalli, S. Modeling studies on simultaneous adsorption of phenol and resorcinol onto granular activated carbon from simulated aqueous solution. Journal of Hazardous Materials 185, 287– 294, (2011).

140. Kumar, V.; Tewari, R.; Singh, K. Comparative Studies of Drying Methods on Yield and Composition of the Essential Oil of Cymbopogon citratus. Journal of Essential Oil Bearing Plants 18, 744-750, (2015).

141. Lahontan Regional Water Quality Control Board. Swrcb.ca.gov. Retrieved 2014-01-06, (2014).

142. Laine, J. M.; Jacangelo, J. G.; Cummings, E.; W Carns, K. E.; Mallevialle, J. Influence of bromide on low-pressure membrane filtration for controlling DBPs in surface water. Journal - American Water Works Association 85, 87-89, (1993).

143. Lalia, B. S.; Kochkodan, V.; Hashaikeh, R.; Hilal, N. A review on membrane fabrication: Structure, properties and performance relationship. Desalination 326, 77–95, (2013).

144. Laxman, K.; Myint, M.T.Z.; Al Abri, M.; Sathe, P.; Dobretsov, S.; Dutta, J. Desalination and disinfection of inland brackish ground water in a capacitive deionization cell using nanoporous activated carbon cloth electrodes. Desalination 362, 126–132, (2015b).

145. Laxman, K.; Myint, M.T.Z.; Khan, R.; Pervez, T.; Dutta, J. Improved desalination by zinc oxide nanorod induced electric field enhancement in capacitive deionization of brackish water. Desalination 359, 64–70, (2015a).

146. Lee J.-Y.; Seo S.-J.; Yun S.- H.; Moon S.-H. Preparation of ion exchanger layered electrodes for advanced membrane capacitive deionization (MCDI). Water Research 45, 5375–5380, (2011).

147. Lee, J. H.; Bae, W.S.; Choi, J.H. Electrode reactions and adsorption/desorption performance related to the applied potential in a capacitive deionization process. Desalination 258, 159–163, (2010).

148. Lee, J.B.; Park, K.K.; Eum, H.M.; Lee, C.W. Desalination of a thermal power plant wastewater by membrane capacitive deionization. Desalination 196, 125-134, (2006).

149. Lee, J.H.; Choi, J.H. Ion-selective composite carbon electrode coated with TiO2 nanoparticles for the application of electrosorption process. Desalination and Water Treatment 51, 503–510, (2013).

150. Lee, J.-H.; Choi, J.-H. The production of ultrapure water by membrane capacitive deionization (MCDI) technology. Journal of Membrane Science 409–410, 251–256, (2012).

151. Lee, J.Y.; Seo, S.J.; Park, J.W.; Moon, S.H. A study on the cell structure for capacitive deionization system. Korean Journal of Chemical Engineering 48, 791-794, (2010).

152. Lee, S.F.; Sherif, S.A. Thermodynamic analysis of a lithium bromide/water absorption system for cooling and heating applications. International Journal of Energy Research 25, 1019-1031, (2001).

153. Leitão, A.; Serrão, R. Adsorption of phenolic compounds from water on activated carbon: prediction of multicomponent equilibrium isotherms using single-component data. Adsorption 11, 167–179, (2005).

154. Li, H.; Gao, Y.; Pan, L.; Zhang, Y.; Chen, Y.; Sun, Z. Electrosorptive desalination by carbon nanotubes and nanofibres electrodes and ion-exchange membranes. Water Research 42, 4923-4928, (2008).

155. Li, H.; Lu, T.; Pan, L.; Zhang, Y.; Sun, Z. Electrosorption behavior of graphene in NaCl solutions. Journal of Materials Chemistry 19, 6773–6779, (2009).

156. Li, H.; Nie, C.; Pan, L.; Sun, Z. The study of membrane capacitive deionization from charge efficiency. Desalination and Water Treatment 42, 210–215, (2012b).

157. Li, H.; Pan, L.; Lu, T.; Zhan, Y.; Nie, C.; Sun, Z. A comparative study on electrosorptive behavior of carbon nanotubes and graphene for capacitive deionization. Journal of Electroanalytical Chemistry 653, 40–44, (2011).

158. Li, H.; Pan, L.; Nie, C.; Liu, Y.; Sun, Z. Reduced graphene oxide and activated carbon composites for capacitive deionization. Journal of Materials Chemistry 22, 15556–15561, (2012a).

159. Li, H.; Pan, L.; Zhang, Y.; Zou, L.; Sun, C.; Zhan, Y.; Sun, Z. Kinetics and thermodynamics study for electrosorption of NaCl onto carbon nanotubes and carbon nanofibers electrodes. Chemical Physics Letters 485, 161–166, (2010a).

160. Li, H.; Zou, L. Ion-exchange membrane capacitive deionization: A new strategy for brackish water desalination. Desalination 275, 62–66, (2011).

161. Li, H.; Zou, L.; Pan, L.; Sun, Z. Novel graphene-like electrodes for capacitive deionization. Environmental Science & Technology 44, 8692–8697, (2010b).

162. Li, H.; Zou, L.; Pan, L.; Sun, Z. Using graphene nano-flakes as electrodes to remove ferric ions by capacitive deionization. Separation and Purification Technology 75, 8–14, (2010c).

163. Li, H.B.; Lu, T.; Pan, L.K.; Zhang, Y.P.; Sun, Z. Electrosorption behavior of graphene in NaCl solutions. Journal of Materials Chemistry 19, 6773–6779, (2009).

164. Li, L.X.; Li, F. The effect of carbonyl, carboxyl and hydroxyl groups on the capacitance of carbon nanotubes. New Carbon Materials 26, 224–228, (2011).

165. Li, Y.; Zhang, C.; Jiang, Y.; Wang, T.J.; Wang, H. Effects of the hydration ratio on the electrosorption selectivity of ions during capacitive deionization. Desalination 399, 171–177, (2016).

166. Li, Z.; Song, B.; Wu, Z.; Lin, Z.; Yao, Y.; Moon, K.-S.; Wong, C.P. 3D porous graphene with ultrahigh surface area for microscale capacitive deionization. Nano Energy 11, 711 – 718, (2015).

167. Liang, P.; Yuan, L.; Yang, X.; Zhou, S.; Huang, X. Coupling ion-exchangers with inexpensive activated carbon fiber electrodes to enhance the performance of capacitive deionization cells for domestic wastewater desalination. Water Research 47, 2523–2530, (2013).

168. Liou, T-H. Preparation and characterization of nano-structured silica from rice husk. Materials Science and Engineering: A 364, 313– 323, (2004).

169. Lipnizki, F.; Boelsmand, J.; Madsen, R. Concept of industrial-scale diafiltration systems. Desalination 144, 179-184, (2001).

170. Liu, J.; Lu, M.; Yang, J.; Cheng, J.; Cai. W. Capacitive desalination of ZnO/activated carbon asymmetric capacitor and mechanism analysis. Electrochimica Acta 151, 312–318, (2015a).

171. Liu, L.; Liao, L.; Meng, Q.; Cao, B. High performance graphene composite microsphere electrodes for capacitive deionization. Carbon 90, 75–84, (2015b).

172. Liu, Y.; Pan, L.; Xu, X.; Lu, T.; Sun, Z.; Chua D.H.C. Enhanced desalination efficiency in modified membrane capacitive deionization by introducing ion-exchange polymers in carbon nanotubes electrodes. Electrochimica Acta 130, 619–624, (2014).

173. Liu, Y.; Pan, L.; Xu, X.; Lu, T.; Sun, Z.; Chua, D.H.C. Enhanced desalination efficiency in modified membrane capacitive deionization by introducing ion-exchange polymers in carbon nanotubes electrodes. Electrochimica Acta 130, 619–624, (2014).

174. Liu, Y.; Xu, X.; Wang, M.; Lu, T.; Sun, Z.; Pan, L. Nitrogen-doped carbon nanorods with excellent capacitive deionization ability. Journal of Materials Chemistry A 3, 17304–17311, (2015c).

175. Losi, M.E.; Frankenberger, W.T. Chromium-resistant microorganisms isolated from evaporation ponds of a metal processing plant. Water, Air, & Soil Pollution 74, 405-413, (1994).

176. Mall, I.D.; Srivastava, V.C.; Agarwal, N.K. Removal of Orange-G and Methyl Violet dyes by adsorption onto bagasse fly ash kinetic study and equilibrium isotherm analyses. Dyes and Pigments 69, 210–223, (2006).

177. Mallevialle, J.; Odendaal, P. E.; Wiesner, M. R. The emergence of membranes in water and wastewater treatment, in: Water Treatment Membrane Processes, Published by Water Research Commission of South Africa, McGraw-Hill Publication, (1996).

178. Manning, A.H.; Mills, C.T.; Morrison, J.M.; Ball, L.B. Insights into controls on hexavalent chromium in groundwater provided by environmental tracers, Sacramento Valley, California, USA. Applied Geochemistry 62, 186-199, (2015).

179. Mason, E.A.; Lonsdale, H.K. Review statistical–mechanical theory of membrane transport. Journal of Membrane Science 51, 1–81, (1990).

180. Mattson, J. S.; Mark, H.B. Activated Carbon, Marcel Dekker, New York, (1971).

181. McLean, R.J.; Beauchemin, D.; Clapham, L.; Beveridge, T.J. Metal-binding characteristics of the gamma-glutamyl capsular polymer of Bacillus licheniformis ATCC 9945. Applied and Environmental Microbiology 56, 3671-3677, (1990).

182. Meenakshi, R.C.; Maheshwari. Fluoride in drinking water and its removal. Journal of Hazardous Materials 137, 456–463, (2006).

183. Mehiguene, K.; Garba, Y.; Taha, S.; Gondrexon, N.; Dorange, G. Influence of operating conditions on the retention of copper and cadmium in aqueous solution by nanofiltration experimental results and modeling. Separation and Purification Technology 15, 181–187, (1999).

184. Mehiguene, K.; Garba, Y.; Taha, S.; Gondrexon, N.; Dorange, G. Influence of operating conditions on the retention of copper and cadmium in aqueous solutions by

nanofiltration: experimental results and modeling. Separation and Purification Technology 15, 181–187, (1999).

185. Mehiguene, K.; Garba, Y.; Taha, S.; Gondrexon, N.; Dorange, G. Influence of operating conditions on the retention of copper and cadmium in aqueous solutions by nanofiltration: experimental results and modeling. Separation and Purification Technology 15, 181–187, (1999).

186. Mezher, T; Fath, H.; Abbas, Z.; Khaled, A. Techno-economic assessment and environmental impacts of desalination technologies. Desalination 266,263–73, (2011).

187. Mishra, D.; Shukla, A.K.; Dixit, A.K.; Singh, K. Aqueous enzymatic extraction of oil from mandarin peels. Journal of Oleo Science 54, 355-359, (2005).

188. Mishra, S.; Bharagava, R.N. Toxic and genotoxic effects of hexavalent chromium in environment and its bioremediation strategies. Journal of Environmental Science and Health, Part C 34, 1-32, (2016).

189. Moghal, A.A.B.; Reddy, K.R.; Mohammed, S.A.S.; Al-Shamrani, M.A.; Zahid, W.M. Lime-Amended Semi-arid Soils in Retaining Copper, Lead, and Zinc from Aqueous Solutions. Water, Air, & Soil Pollution 227, 372, 1-19, (2016).

190. Mohammadpour, A.; Waghmare, P.R.; Mitra, S.K.; Shankar, K. Anodic growth of large-diameter multipodal TiO_2 nanotubes. Acs Nano 4, 7421-7430, (2010).

191. Mossad, M.; Zou, L. A study of the capacitive deionisation performance under various operational conditions. Journal of Hazardous Materials 213, 491–497, (2012).

192. Mulder, M. Basic Principles of Membrane Technology, Kluwer Academic Publishers, Dordrecht, (1991).

193. Murthy, Z.V.P.; Chaudhari, L.B. Application of nanofiltration for the rejection of nickel ions from aqueous solutions and estimation of membrane transport parameters. Journal of Hazardous Materials 160, 70–77, (2008).

194. Murthy, Z.V.P.; Chaudhari, L.B. Rejection behavior of nickel ions from synthetic wastewater containing Na_2SO_4, $NiSO_4$, $MgCl_2$ and CaCl2 salts by nanofiltration and characterization of the membrane. Desalination, 247, 610-622, (2009).

195. Murthy, Z.V.P.; Choudhary, A. Separation and estimation of nanofiltration membrane transport parameters for cerium and neodymium. Rare Metals 31, 500-506, (2012).

196. Murthy, Z.V.P.; Choudhary, A. Separation of cerium from feed solution by nanofiltration. Desalination 279, 428-432, (2011).

197. Murthy, Z.V.P.; Gaikwad, M.S. Separation of praseodymium (III) from aqueous solutions by nanofiltration. Canadian Metallurgical Quarterly 52, 18-22, (2013).

198. Murthy, Z.V.P.; Gupta, S. K. Estimation of mass transfer coefficient using a combined non linear membrane transport and film theory model. Desalination 109, 39-49, (1997).

199. Murthy, Z.V.P.; Gupta, S.K. Sodium cyanide separation and parameter estimation for reverse osmosis thin film composite polyamide membrane. Journal of Membrane Science 154, 89-103, (1999).

200. Murthy, Z.V.P.; Gupta, S.K. Thin film composite polyamide membrane parameters estimation for phenol-water system by reverse osmosis. Separation Science and Technology 33, 2541–2557, (1998).

201. Myint, M.T.Z.; Dutta, J. Fabrication of zinc oxide nanorods modified activated carbon cloth electrode for desalination of brackish water using capacitive deionization approach. Desalination 305, 24–30, (2012).

202. Nadakatti, S.; Tendulkar, M.; Kadam, M. Use of mesoporous conductive carbon black to enhance performance of activated carbon electrodes in capacitive deionization technology. Desalination 268, 182–88, (2011).

203. Nanduri, V.; Das, T.K. A survey of critical research areas in the energy segment of restructured electric power markets. International Journal of Electrical Power & Energy Systems 31, 181-191, (2009).

204. Nanduri, V.; Das, T.K.; Rocha, P. Generation capacity expansion in energy markets using a two-level game-theoretic model. IEEE Transactions on Power Systems 24, 1165-1172, (2009).

205. Nath, K.; Singh, D.; Shyam, S.; Sharma, Y.K. Phytotoxic effects of chromium and tannery effluent on growth and metabolism of Phaseolus mungo Roxb. Journal of Environmental Biology 30, 227–234, (2009).

206. Nguyen, N.C.; Chen, S.S.; Hsu, H.T.; Li, C.W. Separation of three divalent cations (Cu 2+, Co 2+ and Ni 2+) by NF membranes from pHs3 to 5. Desalination 328, 51-57, (2013).

207. Nie, C.; Zhan, Y.; Pan, L.; Li, H.; Sun, Z. Electrosorption of different cations and anions with membrane capacitive deionization based on carbon nanotube/nanofiber electrodes and ion exchange membranes. Desalination and Water Treatment 30, 266–271, (2011).

208. Nightingale, E.R. Phenomenological theory of ion solvation effective radii of hydrated ions. The Journal of Physical Chemistry 63, 1381–1387, (1959).

209. Nriagu, J.O.; Nieboer, E. eds. Chromium in the natural and human environments. John Wiley & Sons 20, 21– 81, (1988).

210. Nugrahenny, A.T.U.; Kim, J.; Lim, S.; Jung, D.-H. Development of high performance cell structure for capacitive deionization using membrane polymer-coated electrode. In The 6th Conference of Indonesian Students Association in Korea, Daejeon, (2013).

211. Oda, H.; Nakagawa, Y. Removal of ionic substances from dilute solution using activated carbon electrodes. Carbon 41, 1037–1047, (2003).

212. Omosebi, A.; Gao, X.; Landon, J.; Liu, K. Asymmetric Electrode Configuration for Enhanced Membrane Capacitive Deionization. ACS Applied Materials & Interfaces 6, 12640−12649, (2014).

213. Omosebi, A.; Gao, X.; Rentschler, J.; Landon, J.; Liu, K. Continuous operation of membrane capacitive deionization cells assembled with dissimilar potential of zero charge electrode pairs. Journal of Colloid and Interface Science 446, 345–351, (2015).

214. Oren, Y. Capacitive deionization (CDI) for desalination and water treatment — past, present and future (a review). Desalination 228, 10–29, (2008).

215. Owlad, M.; Aroua, M.K.; Daud, W.A.W.; Baroutian, S. Removal of hexavalent chromium-contaminated water and wastewater: a review. Water, Air, & Soil Pollution 200, 59-77, (2009).

216. Pan, H.; Yang, J.; Wang, S.; Xiong, Z.; Cai, W.; Liu, J. Facile fabrication of porous carbon nanofibers by electrospun PAN/dimethyl sulfone for capacitive deionization. Journal of Materials Chemistry A 3, 13827−13834, (2015).

217. Pan, L. K.; Wang, X. Z.; Gao, Y.; Zhang, Y. P.; Chen, Y. W.; Sun, Z. Electrosorption of anions with carbon nanotube and nanofibre composite film electrodes. Desalination 244, 139–143, (2009).

218. Panigrahi, A.; Pilli, S. R.; Mohanty, K. Selective separation of Bisphenol A from aqueous solution using supported ionic liquid membrane. Separation and Purification Technology, 107, 70-78, (2013).

219. Park, B.H.; Kim, Y.J.; Park, J. S.; Choi, J. Capacitive deionization using a carbon electrode prepared with water-soluble poly(vinyl alcohol) binder. Journal of Industrial and Engineering Chemistry 17,717–722, (2011).

220. Peeters, J. M.; Boom, J. P.; Mulder, M. H. V.; Strathmann, H. Retention measurements of nanofiltration membranes with electrolyte solution. Journal of Membrane Science 145, 199-209, (1998).

221. Pellerin, C.; Booker, S.M. Reflections on hexavalent chromium: health hazards of an industrial heavyweight. Environmental Health Perspectives 108, A402, (2000).

222. Peng, Z.; Zhang, D.; Shi, L.; Yan, T. High performance ordered mesoporous carbon/carbon nanotube composite electrodes for capacitive deionization. Journal of Materials Chemistry 22, 6603–6612, (2012).

223. Perrin, J. Mecanisme de l'klectrisation de contact et solutions colloidales. Journal de Chimie Physique 2, 601- 665, (1904).

224. Porada, S.; Zhao, R.; van der Wal, A.; Presser, V.; Biesheuvel, P.M. Review on the science and technology of water desalination by capacitive deionization. Progress in Materials Science 58, 1388–1442, (2013).

225. Pusch, W. Determination of transport parameters of synthetic membranes by hyperfiltration experiments. Part I. Derivation of transport relationship from linear relations of thermodynamics of irreversible processes. Berichte der Bunsengesellschaft für physikalische Chemie 81, 269–276, (1997).

226. Qadir, M.; Sharma, B.R.; Bruggeman, A.; Choukr-Allah, R.; Karajeh, F. Nonconventional water resources and opportunities for water augmentation to achieve food security in water scarce countries. Agricultural Water Management 87, 2–22, (2007).

227. Quincke, G. Ueber die Fortführung materieller Theilchen durch strömende Elektricität. Annals of Physics189, 513–598, (1861).

228. Radjenovic, J.; Petrovic, M.; Ventura, F.; Barcelo, D. Rejection of pharmaceuticals in nanofiltration and reverse osmosis membrane drinking water treatment. Water Research 42, 3601–3610, (2008).

229. Rakhshaee, R.; Khosravi, M.; Ganji, M.T. Kinetic modeling and thermodynamic study to remove Pb (II), Cd (II), Ni (II) and Zn (II) from aqueous solution using dead and living Azolla filiculoides. Journal of Hazardous Materials 134, 120–129, (2006).

230. Raman, L.P.; Cheryan, M.; Rajagopalan, N. Consider nanofiltration for membrane separation. Chemical Engineering Progress 68-74, (1994).

231. Rasines, G.; Lavela, P.; Macias, C.; Haro, M.; Ania, C.O.; Tirado, J. L. Improvement of desalination efficiency in capacitive deionization using a carbon electrode coated with an ion-exchange polymer. Journal of Electroanalytical Chemistry 671, 92–98, (2012).

232. Rautenbach, R.; Gröschl, A. Separation potential of nanofiltration membrane. Desalination 77, 73-84, (1990).

233. Ravanchia, M.T.; Kaghazchia, T.; Kargarib, A. Application of membrane separation processes in petrochemical industry: a review. Desalination 235, 199–244, (2009).

234. Ray, D.; Aswal, V.K. Multi-technique approach for the study of block copolymer-mediated gold nanoparticles. Nanoscience and Nanotechnology Letters 3, 603–611, (2011).

235. Ray, D.; Aswal, V.K.; Kohlbrecher J. Synthesis and characterization of high concentration block copolymer-mediated gold nanoparticles. Langmuir 27, 4048–4056, (2011).

236. Ray, D.; Aswal, V.K.; Srivastava, D. Concentration effect on tuning of block copolymer-mediated synthesis of gold nanoparticles. Journal of Nanoscience and Nanotechnology 10, 6356–6362, (2010).

237. Reardon, E.J.; Wang, Y. A Limestone Reactor for fluoride removal from wastewaters. Environmental Science & Technology 34, 3247–3253, (2000).

238. Reddy, K.R.; Xie, T.; Dastgheibi, S. Removal of heavy metals from urban stormwater runoff using different filter materials. Journal of Environmental Chemical Engineering 2, 282-292, (2014).

239. Reddy, N.B.; Prasad, K.S.S. Pyroclastic fluoride in ground waters in someparts of Tadpatri Taluk, Anantapur district, Andhra Pradesh. Indian Journal of Environmental Health 45, 285–288, (2003).

240. Ren, X.; Zhao, C.; Du, S.; Wang, T.; Luan, Z.; Wang, J.; Hou, D. Fabrication of asymmetric poly (m-phenylene isophthalamide) nanofiltration membrane for chromium(VI) removal. Journal of Environmental Sciences 22, 1335–1341, (2010).

241. Rengaraj, S.; Joo, C.K.; Kim, Y.; Yi, J. Kinetics of removal of chromium from water and electronic process wastewater by ion exchange resins: 1200H, 1500H and IRN97H. Journal of Hazardous Materials 102,257-275, (2003).

242. Richards, L.A.; Vuachere, M.; Schafer, A.I. Impact on pH on the removal of fluoride, nitrate and boron by nanofiltration/reverse osmosis. Desalination 261, 331–337, (2010).

243. Rosa, M.; de Pinho, M. The role of ultrafiltration and nanofiltration on the minimization of the environmental-impact of bleached pulp effluents. Journal of Membrane Science 102, 155-161, (1995).

244. Rout, P.R.; Bhunia, P.; Dash, R.R. A mechanistic approach to evaluate the effectiveness of red soil as a natural adsorbent for phosphate removal from wastewater. Desalination and Water Treatment 54, 358-373, (2015).

245. Rout, P.R.; Bhunia, P.; Dash, R.R. Modeling isotherms, kinetics and understanding the mechanism of phosphate adsorption onto a solid waste: ground burnt patties. Journal of Environmental Chemical Engineering 2, 1331-1342, (2014).

246. Ryoo, M.W.; Seo, G. Improvement in capacitive deionization function of activated carbon cloth by titania modification. Water Research 37, 1527–34, (2003).

247. Ryu, T.; Lee, D.-H.; Ryu, J.C.; Shin, J.; Chung, K.-S.; Kim, Y.H. Lithium recovery system using electrostatic field assistance. Hydrometallurgy 151, 78–83, (2015).

248. Sahu, S.K.; Verma, V.K.; Bagchi, D.; Kamar, V.; Pandey, B.B. Recovery of chromium (VI) from electroplating effluent by solvent extraction with tributyl phosphate. Indian Journal of Chemical Technology 15, 397–402, (2008).

249. Samal, K.; Das, C.; Mohanty, K. Development of Hybrid Membrane Process for Pb bearing Wastewater Treatment. Journal of Water Process Engineering, 10, 30-38, (2016).

250. Sato, Y.; Kang, M.; Kamei, T.; Magara, Y. Performance of nanofiltration for arsenic removal. Water Research 36, 3371-3377, (2002).

251. Seo, S. J.; Jeon, H.; Lee, J. K.; Kim, G. Y.; Park, D.; Nojima, H.; Lee, J.; Moon, S. H.; 2010. Investigation on removal of hardness ions by capacitive deionization (CDI) for water softening applications. Water Research 44, 2267–75, (2010).

252. Shen, F.; Chen, X.; Gao, P. Electrochemical removal of fluoride ions from industrial wastewater. Chemical Engineering Science, 58, 987-993, (2003).

253. Shen, J.; Schäfer, A. Removal of fluoride and uranium by nanofiltration and reverse osmosis:A review. Chemosphere 117,679–691, (2014).

254. Sherif, S.A.; Barbir, F.; Veziroglu, T.N. Wind energy and the hydrogen economy—review of the technology. Solar energy 78, 647-660, (2005).

255. Si, Y; Samulski, E.T. Synthesis of water soluble graphene. Nano Letters 8, 1679-1682, (2008).

256. Soin, N.; Roy, S.S.; Mitra, S.K.; Thundat, T.; McLaughlin, J.A. Nanocrystalline ruthenium oxide dispersed Few Layered Graphene (FLG) nanoflakes as supercapacitor electrodes. Journal of Materials Chemistry, 22, 14944-14950, (2012).

257. Spiegler, K. S.; Kedem, O. Thermodynamics of hyperfiltration (reverse osmosis): criteria for efficient membrane. Desalination 1, 311-326, (1966).

258. Srivastava, S.; Srivastava, A.K. Biological phosphate removal by model based fed-batch cultivation of Acinetobacter calcoaceticus. Biochemical Engineering Journal 40, 227-232, (2008).

259. Srivastava, S.; Srivastava, A.K. Biological phosphate removal by model based continuous cultivation of Acinetobacter calcoaceticus. Process Biochemistry 41,624-630, (2006).

260. State Communicate of Standard of Poland Council of Ministers. Standard 937 for Drinking Water, Decree No. 82, (2000).

261. Stern, A.H.; Fagliano, J.A.; Savrin, J.E.; Freeman, N.C.; Lioy, P.J. The association of chromium in household dust with urinary chromium in residences adjacent to chromate production waste sites. Environmental Health Perspectives 106, 833, (1998).

262. Sun, K.; Jiang, J. C.; Cui, D.D. Preparation of activated carbon with highly developed mesoporous structure from Camellia oleifera shell through water vapor gasification and phosphoric acid modification. Biomass Bioenergy 35, 3643–3647, (2011).

263. Szöke, S.; Pátzay, G.; Weiser, L. Cobalt (III) EDTA complex removal from aqueous alkaline borate solutions by nanofiltration. Desalination 175, 179-185, (2005).

264. Tang, W.; Kovalsky, P.; He D., Waite, T.D. Fluoride and nitrate removal from brackish groundwaters by batch-mode capacitive deionization. Water Research 84, 342-349, (2015).

265. Tian, G.; Liu, L.; Meng, Q.; Cao, B. Preparation and characterization of cross-linked quaternised polyvinyl alcohol membrane/activated carbon composite electrode for membrane capacitive deionization. Desalination 354,107–115, (2014).

266. U.S. Environmental Protection Agency. Consumer Factsheet on: Chromium. Archived October 10, at the Wayback Machine, (2008).

267. United States of Environmental Protection Agency. Drinking water health advisory for chromium. Prepared by the Office of Health and Environmental Assessment, Environmental Criteria and Assessment Office. Cincinnati, OH and Washington, DC: Office of Drinking Water, (1985).

268. Vaidya, S.Y.; Simaria, A.V.; Murthy, Z.V.P. Reverse osmosis transport models evaluation: a new approach. Indian Journal of Chemical Technology 8, 335–343, (2001).

269. Van der Bruggen, B.; Everaert, K.; Wilms, D.; Vandecasteele, C. Application of nanofiltration for removal of pesticides, nitrate and hardness from ground water: rejection properties and economic evaluation. Journal of Membrane Science 193, 239-248, (2001).

270. Van der Bruggen, B.; Koninckx, A.; Vandecasteele, C. Separation of monovalent and divalent ions from aqueous solution by electrodialysis and nanofiltration. Water Research 38(5), 1347-1353, (2004).

271. van Limpt, B.; van der Wal, A. Water and chemical savings in cooling towers by using membrane capacitive deionization. Desalination 342,148–155, (2014).

272. Vergili, I. 2013. Application of nanofiltration for the removal of carbamazepine, diclofenac and ibuprofen from drinking water sources. Journal of Environmental Management 127,177-187, (2013).

273. Verma, A.K.; Dash, R.R.; Bhunia, P. A review on chemical coagulation/flocculation technologies for removal of colour from textile wastewaters. Journal of Environmental Management 93(1), 154-168, (2012).

274. W.H.O., Guidelines for drinking water quality, 1 (4), 178, (2011).

275. W.H.O., Guidelines for Drinking Water Quality, Geneva, (2004).

276. Wagner, J. Membrane filtration handbook-practical tips and hints, Osmonics Inc., (2001).

277. Wang, G.; Pan, C.; Wang, L.P.; Dong, Q.; Yu, C.; Zhao, Z.B.; Qiu, J.S. Activated carbon nanofiber webs made by electrospinning for capacitive deionization Electrochimica Acta 69, 65–70, (2012a).

278. Wang, G.; Qian, B.Q.; Dong, Q.; Yang, J.Y.; Zhao, Z.B.; Qiu, J.S. Highly mesoporous activated carbon electrode for capacitive deionization. Separation and Purification Technology 103 216–221, (2013b).

279. Wang, H. J.; Xi, X. K.; Kleinhammes, A.; Wu, Y. Temperature-Induced Hydrophobic-Hydrophilic Transition Observed by Water Adsorption. Science 322, 80–83, (2008).

280. Wang, H.; Zhang, D.; Yan, T.; Wen, X.; Zhang, J.; Shi, L.; Zhong, Q. Three-dimensional macroporous graphene architectures as high performance electrodes for capacitive deionization. Journal of Materials Chemistry A 1, 11778–11789, (2013a).

281. Wang, X.Z.; Li, M.G.; Chen, Y.W.; Cheng, R.M.; Huang, S.M.; Pan, L.K.; Sun, Z. Electrosorption of NaCl solutions with carbon nanotubes and nanofibers composite film electrodes. Electrochemical and Solid-State Letters 9, E23–E26, (2006).

282. Wang, Y.; Han, X.; Wang, R.; Xu, S.; Wang, J. Preparation optimization on the coating-type polypyrrole/carbon nanotube composite electrode for capacitive deionization. Electrochimica Acta 182, 81–88, (2015).

283. Wang, Y.; Zhang, L.; Wu, Y.; Xu, S.; Wang J. Polypyrrole/carbon nanotube composites as cathodematerial for performance enhancing of capacitive deionization technology. Desalination 354, 62–67, (2014).

284. Wang, Z.; Dou, B.; Zheng, L.; Zhang, G.; Liu, Z.; Hao, Z. Effective desalination by capacitive deionization with functional graphene nanocomposite as novel electrode material. Desalination 299, 96–102, (2012b).

285. Wankat, P.C. Rate-controlled separation, Elsevier applied science publication, London, (1990).

286. Wei-fang, M.A.; WEN-jun, L.; Guo-wei, C. Factors influencing the removal of fluoride from groundwater by nanofiltration. Proc. ICBBE'09. International Conference on Bioinformatics and Biomedical Engineering, Beijing, (2009).

287. Welgemoed, T. J.; Schutte, C. F. Capacitive deionization technology™: An alternative desalination solution. Desalination 183, 327–40, (2005).

288. Wen, Q. X.; Yang, H.; Chen, Z.Q.; Zhang, H.C. Microbial Desalination Cell Combined with Capacitive Deionization/Membrane Capacitive Deionization to Desalinate Seawater. Advanced Materials Research 807, 373–379, (2013).

289. Wen, X.; Zhang, D.; Yan, T.; Zhang, J.; Shi, L. Three-dimensional graphene-based hierarchically porous carbon composites prepared by a dual-template strategy for capacitive deionization. Journal of Materials Chemistry A 1, 12334–12344, (2013).

290. Wijmans, J.G.; Baker, R.W. The solution-diffusion model: a review. Journal of Membrane Science 107, 1–21, (1995).

291. Wimalasiri, Y.; Mossad, M.; Zou, L. Thermodynamics and kinetics of adsorption of ammonium ions by graphene laminate electrodes in capacitive deionization. Desalination 357178–357188, (2015).

292. Wimalasiri, Y.; Zou, L. Carbon nanotube/graphene composite for enhanced capacitive deionization performance. Carbon 59, 464–71, (2013).

293. Wouters, J.J.; Lado, J.J.; Tejedor-Tejedor, M.I.; Perez-Roa, R.; Anderson, M.A. Carbon fiber sheets coated with thin-films of SiO2 and γ-Al2O3 as electrodes in capacitive deionization: Relationship between properties of the oxide films and electrode performance. Electrochimica Acta 112,763–773, (2013).

294. Wu, P.; Xia, L.; Dai, M.; Lin, L.L.; Song, S.X. Electrosorption of fluoride on TiO2-loaded activated carbon in water. Colloids and Surfaces A 502, 66–73, (2016).

295. Xie, M.; Nghiem, L.D.; Price, W.E.; Elimelech, M. Comparison of the removal of hydrophobic trace organic contaminants by forward osmosis and reverse osmosis. Water Research 46, 2683–2692, (2012a).

296. Xu, P.; Drewes, J. E.; Heil, D.; Wang, G. Treatment of brackish produced water using carbon aerogel-based capacitive deionization technology. Water Research 42, 2605–2617, (2008).

297. Xu, P.; Drewes, J.E.; Kim, T.-U.; Bellona, C.; Amy, G. Effect of membrane fouling on transport of organic contaminants in NF/RO membrane applications. Journal of Membrane Science 279, 165–175, (2006).

298. Xu, T. Ion exchange membranes: State of their development and perspective. Journal of Membrane Science 263, 1–29, (2005).

299. Xu, X.; Liu, Y.; Lu, T.; Sun, Z.; Chua, D.H.C., Pan, L. Rational design and fabrication of graphene/ carbon nanotubes hybrid sponge for high-performance capacitive deionization. Journal of Materials Chemistry A 3, 13418–13425, (2015b).

300. Xu, X.; Pan, L.; Liu, Y.; Lu, T.; Sun, Z. Enhanced capacitive deionization performance of graphene by nitrogen doping. Journal of Colloid and Interface Science, 445, 143–150, (2015a).

301. Xu, X.; Pan, L.; Liu, Y.; Lu, T.; Sun, Z.; Chua, D.H. C. Facile synthesis of novel graphene sponge for high performance capacitive deionization. Scientific Reports 5, 8458, (2015c).

302. Xu, X.; Sun, Z.; Chua, D.H. C.; Pan, L. Novel nitrogen doped graphene sponge with ultrahigh capacitive deionization performance. Scientific Reports 5, 11225, (2015d).

303. Yan C.; Zou L., Short R. Polyaniline-modified activated carbon electrodes for capacitive deionization. Desalination 333, 101–106, (2014).

304. Yan, C.; Kanaththage, Y. W.; Short, R.; Gibson, C. T.; Zou, L. Graphene/Polyaniline nanocomposite as electrode material for membrane capacitive deionization. Desalination 344, 274–279, (2014).

305. Yang, J.; Zou, L.; Song, H. Preparing MnO_2/PSS/CNTs composite electrodes by layer-by-layer deposition of MnO_2 in the membrane capacitive deionization. Desalination 286, 108–114, (2012).

306. Yang, J.; Zou, L.; Song, H.; Hao. Z. Development of novel MnO_2/nanoporous carbon composite electrodes in capacitive deionization technology. Desalination 276, 199–206, (2011).

307. Yang, Y.; Lin, X.; Huang, H.; Feng, D.; Ba, Y.; Cheng, X.; Cui, L. Sodium fluoride induces apoptosis through reactive oxygen species-mediated endoplasmic reticulum stress pathway in Sertoli cells. Journal of Environmental Sciences 30, 81–89, (2015).

308. Yang, Z.Y.; Jin, L.J.; Lu, G.Q.; Xiao, Q.Q.; Zhang, Y.X.; Jing, L.; Zhan, X.X.; Yan, Y.M.; Sun, K.N. Sponge-templated preparation of high surface area graphene with

ultrahighcapacitive deionization performance. Advanced Functional Materials 24, 3917–3925, (2014).

309. Yantasee, W.; Fryxell, G. E.; Addleman, R. S.; Wiacek, R. J.; Koonsiripaiboon, V.; Pattamakomsan, K.; Sukwarotwat, V. Selective removal of lanthanides from natural waters, acidic streams and dialysate. Journal of Hazardous Materials 168, 1233-1238, (2009).

310. Yaroshchuk, E. Dielectric exclusion of ions from membranes. Advances in Colloid and Interface Science 85, 193-230, (2000).

311. Yaroshchuk, E. Non-steric mechanisms of nanofiltration: superposition of Donnan and dielectric exclusion. Separation and Purification Technology 22-23, 143 – 158, (2001).

312. Yin, H.; Zhao, S.; Wan, J.; Tang, H.; Chang, L.; He, L.; Zhao, H.; Gao, Y.; Tang, Z. Three-Dimensional Graphene/Metal Oxide Nanoparticle Hybrids for High-Performance Capacitive Deionization of Saline Water. Advanced Materials 25, 6270–6276, (2013).

313. Ying, T. Y.; Yang, K. L.; Yiacoumi, S.; Tsouris, C. Electrosorption of Ions from Aqueous Solutions by Nanostructured Carbon Aerogel. Journal of Colloid and Interface Science 250, 18–27, (2002).

314. Yoon, J.; Amy, G.; Chung, J.; Sohn, J.; Yoon, Y. Removal of toxic ions (chromate, arsenate, and perchlorate) using reverse osmosis, nanofiltration, and ultrafiltration membranes. Chemosphere 77, 228-235, (2009).

315. Yuan, L.; Yang, X.; Liang, P.; Wang, L.; Huang, Z. H.; Wei, J.; Huang, X. Capacitive deionization coupled with microbial fuel cells to desalinate low-concentration salt water. Bioresource Technology 110,735–38, (2012).

316. Zahrim, A.Y.; Hilal, N.; Tizaoui, C. Tubular nanofiltration of highly concentrated C.I. Acid Black 210 dye. Water Science & Technology 67, 901–906, (2013).

317. Zhang, D.; Yan, T.; Shi, L.; Peng, Z.; Wen, X.; Zhang, J. Enhanced capacitive deionization performance of graphene/carbon nanotube composites. Journal of Materials Chemistry 22, 14696–14704, (2012).

318. Zhang, W.; Mossad, M.; Yazdi, J.S.; Zou, L. A statistical experimental investigation on arsenic removal using capacitive deionization. Desalination and Water Treatment 57, 3254–3260, (2016).

319. Zhang, Y.; Zou, L.; Wimalasiri, Y.; Lee, J.-Y.; Chun, Y. Reduced graphene oxide/polyaniline conductive anion exchange membranes in capacitive deionisation process. Electrochimica Acta 182, 383–390, (2015).

320. Zhao, R.; Biesheuvel, P. M.; van der Wal, A. Energy consumption and constant current operation in membrane capacitive deionization. Energy & Environmental Science 5, 9520–9527, (2012).

321. Zhao, R.; Porada, S.; Biesheuvel, P.M.; van der Wal, A. Energy consumption in membrane capacitive deionization for different water recoveries and flow rates, and comparison with reverse osmosis. Desalination 330, 35–41, (2013a).

322. Zhao, Y.; Wang, Y.; Wang, R.; Wu, Y.; Xu, S.; Wang, J. Performance comparison and energy consumption analysis of capacitive deionization and membrane capacitive deionization processes. Desalination 324, 127–133, (2013b).

323. Zhitkovich, A. Chromium in drinking water: sources, metabolism, and cancer risks. Chemical Research in Toxicology 24, 1617-1629, (2011).

324. Zhou, P.; Brown, G. M.; Gu, B. Membrane and other treatment technologies –pros and cons. In Perchlorate, eds. B. Gu, and J. Coates 389–404, Springer, New York (2006).

325. Zou, L.; Li, L.X.; Song, H.H.; Morris, G. Using mesoporous carbon electrodes for brackish water desalination. Water Research 42, 2340–2348, (2008).

Table A.1 Input and output data for experiment on effect of applied pressure and feed concentration on permeate flux with NF300.

Sr. No.	Membrane used	Pressure (bar)	Feed concentration (mg/L)	Cross flowrate (L/min)	Permeate flux (L/m²hr)	Experiment No.
1	NF300	2	5	16	17	1
2	NF300	4	5	16	35	1
3	NF300	6	5	16	47	1
4	NF300	8	5	16	61	1
5	NF300	10	5	16	74	1
6	NF300	2	10	16	15	1
7	NF300	4	10	16	33	1
8	NF300	6	10	16	44	1
9	NF300	8	10	16	58	1
10	NF300	10	10	16	71	1
11	NF300	2	50	16	12	1
12	NF300	4	50	16	30	1
13	NF300	6	50	16	40	1
14	NF300	8	50	16	55	1
15	NF300	10	50	16	67	1
16	NF300	2	100	16	8	1

17	NF300	4	100	16	25	1
18	NF300	6	100	16	34	1
19	NF300	8	100	16	49	1
20	NF300	10	100	16	60	1

Table A.2 Input and output data for experiment on effect of applied pressure and feed concentration on permeate flux with PN40.

Sr. No.	Membrane used	Pressure (bar)	Feed concentration (mg/L)	Cross flowrate (L/min)	Permeate flux (L/m²hr)	Experiment No.
1	PN40	2	5	16	36	4
2	PN40	4	5	16	74	4
3	PN40	6	5	16	99	4
4	PN40	8	5	16	126	4
5	PN40	10	5	16	152	4
6	PN40	2	10	16	34	4
7	PN40	4	10	16	72	4
8	PN40	6	10	16	97	4
9	PN40	8	10	16	124	4
10	PN40	10	10	16	150	4
11	PN40	2	50	16	31	4
12	PN40	4	50	16	69	4

13	PN40	6	50	16	94	4
14	PN40	8	50	16	121	4
15	PN40	10	50	16	147	4
16	PN40	2	100	16	26	4
17	PN40	4	100	16	63	4
18	PN40	6	100	16	89	4
19	PN40	8	100	16	116	4
20	PN40	10	100	16	143	4

Table A.3 Input and output data for experiment on effect of applied pressure and feed concentration on permeate flux with NF500.

Sr. No.	Membrane used	Pressure (bar)	Feed concentration (mg/L)	Cross flowrate (L/min)	Permeate flux (L/m^{2}hr)	Experiment No.
1	NF500	2	5	16	31	7
2	NF500	4	5	16	66	7
3	NF500	6	5	16	93	7
4	NF500	8	5	16	117	7
5	NF500	10	5	16	136	7
6	NF500	2	10	16	29	7
7	NF500	4	10	16	64	7
8	NF500	6	10	16	91	7

9	NF500	8	10	16	115	7
10	NF500	10	10	16	134	7
11	NF500	2	25	16	28	7
12	NF500	4	25	16	63	7
13	NF500	6	25	16	90	7
14	NF500	8	25	16	114	7
15	NF500	10	25	16	133	7
16	NF500	2	50	16	26	7
17	NF500	4	50	16	61	7
18	NF500	6	50	16	88	7
19	NF500	8	50	16	112	7
20	NF500	10	50	16	131	7
21	NF500	2	100	16	21	7
22	NF500	4	100	16	55	7
23	NF500	6	100	16	83	7
24	NF500	8	100	16	107	7
25	NF500	10	100	16	127	7

Table A.4 Input and output data for experiment on effect of applied pressure and feed concentration on permeate flux with RO membrane.

Sr. No.	Membrane used	Pressure (bar)	Feed concentration (mg/L)	Cross flowrate (L/min)	Permeate flux (L/m^{2}hr)	Experiment No.
1	RO flat sheet	4	5	16	18	10
2	RO flat sheet	8	5	16	36	10
3	RO flat sheet	12	5	16	54	10
4	RO flat sheet	16	5	16	74	10
5	RO flat sheet	20	5	16	93	10
6	RO flat sheet	4	50	16	16	10
7	RO flat sheet	8	50	16	34	10
8	RO flat sheet	12	50	16	54	10
9	RO flat sheet	16	50	16	72	10
10	RO flat sheet	20	50	16	92	10
11	RO flat sheet	4	100	16	14	10
12	RO flat sheet	8	100	16	32	10
13	RO flat sheet	12	100	16	52	10
14	RO flat sheet	16	100	16	71	10
15	RO flat sheet	20	100	16	90	10
16	RO flat sheet	4	400	16	9	10
17	RO flat sheet	8	400	16	27	10

18	RO flat sheet	12	400	16	47	10
19	RO flat sheet	16	400	16	66	10
20	RO flat sheet	20	400	16	85	10

Table A.5 Input and output data for experiment on effect of applied pressure and feed concentration on removal percentage of Cr(VI) and fluoride with NF300.

Sr. No.	Membrane used	Pressure (bar)	Feed concentration (mg/L)	Cross flowrate (L/min)	Removal percentage of Cr(VI)	Removal percentage of fluoride	Experiment No.
1	NF300	2	5	16	89	86	2
2	NF300	4	5	16	92	88	2
3	NF300	6	5	16	94	90	2
4	NF300	8	5	16	96	91.5	2
5	NF300	10	5	16	97	92	2
6	NF300	2	10	16	86	80	2
7	NF300	4	10	16	88	84	2
8	NF300	6	10	16	91	87	2
9	NF300	8	10	16	93	89.5	2
10	NF300	10	10	16	93.5	90	2
11	NF300	2	50	16	78	72	2
12	NF300	4	50	16	80	74.2	2

13	NF300	6	50	16	82.1	76	2
14	NF300	8	50	16	84	79.2	2
15	NF300	10	50	16	85	80	2
16	NF300	2	100	16	70	61.2	2
17	NF300	4	100	16	72	63.4	2
18	NF300	6	100	16	74.3	66.5	2
19	NF300	8	100	16	76	68	2
20	NF300	10	100	16	77	69	2

Table A. 6 Input and output data for experiment on effect of applied pressure and feed concentration on removal percentage of Cr(VI) and fluoride with PN40.

Sr. No.	Membrane used	Pressure (bar)	Feed concentration (mg/L)	Cross flowrate (L/min)	Removal percentage of Cr(VI)	Removal percentage of fluoride	Experiment No.
1	PN40	2	5	16	78	75.8	5
2	PN40	4	5	16	80.2	78	5
3	PN40	6	5	16	83.5	80	5
4	PN40	8	5	16	86	81.50	5
5	PN40	10	5	16	88	82	5
6	PN40	2	10	16	74.5	74	5
7	PN40	4	10	16	77	76.21	5

267

8	PN40	6	10	16	79	79.34	5
9	PN40	8	10	16	81	80.14	5
10	PN40	10	10	16	82	80.56	5
11	PN40	2	50	16	67	61.20	5
12	PN40	4	50	16	69	64.10	5
13	PN40	6	50	16	71	66.80	5
14	PN40	8	50	16	73	69	5
15	PN40	10	50	16	74	70	5
16	PN40	2	100	16	60	51.80	5
17	PN40	4	100	16	62	55	5
18	PN40	6	100	16	64.1	57	5
19	PN40	8	100	16	66	59.20	5
20	PN40	10	100	16	67	60	5

Table A. 7 Input and output data for experiment on effect of applied pressure and feed concentration on removal percentage of Cr(VI) and fluoride with NF500.

Sr. No.	Membrane used	Pressure (bar)	Feed concentration (mg/L)	Cross flowrate (L/min)	Removal percentage of Cr(VI)	Removal percentage of fluoride	Experiment No.
1	NF500	2	5	16	84	78.6	8
2	NF500	4	5	16	86	80.5	8

3	NF500	6	5	16	88	82	8
4	NF500	8	5	16	90	84.1	8
5	NF500	10	5	16	91	85	8
6	NF500	2	10	16	80	76	8
7	NF500	4	10	16	82	78.2	8
8	NF500	6	10	16	84	80.3	8
9	NF500	8	10	16	86	82.5	8
10	NF500	10	10	16	87	83	8
11	NF500	2	25	16	76	73	8
12	NF500	4	25	16	77.5	75.8	8
13	NF500	6	25	16	79	77	8
14	NF500	8	25	16	82	78.9	8
15	NF500	10	25	16	83	80	8
16	NF500	2	50	16	70.5	67	8
17	NF500	4	50	16	72	69	8
18	NF500	6	50	16	74	71.5	8
19	NF500	8	50	16	75.6	73.1	8
20	NF500	10	50	16	77	74	8
21	NF500	2	100	16	65	56.2	8
22	NF500	4	100	16	67	58	8
23	NF500	6	100	16	69	60	8
24	NF500	8	100	16	70	61.2	8

25	NF500	10	100	16	71	63	8

Table A. 8 Input and output data for experiment on effect of applied pressure and feed concentration on removal percentage of Cr(VI) and fluoride with RO membrane.

Sr.No.	Membrane used	Pressure (bar)	Feed concentration (mg/L)	Cross flowrate (L/min)	Removal percentage of Cr(VI)	Removal percentage of fluoride	Experiment No.
1	RO	4	5	16	99.7	94	11
2	RO	8	5	16	99.79	94.11	11
3	RO	12	5	16	99.88	94.66	11
4	RO	16	5	16	99.97	94.99	11
5	RO	20	5	16	99.86	94.6	11
6	RO	4	50	16	99.65	93.95	11
7	RO	8	50	16	99.74	94.06	11
8	RO	12	50	16	99.83	94.61	11
9	RO	16	50	16	99.93	94.95	11
10	RO	20	50	16	99.82	94.56	11
11	RO	4	100	16	98.66	92.96	11
12	RO	8	100	16	98.75	93.07	11
13	RO	12	100	16	98.86	93.64	11
14	RO	16	100	16	99	94.02	11

15	RO	20	100	16	98.82	93.56	11
16	RO	4	400	16	98.13	92.43	11
17	RO	8	400	16	98.22	92.54	11
18	RO	12	400	16	98.35	93.13	11
19	RO	16	400	16	98.5	93.52	11
20	RO	20	400	16	98.34	93.08	11

Table A. 9 Input and output data for experiment on effect of pH on removal percentage of Cr(VI) and fluoride with NF300 membrane.

Sr. No.	Membrane used	Pressure (bar)	pH of feed	Feed concentration (mg/L)	Cross flowrate (L/min)	Removal percentage of Cr(VI)	Removal percentage of fluoride	Experiment No.
1	NF300	10	3	5	16	45	37	3
2	NF300	10	5	5	16	60	52	3
3	NF300	10	7	5	16	72	65	3
4	NF300	10	8	5	16	97	92	3
5	NF300	10	9	5	16	97.1	92.3	3
6	NF300	10	3	100	16	21	17	3
7	NF300	10	5	100	16	30	25	3
8	NF300	10	7	100	16	44	32	3
9	NF300	10	8	100	16	77	69	3

271

10	NF300	10	9	100	16	77.3	69.3	3

Table A. 10 Input and output data for experiment on effect of pH on removal percentage of Cr(VI) and fluoride with PN40 membrane.

Sr. No.	Membrane used	Pressure (bar)	pH of feed	Feed concentration (mg/L)	Cross flowrate (L/min)	Removal percentage of Cr(VI)	Removal percentage of fluoride	Experiment No.
1	PN40	10	3	5	16	34	28	6
2	PN40	10	5	5	16	51	44	6
3	PN40	10	7	5	16	58	56	6
4	PN40	10	8	5	16	88	82	6
5	PN40	10	9	5	16	88.5	82.3	6
6	PN40	10	3	100	16	18	14	6
7	PN40	10	5	100	16	24	20	6
8	PN40	10	7	100	16	29	25	6
9	PN40	10	8	100	16	67	60	6
10	PN40	10	9	100	16	67.2	60.1	6

Table A. 11 Input and output data for experiment on effect of pH on removal percentage of Cr(VI) and fluoride with NF500 membrane.

Sr. No.	Membrane used	Pressure (bar)	pH of feed	Feed concentration (mg/L)	Cross flowrate (L/min)	Removal percentage of Cr(VI)	Removal percentage of fluoride	Experiment No.
1	NF500	10	2	5	16	38	32	9
2	NF500	10	4	5	16	55	47	9
3	NF500	10	6	5	16	62	60	9
4	NF500	10	8	5	16	91	85	9
5	NF500	10	10	5	16	91.2	85.1	9
6	NF500	10	2	25	16	30	24	9
7	NF500	10	4	25	16	46	35	9
8	NF500	10	6	25	16	53	45	9
9	NF500	10	8	25	16	83	80	9
10	NF500	10	10	25	16	83.1	80.5	9
11	NF500	10	2	100	16	19	16	9
12	NF500	10	4	100	16	28	22	9
13	NF500	10	6	100	16	33	29	9
14	NF500	10	8	100	16	71	63	9
15	NF500	10	10	100	16	71.2	63.6	9

Table A. 12 Input and output data for experiment on effect of pH on removal percentage of Cr(VI) and fluoride with RO membrane.

Sr. No.	Membrane used	Pressure (bar)	pH of feed	Feed concentration (mg/L)	Cross flowrate (L/min)	Removal percentage of Cr(VI)	Removal percentage of fluoride	Experiment No.
1	RO	16	3	5	16	99.1	94	12
2	RO	16	5	5	16	99.24	94.15	12
3	RO	16	7	5	16	99.88	94.66	12
4	RO	16	8	5	16	99.97	94.99	12
5	RO	16	9	5	16	99.98	95	12
6	RO	16	3	50	16	98.24	93.12	12
7	RO	16	5	50	16	98.65	93.3	12
8	RO	16	7	50	16	99.83	94.61	12
9	RO	16	8	50	16	99.93	94.8	12
10	RO	16	9	50	16	99.93	94.82	12
11	RO	16	3	100	16	97.19	92.13	12
12	RO	16	5	100	16	97.64	92.65	12
13	RO	16	7	100	16	98.69	93.64	12
14	RO	16	8	100	16	99	94.02	12
15	RO	16	9	100	16	99.1	94	12
16	RO	16	3	400	16	96.1	91.28	12
17	RO	16	5	400	16	96.58	91.83	12

18	RO	16	7	400	16	98.35	92.95	12
19	RO	16	8	400	16	98.5	93.52	12
20	RO	16	9	400	16	98.49	93.53	12

Table A. 13 Input and output data for experiment on effect of applied voltage on conductivity change of binary feed of Cr(VI) and fluoride with CAC electrode.

Sr. No.	Electrode used	Voltage applied (V)	Feed concentration (mg/L)	Initial feed conductivity (µS/cm)	Time (min)	Conductivity change (µS/cm)	Experiment No.
1	CAC	0.4	10	75.54	0	75.54	13
2	CAC	0.4	10	75.54	5	69.00	13
3	CAC	0.4	10	75.54	10	59.00	13
4	CAC	0.4	10	75.54	15	52.00	13
5	CAC	0.4	10	75.54	20	46.00	13
6	CAC	0.4	10	75.54	25	41.00	13
7	CAC	0.4	10	75.54	30	39.00	13
8	CAC	0.4	10	75.54	35	37.00	13
9	CAC	0.4	10	75.54	40	36.10	13
10	CAC	0.4	10	75.54	45	35.20	13
11	CAC	0.4	10	75.54	50	34.80	13
12	CAC	0.4	10	75.54	55	34.70	13
13	CAC	0.4	10	75.54	60	34.60	13
14	CAC	0.4	10	75.54	65	34.55	13
15	CAC	0.4	10	75.54	70	34.50	13

16	CAC	0.4	10	75.54	75	34.45	13
17	CAC	0.4	10	75.54	80	34.40	13
18	CAC	0.4	10	75.54	85	34.36	13
19	CAC	0.4	10	75.54	90	34.30	13
20	CAC	0.4	10	75.54	95	34.24	13
21	CAC	0.4	10	75.54	100	34.20	13
22	CAC	0.4	10	75.54	105	34.18	13
23	CAC	0.4	10	75.54	110	34.12	13
24	CAC	0.4	10	75.54	115	34.10	13
25	CAC	0.4	10	75.54	120	34.00	13
26	CAC	0.8	10	75.54	0	75.54	13
27	CAC	0.8	10	75.54	5	60.00	13
28	CAC	0.8	10	75.54	10	50.00	13
29	CAC	0.8	10	75.54	15	40.10	13
30	CAC	0.8	10	75.54	20	36.00	13
31	CAC	0.8	10	75.54	25	32.61	13
32	CAC	0.8	10	75.54	30	31.24	13
33	CAC	0.8	10	75.54	35	30.43	13
34	CAC	0.8	10	75.54	40	30.30	13
35	CAC	0.8	10	75.54	45	29.83	13
36	CAC	0.8	10	75.54	50	29.49	13
37	CAC	0.8	10	75.54	55	28.95	13

38	CAC	0.8	10	75.54	60	28.57	13
39	CAC	0.8	10	75.54	65	27.60	13
40	CAC	0.8	10	75.54	70	27.48	13
41	CAC	0.8	10	75.54	75	27.41	13
42	CAC	0.8	10	75.54	80	27.14	13
43	CAC	0.8	10	75.54	85	27.05	13
44	CAC	0.8	10	75.54	90	27.00	13
45	CAC	0.8	10	75.54	95	26.90	13
46	CAC	0.8	10	75.54	100	26.90	13
47	CAC	0.8	10	75.54	105	26.82	13
48	CAC	0.8	10	75.54	110	26.71	13
49	CAC	0.8	10	75.54	115	26.57	13
50	CAC	0.8	10	75.54	120	26.50	13
51	CAC	1.2	10	75.54	0	75.54	13
52	CAC	1.2	10	75.54	5	54.97	13
53	CAC	1.2	10	75.54	10	41.26	13
54	CAC	1.2	10	75.54	15	35.26	13
55	CAC	1.2	10	75.54	20	32.26	13
56	CAC	1.2	10	75.54	25	29.44	13
57	CAC	1.2	10	75.54	30	27.46	13
58	CAC	1.2	10	75.54	35	26.26	13
59	CAC	1.2	10	75.54	40	25.49	13

60	CAC	1.2	10	75.54	45	24.38	13
61	CAC	1.2	10	75.54	50	23.69	13
62	CAC	1.2	10	75.54	55	22.84	13
63	CAC	1.2	10	75.54	60	22.15	13
64	CAC	1.2	10	75.54	65	20.95	13
65	CAC	1.2	10	75.54	70	20.53	13
66	CAC	1.2	10	75.54	75	20.09	13
67	CAC	1.2	10	75.54	80	19.54	13
68	CAC	1.2	10	75.54	85	19.15	13
69	CAC	1.2	10	75.54	90	18.90	13
70	CAC	1.2	10	75.54	95	18.60	13
71	CAC	1.2	10	75.54	100	18.40	13
72	CAC	1.2	10	75.54	105	18.22	13
73	CAC	1.2	10	75.54	110	18.06	13
74	CAC	1.2	10	75.54	115	17.87	13
75	CAC	1.2	10	75.54	120	17.79	13

Table A. 14 Input and output data for experiment on effect of flowrate on conductivity of binary feed of Cr(VI) and fluoride with CAC electrode.

Sr. No.	Electrode used	Voltage applied (V)	Feed concentration (mg/L)	Flowrate (mL/min)	Initial feed conductivity (µS/cm)	Time (min)	Conductivity change (µS/cm)	Experiment No.
1	CAC	1.2	10	4	75.48	0	75.48	14
2	CAC	1.2	10	4	75.48	10	56.81	14
3	CAC	1.2	10	4	75.48	20	46.77	14
4	CAC	1.2	10	4	75.48	30	42.01	14
5	CAC	1.2	10	4	75.48	40	40.04	14
6	CAC	1.2	10	4	75.48	50	38.24	14
7	CAC	1.2	10	4	75.48	60	36.7	14
8	CAC	1.2	10	4	75.48	70	35.08	14
9	CAC	1.2	10	4	75.48	80	34.09	14
10	CAC	1.2	10	4	75.48	90	33.45	14
11	CAC	1.2	10	4	75.48	100	32.95	14
12	CAC	1.2	10	4	75.48	110	32.61	14
13	CAC	1.2	10	4	75.48	120	32.34	14
14	CAC	1.2	10	8	75.61	0	75.61	14
15	CAC	1.2	10	8	75.61	10	52.36	14

16	CAC	1.2	10	8	75.61	20	42.32	14
17	CAC	1.2	10	8	75.61	30	37.56	14
18	CAC	1.2	10	8	75.61	40	35.59	14
19	CAC	1.2	10	8	75.61	50	33.79	14
20	CAC	1.2	10	8	75.61	60	32.25	14
21	CAC	1.2	10	8	75.61	70	30.63	14
22	CAC	1.2	10	8	75.61	80	29.64	14
23	CAC	1.2	10	8	75.61	90	29.00	14
24	CAC	1.2	10	8	75.61	100	28.5	14
25	CAC	1.2	10	8	75.61	110	28.16	14
26	CAC	1.2	10	8	75.61	120	27.89	14
27	CAC	1.2	10	12	75.72	0	75.72	14
28	CAC	1.2	10	12	75.72	10	47.58	14
29	CAC	1.2	10	12	75.72	20	37.54	14
30	CAC	1.2	10	12	75.72	30	32.78	14
31	CAC	1.2	10	12	75.72	40	30.81	14
32	CAC	1.2	10	12	75.72	50	29.01	14
33	CAC	1.2	10	12	75.72	60	27.47	14
34	CAC	1.2	10	12	75.72	70	25.85	14
35	CAC	1.2	10	12	75.72	80	24.86	14
36	CAC	1.2	10	12	75.72	90	24.22	14
37	CAC	1.2	10	12	75.72	100	23.72	14

38	CAC	1.2	10	12	75.72	110	23.38	14
39	CAC	1.2	10	12	75.72	120	23.11	14
40	CAC	1.2	10	16	75.64	0	75.64	14
41	CAC	1.2	10	16	75.64	10	42.26	14
42	CAC	1.2	10	16	75.64	20	32.22	14
43	CAC	1.2	10	16	75.64	30	27.46	14
44	CAC	1.2	10	16	75.64	40	25.49	14
45	CAC	1.2	10	16	75.64	50	23.69	14
46	CAC	1.2	10	16	75.64	60	22.15	14
47	CAC	1.2	10	16	75.64	70	20.53	14
48	CAC	1.2	10	16	75.64	80	19.54	14
49	CAC	1.2	10	16	75.64	90	18.9	14
50	CAC	1.2	10	16	75.64	100	18.4	14
51	CAC	1.2	10	16	75.64	110	18.06	14
52	CAC	1.2	10	16	75.64	120	17.79	14
53	CAC	1.2	10	20	75.72	0	75.72	14
54	CAC	1.2	10	20	75.72	10	45.4	14
55	CAC	1.2	10	20	75.72	20	34.36	14
56	CAC	1.2	10	20	75.72	30	29.6	14
57	CAC	1.2	10	20	75.72	40	27.63	14
58	CAC	1.2	10	20	75.72	50	25.83	14
59	CAC	1.2	10	20	75.72	60	24.29	14

60	CAC	1.2	10	20	75.72	70	22.67	14
61	CAC	1.2	10	20	75.72	80	21.68	14
62	CAC	1.2	10	20	75.72	90	21.04	14
63	CAC	1.2	10	20	75.72	100	20.54	14
64	CAC	1.2	10	20	75.72	110	20.2	14
65	CAC	1.2	10	20	75.72	120	19.93	14

Table A. 15 Input and output data for experiment on pH effect on Cr(VI) and fluoride removal by CAC electrode.

Sr. No.	Electrode used	Voltage applied (V)	Feed concentration (mg/L)	Flowrate (mL/min)	pH	Time (min)	Removal % of Cr(VI)	Removal % of fluoride	Experiment No.
1	CAC	1.2	10	16	3	120	85.44	74.82	15
2	CAC	1.2	10	16	5	120	90.12	82.56	15
3	CAC	1.2	10	16	7	120	96.98	93.87	15
4	CAC	1.2	10	16	8	120	97.1	94.2	15
5	CAC	1.2	10	16	9	120	97.84	94.75	15

Table A. 16 Input and output data for experiment on electrosorption of Cr(VI) and fluoride and regeneration of CAC electrode.

Sr. No.	Electrode used	Voltage applied (V)	Feed concentration (mg/L)	Flowrate (mL/min)	Mode (Electrosorption/ Regeneration)	Time (min)	Conductivity change (µS/cm)	Experiment No.
1	CAC	1.2	10	16	Electrosorption	0	75.54	16
2	CAC	1.2	10	16	Electrosorption	5	54.97	16
3	CAC	1.2	10	16	Electrosorption	10	41.26	16
4	CAC	1.2	10	16	Electrosorption	15	35.26	16
5	CAC	1.2	10	16	Electrosorption	20	32.26	16
6	CAC	1.2	10	16	Electrosorption	25	29.44	16
7	CAC	1.2	10	16	Electrosorption	30	27.46	16
8	CAC	1.2	10	16	Electrosorption	35	26.26	16
9	CAC	1.2	10	16	Electrosorption	40	25.49	16
10	CAC	1.2	10	16	Electrosorption	45	24.38	16
11	CAC	1.2	10	16	Electrosorption	50	23.69	16
12	CAC	1.2	10	16	Electrosorption	55	22.84	16
13	CAC	1.2	10	16	Electrosorption	60	22.15	16
14	CAC	1.2	10	16	Electrosorption	65	20.95	16
15	CAC	1.2	10	16	Electrosorption	70	20.53	16

16	CAC	1.2	10	16	Electrosorption	75	20.09	16
17	CAC	1.2	10	16	Electrosorption	80	19.54	16
18	CAC	1.2	10	16	Electrosorption	85	19.15	16
19	CAC	1.2	10	16	Electrosorption	90	18.9	16
20	CAC	1.2	10	16	Electrosorption	95	18.6	16
21	CAC	1.2	10	16	Electrosorption	100	18.4	16
22	CAC	1.2	10	16	Electrosorption	105	18.22	16
23	CAC	1.2	10	16	Electrosorption	110	18.06	16
24	CAC	1.2	10	16	Electrosorption	115	17.87	16
25	CAC	1.2	10	16	Electrosorption	120	17.79	16
26	CAC	0.0	10	16	Regeneration	125	17.79	16
27	CAC	0.0	10	16	Regeneration	130	41.5	16
28	CAC	0.0	10	16	Regeneration	135	50.5	16
29	CAC	0.0	10	16	Regeneration	140	55.3	16
30	CAC	0.0	10	16	Regeneration	145	57.7	16
31	CAC	0.0	10	16	Regeneration	150	59.67	16
32	CAC	0.0	10	16	Regeneration	155	61.12	16
33	CAC	0.0	10	16	Regeneration	160	62.36	16
34	CAC	0.0	10	16	Regeneration	165	63.22	16
35	CAC	0.0	10	16	Regeneration	170	63.91	16
36	CAC	0.0	10	16	Regeneration	175	64.36	16
37	CAC	0.0	10	16	Regeneration	180	64.74	16

38	CAC	0.0	10	16	Regeneration	185	64.97	16
39	CAC	0.0	10	16	Regeneration	190	65.02	16
40	CAC	1.2	10	16	Electrosorption	195	55.74	16
41	CAC	1.2	10	16	Electrosorption	200	46.38	16
42	CAC	1.2	10	16	Electrosorption	205	38.12	16
43	CAC	1.2	10	16	Electrosorption	210	33.35	16
44	CAC	1.2	10	16	Electrosorption	215	31.37	16
45	CAC	1.2	10	16	Electrosorption	220	29.68	16
46	CAC	1.2	10	16	Electrosorption	225	28.35	16
47	CAC	1.2	10	16	Electrosorption	230	27.32	16
48	CAC	1.2	10	16	Electrosorption	235	27.01	16
49	CAC	1.2	10	16	Electrosorption	240	26	16
50	CAC	1.2	10	16	Electrosorption	245	24.97	16
51	CAC	1.2	10	16	Electrosorption	250	24.22	16
52	CAC	1.2	10	16	Electrosorption	255	23.1	16
53	CAC	1.2	10	16	Electrosorption	260	22.84	16
54	CAC	1.2	10	16	Electrosorption	265	22.32	16
55	CAC	1.2	10	16	Electrosorption	270	21.86	16
56	CAC	1.2	10	16	Electrosorption	275	21.33	16
57	CAC	1.2	10	16	Electrosorption	280	21.1	16
58	CAC	1.2	10	16	Electrosorption	285	20.87	16
59	CAC	1.2	10	16	Electrosorption	290	20.69	16

60	CAC	1.2	10	16	Electrosorption	295	20.52	16
61	CAC	1.2	10	16	Electrosorption	300	20.39	16
62	CAC	1.2	10	16	Electrosorption	305	20.22	16
63	CAC	1.2	10	16	Electrosorption	310	20.09	16
64	CAC	0.0	10	16	Regeneration	315	20.09	16
65	CAC	0.0	10	16	Regeneration	320	35.31	16
66	CAC	0.0	10	16	Regeneration	325	45.3	16
67	CAC	0.0	10	16	Regeneration	330	50.7	16
68	CAC	0.0	10	16	Regeneration	335	52.98	16
69	CAC	0.0	10	16	Regeneration	340	55.5	16
70	CAC	0.0	10	16	Regeneration	345	57.31	16
71	CAC	0.0	10	16	Regeneration	350	58.31	16
72	CAC	0.0	10	16	Regeneration	355	59.14	16
73	CAC	0.0	10	16	Regeneration	360	59.54	16
74	CAC	0.0	10	16	Regeneration	365	59.84	16
75	CAC	0.0	10	16	Regeneration	370	60.28	16
76	CAC	0.0	10	16	Regeneration	375	60.53	16
77	CAC	0.0	10	16	Regeneration	380	60.66	16
78	CAC	1.2	10	16	Electrosorption	385	55.45	16
79	CAC	1.2	10	16	Electrosorption	390	45.38	16
80	CAC	1.2	10	16	Electrosorption	395	39.38	16
81	CAC	1.2	10	16	Electrosorption	400	36.37	16

82	CAC	1.2	10	16	Electrosorption	405	33.97	16
83	CAC	1.2	10	16	Electrosorption	410	32.14	16
84	CAC	1.2	10	16	Electrosorption	415	30.87	16
85	CAC	1.2	10	16	Electrosorption	420	29.97	16
86	CAC	1.2	10	16	Electrosorption	425	29.26	16
87	CAC	1.2	10	16	Electrosorption	430	28.41	16
88	CAC	1.2	10	16	Electrosorption	435	27.47	16
89	CAC	1.2	10	16	Electrosorption	440	26.75	16
90	CAC	1.2	10	16	Electrosorption	445	25.59	16
91	CAC	1.2	10	16	Electrosorption	450	25.25	16
92	CAC	1.2	10	16	Electrosorption	455	24.77	16
93	CAC	1.2	10	16	Electrosorption	460	24.26	16
94	CAC	1.2	10	16	Electrosorption	465	23.81	16
95	CAC	1.2	10	16	Electrosorption	470	23.56	16
96	CAC	1.2	10	16	Electrosorption	475	23.3	16
97	CAC	1.2	10	16	Electrosorption	480	23.11	16
98	CAC	1.2	10	16	Electrosorption	485	22.93	16
99	CAC	1.2	10	16	Electrosorption	490	22.79	16
100	CAC	1.2	10	16	Electrosorption	495	22.61	16
101	CAC	1.2	10	16	Electrosorption	500	22.51	16
102	CAC	0.0	10	16	Regeneration	505	22.51	16
103	CAC	0.0	10	16	Regeneration	510	35.27	16

104	CAC	0.0	10	16	Regeneration	515	49.46	16
105	CAC	0.0	10	16	Regeneration	520	54.26	16
106	CAC	0.0	10	16	Regeneration	525	56.66	16
107	CAC	0.0	10	16	Regeneration	530	58.63	16
108	CAC	0.0	10	16	Regeneration	535	60.08	16
109	CAC	0.0	10	16	Regeneration	540	61.32	16
110	CAC	0.0	10	16	Regeneration	545	62.18	16
111	CAC	0.0	10	16	Regeneration	550	62.87	16
112	CAC	0.0	10	16	Regeneration	555	63.32	16
113	CAC	0.0	10	16	Regeneration	560	63.7	16
114	CAC	0.0	10	16	Regeneration	565	63.8	16
115	CAC	0.0	10	16	Regeneration	570	63.92	16

Table A. 17 Input and output data for experiment on electrosorption of Cr(VI) and fluoride and regeneration of TWBAC electrode.

Sr. No.	Electrode used	Voltage applied (V)	Feed concentration (mg/L)	Flowrate (mL/min)	Mode (Electrosorption/ Regeneration)	Time (min)	Conductivity change (µS/cm)	Experiment No.
1	TWBAC	1.2	10	16	Electrosorption	0	75.54	18
2	TWBAC	1.2	10	16	Electrosorption	5	59.51	18
3	TWBAC	1.2	10	16	Electrosorption	10	46.49	18

4	TWBAC	1.2	10	16	Electrosorption	15	40.49	18
5	TWBAC	1.2	10	16	Electrosorption	20	37.49	18
6	TWBAC	1.2	10	16	Electrosorption	25	34.66	18
7	TWBAC	1.2	10	16	Electrosorption	30	32.69	18
8	TWBAC	1.2	10	16	Electrosorption	35	31.49	18
9	TWBAC	1.2	10	16	Electrosorption	40	30.72	18
10	TWBAC	1.2	10	16	Electrosorption	45	29.61	18
11	TWBAC	1.2	10	16	Electrosorption	50	27.85	18
12	TWBAC	1.2	10	16	Electrosorption	55	27.12	18
13	TWBAC	1.2	10	16	Electrosorption	60	26.45	18
14	TWBAC	1.2	10	16	Electrosorption	65	26.00	18
15	TWBAC	1.2	10	16	Electrosorption	70	25.76	18
16	TWBAC	1.2	10	16	Electrosorption	75	25.31	18
17	TWBAC	1.2	10	16	Electrosorption	80	24.77	18
18	TWBAC	1.2	10	16	Electrosorption	85	24.38	18
19	TWBAC	1.2	10	16	Electrosorption	90	24.12	18
20	TWBAC	1.2	10	16	Electrosorption	95	23.82	18
21	TWBAC	1.2	10	16	Electrosorption	100	23.63	18
22	TWBAC	1.2	10	16	Electrosorption	105	23.45	18
23	TWBAC	1.2	10	16	Electrosorption	110	23.29	18
24	TWBAC	1.2	10	16	Electrosorption	115	23.09	18
25	TWBAC	1.2	10	16	Electrosorption	120	23.02	18

26	TWBAC	0.0	10	16	Regeneration	125	23.15	18
27	TWBAC	0.0	10	16	Regeneration	130	42.86	18
28	TWBAC	0.0	10	16	Regeneration	135	48.69	18
29	TWBAC	0.0	10	16	Regeneration	140	51.86	18
30	TWBAC	0.0	10	16	Regeneration	145	54.17	18
31	TWBAC	0.0	10	16	Regeneration	150	55.80	18
32	TWBAC	0.0	10	16	Regeneration	155	57.17	18
33	TWBAC	0.0	10	16	Regeneration	160	58.16	18
34	TWBAC	0.0	10	16	Regeneration	165	58.97	18
35	TWBAC	0.0	10	16	Regeneration	170	59.53	18
36	TWBAC	0.0	10	16	Regeneration	175	59.92	18
37	TWBAC	0.0	10	16	Regeneration	180	60.25	18

Table A. 18 Input and output data for experiment on electrosorption of Cr(VI) and fluoride and regeneration of RHAC electrode

Sr. No.	Electrode used	Voltage applied (V)	Feed concentration (mg/L)	Flowrate (mL/min)	Mode (Electrosorption/ Regeneration)	Time (min)	Conductivity change (μS/cm)	Experiment No.
1	RHAC	1.2	10	16	Electrosorption	0	75.54	20
2	RHAC	1.2	10	16	Electrosorption	5	61.88	20
3	RHAC	1.2	10	16	Electrosorption	10	49.63	20

4	RHAC	1.2	10	16	Electrosorption	15	43.63	20
5	RHAC	1.2	10	16	Electrosorption	20	40.63	20
6	RHAC	1.2	10	16	Electrosorption	25	37.80	20
7	RHAC	1.2	10	16	Electrosorption	30	35.83	20
8	RHAC	1.2	10	16	Electrosorption	35	34.63	20
9	RHAC	1.2	10	16	Electrosorption	40	33.86	20
10	RHAC	1.2	10	16	Electrosorption	45	32.74	20
11	RHAC	1.2	10	16	Electrosorption	50	32.06	20
12	RHAC	1.2	10	16	Electrosorption	55	31.20	20
13	RHAC	1.2	10	16	Electrosorption	60	30.52	20
14	RHAC	1.2	10	16	Electrosorption	65	29.32	20
15	RHAC	1.2	10	16	Electrosorption	70	28.90	20
16	RHAC	1.2	10	16	Electrosorption	75	28.45	20
17	RHAC	1.2	10	16	Electrosorption	80	27.90	20
18	RHAC	1.2	10	16	Electrosorption	85	27.52	20
19	RHAC	1.2	10	16	Electrosorption	90	27.26	20
20	RHAC	1.2	10	16	Electrosorption	95	26.96	20
21	RHAC	1.2	10	16	Electrosorption	100	26.76	20
22	RHAC	1.2	10	16	Electrosorption	105	26.58	20
23	RHAC	1.2	10	16	Electrosorption	110	26.43	20
24	RHAC	1.2	10	16	Electrosorption	115	26.23	20
25	RHAC	1.2	10	16	Electrosorption	120	26.10	20

26	RHAC	0.0	10	16	Regeneration	125	37.28	20
27	RHAC	0.0	10	16	Regeneration	130	50.96	20
28	RHAC	0.0	10	16	Regeneration	135	55.85	20
29	RHAC	0.0	10	16	Regeneration	140	61.02	20
30	RHAC	0.0	10	16	Regeneration	145	64.33	20
31	RHAC	0.0	10	16	Regeneration	150	65.96	20
32	RHAC	0.0	10	16	Regeneration	155	67.03	20
33	RHAC	0.0	10	16	Regeneration	160	67.62	20
34	RHAC	0.0	10	16	Regeneration	165	68.13	20
35	RHAC	0.0	10	16	Regeneration	170	68.68	20
36	RHAC	0.0	10	16	Regeneration	175	69.08	20
37	RHAC	0.0	10	16	Regeneration	180	69.41	20
38	RHAC	0.0	10	16	Regeneration	185	69.52	20
39	RHAC	1.2	10	16	Electrosorption	190	63.01	20
40	RHAC	1.2	10	16	Electrosorption	195	50.75	20
41	RHAC	1.2	10	16	Electrosorption	200	44.75	20
42	RHAC	1.2	10	16	Electrosorption	205	41.75	20
43	RHAC	1.2	10	16	Electrosorption	210	38.92	20
44	RHAC	1.2	10	16	Electrosorption	215	36.95	20
45	RHAC	1.2	10	16	Electrosorption	220	35.75	20
46	RHAC	1.2	10	16	Electrosorption	225	34.98	20
47	RHAC	1.2	10	16	Electrosorption	230	33.87	20

48	RHAC	1.2	10	16	Electrosorption	235	33.18	20
49	RHAC	1.2	10	16	Electrosorption	240	32.33	20
50	RHAC	1.2	10	16	Electrosorption	245	31.64	20
51	RHAC	1.2	10	16	Electrosorption	250	30.44	20
52	RHAC	1.2	10	16	Electrosorption	255	30.02	20
53	RHAC	1.2	10	16	Electrosorption	260	29.58	20
54	RHAC	1.2	10	16	Electrosorption	265	29.03	20
55	RHAC	1.2	10	16	Electrosorption	270	28.64	20
56	RHAC	1.2	10	16	Electrosorption	275	28.38	20
57	RHAC	1.2	10	16	Electrosorption	280	28.08	20
58	RHAC	1.2	10	16	Electrosorption	285	27.89	20
59	RHAC	1.2	10	16	Electrosorption	290	27.71	20
60	RHAC	1.2	10	16	Electrosorption	295	27.55	20
61	RHAC	1.2	10	16	Electrosorption	300	27.36	20
62	RHAC	1.2	10	16	Electrosorption	305	27.23	20
63	RHAC	0.0	10	16	Regeneration	310	34.41	20
64	RHAC	0.0	10	16	Regeneration	315	48.08	20
65	RHAC	0.0	10	16	Regeneration	320	52.97	20
66	RHAC	0.0	10	16	Regeneration	325	58.14	20
67	RHAC	0.0	10	16	Regeneration	330	61.45	20
68	RHAC	0.0	10	16	Regeneration	335	63.08	20
69	RHAC	0.0	10	16	Regeneration	340	64.15	20

70	RHAC	0.0	10	16	Regeneration	345	64.74	20
71	RHAC	0.0	10	16	Regeneration	350	65.25	20
72	RHAC	0.0	10	16	Regeneration	355	65.81	20
73	RHAC	0.0	10	16	Regeneration	360	66.20	20
74	RHAC	0.0	10	16	Regeneration	365	66.54	20
75	RHAC	0.0	10	16	Regeneration	370	66.71	20
76	RHAC	1.2	10	16	Electrosorption	375	64.05	20
77	RHAC	1.2	10	16	Electrosorption	380	51.80	20
78	RHAC	1.2	10	16	Electrosorption	385	45.80	20
79	RHAC	1.2	10	16	Electrosorption	390	42.80	20
80	RHAC	1.2	10	16	Electrosorption	395	39.97	20
81	RHAC	1.2	10	16	Electrosorption	400	38.00	20
82	RHAC	1.2	10	16	Electrosorption	405	36.80	20
83	RHAC	1.2	10	16	Electrosorption	410	36.03	20
84	RHAC	1.2	10	16	Electrosorption	415	34.91	20
85	RHAC	1.2	10	16	Electrosorption	420	34.23	20
86	RHAC	1.2	10	16	Electrosorption	425	33.37	20
87	RHAC	1.2	10	16	Electrosorption	430	32.69	20
88	RHAC	1.2	10	16	Electrosorption	435	31.49	20
89	RHAC	1.2	10	16	Electrosorption	440	31.07	20
90	RHAC	1.2	10	16	Electrosorption	445	30.62	20
91	RHAC	1.2	10	16	Electrosorption	450	30.07	20

92	RHAC	1.2	10	16	Electrosorption	455	29.69	20
93	RHAC	1.2	10	16	Electrosorption	460	29.43	20
94	RHAC	1.2	10	16	Electrosorption	465	29.13	20
95	RHAC	1.2	10	16	Electrosorption	470	28.93	20
96	RHAC	1.2	10	16	Electrosorption	475	28.75	20
97	RHAC	1.2	10	16	Electrosorption	480	28.60	20
98	RHAC	1.2	10	16	Electrosorption	485	28.40	20
99	RHAC	1.2	10	16	Electrosorption	490	28.27	20
100	RHAC	0.0	10	16	Regeneration	495	37.99	20
101	RHAC	0.0	10	16	Regeneration	500	51.67	20
102	RHAC	0.0	10	16	Regeneration	505	56.55	20
103	RHAC	0.0	10	16	Regeneration	510	61.72	20
104	RHAC	0.0	10	16	Regeneration	515	65.04	20
105	RHAC	0.0	10	16	Regeneration	520	66.67	20
106	RHAC	0.0	10	16	Regeneration	525	67.74	20
107	RHAC	0.0	10	16	Regeneration	530	68.32	20
108	RHAC	0.0	10	16	Regeneration	535	68.84	20
109	RHAC	0.0	10	16	Regeneration	540	69.39	20
110	RHAC	0.0	10	16	Regeneration	545	69.79	20
111	RHAC	0.0	10	16	Regeneration	550	70.12	20
112	RHAC	0.0	10	16	Regeneration	555	70.25	20

Table A. 19 Input and output data for experiment on electrosorption of Cr(VI) and fluoride and regeneration of LASAC electrode at 1.2 V.

Sr. No.	Electrode used	Feed concentration (mg/L)	Flowrate (mL/min)	Mode (Electrosorption/ Regeneration)	Time (min)	Conductivity change (µS/cm)	Experimental No.
1	LASAC	10	16	Electrosorption	0	75.54	22
2	LASAC	10	16	Electrosorption	5	57.76	22
3	LASAC	10	16	Electrosorption	10	44.22	22
4	LASAC	10	16	Electrosorption	15	38.22	22
5	LASAC	10	16	Electrosorption	20	35.22	22
6	LASAC	10	16	Electrosorption	25	32.39	22
7	LASAC	10	16	Electrosorption	30	30.42	22
8	LASAC	10	16	Electrosorption	35	29.22	22
9	LASAC	10	16	Electrosorption	40	28.45	22
10	LASAC	10	16	Electrosorption	45	27.34	22
11	LASAC	10	16	Electrosorption	50	26.65	22
12	LASAC	10	16	Electrosorption	55	25.79	22
13	LASAC	10	16	Electrosorption	60	25.11	22
14	LASAC	10	16	Electrosorption	65	23.91	22
15	LASAC	10	16	Electrosorption	70	23.49	22
16	LASAC	10	16	Electrosorption	75	23.04	22
17	LASAC	10	16	Electrosorption	80	22.49	22

18	LASAC	10	16	Electrosorption	85	22.11	22
19	LASAC	10	16	Electrosorption	90	21.85	22
20	LASAC	10	16	Electrosorption	95	21.55	22
21	LASAC	10	16	Electrosorption	100	21.36	22
22	LASAC	10	16	Electrosorption	105	21.18	22
23	LASAC	10	16	Electrosorption	110	21.02	22
24	LASAC	10	16	Electrosorption	115	20.82	22
25	LASAC	10	16	Electrosorption	120	20.75	22
26	LASAC	10	16	Regeneration	125	40.12	22
27	LASAC	10	16	Regeneration	130	53.80	22
28	LASAC	10	16	Regeneration	135	58.69	22
29	LASAC	10	16	Regeneration	140	63.86	22
30	LASAC	10	16	Regeneration	145	67.17	22
31	LASAC	10	16	Regeneration	150	68.80	22
32	LASAC	10	16	Regeneration	155	69.87	22
33	LASAC	10	16	Regeneration	160	70.46	22
34	LASAC	10	16	Regeneration	165	70.97	22
35	LASAC	10	16	Regeneration	170	71.53	22
36	LASAC	10	16	Regeneration	175	71.92	22
37	LASAC	10	16	Regeneration	180	72.25	22
38	LASAC	10	16	Regeneration	185	72.41	22
39	LASAC	10	16	Electrosorption	190	58.88	22

40	LASAC	10	16	Electrosorption	195	45.34	22
41	LASAC	10	16	Electrosorption	200	39.34	22
42	LASAC	10	16	Electrosorption	205	36.34	22
43	LASAC	10	16	Electrosorption	210	33.52	22
44	LASAC	10	16	Electrosorption	215	31.55	22
45	LASAC	10	16	Electrosorption	220	30.35	22
46	LASAC	10	16	Electrosorption	225	29.57	22
47	LASAC	10	16	Electrosorption	230	28.46	22
48	LASAC	10	16	Electrosorption	235	27.78	22
49	LASAC	10	16	Electrosorption	240	26.92	22
50	LASAC	10	16	Electrosorption	245	26.23	22
51	LASAC	10	16	Electrosorption	250	25.03	22
52	LASAC	10	16	Electrosorption	255	24.61	22
53	LASAC	10	16	Electrosorption	260	24.17	22
54	LASAC	10	16	Electrosorption	265	23.62	22
55	LASAC	10	16	Electrosorption	270	23.23	22
56	LASAC	10	16	Electrosorption	275	22.98	22
57	LASAC	10	16	Electrosorption	280	22.68	22
58	LASAC	10	16	Electrosorption	285	22.48	22
59	LASAC	10	16	Electrosorption	290	22.30	22
60	LASAC	10	16	Electrosorption	295	22.15	22
61	LASAC	10	16	Electrosorption	300	21.95	22

62	LASAC	10	16	Electrosorption	305	21.87	22
63	LASAC	10	16	Regeneration	310	37.25	22
64	LASAC	10	16	Regeneration	315	50.93	22
65	LASAC	10	16	Regeneration	320	55.81	22
66	LASAC	10	16	Regeneration	325	60.98	22
67	LASAC	10	16	Regeneration	330	64.30	22
68	LASAC	10	16	Regeneration	335	65.92	22
69	LASAC	10	16	Regeneration	340	66.99	22
70	LASAC	10	16	Regeneration	345	67.58	22
71	LASAC	10	16	Regeneration	350	68.09	22
72	LASAC	10	16	Regeneration	355	68.65	22
73	LASAC	10	16	Regeneration	360	69.04	22
74	LASAC	10	16	Regeneration	365	69.38	22
75	LASAC	10	16	Regeneration	370	69.53	22
76	LASAC	10	16	Electrosorption	375	59.93	22
77	LASAC	10	16	Electrosorption	380	46.39	22
78	LASAC	10	16	Electrosorption	385	40.39	22
79	LASAC	10	16	Electrosorption	390	37.39	22
80	LASAC	10	16	Electrosorption	395	34.56	22
81	LASAC	10	16	Electrosorption	400	32.59	22
82	LASAC	10	16	Electrosorption	405	31.39	22
83	LASAC	10	16	Electrosorption	410	30.62	22

84	LASAC	10	16	Electrosorption	415	29.51	22
85	LASAC	10	16	Electrosorption	420	28.82	22
86	LASAC	10	16	Electrosorption	425	27.96	22
87	LASAC	10	16	Electrosorption	430	27.28	22
88	LASAC	10	16	Electrosorption	435	26.08	22
89	LASAC	10	16	Electrosorption	440	25.66	22
90	LASAC	10	16	Electrosorption	445	25.21	22
91	LASAC	10	16	Electrosorption	450	24.66	22
92	LASAC	10	16	Electrosorption	455	24.28	22
93	LASAC	10	16	Electrosorption	460	24.02	22
94	LASAC	10	16	Electrosorption	465	23.72	22
95	LASAC	10	16	Electrosorption	470	23.52	22
96	LASAC	10	16	Electrosorption	475	23.34	22
97	LASAC	10	16	Electrosorption	480	23.19	22
98	LASAC	10	16	Electrosorption	485	22.99	22
99	LASAC	10	16	Electrosorption	490	22.92	22
100	LASAC	10	16	Regeneration	495	40.83	22
101	LASAC	10	16	Regeneration	500	54.51	22
102	LASAC	10	16	Regeneration	505	59.39	22
103	LASAC	10	16	Regeneration	510	64.57	22
104	LASAC	10	16	Regeneration	515	67.88	22
105	LASAC	10	16	Regeneration	520	69.51	22

106	LASAC	10	16	Regeneration	525	70.58	22
107	LASAC	10	16	Regeneration	530	71.17	22
108	LASAC	10	16	Regeneration	535	71.68	22
109	LASAC	10	16	Regeneration	540	72.23	22
110	LASAC	10	16	Regeneration	545	72.63	22
111	LASAC	10	16	Regeneration	550	72.96	22
112	LASAC	10	16	Regeneration	555	73.16	22

Table A. 20 Input and output data for experiment on removal percentage and electrosorption capacity of Cr(VI) and fluoride with CAC electrode.

Sr. No.	Electrode used	Voltage applied (V)	Feed concentration (mg/L)	Flow rate (mL/min)	Time (min)	Removal percentage of Cr(VI)	Removal percentage of fluoride	Electrosorption capacity of Cr(VI)	Electrosorption capacity of fluoride	Exp. No.
1	CAC	1.2	10	16	120	97.1	94.20	0.85	0.82425	17
2	CAC	1.2	25	16	120	92.52	86.00	2.023875	1.88125	17
3	CAC	1.2	50	16	120	63.8	55.80	2.79125	2.44125	17
4	CAC	1.2	100	16	120	42	36.80	3.675	3.22	17

Table A. 21 Input and output data for experiment on removal percentage and electrosorption capacity of Cr(VI) and fluoride with TWBAC electrode.

Sr. No.	Electrode used	Voltage applied (V)	Feed concentration (mg/L)	Flow rate (mL/ min)	Time (min)	Removal percentage of Cr(VI)	Removal percentage of fluoride	Electrosorption capacity of Cr(VI)	Electrosorption capacity of fluoride	Exp. No.
1	TWBAC	1.2	10	16	120	88.5	85.2	0.77	0.7455	19
2	TWBAC	1.2	25	16	120	84.12	79.16	1.840125	1.731625	19
3	TWBAC	1.2	50	16	120	54.56	46.88	2.387	2.051	19
4	TWBAC	1.2	100	16	120	32.45	28.52	2.839375	2.4955	19

Table A. 22 Input and output data for experiment on removal percentage and electrosorption capacity of Cr(VI) and fluoride with RHAC electrode.

Sr. No.	Electrode used	Voltage applied (V)	Feed concentration (mg/L)	Flow rate (mL/ min)	Time (min)	Removal percentage of Cr(VI)	Removal percentage of fluoride	Electrosorption capacity of Cr(VI)	Electrosorption capacity of fluoride	Exp. No.
1	RHAC	1.2	10	16	120	83.1	80.4	0.727125	0.7035	21
2	RHAC	1.2	25	16	120	80.2	75.12	1.754375	1.64325	21
3	RHAC	1.2	50	16	120	50.96	42.14	2.2295	1.843625	21
4	RHAC	1.2	100	16	120	28.28	26.75	2.4745	2.340625	21

Table A. 23 Input and output data for experiment on removal percentage and electrosorption capacity of Cr(VI) and fluoride with LASAC electrode.

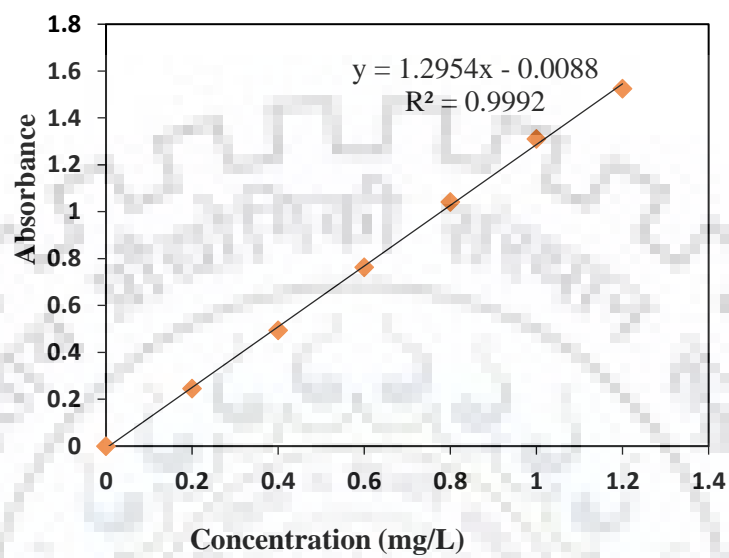| Sr. No.	Electrode used	Voltage applied (V)	Feed concentration (mg/L)	Flow rate (mL/min)	Time (min)	%Removal of Cr(VI)	%Removal of Fluoride	Electrosorption capacity of Cr(VI)	Electrosorption capacity of fluoride	Exp. No.
1	LASAC	1.2	10	16	120	92.2	89.2	0.80675	0.7805	23
2	LASAC	1.2	25	16	120	87.2	81.8	1.9075	1.789375	23
3	LASAC	1.2	50	16	120	58.88	50.16	2.576	2.1945	23
4	LASAC	1.2	100	16	120	36.88	31.49	3.227	2.755375	23

Calibration curve of Cr(VI)

Fig. A1 Calibration curve of Cr(VI).